NON-LINEAR HOMOGENIZATION OF MAGNETORHEOLOGICAL ELASTOMERS AT FINITE STRAIN

Evan Galipeau

A DISSERTATION

in

Mechanical Engineering and Applied Mechanics

Presented to the Faculties of the University of Pennsylvania

in

Partial Fulfillment of the Requirements for the

Degree of Doctor of Philosophy

2012

Professor Pedro Ponte Castañeda
Department of Mechanical Engineering and Applied Mechanics
Supervisor of Dissertation

Associate Professor Jennifer R. Lukes
Department of Mechanical Engineering and Applied Mechanics
Graduate Group Chairperson

Dissertation Committee:

Professor John L. Bassani,
Department of Mechanical Engineering and Applied Mechanics
Associate Professor Prashant Purohit,
Department of Mechanical Engineering and Applied Mechanics

ACKNOWLEDGEMENT

I would like to express my gratitude to my advisor, Dr. Pedro Ponte Castañeda and the mechanical engineering graduate group. This work would not have been possible without Pedro Ponte Castañeda's exceptional knowledge of homogenization and prior work. I would also like to thank the members of my thesis committee: Dr. John L. Bassani and Prashant Purohit.

Chapter 5 of this work represents a collaboration with Gal de Botton and Stephan Rudykh. I am grateful for the opportunity to work with them and for the opportunity to visit Israel.

The endless hours spent in the office were made enjoyable by my officemates. Discussions with Morteza, Reza, and Michalis were critical to the development of this thesis.

Last but not the least, I would like to thank my wife Kendra and my son Russell for their love. Their support, kindness, and patience throughout my graduate studies has been ceaseless.

ABSTRACT

NON-LINEAR HOMOGENIZATION OF MAGNETORHEOLOGICAL ELASTOMERS AT FINITE STRAIN

Evan Galipeau

Pedro Ponte Castañeda

Magnetorheological elastomers (MREs) are composite materials consisting of magnetizable particles embedded in an elastomeric matrix material. They are capable of magnetostriction, generating actuation traction, and magnetic field-dependent modulus effects. Because of these properties, MREs have a myriad of potential applications including magnetic position sensors, electromagnetic shielding, and flexible magnets, as well as controllable mounts, clutches and vibration absorbers. While experimental results demonstrate the promise of these materials, the effects that can be obtained are still relatively small. The goal of this thesis is to provide a better understanding of the properties of MREs using theoretical methods to help guide their continued development. For this purpose, we use homogenization, which determines an effective macroscopic constitutive model for an MRE based on the properties of the constituent phases and their arrangement within the composite. Variational homogenization methods were developed in this work which provide a framework to predict the behavior of general magnetoelastic composites. However, specializing this work to MREs, a somewhat simplified approach is developed which assumes that the microstructure evolves exactly as it would in the purely mechanical problem; we refer to it as the "partial decoupling approximation." Specific constitutive models for MREs made with rigid inclusions are derived which incorporate the non-linear effects of

magnetic saturation and the non-linearity inherent in finite strain mechanics. While the magnetoelastic coupling in MREs can be accounted for by considering the torques and forces exerted on particles by the applied magnetic field, the variational approach used here circumvents the need to explicitly compute these forces and torques. The results demonstrate that for aligned loading, where the magnetic torques vanish, the magnetoelastic coupling is proportional to the square of the particle concentrations to leading order. For non-aligned loading, the associated torques have effects proportional to the concentration and can be significantly larger. We optimize magnetoelastic properties like magnetostriction, actuation traction, and magnetoelastic modulus with respect to the microstructure. Furthermore, we investigate multi-scale composites that utilize magnetic torques and particle rotations to produce strong magnetoelastic coupling.

Contents

List of Tables

List of Figures

Chapter 1

Introduction

Magnetorheological elastomers (MREs) are composite materials consisting of magnetizable particles embedded in an elastomeric matrix material capable of finite strains. Typical materials used for the matrix include natural rubber, silicone rubber, and polyurethane, while carbonyl iron, Terfenol-D, and other more exotic materials have been used for the particles (Rigbi and Jilken, 1983; Sohoni and Mark, 1987; Ginder et al., 1999; Carson and Jolly, 2000; Ginder et al., 2002; Lanotte et al., 2003a,b; Guan et al., 2008; von Lockette et al., 2011; Danas et al., 2012). Because of the magnetic interactions among the particles, these composites can undergo "spontaneous" strain when subjected to a magnetic field, a phenomenon that is more generally known as *magnetostriction*. Moreover the macroscopic stiffness of MREs can be modified quickly, smoothly, and reversibly by application of a magnetic field. This means that they are good candidates for application as actuators, since their macroscopic response can be actively controlled in real-time. Additionally the appearance of strain in the composite can lead to changes in the overall magnetization (magnitude and/or direction), which could be detected by external means. This implies that MREs have great potential for use as sensors. MREs have already been proposed for use as media for magnetic data storage, magnetic position sensors, electromagnetic shielding, flexible magnets, and touch-screen displays, as well as controllable mounts, clutches and vibration absorbers in the automotive industry. MREs have favorable processing properties—they can be formed into objects of any shape and size—so they are expected to find use in many other industrial applications.

Three primary mechanisms are responsible for the magneto-mechanical coupling in MREs: magnetostriction of the inclusions, magnetic torques on particles, and magnetic interactions between particles. For MREs containing particles of giant magnetostrictive materials, such as Terfenol-D and Ni_2MnGa, all three mechanisms can be important (Duenas and Carman, 2000). For other inclusion materials, such as carbonyl iron, nickel, or cobalt, which have very small magnetostriction, the particles are effectively rigid, and the primary mechanisms are magnetic torques and magnetic interactions between particles (Jolly et al., 1996; Bednarek, 1999; Ginder et al., 2002; Guan et al., 2008).

A significant body of literature lays the foundation for this work. Numerous experiments have been performed on MREs composed of rigid, magnetic particles by various researchers. The particles can either be distributed randomly in the composite or aligned in chain structures by curing the elastomer under application of

a magnetic field. Jolly et al. (1996) and Danas et al. (2012) performed shear tests on chain-structured MREs and showed that the magnetic field increases the effective shear modulus of the composite. Bednarek (1999) measured the magnetostriction of composites made with randomly distributed particles subjected to very high magnetic fields. Ginder et al. (2002) and Guan et al. (2008) experimentally determined the magnetostriction of random and chain-structured MREs. Lanotte et al. (2003b) investigated the effect of particle rotation on the average magnetization of the composite. More recently, Diguet et al. (2010) have provided experimental and theoretical results for the magnetostriction and magnetic saturation of composite samples formed into a cylindrical shape and exposed to a remotely applied magnetic field. Work has also been done on MREs with particles which undergo large magnetostriction. For instance, Duenas and Carman (2000) obtained experimental results for MREs made with Terfenol-D inclusions at concentrations ranging from 10% to 50% and estimated the concentration which maximizes the composite magnetostriction.

While the experimental results demonstrate the promise of these materials, the overall effects that can be obtained are still relatively small. Experimental studies to improve these materials are likely to be time-consuming and expensive while theoretical methods may allow for the design of better MREs while avoiding the costs associated with experimentation. Additionally, theoretical studies can provide insight into the underlying mechanisms responsible for the coupling of MREs. Several papers have been published recently attempting to postulate constitutive models for magnetoelastic, and in particular MRE materials, using "macroscopic" (i.e. continuum mechanics) methods (Brown, 1963, 1966; Kovetz, 2000; Eringen and Maugin, 1990; Tiersten, 1964, 1965; Toupin, 1956; Truesdell and Toupin, 1960). Examples of the use of this type of approach include the works of Brigadnov and Dorfmann (2003); Dorfmann and Ogden (2004); Kankanala and Triantafyllidis (2004), and Danas et al. (2012) (see also Suo et al. (2008) for an analogous theory for deformable dielectrics). Although the continuum theories have been helpful in describing the "macroscopic" magneto-mechanical response of MREs and have the advantage of considering large strain, gaining further improvements in the properties of these complex materials will depend crucially on a better understanding of the highly coupled and nonlinear structure-property relations for these materials.

A natural tool to study the effective behavior of MREs is homogenization, which determines a constitutive model for an MRE based on the properties of the consti-

tutive phases and their arrangement within the composite. For MREs made from particles with small magnetostriction, Borcea and Bruno (2001) developed a small-strain model for composites composed of rigid, isotropic, ferromagnetic spheres by considering particle-particle forces. They obtained estimates that aim to account for interactions to second order in the volume fraction. Their results agree with the dilute limit of a rigidly reinforced composite to first order in the volume fraction because the inter-particle forces vanish in this limit. Furthermore, the isotropic spheres cannot experience magnetic torques. Yin and Sun (2006) also developed small-strain models for composites with randomly distributed isotropic spheres; however, the particles could deform elastically but were assumed to exhibit linear magnetic behavior. The pairwise particle interactions were used to compute an average stress over the composite and to obtain magnetoelastic constitutive relations in their work. Yin et al. (2006) extended this approach to MREs where the magnetic particles form chain structures but still preserve their spherical shape. In addition, Liu et al. (2006) have calculated the effective properties of composites made of a dilute concentration of magnetostrictive particles dispersed in a magnetically transparent, linear-elastic matrix, by means of the "constrained theory" of micromagnetics (DeSimone and James, 2002). These homogenization approaches have been restricted essentially to *infinitesimal deformations* and very specific microstructures, which limits their usefulness. On the other hand, in the context of electro-active polymers deBotton et al. (2007) have recently generated finite-strain estimates for the macroscopic response of material systems with a special type of sequentially laminated microstructures and linear electrostatic response for the inclusion phase.

There is a need to accurately model the macroscopic response of these material systems and its dependence on the microstructure to aid in the development of MREs. In fact the magnetic interactions among the particles in these materials depend critically on their distribution in space, as well as on their shape and orientation. The orientation of the magnetization in the particles should be taken into account for the case of magnetically anisotropic particles. Furthermore, the relative position and orientation of the particles can change because of the large deformations that these elastomer-based materials are capable of developing. This evolution of the microstructure must be considered and is in fact critical for determining the coupled behavior of MREs. The natural tool for accounting for all these effects is homogenization, but until recently, the state of the art in homogenization theory was not sufficiently ad-

vanced to undertake this enterprize in its full generality. Accounting for *constitutive* and *geometric* nonlinearities in the context of homogenization is extremely difficult, and this is presumably the reason why this approach has not yet been attempted for magnetoelasticity at finite strains.

Determining the effective behavior MREs is a quite complicated problem and indeed homogenization of MREs reduces to the homogenization of mechanical composites at finite strain in the limit when the magnetic field vanishes. Finite strain homogenization of this type in the purely mechanical context is already a difficult problem and we make use of many recent developments in that field. Significant progress was made by Ponte Castañeda and Tiberio (2000) in deriving second-order homogenization estimates for hyperelastic composites at finite strains using the "tangent linear comparison" method. This in turn was built on progressive advances in nonlinear homogenization (Talbot and Willis, 1985; Ponte Castañeda, 1991; Suquet, 1993; Ponte Castañeda, 1996; Ponte Castañeda and Suquet, 1998; Ponte Castañeda and Willis, 1999). More robust estimates, which are capable of capturing the highly nonlinear incompressibility constraint in rubber-like materials, have been developed more recently by Lopez-Pamies and Ponte Castañeda (2006a) making use of the "generalized secant" approach of Ponte Castañeda (2002), which incorporates the use of field fluctuations in the earlier second-order estimates.

The goal of this thesis is to provide a better understanding of the properties of MREs using theoretical methods in order to guide their continued development. To this end homogenization methods were developed which provide a framework to predict the behavior of MREs based on the properties of the constituent phases and their arrangement within the composite. Moreover, the methods also provide a basis for the analogous electro-magneto-elastic homogenization. It should be noted that the homogenization methods developed in this work apply to more general magnetoelastic composites, not only MREs, and that the previously mentioned linear comparison techniques can be brought to bear directly on the magnetoelastic homogenization. However in this work a somewhat simplified approach which assumes effectively rigid inclusions and utilizes a "partial decoupling approximation" will be used. Specific constitutive models for MREs made with rigid inclusions are derived which include the non-linear effects of magnetic saturation and the non-linearity inherent in finite strain mechanics. Furthermore, the magnetoelastic properties of these materials were optimized with respect to effects like magnetostriction, actuation traction, and mag-

netoelastic modulus. These methods were employed to develop designer materials capable of more pronounced magnetoelastic effects.

This thesis is laid out as follows. Chapter 2 provides background information. Since this thesis is primarily directed at the mechanics community, a brief overview of the physics of magnetism is provided. This provides the foundation for the constitutive models we use to describe the magnetic inclusions in MREs. Then the necessary background on the coupled magnetoelastic variational methods and energy functions which serve as the basis for this work is given. We will also discuss the proper application of magnetoelastic energy functions as there are some important practical differences between measuring magnetoelastic and purely mechanical material properties.

Chapter 3 introduces the homogenization framework based on the energy methods outlined in Chapter 2. First a variational homogenization formulation is developed for magnetoelastic composites at finite strain, generalizing the corresponding formulation of Hill (1972) for hyperelastic composites. This formulation makes use of a Lagrangian constitutive framework originally proposed by Dorfmann and Ogden (2004) for magnetoelasticity, as well as of variational principles exploiting this framework, recently advanced by Bustamante et al. (2008). Next a "partial decoupling" of the magnetoelastic homogenization problem is accomplished taking advantage of the special character of the microstructure and its evolution in MREs. In essence the microstructure is assumed to evolve with the "purely mechanical" deformation, thus splitting the original problem into a purely mechanical homogenization problem, together with a magnetostatic homogenization problem in the deformed configuration. In turn both of these sub-problems can be solved by means of the "linear comparison" homogenization techniques together with the linear homogenization estimates of Ponte Castañeda and Willis (1995) for composites with particulate microstructures of the type exhibited by the MREs. The approximation is argued to be very accurate at least in the "stiff matrix" limit. Furthermore explicit results are provided for MREs with magnetically linear anisotropic behavior, which are later shown to also be valid for magnetically nonlinear behavior provided that the magnetic permeability of the relevant "linear comparison composite" can be computed from the secant modulus (Ponte Castañeda et al., 1992) of the nonlinear material evaluated at the average magnetic field in the inclusions. Results are also provided for MREs where the inclusions exhibit permanent magnetization. The results demonstrate that there

is an "extra" stress—beyond the usual "purely mechanical" and "vacuum magnetic" stresses—which can be directly related to deformation-induced changes in the volume fraction, orientation and distribution of the particles. Finally some concluding remarks are offered concerning applications of the above-described theory to specific MRE systems, as well as possible extensions/generalizations for other electro- and magnetoelastic material systems. The work in this chapter was discussed in Ponte Castañeda and Galipeau (2011).

Chapter 4 explores the effects of magnetic torques and particle rotations when the magnetic and mechanical fields are not aligned with the geometric axes of the particles. We will consider magnetically isotropic particles for simplicity, although the general theory can account for magnetic anisotropy. In this case, the theoretical results of Chapter 3 (Ponte Castañeda and Galipeau, 2011) suggest that the effect of the particle rotations should be of order volume fraction, since these effects derive from the direct interaction of the particles with the applied magnetic field. The MREs of interest in this work consist of stiff, aligned cylindrical fibers of a magnetizable material that are distributed with "elliptical" two-point correlations in a soft elastomeric matrix. The fibers have elliptical cross-section and their in-plane axes are also aligned. The resulting MRE systems are subjected to combined in-plane mechanical and magnetic loading, and estimates are obtained for their magnetoelastic stored-energy function using the finite-strain homogenization framework and "partial decoupling approximation" of Chapter 3 (Ponte Castañeda and Galipeau, 2011). It is demonstrated that the tractions that are required to maintain a specified deformation of the MRE have a resultant torque when the macroscopic magnetic field is not aligned with the geometric axes of the particles. More importantly, it is shown that the magnetoelastic effects are generally enhanced in this case due to the increased potential for particle rotations. The effects of having permanent magnets included in the particulate microstructures is also included. The results of this section provided the basis for part of the work presented in Galipeau and Ponte Castañeda (2012).

Chapter 5 shows how the homogenization framework can be naturally extended to include magnetoelastic effects in periodic media. An in-depth analysis and comparison of the magnetoelastic effects in periodic and random media is considered in this chapter. The presence of magnetic particles modifies the magnetic stress even for dilute particle concentrations; however, accounting for the Maxwell stress outside the material shows that the magnetoelastic coupling depends to leading order

on the concentration squared. This implies that higher order information about the microstructure is necessary to accurately describe the magnetoelastic coupling. Moreover, we find that linearly magnetic materials with the same susceptibilities can have rather different magnetoelastic coupling. We demonstrate that the main governing parameter for the magnetoelastic coupling is the derivative of susceptibility with respect to deformation. These effects are illustrated and confirmed by comparison of the responses of the MREs with random and periodic distributions of the particles. We show how magnetic susceptibility as a function of deformation is related to the coupled magnetoelastic behavior in MREs. As a result parameters useful in characterizing the coupled behavior of MREs are defined. These quantities are evaluated for random, quasi-hexagonal, and rectangular periodic microstructures over a wide range of concentrations and particle aspect ratios. Finally, we evaluate the magnetostriction for these materials to provide direction in developing MREs with strongly coupled behavior. It is revealed that periodic materials have stronger magnetoelastic effects than randomly generated materials, but in both cases the effects are greatly influenced by the concentration and relative positions of the particles. This chapter was completed in collaboration with Stephan Rudykh and Gal deBotton at Ben-Gurion University, in Beer-Sheva, Israel, who performed the finite element simulations. This work was presented in Galipeau et al. (2013).

In Chapter 6 laminates consisting of the previously defined MRE systems with plus/minus orientations of the fibers relative to the layers' normal are constructed. Because of the symmetry of the microstructure, the macroscopic torques on the sample can be eliminated—while still preserving the enhanced coupling effects of the particle rotations—by application of the magnetic field and mechanical tractions along the layers' normal. These laminated MRE samples are found to exhibit greatly increased actuation and magnetostriction, as well as greater sensitivity of the Young's modulus to the applied magnetic field. Additionally, certain instabilities are revealed and discussed in the process of evaluating these laminated composites. We also consider the limit where the aspect ratio of the particles in the plus/minus phases becomes extremely large and the composite becomes a rank 2 laminate. We also evaluate this material as a function of the microstructure. Portions of this chapter were presented in Galipeau and Ponte Castañeda (2013).

Chapter 7 investigates a 3D model in the small-strain limit. The homogenization technique is applied to composites with "ellipsoidal" microstructures subjected

to aligned loading conditions. The results are specialized for small strains. Expressions are given for the surface traction in composite materials consisting of spheroidal particles with nonlinear magnetic behavior, distributed spheroidally in an isotropic non-magnetic matrix, and subjected to aligned loadings. Then the results are utilized for uniaxial loading aligned with the symmetry axis of the spheroidal inclusions. Various parameters are defined, including an actuator energy density, to evaluate these materials and investigate in some detail the effects of particle shape and concentration on the magnetoelastic behavior of the composite in the uniaxial tension test. Additionally we provide predictions of the multidirectional magnetostriction when the magnetic field is applied transverse to the spheroidal axis. This chapter provided the basis for Galipeau and Ponte Castañeda (2012).

Finally Chapter 8 provides some concluding remarks as well as some directions for future work.

In this thesis, scalars will be denoted by italic Roman, a and G, or Greek letters, α; vectors by boldface Roman letters, $\mathbf{b}$; second-order tensors by boldface italic Roman letters, $\boldsymbol{P}$, or bold face Greek letters, $\boldsymbol{\epsilon}$; and fourth-order by tensors barred letters, $\mathbb{C}$. When necessary Cartesian components will be introduced; for example, C_{ijkl} are the Cartesian components of $\mathbb{C}$.

1.1 List of publications resulting from this dissertation work

1. Ponte Castañeda, P., Galipeau, E., 2011. Homogenization-based constitutive models for magnetorheological elastomers at finite strain. J. Mech. Phys. Solids 59, 194-215

2. Galipeau, E., Ponte Castañeda, P., 2012. The effect of particle shape and distributions on the macroscopic behavior of magnetoelastic composites. Int. J. Solids Struct. 49, 1-17

3. Galipeau, E., Ponte Castañeda, P., 2013. A finite-strain constitutive model for magnetorheological elastomers: magnetic torques and particle rotations. J. Mech. Phys. Solids, Submitted

4. Galipeau, E., Rudykh, S., deBotton, G., Ponte Castañeda, P., 20–. The effect of microstructure on coupled magnetoelastic behavior for random and periodic composites. 00, 000-000

5. Galipeau, E., Ponte Castañeda, P., Layered microstructures for enhanced magnetoelastic effects, in preparation

Chapter 2

Background

2.1 Fundamentals of rigid magnetic materials

Magnetism occurs at a variety of length scales with very different effects and consequences. The aim of this section to provide a foundation for understanding the terminology found in literature about magnetism and magnetorheological materials and how this work relates to it. Magnetic materials exhibit strong-nonlinearity and empirical parameters are used in order to simply quantify these materials. The following discussion will describe how those parameters relate to the non-linear constitutive relations used in this work. In this regard, the critical information from books on electro-magnetism including Jackson (1975), Ohanian (2006), and Kovetz (2000) is compiled and explained.

2.1.1 Magnetostatic fields and magnetic materials

Here we will consider the field equations governing magnetostatics since we are primarily interested the quasi-static behavior of MREs. A nice presentation is given by Kovetz (2000) who considered the full electomagnetic system. Reducing this to the quasi-static case, the fundamental quantities necessary to understand the magnetic effects are the magnetic flux $\mathbf{b}$ and the magnetic intensity $\mathbf{h}$. The fields satisfy these differential equations

$$\operatorname{curl} \mathbf{h} = 0 \qquad \mathbf{n} \times [[\mathbf{h}]] = \mathbf{j} \tag{2.1}$$

$$\operatorname{div} \mathbf{b} = 0 \qquad \mathbf{n} \cdot [[\mathbf{b}]] = 0 \tag{2.2}$$

where $\mathbf{j}$ is the steady state free current and the curl and div operators are with respect to the current configuration. These equations are very similar to stress-strain relations with $\mathbf{b}$ being divergence-free like the stress field, and $\mathbf{h}$ being the derivative of a potential or curl-free like the displacement field.

Similar to the mechanics analogy the relationship between $\mathbf{b}$ and $\mathbf{h}$ is determined by the material occupying the space in question and can be considered as a material constitutive relation. However within a vacuum $\mathbf{b}$ and $\mathbf{h}$ have a non-trivial relationship, which is

$$\mathbf{b} = \mu_0 \mathbf{h} \tag{2.3}$$

where μ_0 is the magnetic permeability of free space.

Within materials electrons circulate in and around atoms which gives rise to the

magnetism in atoms or molecules. When a large number of magnetized atoms or molecules are together we can define the contribution to the magnetic field from the particles as a magnetization vector $\mathbf{m}$. This quantity is only defined in an average sense in the context of a region containing a sufficiently high number of atoms. This magnetization has the effect of increasing (or decreasing when $\mathbf{m}$ is negative) the magnetic flux $\mathbf{b}$ making the constitutive relation within a magnetic material

$$\mathbf{b} = \mu_0(\mathbf{h} + \mathbf{m}). \tag{2.4}$$

This formulation can make it appear that there are two independent variables, for example $\mathbf{h}$ and $\mathbf{m}$ determining $\mathbf{b}$; however one of the three quantities determines the other two. A specified $\mathbf{h}$ field within a material can cause the material to respond with a certain magnetization and therefore a magnetic flux $\mathbf{b}$. As it turns out these functions are in general not necessarily single valued and can depend in a very complicated way on the history and present state of the magnetic fields. Also note that $\mathbf{b}$, $\mathbf{h}$, and $\mathbf{m}$ are vectors and the relationship between them can be anisotropic which implies the vectors may not be coaxial. For simplicity in this section we will only consider isotropic material behavior such that the vectors are coaxial. The figures represent the magnitude of the respective fields.

2.1.2 Fundamental characteristics of diamagnetic, paramagnetic and ferromagnetic materials

Different materials can respond to magnetic excitation in very different ways. There are many classifications for magnetic materials; however the difference between these characterizations depends somewhat on the length scales of the material involved.

On the molecular length scale the three major groups of magnetic materials, diamagnetic, paramagnetic, and ferromagnetic referring to different atomic responses to magnetic excitation. Most, if not all, materials show some degree of all three types of behavior at the molecular length scale. The degree to which one behavior overshadows the others determines how one should classify the bulk material. Paramagnetic and diamagnetic effects are actually properties of atoms whereas ferromagnetic behaviors are properties of the molecular structure in combination with the magnetic properties of atoms. This means that it is possible to discuss whether atoms may be paramagnetic or diamagnetic, but a material being ferromagnetic must refer to a

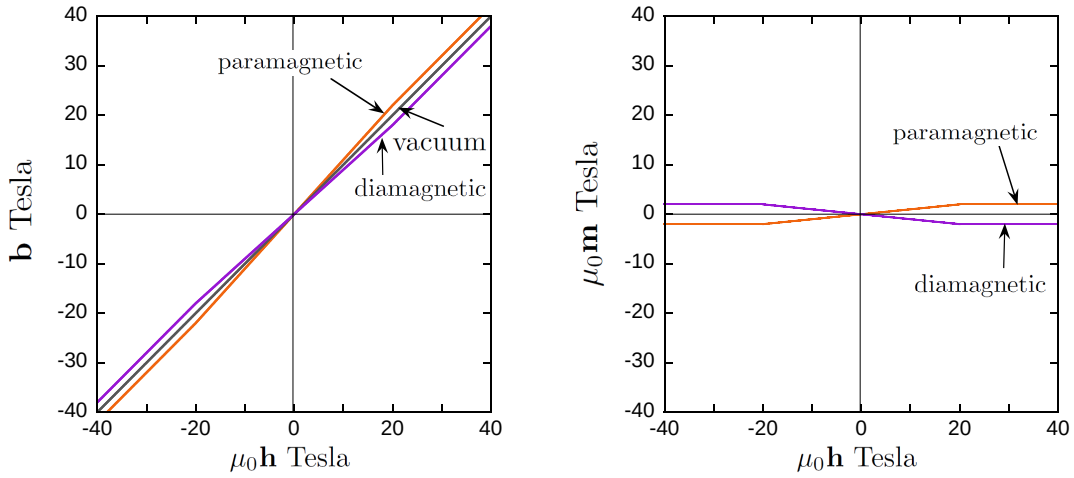

(a) (b)

Figure 2.1: Magnetic constitutive relations for paramagnetic and diamagnetic materials relative to vacuum. (a) $\mathbf{b}$ as a function of $\mathbf{h}$. (b) $\mathbf{m}$ as a function of $\mathbf{h}$.

material with some form of structure (Kovetz, 2000).

The properties which we will be concerned with will be properties of magnetic materials in which large groups of atoms combine to give materials with bulk magnetic properties. In the bulk these atomic interactions give rise to very different relations between $\mathbf{b}$, $\mathbf{h}$, and $\mathbf{m}$, depending on the type of material.

The diagrams in Figure 2.1 illustrate the macroscopic behavior of paramagnetic and diamagnetic materials in relation to vacuum. It is at this length scale that the qualitative differences in the $\mathbf{b} - \mathbf{h}$ relations determine how to classify materials. Paramagnetic materials have a magnetization which increases the magnetic flux relative to vacuum and diamagnetic materials have a magnetization which decreases the magnetic flux relative to vacuum. As discussed before, all materials will have some degree of both paramagnetic and diamagnetic material response at the molecular level and their combined effect determines their macroscopic response.

For small applied magnetic fields the relations are well approximated as linear and a very common way of describing the material properties is to describe $\mathbf{b}$ or $\mathbf{m}$ as a linear function of $\mathbf{h}$. For these materials the constitutive relation is often written as

$$\mathbf{b} = \mu\mathbf{h} \tag{2.5}$$

where μ is the magnetic permeability of the material. Relations of this type are also given in terms of the susceptibilities $\chi_h = \mu - \mu_0$ and $\chi_b = \frac{\mu-\mu_0}{\mu}$ which define the magnetization as

$$\mathbf{m} = \chi_h \mathbf{h} \qquad \text{and} \qquad \mathbf{m} = \chi_b \frac{\mathbf{b}}{\mu_0}. \tag{2.6}$$

This approximation is good for a large range of excitations; however at large enough $\mathbf{h}$ fields the material becomes saturated. This means that an increase in the applied field can cause no further magnetization. At this point the magnetization is constant and the increase in magnetic flux is proportional to the increase in magnetic intensity with the same coefficient as vacuum. A very large magnetic field is required to reach saturation (about 20 tesla) so that these materials are well approximated by linear functions in most cases. The permeability for most materials is in the range of $\mu = \mu_0(1 \pm 0.003)$. Materials with the coefficient of μ_0 less than one are diamagnetic and materials with a coefficient greater than one are considered paramagnetic. For these materials the magnetic behavior is independent of the size of the sample, which is not the case for the ferromagnetic materials we are about to discuss. All these materials are non-magnetic for most practical purposes because the magnetization is too small to generate a noticeable effect, especially when compared to ferromagnetic materials. In this thesis we consider the elastomer matrix to be non-magnetic with $\mu = \mu_0$ even though in truth it probably exhibits some paramagnetic or diamagnetic behavior.

The $\mathbf{b} - \mathbf{h}$ relations for a typical ferromagnetic are drawn in Figure 2.2 (Kovetz, 2000). The relation is no longer single valued. Small values of $\mathbf{h}$ give rise to three different equilibrium solutions for the resulting magnetic flux and magnetization. It turns out that solutions with negative slope correspond to unstable solutions leaving two stable solutions. Also of interest is that for zero applied magnetic field there is a net magnetization. This spontaneous magnetization is the result of the crystalline structure and the magnetic moments of the atoms. It is because of this spontaneous magnetization that ferromagnetic materials are always magnetized at a small enough length scale. Iron samples on the order of 20 nm can show uniform spontaneous magnetization with no applied magnetic intensity.

For large samples when the differential equations governing magneto-statics are solved with a uniform magnetization, the $\mathbf{h}$ that results is sufficient to reverse the magnetization. If the entire sample were to reverse magnetization the resulting $\mathbf{h}$ would

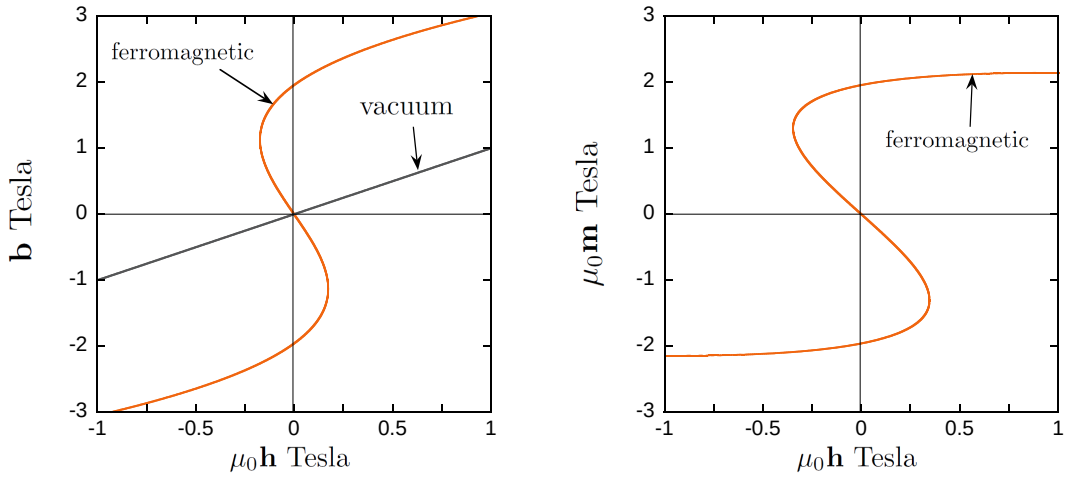

(a) (b)

Figure 2.2: Magnetic constitutive relations for single domain ferromagnetic materials. (a) **b** as a function of **h**. (b) **m** as a function of **h**.

reverse the magnetization again. Therefore uniform magnetization is not possible in larger specimens of ferromagnetic materials. The result is that bulk ferromagnetic materials divide themselves into magnetic domains. It would seem from solving the equations of magnetization that any ferromagnetic would continually subdivide into infinitesimally small domains. However there is a surface energy for magnetic domains which limits their subdivision. For larger magnetic fields the solutions eventually become singled valued and the individual domains can vanish.

Most practical magnetic particles consist of sufficiently many domains and the particle magnetization can be thought of as the average over many magnetic domains. Spontaneous magnetization averages to give a bulk magnetization behavior for a sample at this length scale. While single domains are in fact always magnetized, a large group of domains can have a net magnetization of zero. Usually the magnetic domains are small relative to the size of bulk samples and the effects of multiple domains decays very rapidly with distance from the sample such that from a macroscopic perspective only the net magnetization needs to be considered. The bulk properties of this material would be determined by minimizing the total energy at the applied **b** or **h** field. The resulting magnetization curves for the bulk material are shown in Figure 2.3. The curves in Figure 2.3 are called the anhysteretic magne-

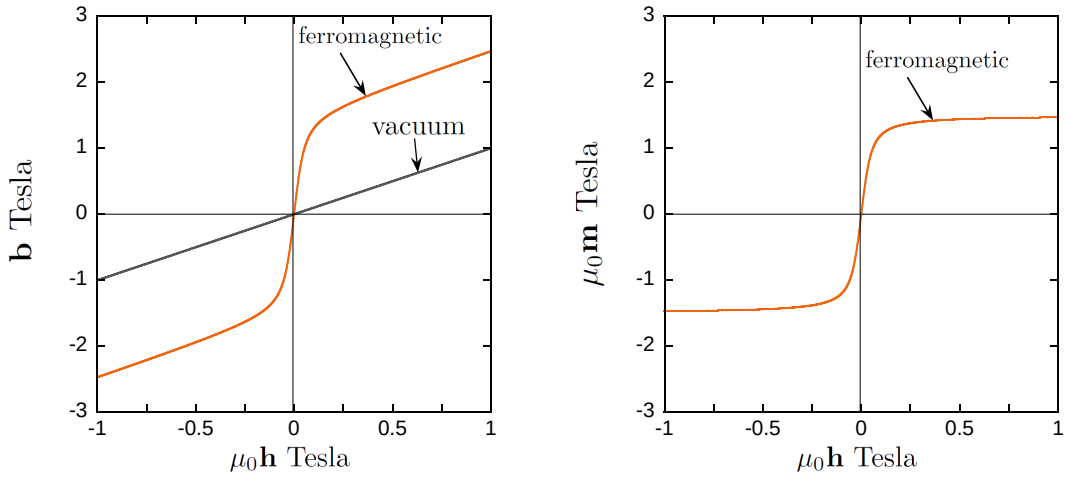

(a) (b)

Figure 2.3: Anhysteric magnetic constitutive relations for bulk ferromagnetic materials. (a) **b** as a function of **h**. (b) **m** as a function of **h**.

tization curves because they ignore hysteresis. These represent the global minimum of the potential energy of the magnetic material. For many materials the time scale to reach the equilibrium state can be very long.

Since the time scale to reach equilibrium is so long the magnetization curves of many ferromagnetic materials do exhibit strong hysteresis such that most ferromagnetic materials have constitutive relations qualitatively similar to the depiction in Figure 2.4. The curve starting at the origin illustrates the constitutive relation as the magnetic intensity is increased from zero in a material which has just been formed or after the material has been allowed to reach it equilibrium state. After the material has been brought to saturation and the applied magnetic field is subsequently decreased, the response of the material follows the upper curve. If the material reaches saturation in the negative direction and the magnetic flux is increased again, it follows the lower curve. The relation is significantly more complicated if the magnetization cycle does not reach saturation. Creating models to describe magnetic constitutive relations is an area of active research.

The explanation for this bulk constitutive behavior based on the properties of the underlying micro-structure is not fully understood; however there is consensus on some of the underlying causes. The individual magnetic domains become stuck in

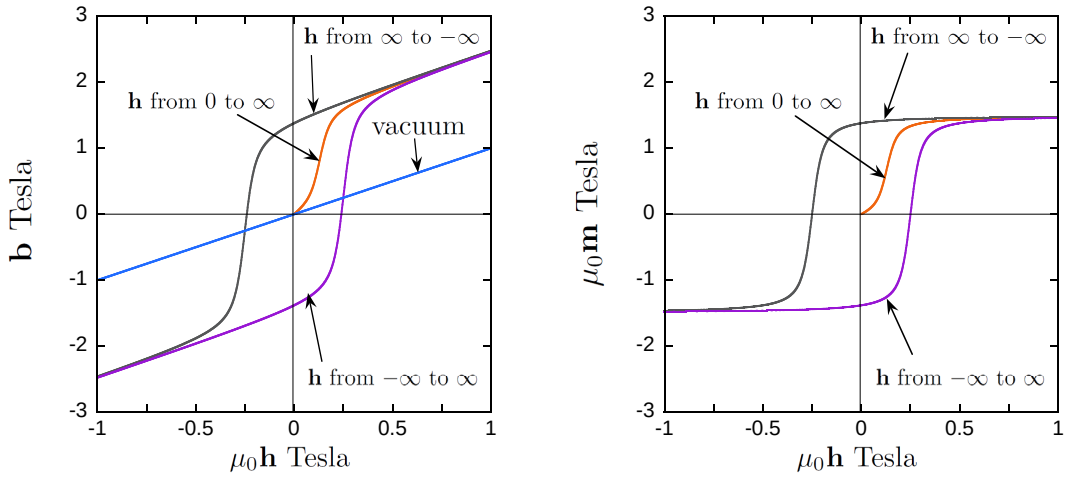

(a) (b)

Figure 2.4: Magnetic constitutive relations for bulk ferromagnetic materials. (a) **b** as a function of **h**. (b) **m** as a function of **h**.

their present configuration, which is called domain pinning, and it takes an increased applied field to reverse the individual magnetic domains. These effects are drastically affected by almost every property of the material and state of the material. Material impurities, lattice structure, crystalline structure, sample size, and other properties intrinsic to the materials, as well as the state of stress in the material, applied electric field, and temperature, plus many others, all influence bulk magnetic materials.

Figure 2.4 serves to define several important parameters in connection with magnetic materials. Magnetic saturation is the maximum amount of magnetization that a material can produce and is the maximum value of **m** as $\mathbf{h} \to \infty$. Remanence is the amount of permanent magnetization that remains after the applied fields are removed and is depicted by the vertical and horizontal intercepts. Hysteresis loss represents the energy expended during a closed magnetization cycle. The area between the upper and lower magnetization curves represents the total hysteresis loss.

2.1.3 Soft ferromagnetism and hard ferromagnetism

Most materials which are considered magnetic exhibit magnetization behavior qualitatively consistent with Figure 2.4. However quantitative differences often significantly

impact our perception of the magnetic behavior. One type of magnetic material model is a soft ferromagnetic material. This material idealization has zero remanence and zero hysteresis. These materials are sometimes called superparamagnetic even though they are usually ferromagnetic materials with minimal domain pinning. Soft ferromagnetic materials reach the anhysteretic magnetization curve very quickly. This means that the magnetization can be approximated as a single valued function of the magnetic intensity. In turn this implies that the materials can be described by an energy function. The homogenization framework developed in Chapter 3 requires the constituent materials to have such energy functions. While no real material achieves this idealization, it is a good approximation in many contexts and can include both isotropic and anisotropic magnets. This is the type of material most extensively considered in this work as it is a good representation of soft iron, nickel, cobalt and their alloys.

The classification of a hard magnetic materials is more complicated. In contrast to soft magnetic materials in which the upper and lower magnetization curves coincide, in hard magnetic materials the upper and lower curves widen. Hard magnetic materials make good permanent magnets because once exposed to a large magnetic field, they retain their magnetization when the external field is removed. However a hard magnetic material may be unmagnetized.

These two very general classes characterize the most common types of magnetic materials, but it is by no means exhaustive. Another useful categorization would be materials which have a one-to-one magnetization vs. magnetic intensity relationship yet retain a remnant magnetization. A magnet with these properties would be hard in the sense that it would be a permanent magnet, but soft because it would exhibit no hysteresis. We use this model to represent inclusion materials with permanent magnetization in Chapters 3 and 4. We deem it to be a reasonable approximation for permanent magnets at least for a small range of applied fields.

2.2 Magneto-elastostatics and magnetoelastic energy functions for deformable materials

Given a brief overview of rigid magnetic materials we now move on to coupled magnetoelastic behaviors. The coupling of electromagnetism and continuum mechanics has been an area of active research for well over 100 years and has only recently been widely accepted. The theoretical foundations of electroelastic and magnetoelastic response from a continuum mechanics (or macroscopic) point of view goes back to the 1960s. Truesdell and Toupin (1960), Tiersten (1964) and Maugin and Eringen (1972) developed the relevant conservation laws and proposed constitutive theories making use of the axioms of continuum mechanics (Toupin (1956) considered the finite strain theory for deformable dielectrics). Tiersten (1965) and Brown (1966) developed variational approaches by employing a suitable ansatz for the free-energy function. These theories have been further developed and nicely presented in the monographs by Eringen and Maugin (1990) and Kovetz (2000). It should also be mentioned that there are more "microscopic" theories of magnetism, such as micromagnetics (Brown, 1963), which aim to account for the phenomenon of "magnetic domains" in ferromagnetic materials. A simplified version of this theory has been developed by DeSimone (1993) in the "large body" limit, while James and Kinderlehrer (1993); DeSimone and James (2002) have proposed a "constrained theory" appropriate for magnetostrictive, single-crystal samples with high anisotropy and mobile variant interfaces.

2.2.1 Background on magneto-elastostatics

Neglecting electrical, thermal, and relativistic effects, and under the hypotheses of quasi-static magnetic and mechanical loadings, the magnetoelasticity problem can be characterized (e.g., Brown (1966); Eringen and Maugin (1990); Kovetz (2000)) as follows. Consider a heterogeneous material occupying a volume Ω_0 in the reference configuration when no magnetic and mechanical fields are applied. The specimen is made up of N different homogeneous phases occupying subdomains $\Omega_0^{(r)}$ $(r = 1, ..., N)$. Let $\mathbf{X}$ denote the position of a given material particle in Ω_0. Under the combined action of magnetic and mechanical loadings, the material particle will move to a new position described by $\mathbf{x}$ in the deformed configuration of the specimen Ω. This mapping of material points from the reference to the deformed configuration defines

a function $\mathbf{x} = \mathbf{x}(\mathbf{X})$, which is assumed to be continuous and one-to-one so that there are neither gaps nor interpenetration regions in the material. The deformation is characterized by the deformation gradient tensor $\boldsymbol{F} = \operatorname{Grad}\mathbf{x}$, with Cartesian components $F_{ij} = \partial x_i/\partial X_j$ and such that $J = \det \boldsymbol{F} > 0$. Note that $\boldsymbol{F}$ may be discontinuous, for example, across a material interface, but its jump must satisfy the condition $[[\boldsymbol{F}]] = \mathbf{A} \otimes \mathbf{N}$, where $\mathbf{N}$ is the normal to the interface in the reference configuration and $\mathbf{A}$ is a vector to be determined from the solution of the problem.

The material satisfies the conservation of mass equation, which in local form becomes $\rho_0 = \rho \det \boldsymbol{F}$, where ρ_0 and ρ are the material densities in the reference and deformed configurations, respectively. Here we will take the density of each phase r in the reference configuration to be a prescribed constant, $\rho_0^{(r)}$, in such a way that $\rho^{(r)} = \rho_0^{(r)}/J$. Note that the $\rho^{(r)}$ depend on the deformation and are not necessarily constant.

Defining $\boldsymbol{T}$ and $\boldsymbol{S} = J\boldsymbol{T}\boldsymbol{F}^{-T}$ as the *total* Cauchy and first Piola-Kirchhoff stress tensors, we enforce the equilibrium equations. They can be written equivalently in Eulerian (in terms of $\boldsymbol{T}$), or Lagrangian (in terms of $\boldsymbol{S}$) forms as

$$\operatorname{div}\boldsymbol{T} + \rho\mathbf{f} = \mathbf{0}, \quad \text{or} \quad \operatorname{Div}\boldsymbol{S} + \rho_0\mathbf{f}_0 = 0, \tag{2.7}$$

where $\mathbf{f}$ and $\mathbf{f}_0$ are the given *mechanical* body force distributions in the deformed and reference configurations, and div and Div are the divergence operators in the deformed and reference configurations (e.g., Div $\boldsymbol{S}$ is the vector with Cartesian components $\partial S_{ij}/\partial X_j$). It is emphasized here, and discussed in more detail further below, that these measures of stress include both mechanical as well as magnetic effects. It is customary by some authors to insert all or part of the magnetic contributions as a body force in the above equilibrium equations. However it is advantageous in the present context to include both effects in the total stress for two reasons. First, unlike the mechanical body force, which is externally prescribed, the magnetic body force is obtained from the solution of the coupled magnetoelastic problem. Second, as a consequence of the first point, the magnetic body force will fluctuate on the same length scale as the microstructure and therefore can not be treated as a *fixed* body force in the homogenization problem. In addition to the above conservation of linear momentum equation, the conservation of angular momentum equation leads to the requirement of symmetry of the Cauchy stress, $\boldsymbol{T} = \boldsymbol{T}^T$, or equivalently,

$\boldsymbol{S}\boldsymbol{F}^T = \boldsymbol{F}\boldsymbol{S}^T$. As with $\boldsymbol{F}$, the stress fields $\boldsymbol{T}$ and $\boldsymbol{S}$ may be discontinuous across a given interface, but must satisfy the jump conditions $[[\boldsymbol{T}]]\mathbf{n} = \mathbf{0}$ (or $[[\boldsymbol{S}]]\mathbf{N} = \mathbf{0}$), where $\mathbf{n}$ (or $\mathbf{N}$) is the normal to the interface in the deformed (reference) configuration.

The equations of magnetostatics are usually expressed in Eulerian form in terms of the true (or Eulerian) magnetic field $\mathbf{h}$ and magnetic induction field $\mathbf{b}$, satisfying Ampere's and Gauss's laws

$$\operatorname{curl}\mathbf{h} = \mathbf{j}, \quad \text{and} \quad \operatorname{div}\mathbf{b} = 0, \tag{2.8}$$

respectively. Here, $\mathbf{j}$ is the prescribed time-independent current density per unit volume in Ω, and curl and div are the usual differential operators with respect to $\mathbf{x}$. However, it is known (Dorfmann and Ogden, 2004; Kankanala and Triantafyllidis, 2004) that these equations can also be written in Lagrangian form as

$$\operatorname{Curl}\mathbf{H} = \mathbf{J}, \quad \text{and} \quad \operatorname{Div}\mathbf{B} = 0, \tag{2.9}$$

where $\mathbf{H} = \boldsymbol{F}^T\mathbf{h}$, $\mathbf{B} = J\boldsymbol{F}^{-1}\mathbf{b}$ and $\mathbf{J} = J\boldsymbol{F}^{-1}\mathbf{j}$ are the Lagrangian counterparts of the magnetic, magnetic induction, and current density fields. These magnetic fields may also be discontinuous at interfaces, but must satisfy the jump conditions $[[\mathbf{b}]] \cdot \mathbf{n} = \mathbf{0}$ (or $[[\mathbf{B}]] \cdot \mathbf{N} = \mathbf{0}$), and $\mathbf{n} \times [[\mathbf{h}]] = \mathbf{k}$ (or $\mathbf{N} \times [[\mathbf{H}]] = \mathbf{K}$), where $\mathbf{k}$ (or $\mathbf{K}$) is the prescribed surface current density per unit deformed surface per unit reference surface. Once again, $\mathbf{n}$ (or $\mathbf{N}$) denotes the normal to the interface in the deformed reference configuration.

Next we describe in some detail the constitutive behavior of the homogeneous magnetoelastic phases in the material. We ignore dissipative and thermal processes by keeping the temperature constant. The constitutive behavior of the magnetoelastic phases is characterized by energy-density functions, or potentials $W^{(r)}$ $(r = 1, ..., N)$, which are taken to be functions of the deformation gradient tensor $\boldsymbol{F}$ and the Lagrangian magnetic induction field $\mathbf{B}$, such that the first Piola-Kirchhoff stress $\boldsymbol{S}$ and the Lagrangian magnetic field $\mathbf{H}$ in phase r are respectively given by

$$\boldsymbol{S} = \frac{\partial W^{(r)}}{\partial \boldsymbol{F}}(\boldsymbol{F}, \mathbf{B}), \quad \text{and} \quad \mathbf{H} = \frac{\partial W^{(r)}}{\partial \mathbf{B}}(\boldsymbol{F}, \mathbf{B}). \tag{2.10}$$

The use of such energy-density functions has been proposed recently by Dorfmann and Ogden (2004), who refer to them as "amended" free-energy functions (see also

Suo et al. (2008)) for the analogous case of deformable dielectrics). It should be noted that the potential $W^{(r)}$ can be related to the more conventional (Kovetz, 2000) specific free-energy density $\Phi^{(r)}$ via

$$W^{(r)}(\boldsymbol{F}, \mathbf{B}) = \rho_0^{(r)} \Phi^{(r)}(\boldsymbol{F}, \mathbf{B}) + \frac{(\boldsymbol{F}\mathbf{B}) \cdot (\boldsymbol{F}\mathbf{B})}{2\mu_0 J}, \tag{2.11}$$

where $\rho_0^{(r)}$ is the material density of phase r in the reference configuration. Furthermore, defining $w^{(r)}(\boldsymbol{F}, \mathbf{b}) = W^{(r)}(\boldsymbol{F}, J\boldsymbol{F}^{-1}\mathbf{b})/J$, we have that

$$w^{(r)}(\boldsymbol{F}, \mathbf{b}) = \rho^{(r)} \phi^{(r)}(\boldsymbol{F}, \mathbf{b}) + \frac{1}{2\mu_0} \mathbf{b} \cdot \mathbf{b}, \tag{2.12}$$

where $\rho^{(r)} = \rho_0^{(r)}/J$ is the material density in the deformed configuration and $\phi^{(r)}(\boldsymbol{F}, \mathbf{b}) = \Phi^{(r)}(\boldsymbol{F}, J\boldsymbol{F}^{-1}\mathbf{b})$ is the specific free-energy density (in Eulerian form). It can then be shown (Kovetz, 2000) that the Cauchy stress $\boldsymbol{T}$ can be written in the form

$$\boldsymbol{T} = \rho^{(r)} \frac{\partial \phi^{(r)}}{\partial \boldsymbol{F}} \boldsymbol{F}^T + (\mathbf{m} \cdot \mathbf{b}) \boldsymbol{I} - \mathbf{m} \otimes \mathbf{b} + \boldsymbol{T}^M, \tag{2.13}$$

where

$$\boldsymbol{T}^M = \frac{1}{\mu_0} \mathbf{b} \otimes \mathbf{b} - \frac{1}{2\mu_0} (\mathbf{b} \cdot \mathbf{b}) \boldsymbol{I} \tag{2.14}$$

is the so-called Maxwell stress. Note that the Maxwell stress is present even when no material is present such as in vacuum, or when the material is magnetically insensitive, in which cases it is known to be self-equilibrated. Also, the Eulerian magnetic field $\mathbf{h}$ can be written in the form

$$\mathbf{h} = \frac{1}{\mu_0} \mathbf{b} - \mathbf{m}, \quad \text{where} \quad \mathbf{m} = -\rho^{(r)} \frac{\partial \phi^{(r)}}{\partial \mathbf{b}} \tag{2.15}$$

is the Eulerian magnetization and μ_0 is the magnetic permeability of vacuum. Alternate, but equivalent forms for the above constitutive equations have been given by earlier authors, including Brown (1966) and Eringen and Maugin (1990), in terms of other choices for the free-energy functions which may be related to the above $\phi^{(r)}$ by means of the Legendre transformation (see Kankanala and Triantafyllidis (2004); Bustamante et al. (2008) for detailed discussions of this point).

In addition, for incompressible materials, the deformation is constrained so that

$$\det \boldsymbol{F} = 1. \tag{2.16}$$

In this case the first Piola-Kirchoff stress is given by

$$\boldsymbol{S} = \frac{\partial W^{(r)}}{\partial \boldsymbol{F}} - p\boldsymbol{F}^{-\mathrm{T}} \tag{2.17}$$

where p is a Lagrange multiplier—the hydrostatic pressure—associated with the incompressibility constraint. In the deformed configuration, the corresponding total Cauchy stress is

$$\boldsymbol{T} = \frac{\partial W^{(r)}}{\partial \boldsymbol{F}}\boldsymbol{F}^{\mathrm{T}} - p\boldsymbol{I} = \rho^{(r)}\frac{\partial \phi^{(r)}}{\partial \boldsymbol{F}}\boldsymbol{F}^{\mathrm{T}} - p\boldsymbol{I} + \frac{1}{\mu_0}\mathbf{b}\otimes\mathbf{b} - \mathbf{m}\otimes\mathbf{b}. \tag{2.18}$$

It should be emphasized that the above constitutive models are fully consistent with thermodynamics (see Kovetz (2000)), but because dissipative and thermal effects are being ignored, the first law will not be needed in this work. On the other hand the stored-energy functions of the phases are required to be *objective* so that $W^{(r)}(\boldsymbol{Q}\boldsymbol{F}, \mathbf{B}) = W^{(r)}(\boldsymbol{F}, \mathbf{B})$ for all proper orthogonal $\boldsymbol{Q}$ and arbitrary deformation gradients $\boldsymbol{F}$ and magnetic induction fields $\mathbf{B}$. In particular, by making use of the polar decomposition $\boldsymbol{F} = \boldsymbol{R}\boldsymbol{U}$, where $\boldsymbol{U}$ is the right stretch tensor and $\boldsymbol{R}$ is the rotation tensor, it follows that $W^{(r)}(\boldsymbol{F}, \mathbf{B}) = W^{(r)}(\boldsymbol{U}, \mathbf{B})$. Alternatively, in terms of the specific free-energy density $\phi^{(r)}$, objectivity requires that $\phi^{(r)}(\boldsymbol{Q}\boldsymbol{F}, \boldsymbol{Q}\mathbf{b}) = \phi^{(r)}(\boldsymbol{F}, \mathbf{b})$, for all proper orthogonal $\boldsymbol{Q}$, which implies (see Kovetz (2000)) that $\phi^{(r)}$ can be written in the form $\phi^{(r)}(\boldsymbol{F}, \mathbf{b}) = \varphi^{(r)}(\boldsymbol{F}^T\boldsymbol{F}, \boldsymbol{F}^T\mathbf{b})$.

Given some assumed convexity in the variable $\mathbf{B}$ of the energy functions of the phases, it is possible to define a partial Legendre-Fenchel transform with respect to $\mathbf{B}$ via

$$U^{(r)}(\boldsymbol{F}, \mathbf{H}) = \inf_{\mathbf{B}} \left\{ W^{(r)}(\boldsymbol{F}, \mathbf{B}) - \mathbf{H}\cdot\mathbf{B} \right\}, \tag{2.19}$$

such that

$$\boldsymbol{S} = \frac{\partial U^{(r)}}{\partial \boldsymbol{F}}(\boldsymbol{F}, \mathbf{H}), \quad \text{and} \quad \mathbf{B} = -\frac{\partial U^{(r)}}{\partial \mathbf{H}}(\boldsymbol{F}, \mathbf{H}). \tag{2.20}$$

Note that the new energy functions $U^{(r)}$ will still be polyconvex in the deformation gradient $\boldsymbol{F}$, but are now concave in the magnetic field $\mathbf{H}$. An analogous definition is

made for the Eulerian form of the energy function $u^{(r)}(\boldsymbol{F}, \mathbf{h})$, which are also concave in $\mathbf{h}$. Several other partial Legendre transforms are possible (Kovetz, 2000; Kankanala and Triantafyllidis, 2004; Bustamante et al., 2008), depending on other variables, such as the magnetization $\mathbf{m}$. However they will not be needed in this work and therefore will not be discussed further.

2.2.2 Energy functions for special magnetic materials

Although the homogenization framework to be developed in the next chapter will be of more general application, in this work we will focus on the special case of rigid, magnetically susceptible particles that are distributed randomly in a hyperelastic, magnetically insensitive elastomer. It is relevant to make the forms of the functions $W^{(r)}$ (and $\phi^{(r)}$) more explicit for these two special types of materials. Recall that the aim of this work is to derive macroscopic forms for the potentials of MREs starting from the constitutive behavior of the constituent phases.

Elastomeric matrix

In this case, the energy-density function (in the reference configuration) $W^{(1)}$ takes the form given by (2.11), where the specific free-energy function is now independent of $\mathbf{B}$. In other words $\rho_0^{(1)}\Phi^{(1)}(\boldsymbol{F}, \mathbf{B}) = W_{me}^{(1)}(\boldsymbol{F})$, so that we can write

$$W^{(1)}(\boldsymbol{F}, \mathbf{B}) = W_{me}^{(1)}(\boldsymbol{F}) + W_{mag}^{(1)}(\boldsymbol{F}, \mathbf{B}), \tag{2.21}$$

where

$$W_{mag}^{(1)}(\boldsymbol{F}, \mathbf{B}) = \frac{(\boldsymbol{F}\mathbf{B}) \cdot (\boldsymbol{F}\mathbf{B})}{2\mu_0 J}, \quad \text{or} \quad w_{mag}^{(1)}(\mathbf{b}) = \frac{W_{mag}^{(1)}(\boldsymbol{F}, J\boldsymbol{F}^{-1}\mathbf{b})}{J} = \frac{\mathbf{b} \cdot \mathbf{b}}{2\mu_0}. \tag{2.22}$$

Note that $w_{mag}^{(1)}$ is independent of $\boldsymbol{F}$, as expected. In expression (2.21), the subscripts *me* and *mag* have been used to emphasize the fact that they correspond to the purely *me*chanical and purely *mag*netic materials in the absence of magnetic and mechanical fields, respectively. In fact for a homogeneous specimen of an elastomer, the corresponding Maxwell stress is self-equilibrated just as it is in vacuum, and the magnetostatic problem becomes fully decoupled from the mechanical problem. However, the presence of magnetic particles affects the magnetic fields in the elastomer for the

problems of interest in this work. The magnetic and mechanical problems become coupled together, as we will see later. In addition to the objectivity condition discussed earlier, the (mechanical) stored-energy functions $W_{me}^{(1)}$ will be assumed (Ball, 1977) to be polyconvex. Note that $W_{mag}^{(1)}$, as given by expression (2.22), is polyconvex (i.e., convex in $\boldsymbol{F}$ and in $\det \boldsymbol{F}$, separately), and so polyconvexity of $W_{me}^{(1)}$ for the elastomeric phase implies polyconvexity of $W^{(1)}$ in $\boldsymbol{F}$ (for fixed $\mathbf{B}$). We also assume that $W_{me}^{(1)}(\boldsymbol{F}) \to \infty$ as $\det \boldsymbol{F} \to 0+$, to ensure the *material impenetrability* condition: $\det \boldsymbol{F}(\mathbf{X}) > 0$ for $\mathbf{X}$ in Ω_0. Note that this condition would be automatically satisfied for incompressible materials, where $\det \boldsymbol{F}$ is required to be identically 1. Examples of $W_{me}^{(1)}$ (in the purely mechanical case) include the standard neo-Hookean and Mooney-Rivlin models, as well as other more realistic models such as the Gent (1996) model. Also note that $W_{mag}^{(1)}$ and $w_{mag}^{(1)}$ (and therefore $W^{(1)}$ and $w^{(1)}$) are convex in $\mathbf{B}$ and $\mathbf{b}$, respectively.

An energy function in the form of equation (2.21) should yield the purely elastic result in the presence of a magnetic field. Extending elasticity theory directly can lead to incorrect results. For example, we get a contribution solely due to the magnetic field if we attempt to follow elasticity and define a material modulus as $\frac{\partial^2 W}{\partial \boldsymbol{F} \partial \boldsymbol{F}}$. However, the measured modulus of rubber does not depend on the magnetic field, so something is amiss. In the next section we will show how the proposed energy function does indeed generate the elastic result.

It is worthwhile to note that the complement of equation (2.21) with respect to $\mathbf{B}$ and $\mathbf{H}$ is

$$U^{(1)}(\boldsymbol{F}, \mathbf{H}) = W_{me}^{(1)}(\boldsymbol{F}) - \frac{\mu_0 J}{2}(\boldsymbol{F}^{-1}\mathbf{H}) \cdot (\boldsymbol{F}^{-1}\mathbf{H}). \tag{2.23}$$

This gives the same expression for the mechanical and magnetic constitutive equation as expression (2.21), and it is easy to compute via a Legendre transform. This would be the appropriate function to use if $\mathbf{H}$ were chosen as the independent variable.

Rigid, magnetizable particles

In this case, perhaps the simplest possible choice for the specific free-energy function (in the reference configuration) would be

$$\rho_0^{(2)}\Phi^{(2)}(\boldsymbol{F}, \mathbf{B}) = W_{me}^{(2)}(\boldsymbol{F}) + \rho_0^{(2)}\Phi_{mag}^{(2)}(\mathbf{B}), \tag{2.24}$$

where the function $W_{me}^{(2)}$ is equal to zero if $\boldsymbol{F}$ is a pure rotation $\boldsymbol{R}^{(2)}$ and infinity otherwise. It serves to enforce the rigidity constraint $\boldsymbol{U} = \boldsymbol{I}$. $\Phi_{mag}^{(2)}$, which can only depend on $\mathbf{B}$ since it cannot depend on $\boldsymbol{R}^{(2)}$ because of objectivity, is assumed to be convex in $\mathbf{B}$. Therefore, we can write the stored-energy function for this material in the form

$$W^{(2)}(\boldsymbol{F}, \mathbf{B}) = W_{me}^{(2)}(\boldsymbol{F}) + W_{mag}^{(2)}(\mathbf{B}), \tag{2.25}$$

where

$$W_{mag}^{(2)}(\mathbf{B}) = \frac{1}{2\mu_0}\mathbf{B}\cdot\mathbf{B} + \rho_0^{(2)}\Phi_{mag}^{(2)}(\mathbf{B}), \tag{2.26}$$

or, in Eulerian form,

$$w_{mag}^{(2)}(\boldsymbol{R}^{(2)}, \mathbf{b}) = W_{mag}^{(2)}({\boldsymbol{R}^{(2)}}^T\mathbf{b}) = \frac{1}{2\mu_0}\mathbf{b}\cdot\mathbf{b} + \rho_0^{(2)}\varphi_{mag}^{(2)}({\boldsymbol{R}^{(2)}}^T\mathbf{b}), \tag{2.27}$$

where we have used the facts that $\boldsymbol{F} = \boldsymbol{R}^{(2)}$ and $\rho^{(2)} = \rho_0^{(2)}$ in the rigid particles, as well as that $\varphi_{mag}^{(2)}({\boldsymbol{R}^{(2)}}^T\mathbf{b}) = \phi_{mag}^{(2)}(\boldsymbol{R}^{(2)}, \mathbf{b}) = \Phi_{mag}^{(2)}({\boldsymbol{R}^{(2)}}^T\mathbf{b})$, because of objectivity. Once again, in expression (2.25) the subscripts *me* and *mag* have been used to highlight the fact that they correspond to the purely mechanical and purely magnetic materials, in the absence of magnetic and mechanical fields, respectively. It should be emphasized, however, that the additive decomposition of the magnetoelastic energy functions $W^{(r)}$ into a mechanical and magnetic components, denoted $W_{me}^{(r)}$ and $W_{mag}^{(r)}$ is not possible in general for magnetoelastic materials. However as we have just seen it is appropriate for both magnetically impermeable, elastic materials, as well as for rigid, magnetizable materials. This property will be exploited in section 3.3 to estimate the macroscopic response of elastomeric materials containing a random distribution of rigid, magnetizable particles.

Rigid, magnetically linear particles

For the special case of linear anisotropic behavior, the function $\Phi_{mag}^{(2)}$ can be taken to be of the form

$$\rho_0^{(2)}\Phi_{mag}^{(2)}(\mathbf{B}) = -\frac{1}{2\mu_0}\mathbf{B}\cdot\boldsymbol{X}^{(2)}\mathbf{B}, \tag{2.28}$$

where $\boldsymbol{X}^{(2)}$ is a constant, second-order tensor defining the anisotropic magnetic susceptibility of the material. It should be noted that the tensor $\boldsymbol{X}^{(2)}$ is fixed in the reference configuration and is therefore independent of the deformation (rotations),

consistent with objectivity. In terms of the Eulerian description, the corresponding free-energy $\varphi^{(2)}_{mag}$ and magnetization $\mathbf{m}$ take the forms

$$\rho^{(2)}\varphi^{(2)}_{mag}(\boldsymbol{R}^{(2)^T}\mathbf{b}) = -\frac{1}{2\mu_0}\mathbf{b}\cdot\boldsymbol{\chi}^{(2)}\mathbf{b}, \quad \text{and} \quad \mathbf{m} = \frac{1}{\mu_0}\boldsymbol{\chi}^{(2)}\mathbf{b}, \tag{2.29}$$

where the tensor $\boldsymbol{\chi}^{(2)} = \boldsymbol{R}^{(2)}\boldsymbol{X}^{(2)}\boldsymbol{R}^{(2)^T}$ now depends on the rotation of the material and again is consistent with the objectivity requirement. Alternatively, the magnetostatic energy $w^{(2)}_{mag}(\boldsymbol{F},\mathbf{b})$, and magnetic field $\mathbf{h}$ are given by

$$w^{(2)}_{mag}(\boldsymbol{R}^{(2)},\mathbf{b}) = \frac{1}{2}\mathbf{b}\cdot\boldsymbol{\mu}^{(2)^{-1}}\mathbf{b}, \quad \text{and} \quad \mathbf{h} = \boldsymbol{\mu}^{(2)^{-1}}\mathbf{b}, \tag{2.30}$$

which provide the standard forms for a linear anisotropic magnet (Jackson, 1975; Kovetz, 2000). $\boldsymbol{\mu}^{(2)} = \mu_0(\boldsymbol{I}-\boldsymbol{\chi}^{(2)})^{-1}$ is the anisotropic magnetic permeability, which depends on the current orientation of the material in phase 2, as determined by $\boldsymbol{\mu}^{(2)} = \boldsymbol{R}^{(2)}\boldsymbol{M}^{(2)}\boldsymbol{R}^{(2)^T}$, where $\boldsymbol{M}^{(2)} = \mu_0(\boldsymbol{I}-\boldsymbol{X}^{(2)})^{-1}$ is the constant magnetic permeability in the reference configuration. It is important to keep in mind that the rigid particles in the elastomer can rotate in the Eulerian formulation of the problem. Consequently $\boldsymbol{\mu}^{(2)}$ generally depends on the deformation unlike $\boldsymbol{M}^{(2)}$. But this dependence disappears for isotropic magnetic behavior, when $\boldsymbol{\mu}^{(2)} = \boldsymbol{M}^{(2)} = \mu^{(2)}\boldsymbol{I}$. It is also important to recall that the magnetic susceptibility $\boldsymbol{\chi}^{(2)}$ is relatively small for both diamagnetic and paramagnetic materials (above the Curie temperature) and therefore for these materials, the magnetic permeability $\boldsymbol{\mu}^{(2)}$ is positive definite. The energy function $W^{(2)}(\boldsymbol{F},\mathbf{B})$ (and $w^{(2)}(\boldsymbol{F},\mathbf{b})$) can be assumed to be convex in $\mathbf{B}$ (and $\mathbf{b}$)).

Rigid, ferromagnetic particles

For sufficiently large, polycrystalline samples of ferromagnetic materials below the Curie temperature, the corresponding energy functions will no longer be quadratic because the magnetization is nonlinear in the magnetic field. In fact, for these materials, the magnetization reaches a saturation state at sufficiently high magnetic fields, beyond which no further increases in the magnetization are possible. On the other hand, if the ferromagnetic material is assumed to be *soft*, so that the hysteresis effects can be neglected, and the particles are assumed to be large compared to the typical magnetic domain size, the material behavior can be idealized as having a single-valued

constitutive response. An example of a constitutive model for characterizing the magnetization behavior of isotropic ferromagnetic particles is the Langevin model, which is defined by

$$\rho^{(2)}\varphi^{(2)}_{mag}(\boldsymbol{R}^{(2)^T}\mathbf{b}) = -\frac{\mu_0 m_s^2}{3\chi^{(2)}}\left[\ln\left(\sinh\left[\frac{3\chi^{(2)}b}{\mu_0 m_s}\right]\right) - \ln\left(\frac{3\chi^{(2)}b}{\mu_0 m_s}\right)\right]. \tag{2.31}$$

In this expression b is the magnitude of $\mathbf{b}$, m_s is the magnetic saturation of the inclusion and $\chi^{(2)}$ is the linearized magnetic susceptibility. Note that the corresponding energy function $w^{(2)}_{mag}$ is still convex in $\mathbf{b}$, and leads to the following expression for the magnetization

$$\mathbf{m} = \frac{m_s}{b}\left[\coth\left(\frac{3\chi^{(2)}b}{\mu_0 m_s}\right) - \frac{\mu_0 m_s}{3\chi^{(2)}b}\right]\mathbf{b}. \tag{2.32}$$

The theory could be applied equally well to other forms for the free-energy $\varphi^{(2)}_{mag}$ of the particles, including threshold-type models for the magnetization. The general theory to be developed in this work will be applied to more specific models in future research.

Rigid particles with permanent magnetization

In many cases the particles may exhibit some amount of permanent magnetization which remains even after the magnetic field is removed. For our purposes this means that the particles exhibit permanent magnetization on the length scale of the particle size. Permanent magnetization of this type can arise in several ways; for sufficiently small particles the magnetization can occur spontaneously when the material is brought below some critical temperature, usually in the presence of an applied magnetic field. On the other hand, the material can be subject to a large applied magnetic field such that when the field is removed some magnetization remains. In either case the permanent magnetization is the result of a magnetic loading cycle where the material exhibits some hysteresis.

The homogenization methods used in this thesis are not general enough to account for hysteresis because the energy and the stress are not uniquely determined by $\boldsymbol{F}$ and $\mathbf{b}$. However, in the case of MREs with rigid particles and a non-susceptible matrix, we can evaluate the stress in the composite provided that the magnetization behavior of the inclusions can be approximated by a linear function for small $\mathbf{b}$. Here

we assume that the magnetization in the inclusion phase can be expressed as

$$\mathbf{m}^{(2)} = \frac{\boldsymbol{\chi}^{(2)}}{\mu_0}\mathbf{b} + \mathbf{m}_0^{(2)} \tag{2.33}$$

where $\mathbf{m}_0^{(2)}$ is the permanent magnetization when $\mathbf{b} = 0$ and $\boldsymbol{\chi}^{(2)}$ is the differential susceptibility in the neighborhood around $\mathbf{b} = 0$. Note that this expression characterizes the magnetic behavior in the current configuration so that both $\boldsymbol{\chi}^{(2)}$ and $\mathbf{m}_0^{(2)}$ depend on the rotation of the inclusion.

When the constitutive relation for the particles is of form (2.33) the energy can be written as

$$w_{mag}^{(2)}(\boldsymbol{F}, \mathbf{b}) = \frac{1}{2\mu_0}\mathbf{b}\cdot\mathbf{b} - \frac{1}{2\mu_0}\mathbf{b}\cdot\boldsymbol{\chi}^{(2)}\mathbf{b} - \mathbf{b}\cdot\mathbf{m}_0^{(2)} + \mathfrak{c}^{(2)}, \tag{2.34}$$

where $\mathfrak{c}^{(2)}$ is a constant with respect to $\mathbf{b}$. The amended free-energy function corresponding to expression (2.34) for the particles is

$$W^{(2)}(\boldsymbol{F}, \mathbf{B}) = W_{\text{rig}}(\boldsymbol{F}) + \frac{1}{2\mu_0}\mathbf{B}\cdot\mathbf{B} - \frac{1}{2\mu_0}\mathbf{B}\cdot\boldsymbol{X}^{(2)}\mathbf{B} - \mathbf{B}\cdot\mathbf{M}_0^{(2)} + \mathfrak{c}^{(2)}. \tag{2.35}$$

In this expression $\mathbf{M}_0^{(2)}$ is a Lagrangian description of the permanent magnetization which is independent of the deformation. It is related to the permanent magnetization in the deformed configuration by $\boldsymbol{R}^{(2)}\mathbf{M}_0^{(2)} = \mathbf{m}_0^{(2)}$ where $\boldsymbol{R}^{(2)}$ is the rotation of the rigid material. Note that the energy functions given by expressions (2.34) and (2.35) are objective.

In the previous expressions note that the $\mathfrak{c}^{(2)}$ term accounts for the energy loss due to hysteresis so we refer to it as a "specific heat". We also argue that $\mathfrak{c}^{(2)}$ does not depend on the deformation because the particles are rigid and objectivity prohibits a dependence on the rotation. Since $\mathfrak{c}^{(2)}$ does not depend on either variable it will not affect the stress or magnetization within the particle or the macroscopic constitutive relation. While the validity of expression (2.33) may be questionable for many materials, it does encompass the case of a pure permanent magnet when $\boldsymbol{\chi}^{(2)} = 0$. The magnetization is independent of the magnetic field in such a case.

Energy function for other deformable magnetic materials

Energy functions for other classes of deformable magnetic materials are interesting but we will not use these functions in this thesis. These functions provide important points of reference when evaluating magnetoelastic energy functions. Energy functions of the form

$$W(\boldsymbol{F}, \mathbf{B}) = W_{me}(\boldsymbol{F}), \quad \text{and} \quad U(\boldsymbol{F}, \mathbf{H}) = \begin{cases} W_{me}(\boldsymbol{F}), & \text{if } \mathbf{H} = 0; \\ -\infty, & \text{otherwise} \end{cases} \tag{2.36}$$

actually correspond to a perfect magnetic material, in that the material can sustain any **b** field with zero **h** field. In other words, it is a material with infinite magnetic susceptibility and no saturation limit. This corresponds to an extreme case, where the amended free energy function does not depend on the **B** field and the **H** field is always zero. While this energy function is only appropriate in a limited sense, it may be a reasonable choice to describe a deformable strong magnet material before the onset of saturation.

Another case to consider is a material where the **B** field is always zero. The energy functions are given below.

$$W(\boldsymbol{F}, \mathbf{B}) = \begin{cases} W_{me}(\boldsymbol{F}), & \text{if } \mathbf{B} = 0; \\ \infty, & \text{otherwise.} \end{cases} \qquad U(\boldsymbol{F}, \mathbf{H}) = W_{me}(\boldsymbol{F}) \tag{2.37}$$

These energy functions correspond to a deformable perfect diamagnet, or a material which will repel all magnetic flux. A perfect diamagnet is a superconductor (Kovetz (2000)), for reasons that are beyond the scope of this document. Once again this energy function would only be valid before the onset of saturation.

It is imperative that any potential magnetoelastic energy function provide reasonable results for both the mechanical and the magnetic constitutive behavior in its proposed range of validity. In specific if the energy function is intended to apply for large magnetic fields, it should exhibit saturation behavior and recover the incremental **h**-**b** relation of vacuum. Accordingly it can also be argued that the magnetoelastic effects should saturate as well.

In summary the above constitutive models for the elastomeric matrix phase and magnetically susceptible, rigid particles have been found to exhibit energies $W^{(r)}$ that

are convex in the variable $\mathbf{B}$, or equivalently, Eulerian energies $w^{(r)}$ that are convex in the variable $\mathbf{b}$. On the other hand the energy functions $W^{(r)}$ of the matrix phase have been found to be polyconvex in the variable $\boldsymbol{F}$ under the assumption that the mechanical response is polyconvex.

The formulation of the magnetoelasticity problem is completed by the specification of appropriate boundary conditions. However, in doing so, it must be kept in mind (Brown, 1966; Kankanala and Triantafyllidis, 2004; Bustamante et al., 2008) that even if the magnetoelastic body is surrounded by vacuum, the vacuum can carry magnetic fields and therefore a (self-equilibrated) stress field this will be discussed in more detail in the next section. For this reason, the "boundary" conditions are best described in terms of the already mentioned "jump" conditions across the boundary between the magnetoelastic material and the surrounding vacuum. As we will see in more detail in Chapter 3, for homogenization purposes, it will be sufficient to specify conditions on the displacement and either the normal component of the magnetic induction field or the tangential component of the magnetic field, depending on which variable is selected as the independent variable.

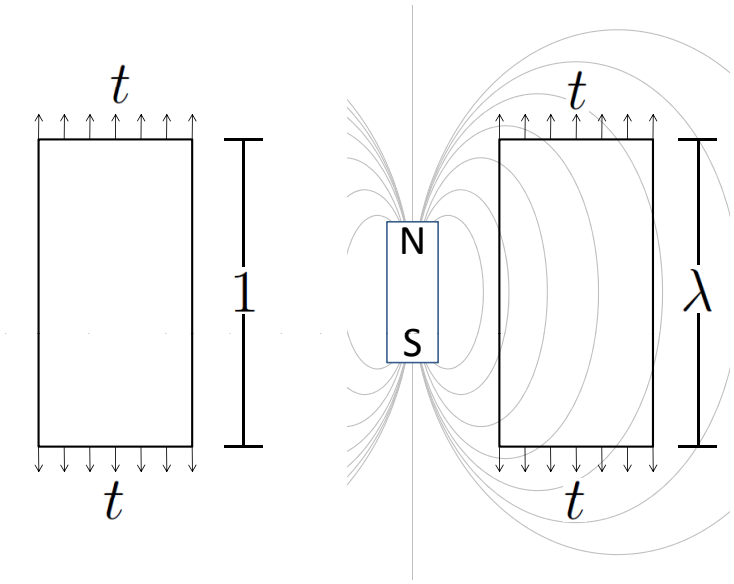

Figure 2.5: During an experiment the magnetic field extends beyond the sample being tested; therefore there is magnetic stress immediately outside the sample. When the material being tested is non-magnetic, the magnetic stress inside cancels exactly the magnetic stress outside the sample. The traction is the same regardless of the magnetic field.

2.3 Measurement of magnetoelastic properties

2.3.1 Accounting for the Maxwell stress in a non-magnetic material

In the previous section we proposed a magnetoelastic energy function for a non-magnetic material. Now it is imperative to describe how this reduces to elasticity even when the material energy function and the stress depend on $\mathbf{b}$. Intuitively we expect that a nonmagnetic material such as rubber should not respond to a magnetic field. We will describe how the theory is consistent with that expectation in this section and explain why the magnetic stress can have no effect on the measured results without the presence of a magnetic material.

Consider an elastic experiment as shown in Figure 2.5. When a mechanical traction is applied to the surface of the material, there is a corresponding displacement of the boundary. The amount of traction is directly related to the stress in the material. Now consider a similar experiment except imagine that we hold a permanent magnet next to the setup, as depicted in Figure 2.5. We expect that when the experiment is

performed, we will observe the same resulting traction displacement relation regardless of the presence of the magnet. However, according to our constitutive relation, there is a stress resulting from the magnetic field which must be taken into account. Notice that the magnetic fields extend past the sample and are unperturbed by the material. Accordingly there is magnetic stress immediately outside the sample. The actual traction measured on the surface is the imbalance between the total stress in the material and the total stress outside the material. For a non-magnetic material the magnetic stress inside the material cancels the magnetic stress outside the material. The traction that is measured is the same as if there were no magnetic field.

It is important to note that this is true even if the magnetic fields are not uniform. The Maxwell stress is such that in a region with no magnetization, it is always divergence-free and its normal component is continuous across any surface. In this way the magnetic stress is completely undetectable by non-magnetic materials.

2.3.2 Applied traction and the total stress

Since there is stress outside the material the relation between the mechanical traction applied on the boundary of the specimen and the total stress within the material must be determined in order to make comparisons with actual experiments. In elasticity the applied traction on the boundary is determined by the appropriate components of the (mechanical) stress tensor inside the material, because the vacuum immediately surrounding the material carries no stress. In magnetoelasticity the magnetic fields extend past the sample being tested and into the vacuum immediately outside the material. This magnetic field generates a Maxwell stress outside the sample, which affects the mechanical traction measured on the outer boundary of the specimen. The magnetic stresses are self-equilibrated and the magnetic fields have no effect on the traction when a non-magnetic material is being tested. However when the material is magnetic, the magnetic stresses are not equilibrated and contribute to the measurable traction on the boundary of the specimen. Based on the jump condition for the total Cauchy stress, $[[\boldsymbol{T}]]\mathbf{n} = 0$, and the magnetic jump conditions, $[[\mathbf{b}]] \cdot \mathbf{n} = 0$ and $[[\mathbf{h}]] \times \mathbf{n} = 0$, the magnetic field and subsequently the magnetic stress outside the material can be determined based on the magnetic fields inside the material. It can be shown (e.g., (Kankanala and Triantafyllidis, 2004)) that the traction on the

boundary of the specimen can be expressed in the form

$$\mathbf{t} = \left[\boldsymbol{T} + \left(\frac{\mu_0}{2}(\mathbf{h}\cdot\mathbf{h})\boldsymbol{I} - \mathbf{h}\otimes\mathbf{b}\right)\right]\mathbf{n} - \frac{\mu_0}{2}\left(\mathbf{m}\cdot\mathbf{n}\right)^2\mathbf{n}, \tag{2.38}$$

where $\boldsymbol{T}$, $\mathbf{h}$, $\mathbf{b}$, and $\mathbf{m}$ are the fields (in the material) just inside the boundary, and $\mathbf{n}$ is the outward normal to the boundary. It should also be emphasized that although this formula is easiest to write in terms of $\boldsymbol{T}, \mathbf{h}, \mathbf{b}$ and $\mathbf{m}$, these are not all independent variables. For instance if we specify $\mathbf{b}$ and $\boldsymbol{F}$, all other variables are determined by the magnetic and mechanical constitutive relations of the material. In addition, note that in the absence of a magnetic field, the above expression reduces to its usual form in the purely mechanical case, $\mathbf{t} = \boldsymbol{T}\mathbf{n}$.

2.3.3 Measurement of material properties

Material properties are evaluated by generating uniform fields within the material. A uniform deformation is accomplished in the purely mechanical context by specifying the position of the boundary as

$$\mathbf{x} = \bar{\boldsymbol{F}}\mathbf{X} \tag{2.39}$$

and an affine traction on the boundary has the form

$$\mathbf{t} = \bar{\boldsymbol{T}}\mathbf{n} \tag{2.40}$$

where $\mathbf{n}$ is the normal to the material surface and $\bar{\boldsymbol{F}}$ and $\bar{\boldsymbol{T}}$ are constant second order tensors. Traction conditions of the form (2.40) have the advantage that the traction components can be directly related components of a second order tensor. In many contexts there is little need to distinguish between the stress and the traction.

In magnetoelasticity $\boldsymbol{T}$, $\mathbf{h}$, $\mathbf{b}$ and $\mathbf{m}$ are all constant within the body if the deformation and magnetic fields are uniform which implies that such an affine traction cannot exist in general. If such an affine traction condition exists we would need to find a $\hat{\boldsymbol{T}}$ such that for all values of $\mathbf{n}$

$$\hat{\boldsymbol{T}}\mathbf{n} = \left[\boldsymbol{T} + \left(\frac{\mu_0\mathbf{h}\cdot\mathbf{h}}{2}\mathbb{I} - \mathbf{h}\otimes\mathbf{b}\right)\right]\mathbf{n} - \frac{\mu_0\left(\mathbf{m}\cdot\mathbf{n}\right)^2}{2}\mathbf{n} \tag{2.41}$$

then we could write $\mathbf{t} = \hat{\boldsymbol{T}}\mathbf{n}$ for the traction. Unfortunately, this is impossible unless $\mathbf{m} = 0$. This can be demonstrated by carefully choosing four different $\mathbf{n}$; this leads

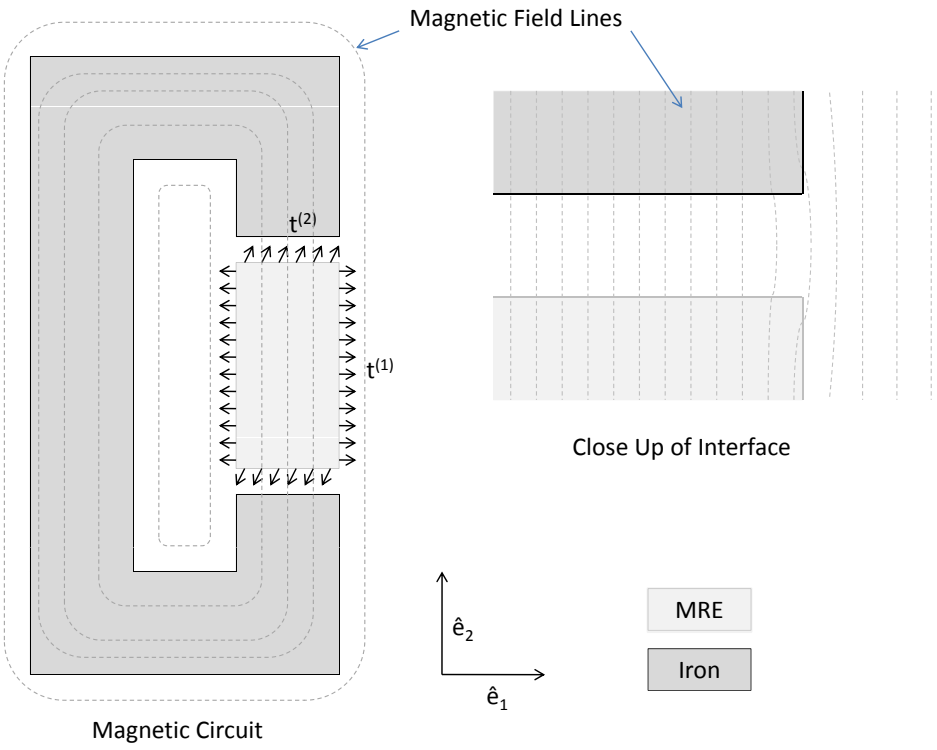

Figure 2.6: The magnetic circuit maintains nearly uniform fields within the sample while uniform traction is applied on the surface. There is a distortion of the magnetic fields near the interface corner. Over the majority of the surface, the fields are uniform.

to inconsistent equations to determine the components of $\hat{\boldsymbol{T}}$. This implies that the traction conditions normally used in elasticity are inconsistent with uniform fields in a magnetoelastic solid surrounded by non-magnetic media as either the traction on the body is not affine or the fields within the material are not uniform. In that case the exact solution would depend on the shape of the sample which implies that the relation is not a material property.

Regardless of this apparent mathematical inconsistency, magnetostriction and magnetoelastic moduli are experimentally measured. We can relate the theory to the practical measurements by carefully considering the experimental setup. Figure 2.6 depicts a typical magnetoelastic experiment. The magnetic circuit, usually made of iron, maintains nearly uniform magnetic fields within the sample. If the space

between the iron and magnetoelastomer is small relative to the size of the sample, the fields immediately outside the sample are uniform over most of the surface. Subsequently, the traction measured on the exposed surfaces is also nearly uniform. This approximation is consistent with experiments which measure magnetoelastic Young's modulus and magnetostriction. This setup avoids the mathematical inconsistency because the sample only has two normal directions. Effectively an affine traction is applied in every actual normal direction.

We call these three values $\mathbf{n}^{(a)}$, where $a = 1, 2, 3$ and consider the three traction vectors $\mathbf{t}^{(a)}$ corresponding to the exposed surfaces. To maintain parity with elasticity we can define $\hat{\boldsymbol{M}}$ and $\hat{\boldsymbol{T}}$ which satisfy the following

$$\frac{\mu_0 \left(\mathbf{m} \cdot \mathbf{n}\right)^2}{2} \mathbf{n} = \hat{\boldsymbol{M}} \mathbf{n} \qquad \forall \mathbf{n} = \mathbf{n}^{(a)}, \tag{2.42}$$

and

$$\mathbf{t}^{(a)} = \hat{\boldsymbol{T}} \mathbf{n} \qquad \forall \mathbf{n} = \mathbf{n}^{(a)}. \tag{2.43}$$

The matrix $\hat{\boldsymbol{T}}$ is a generalized applied traction "tensor" corresponding to an affine applied traction analogous to the purely mechanical. Then

$$\hat{\boldsymbol{T}} = \left[\boldsymbol{T} + \left(\frac{\mu_0 \mathbf{h} \cdot \mathbf{h}}{2} \mathbb{I} - \mathbf{h} \otimes \mathbf{b} \right) \right] - \hat{\boldsymbol{M}} \tag{2.44}$$

for every physical normal direction of the sample. We have gone through considerable effort to keep the equation in this form because this completes the analogy to elasticity. This form also allows us to observe many interesting facts about the applied traction. First notice the potentially non-symmetric $\mathbf{h} \otimes \mathbf{b}$ term. We know that $\boldsymbol{T}$ is always symmetric and $\hat{\boldsymbol{M}}$ can be made symmetric by choosing orthogonal normals. Consequently, there must be some antisymmetric part of $\hat{\boldsymbol{T}}$ for this cuboid to be in static equilibrium. This is reasonable because magnets will experience a net torque aligning them with an external magnetic field. The antisymmetric part of $\hat{\boldsymbol{T}}$ accounts for this torque.

One interesting example where this is important is magnetostriction. Magnetostriction is the effective deformation which solves equation (2.44) when $\hat{\boldsymbol{T}} = 0$. If $\hat{\boldsymbol{T}} = 0$, then $\mathbf{h} \otimes \mathbf{b}$ must be symmetric at equilibrium. This makes sense because if we apply no torque, the magnet will rotate to align its magnetization with the applied field.

2.3.4 Uniaxial tension test, magnetostriction and magnetoelastic moduli

In practice the magnetic uniaxial tension test and magnetostriction are measured along a symmetry axis of the material. This implies that $\mathbf{h}$ and $\mathbf{b}$ are always aligned during a test. This also implies that the applied traction is always normal to the surface and there are three independent equations of static equilibrium from equation (2.44), where $\mathbf{t}_a^{(a)}$ is the normal traction on surface $\mathbf{n}^{(a)}$ (Kankanala and Triantafyllidis, 2008). If $\mathbf{n}^{(1)}$ is aligned with the magnetic fields

$$t_1^{(1)} = T_{11} - \frac{\mathbf{b}\cdot\mathbf{b}}{2\mu_0}, \qquad t_2^{(2)} = T_{22} + \frac{\mu_0\mathbf{h}\cdot\mathbf{h}}{2}, \qquad \text{and} \qquad t_3^{(3)} = T_{33} + \frac{\mu_0\mathbf{h}\cdot\mathbf{h}}{2}. \tag{2.45}$$

These equations define the traction on the surfaces for any value of the deformation and applied magnetic field. Additionally, magnetostriction is determined by finding the deformation which results in no traction.

Since only the applied traction can be measured, effects such as the modulus are with respect to the applied traction as opposed to the total stress. The magnetic field affects the modulus even for a non-magnetic material if the modulus were measured with respect to the total stress. This makes theoretical evaluation of these properties slightly more complicated than the purely mechanical case.

It is also imperative to realize that there are many different magnetoelastic moduli. In thermoelasticity there are isentropic and isothermal moduli, as well as more general thermoelastic moduli. If we consider the stress to be a function of temperature and deformation, we must define the temperature as a function of the deformation to compute a modulus. The temperature is implicitly defined to be constant as a function of deformation in the case of isothermal moduli. Three obvious choices are fixed $\mathbf{h}$, $\mathbf{m}$ and fixed $\mathbf{b}$ moduli. We could also consider fixed $\mathbf{H}$ and fixed $\mathbf{B}$ moduli. In practice the modulus would be specified by the experimenter.

2.4 Concluding remarks

This section has outlined how we deal with coupled magnetoelastic phenomena. In the next section this energy framework is extended to a homogenization framework capable of describing the effective behavior of not only MREs but also general magne-

toelastic composites. This will provide constitutive relations for deformable magnetic materials beyond the rather exceptional examples given here. We will then evaluate these materials for a variety of conditions and microstructures.

Chapter 3

Homogenization-based constitutive models for magnetoelastic composites at finite strain

Although the continuum theories have been helpful in describing the "macroscopic" magneto-mechanical response of MREs, further improvements in the properties of these complex materials will depend crucially on better understanding of the highly coupled and nonlinear structure-property relations for these materials. To aid in this process, we propose a homogenization-based approach to accurately model the macroscopic response of these material systems, and its dependence on the microstructure.

3.1 Homogenization framework for magnetoelastic composites

As done previously, we assume that the magnetoelastic material occupies a domain Ω_0 (in the reference configuration), which is made up of N randomly distributed (homogeneous) phases, occupying sub-domains $\Omega_0^{(r)}$ in Ω_0. The distribution of the phases, or microstructure, for a particular realization of the material can be described by means of characteristic functions $\Theta_0^{(r)}$ $(r = 1, ..., N)$, such that $\Theta_0^{(r)}$ is equal to 1 if the position vector $\mathbf{X}$ is inside phase r (*i.e.*, $\mathbf{X} \in \Omega_0^{(r)}$) and zero otherwise. In this work, we are interested in *composite materials*, which are defined here to be a special class of heterogeneous materials satisfying the *separation of length scales* hypothesis. More precisely, the characteristic functions $\Theta_0^{(r)}$ vary on a length scale, called the microscopic length scale, that is much smaller than the size of the specimen Ω_0, defining the macroscopic length scale. Furthermore, the microstructures are taken to be statistically uniform, so that ergodicity can be used to replace ensemble averages by volume averages over Ω_0. Here we will denote volume averages over $\mathbf{X}$ in the reference configuration (Ω_0) and over $\mathbf{x}$ in the deformed configuration (Ω) by

$$\langle\cdot\rangle_0 = \frac{1}{|\Omega_0|}\int_{\Omega_0}(\cdot)\,dV, \quad \text{and} \quad \langle\cdot\rangle = \frac{1}{|\Omega|}\int_{\Omega}(\cdot)\,dv \tag{3.1}$$

respectively. Under these hypotheses, the probability of finding phase r at point $\mathbf{X}$ is given by its volume fraction $c_0^{(r)} = \left\langle \Theta_0^{(r)} \right\rangle_0$, while the probability of finding phase r at point $\mathbf{X}$ and s at point $\mathbf{X}'$ is given by translation-invariant functions $p_0^{(rs)}(\mathbf{X}' - \mathbf{X}) = \langle \Theta_0^{(r)}(\mathbf{X}' - \mathbf{X}'')\Theta_0^{(s)}(\mathbf{X} - \mathbf{X}'')\rangle_0$ (the integral is over $\mathbf{X}''$), which are assumed to be known.

For later reference, we note that the composite material can also be described in terms of its deformed configuration Ω, where the phases now occupy subdomains $\Omega^{(r)}$. The distribution of the phases in the deformed configuration can be described in terms of characteristic functions $\Theta^{(r)}$ $(r = 1, ..., N)$, such that $\Theta^{(r)}$ is equal to 1 if the position vector (in the deformed configuration) $\mathbf{x}$ is inside phase r (*i.e.*, $\mathbf{X} \in \Omega^{(r)}$) and zero otherwise. In terms of these deformed characteristic functions, we can define analogously volume fractions and two-point probability functions via $c^{(r)} = \langle \Theta^{(r)} \rangle$, and $p^{(rs)}(\mathbf{x}' - \mathbf{x}) = \langle \Theta^{(r)}(\mathbf{x}' - \mathbf{x}'')\Theta^{(s)}(\mathbf{x} - \mathbf{x}'') \rangle$, respectively.

Since the initial density, $\rho_0^{(r)}$, and the constitutive properties, as determined by $W^{(r)}$, of phase r are assumed to be uniform (i.e., independent of $\mathbf{X}$), it is useful to introduce the notations

$$\rho_0(\mathbf{X}) = \sum_{s=1}^{N} \Theta_0^{(s)}(\mathbf{X})\ \rho_0^{(s)}, \quad \text{and} \quad W(\mathbf{X}, \boldsymbol{F}, \mathbf{B}) = \sum_{s=1}^{N} \Theta_0^{(s)}(\mathbf{X})\ W^{(s)}(\boldsymbol{F}, \mathbf{B}), \tag{3.2}$$

to describe the position dependence of the density and energy functions within Ω_0. Thus, ρ_0 and W vary on the microscopic length scale. On the other hand, the prescribed mechanical and magnetic forcing functions, including the body force $\mathbf{f}_0$, and the surface and body current densities, $\mathbf{K}$ and $\mathbf{J}$, are assumed to vary on the macroscopic length scale. Finally, if the boundary conditions are also assumed to vary on the macroscopic length scale, it is expected on physical grounds that it may be possible to replace the heterogeneous material by an equivalent homogeneous material with some effective, or homogenized, energy function $\tilde{W}$. (Note that, because dynamical effects are being ignored, we anticipate that the effective density $\tilde{\rho}_0$ should be the average of the densities of the phases, i.e., $\tilde{\rho}_0 = \langle \rho_0 \rangle_0$.) Homogenization is concerned with the formalization of this averaging process, and with the computation of the effective properties of the composite.

In this section, we develop a homogenization framework for magnetoelasticity in the finite strain and quasi-static contexts, generalizing the heuristic approach of Hill (1972) in finite elasticity. The basic idea is to prescribe boundary conditions that are consistent with "macroscopically uniform" fields in the composite. Although, there are several different possible choices of conditions leading to macroscopically uniform fields in the composite, here we prescribe the following conditions:

$$\mathbf{x} = \bar{\boldsymbol{F}}\mathbf{X}, \quad \text{and} \quad \mathbf{B} \cdot \mathbf{N} = \overline{\mathbf{B}} \cdot \mathbf{N}, \quad \text{on} \quad \partial\Omega_0, \tag{3.3}$$

where $\bar{\boldsymbol{F}}$ and $\overline{\mathbf{B}}$ are a prescribed constant tensor and vector, and $\mathbf{N}$ is the outward unit normal to the boundary of the composite $\partial\Omega_0$. Given these boundary conditions, it follows from the divergence theorem that the "macroscopic averages" (over Ω_0) for the deformation gradient and magnetic induction fields are given by

$$\langle \boldsymbol{F} \rangle_0 = \bar{\boldsymbol{F}}, \quad \text{and} \quad \langle \mathbf{B} \rangle_0 = \overline{\mathbf{B}}, \tag{3.4}$$

so that $\bar{\boldsymbol{F}}$ and $\overline{\mathbf{B}}$ can be interpreted as the macroscopic, or average deformation gradient and magnetic induction field in the composite Ω_0. It should be noted that it is also possible to prescribe uniform conditions on the magnetic field, or the traction on the boundary of the specimen, although the latter may be more difficult to achieve experimentally, due to the coupling of the mechanical tractions with the Maxwell stress in the vacuum surrounding the specimen. As we will see below, however, the boundary conditions (3.3) have the additional advantage that they lead to minimum-type (as opposed to min-max) variational formulations for the homogenization problem.

Thus, following an analogous analysis by Hill (1972) for purely elastic composites, we define the homogenized energy function for the magnetoelastic composite as the volume average of the magnetoelastic energy that is stored in the composite under the above-prescribed boundary conditions. (We ignore the prescribed forcing functions $\mathbf{f}_0$, $\mathbf{J}$, and $\mathbf{K}$, since they vary on the macroscopic length scale and are not expected to affect the homogenization problem.) In this case, we define the homogenized energy potential as a function of the applied macroscopic deformation gradient $\bar{\boldsymbol{F}}$ and magnetic induction $\overline{\mathbf{B}}$ fields via

$$\widetilde{W}(\bar{\boldsymbol{F}}, \overline{\mathbf{B}}) = \inf_{\mathbf{F} \in \mathcal{K}(\bar{\mathbf{F}})} \inf_{\mathbf{B} \in \mathcal{B}_0(\overline{\mathbf{B}})} \langle W(\mathbf{X}, \boldsymbol{F}, \mathbf{B}) \rangle_0, \tag{3.5}$$

where

$$\mathcal{K}(\bar{\boldsymbol{F}}) = \{ \boldsymbol{F} \mid \exists\ \mathbf{x} = \mathbf{x}(\mathbf{X}) \text{ with } \boldsymbol{F} = \operatorname{Grad} \mathbf{x} \text{ in } \Omega_0,\ \mathbf{x} = \bar{\boldsymbol{F}}\mathbf{X} \text{ on } \partial\Omega_0 \}, \tag{3.6}$$

and

$$\mathcal{B}_0(\overline{\mathbf{B}}) = \{ \mathbf{B} \mid \operatorname{Div} \mathbf{B} = \mathbf{0} \text{ in } \Omega_0,\ \mathbf{B} \cdot \mathbf{N} = \overline{\mathbf{B}} \cdot \mathbf{N} \text{ on } \partial\Omega_0 \}. \tag{3.7}$$

It is easily verified by computing the first variation of the functional in (3.5), and

integrating by parts in the usual fashion, that

$$\frac{1}{|\Omega_0|}\int_{\Omega_0}\frac{\partial}{\partial X_j}(\frac{\partial W}{\partial F_{ij}})\,\delta u_i\,dV+\frac{1}{|\Omega_0|}\int_{\Omega_0}e_{ijk}\frac{\partial}{\partial X_j}(\frac{\partial W}{\partial B_k})\,\delta A_i\,dV=0, \tag{3.8}$$

where e_{ijk} is the permutating symbol and $\mathbf{A}$ is the magnetic potential, such that $\mathbf{B}=\operatorname{Curl}\mathbf{A}$. It then follows by making use of the constitutive relations (2.10) that the Euler-Lagrange equations are given by the equilibrium equations $(2.7)_2$ (with $\mathbf{f}_0=0$), and the magnetostatic equations $(2.9)_1$ (with $\mathbf{J}=0$), so that the minimizers in expression (3.5) (assuming that they exist) are solutions of the magnetoelastic problem with boundary conditions (3.3). Although we are not aware of mathematically rigorous results for the above magnetoelastic variational problem, it is known (Ball, 1977) that the constitutive hypothesis of polyconvexity (together with appropriate growth conditions) in $\boldsymbol{F}$ is sufficient to ensure the existence of minimizers in the purely mechanical counterpart of problem (3.5). Similarly, convexity (and appropriate growth conditions) with respect to the variable $\mathbf{B}$ is sufficient to ensure the existence of minimizers in the purely magnetostatic problem. Building on these facts, Kankanala and Triantafyllidis (2004) have proposed recently a generalization of quasiconvexity for magnetoelastic materials. On the other hand, DeSimone and James (2002) have proposed other conditions that are especially well suited for magnetostrictive materials at microscopic length scales. Thus, it would seem reasonable that minimizers of the above-defined magnetoelastic problem should exist for the materials models described in the previous section for the matrix and inclusion phases of the MREs, at least for sufficiently small applied magnetic and mechanical fields. The determination of precise mathematical conditions ensuring the existence of minimizers in expression (3.5) is beyond the scope of this work, and it will simply be assumed here that such minimizers exist, at least for sufficiently small field intensities.

It is also relevant to emphasize in the context of expression (3.5) that $\widetilde{W}(\bar{\boldsymbol{F}},\overline{\mathbf{B}})$ corresponds to the magnetoelastic energy that is stored in the composite under the action of the applied fields $\bar{\boldsymbol{F}}$ and $\overline{\mathbf{B}}$, as determined by boundary conditions (3.3). In general, energy will also be stored through the magnetic fields in the surrounding vacuum. However, as shown next, only the energy stored inside the composite is relevant for the homogenization problem. Indeed, it can be shown in the usual way by means of Hill's (div-curl) lemma (see, for example, Ponte Castañeda and Suquet (1998) that the *average stress* and *average magnetic* fields, as determined by $\bar{\boldsymbol{S}}=\langle\boldsymbol{S}\rangle_0$

and $\overline{\mathbf{H}} = \langle \mathbf{H} \rangle_0$, are respectively given in terms of $\widetilde{W}$ by the relations

$$\bar{\boldsymbol{S}} = \frac{\partial \widetilde{W}}{\partial \bar{\boldsymbol{F}}}, \quad \text{and} \quad \overline{\mathbf{H}} = \frac{\partial \widetilde{W}}{\partial \overline{\mathbf{B}}}. \tag{3.9}$$

As it is known from expressions (3.4) that $\bar{\boldsymbol{F}}$ and $\overline{\mathbf{B}}$ correspond to the average deformation gradient and magnetic induction fields, it follows that expressions (3.9) provide the macroscopic, or homogenized constitutive relations for the composite, and therefore the effective energy function $\widetilde{W}$, as defined by (3.5), completely describes the macroscopic response of the magnetoelastic composite, in the same sense as the local energy functions $W^{(r)}$ characterize the response of the constituent phases. Moreover, it follows from the objectivity of $W^{(r)}$ and the definition (3.5) that $\widetilde{W}$ is objective, namely, $\widetilde{W}(\bar{\boldsymbol{F}}, \overline{\mathbf{B}}) = \widetilde{W}(\bar{\boldsymbol{U}}, \overline{\mathbf{B}})$, where $\bar{\boldsymbol{U}}$ represents the macroscopic right-stretch tensor associated with the macroscopic polar decomposition $\bar{\boldsymbol{F}} = \bar{\boldsymbol{R}}\, \bar{\boldsymbol{U}}$. It should also be noted that the above-described variational homogenization framework reduces naturally to the corresponding framework of Talbot and Willis (1985) for nonlinear dielectrics, when the appropriate conversions are made between the magnetic and electrical cases.

For later use, we define next an effective specific free-energy function $\widetilde{\Phi}$, such that

$$\widetilde{W}(\bar{\boldsymbol{F}}, \overline{\mathbf{B}}) = \bar{\rho}_0 \widetilde{\Phi}(\bar{\boldsymbol{F}}, \overline{\mathbf{B}}) + \frac{(\bar{\boldsymbol{F}}\, \overline{\mathbf{B}}) \cdot (\bar{\boldsymbol{F}}\, \overline{\mathbf{B}})}{2\mu_0 \bar{J}}, \tag{3.10}$$

where $\bar{\rho}_0 = \langle \rho_0 \rangle_0$ is the average material density of the composite in the reference configuration. Then, we can write the macroscopic stress and magnetic fields in the forms

$$\bar{\boldsymbol{S}} = \bar{\rho}_0 \frac{\partial \tilde{\Phi}}{\partial \bar{\boldsymbol{F}}} + \bar{\boldsymbol{S}}^M, \quad \text{and} \quad \overline{\mathbf{H}} = \bar{\rho}_0 \frac{\partial \widetilde{\Phi}}{\partial \overline{\mathbf{B}}} + \frac{1}{\mu_0 \bar{J}} \left(\bar{\boldsymbol{F}}^T \bar{\boldsymbol{F}} \right) \overline{\mathbf{B}} \tag{3.11}$$

where

$$\bar{\boldsymbol{S}}^M = \frac{1}{\mu_0 \bar{J}} \bar{\boldsymbol{F}}\, \overline{\mathbf{B}} \otimes \overline{\mathbf{B}} - \frac{1}{2\mu_0 \bar{J}} \left[\overline{\mathbf{B}} \cdot \left(\bar{\boldsymbol{F}}^T \bar{\boldsymbol{F}} \right) \overline{\mathbf{B}} \right] \bar{\boldsymbol{F}}^{-T} \tag{3.12}$$

is the Lagrangian form of the Maxwell stress, and where $\bar{J} = \det \bar{\boldsymbol{F}}$. Note that the Maxwell stress satisfies the rotational equilibrium condition $\bar{\boldsymbol{S}}^M\, \bar{\boldsymbol{F}}^T = \bar{\boldsymbol{F}}\, \bar{\boldsymbol{S}}^{M^T}$, and it follows from the objectivity of $\widetilde{\Phi}$ that the macroscopic stress also satisfies the macroscopic rotational balance relation $\bar{\boldsymbol{S}}\, \bar{\boldsymbol{F}}^T = \bar{\boldsymbol{F}}\, \bar{\boldsymbol{S}}^T$, just as in the purely elastic case (Hill, 1972).

It is also of interest to write the constitutive relations for the magnetoelastic composite in a form analogous to relation (2.13) in terms of the volume averages (over the deformed configuration Ω of the composite) of the true (or Eulerian) fields, $\bar{\boldsymbol{T}} = \langle \boldsymbol{T} \rangle$, $\bar{\mathbf{b}} = \langle \mathbf{b} \rangle$ and $\bar{\mathbf{h}} = \langle \mathbf{h} \rangle$. This first requires observing that

$$\bar{\boldsymbol{T}} = \bar{J}^{-1} \bar{\boldsymbol{S}} \, \bar{\boldsymbol{F}}^T, \quad \bar{\mathbf{h}} = \bar{\boldsymbol{F}}^{-T} \overline{\mathbf{H}}, \quad \text{and} \quad \bar{\mathbf{b}} = \bar{J}^{-1} \bar{\boldsymbol{F}} \, \overline{\mathbf{B}}, \tag{3.13}$$

which follow by use of the Hill's lemma (in the context of the second expression, it is useful to recall that Div $\left(J\boldsymbol{F}^{-T}\right) = \mathbf{0}$). A detailed derivation of these expressions is given in Appendix A. Then, it can be shown (see Kankanala and Triantafyllidis (2004); Bustamante et al. (2008); Vu and Steinmann (2007) for similar developments) that the effective energy density (per unit volume in the deformed configuration Ω), defined by $\tilde{w}(\bar{\boldsymbol{F}}, \overline{\mathbf{b}}) = \widetilde{W}(\bar{\boldsymbol{F}}, \overline{\mathbf{B}})/\bar{J}$, is alternatively determined by the variational statement

$$\widetilde{w}(\bar{\boldsymbol{F}}, \overline{\mathbf{b}}) = \inf_{\mathbf{F} \in \mathcal{K}(\overline{\mathbf{F}})} \inf_{\mathbf{b} \in \mathcal{B}(\overline{\mathbf{b}})} \langle w(\mathbf{x}, \boldsymbol{F}, \mathbf{b}) \rangle, \tag{3.14}$$

where $w(\mathbf{x}, \boldsymbol{F}, \mathbf{b}) = \sum_{r=1}^{N} \Theta^{(r)}(\mathbf{x}) \; w^{(r)}(\boldsymbol{F}, \mathbf{b})$, $\mathcal{K}(\bar{\boldsymbol{F}})$ is still given by (3.6) and

$$\mathcal{B}(\overline{\mathbf{b}}) = \{ \mathbf{b} \mid \operatorname{div} \mathbf{b} = \mathbf{0} \text{ in } \Omega, \; \mathbf{b} \cdot \mathbf{n} = \overline{\mathbf{b}} \cdot \mathbf{n} \text{ on } \partial\Omega \}. \tag{3.15}$$

It should be noted that this hybrid expression involves both the Lagrangian field $\boldsymbol{F}$ and the Eulerian field $\mathbf{b}$, and should be interpreted as a problem in the deformed configuration for the magnetic induction field $\mathbf{b}$, but the problem for the deformation $\boldsymbol{F}$ should still be referred to the reference configuration. In addition, we can define an effective specific free-energy function $\tilde{\phi}(\bar{\boldsymbol{F}}, \overline{\mathbf{b}}) = \widetilde{\Phi}(\bar{\boldsymbol{F}}, \bar{J} \, \bar{\boldsymbol{F}}^{-1} \overline{\mathbf{b}}) = \widetilde{\Phi}(\bar{\boldsymbol{F}}, \overline{\mathbf{B}})$, such that

$$\tilde{w}(\bar{\boldsymbol{F}}, \overline{\mathbf{b}}) = \bar{\rho} \, \tilde{\phi}(\bar{\boldsymbol{F}}, \overline{\mathbf{b}}) + \frac{1}{2\mu_0} \overline{\mathbf{b}} \cdot \overline{\mathbf{b}}, \tag{3.16}$$

where $\bar{\rho} = \langle \rho \rangle = \bar{\rho}_0 / \bar{J}$ is the average material density in the deformed configuration. It then follows that the (above-defined) average Cauchy stress $\bar{\boldsymbol{T}}$ and (Eulerian) magnetization $\bar{\mathbf{m}}$ (defined by $\bar{\mathbf{m}} = (1/\mu_0)\bar{\mathbf{b}} - \bar{\mathbf{h}}$) can be written in the forms

$$\bar{\boldsymbol{T}} = \bar{\boldsymbol{T}}^M + (\bar{\mathbf{m}} \cdot \bar{\mathbf{b}}) \boldsymbol{I} - \bar{\mathbf{m}} \otimes \bar{\mathbf{b}} + \bar{\rho} \, \frac{\partial \tilde{\phi}}{\partial \bar{\boldsymbol{F}}} \bar{\boldsymbol{F}}^T, \quad \text{and} \quad \bar{\mathbf{m}} = -\bar{\rho} \frac{\partial \tilde{\phi}}{\partial \bar{\mathbf{b}}}, \tag{3.17}$$

where

$$\bar{\boldsymbol{T}}^M = \frac{1}{\mu_0}\bar{\mathbf{b}} \otimes \bar{\mathbf{b}} - \frac{1}{2\mu_0}(\bar{\mathbf{b}} \cdot \bar{\mathbf{b}})\boldsymbol{I} \tag{3.18}$$

is the (true) Maxwell stress in the composite.

As with the local potentials, the objectivity of $\widetilde{W}$ implies that $\tilde{\phi}$ can be written in the form $\tilde{\phi}(\bar{\boldsymbol{F}}, \bar{\mathbf{b}}) = \tilde{\varphi}(\bar{\boldsymbol{C}}, \widehat{\mathbf{b}})$, with $\bar{\boldsymbol{C}} = \bar{\boldsymbol{F}}^T\bar{\boldsymbol{F}}$ and $\widehat{\mathbf{b}} = \bar{\boldsymbol{F}}^T\bar{\mathbf{b}}$, from which it follows that the average Cauchy stress and magnetization can also be written as

$$\bar{\boldsymbol{T}} = \bar{\boldsymbol{T}}^M + (\bar{\mathbf{m}} \cdot \bar{\mathbf{b}})\boldsymbol{I} - \bar{\mathbf{m}} \otimes \bar{\mathbf{b}} - \bar{\mathbf{b}} \otimes \bar{\mathbf{m}} + 2\bar{\rho}\,\bar{\boldsymbol{F}}\,\frac{\partial \tilde{\varphi}}{\partial \bar{\boldsymbol{C}}}\,\bar{\boldsymbol{F}}^T, \quad \text{and} \quad \bar{\mathbf{m}} = -\bar{\rho}\,\bar{\boldsymbol{F}}\,\frac{\partial \tilde{\varphi}}{\partial \widehat{\mathbf{b}}}. \tag{3.19}$$

Note that it is evident from the first of these relations that $\bar{\boldsymbol{T}}$ is symmetric, a condition which, in turn, is also consistent with the macroscopic rotational balance relation $\bar{\boldsymbol{S}}\,\bar{\boldsymbol{F}}^T = \bar{\boldsymbol{F}}\,\bar{\boldsymbol{S}}^T$ discussed above.

For completeness, it should be noted that it is sometimes more convenient to prescribe the magnetic field $\overline{\mathbf{H}}$ instead of the magnetic induction field $\overline{\mathbf{B}}$. The above-described formulation can be easily adapted to handle this situation by taking advantage of the Legendre transformation (2.19) introduced in connection with the dual energy functions $U^{(r)}$. Briefly, we replace the boundary conditions (3.3) by

$$\mathbf{x} = \bar{\boldsymbol{F}}\mathbf{X}, \quad \text{and} \quad \mathbf{H} \times \mathbf{N} = \overline{\mathbf{H}} \times \mathbf{N}, \quad \text{on} \quad \partial\Omega_0, \tag{3.20}$$

so that $\langle \boldsymbol{F} \rangle_0 = \bar{\boldsymbol{F}}$ still, but now $\langle \mathbf{H} \rangle_0 = \overline{\mathbf{H}}$. Then, it can be shown that the average stress $\bar{\boldsymbol{S}} = \langle \boldsymbol{S} \rangle_0$ and average magnetic induction $\overline{\mathbf{B}} = \langle \mathbf{B} \rangle_0$ are determined via

$$\bar{\boldsymbol{S}} = \frac{\partial \widetilde{U}}{\partial \bar{\boldsymbol{F}}} \quad \text{and} \quad \overline{\mathbf{B}} = -\frac{\partial \widetilde{U}}{\partial \overline{\mathbf{H}}} \tag{3.21}$$

in terms of the effective dual potential

$$\widetilde{U}(\bar{\boldsymbol{F}}, \overline{\mathbf{H}}) = \inf_{\mathbf{F} \in \mathcal{K}(\overline{\mathbf{F}})} \sup_{\mathbf{H} \in \mathcal{H}_0(\overline{\mathbf{H}})} \langle U(\mathbf{X}, \boldsymbol{F}, \mathbf{H}) \rangle_0, \tag{3.22}$$

where $\mathcal{K}(\overline{\mathbf{F}})$ is as given by (3.6), and

$$\mathcal{H}_0(\overline{\mathbf{H}}) = \{\mathbf{H} \mid \operatorname{Curl} \mathbf{H} = \mathbf{0} \text{ in } \Omega_0,\ \mathbf{H} \times \mathbf{N} = \overline{\mathbf{H}} \times \mathbf{N} \text{ on } \partial\Omega_0\}. \tag{3.23}$$

It should be noted that the effective potential $\widetilde{U}$ is related to the effective potential

$\widetilde{W}$ by the same Legendre-Fenchel transformation (2.19) as the corresponding local potentials $U^{(r)}$ and $W^{(r)}$, namely

$$\widetilde{U}(\bar{\boldsymbol{F}}, \overline{\mathbf{H}}) = \inf_{\overline{\mathbf{B}}} \left\{ \widetilde{W}(\bar{\boldsymbol{F}}, \overline{\mathbf{B}}) - \overline{\mathbf{H}} \cdot \overline{\mathbf{B}} \right\}. \tag{3.24}$$

Unfortunately, the variational formulation for the effective energy function $\widetilde{U}$ of the magnetoelastic composite does not involve a minimum principle, but a min-max principle, which is less useful for the purpose of generating bounds on $\widetilde{U}$, and therefore on $\widetilde{W}$.

3.2 Magnetoelastic instabilities and loss of ellipticity

As already stated, to the best of our knowledge, mathematically rigorous results are not yet available in the context of magnetoelastic homogenization. However mathematically precise definitions of the effective energy $\widetilde{W}$ for purely elastic composites with *periodic* microstructures have been given by Braides (1985) and Müller (1987). Such definitions generalize the classical definition of the effective energy for periodic media with convex energies (Marcellini, 1978) by accounting for the fact that, in the non-convex case, it is not sufficient to consider one-cell periodic solutions, as solutions involving interactions between several unit cells may lead to lower overall energies. Physically, this corresponds to the possible development of "microscopic" instabilities in the composite at sufficiently high deformation. In this connection it is important to remark that Geymonat et al. (1993), following earlier work by Triantafyllidis and Maker (1985) for laminated materials, have shown rigorously that the loss of strong ellipticity in the homogenized behavior of the composite corresponds to the development of long-wavelength (*i.e.,* "macroscopic") instabilities in the form of localized shear bands. Furthermore, the "failure surfaces" defined by the loss of strong ellipticity condition of this homogenized behavior provide, in some loose sense, upper bounds for the onset of other types of instabilities (Michel et al., 2007).

Because of the difficulties associated with the computation of the microscopic instabilities mentioned in the previous paragraph, especially for composites with random microstructures, a more pragmatic approach will be followed here. We assume

that the materials of interest have a stress-free configuration at $\boldsymbol{F} = \boldsymbol{I}$ and $\mathbf{B} = \mathbf{0}$ and that their mechanical behavior is characterized by the standard theory of linear elasticity for small enough deformations and magnetic fields. It follows that, at least in a neighborhood of $\boldsymbol{F} = \boldsymbol{I}$ and $\mathbf{B} = \mathbf{0}$, the solution of the Euler-Lagrange equations associated with the variational problem (3.5) is unique and gives the minimum energy. The composite material may reach a point at which this "principal" solution bifurcates into lower-energy solutions as the deformation progresses into the nonlinear deformation range. This point corresponds to the onset of a *microscopic* instability beyond which the applicability of the "principal" solution becomes questionable. However, it is still possible to extract useful information from the principal solution by computing the associated *macroscopic* instabilities from the loss of strong ellipticity of the homogenized behavior. In any case, the computation of such macro-instabilities for magnetoelastic composites requires the development of specific constitutive models for these materials such as the ones developed in this thesis.

As previously discussed there are some important differences between the purely mechanical case and the magnetoelastic case when considering the traction and the total stress. In the context of instabilities one must carefully account for the magnetic field outside the sample to determine the stability of the applied traction such as the approach followed by Bertoldi and Gei (2011). The fields outside the material are also important in the work of Ottenio et al. (2008) (and Dorfmann and Ogden (2010) in the electrostatic context) who described the necessary incremental constitutive equations and governing equations to consider the problem of surface instability in a magnetoelastic half-space. However loss of ellipticity is a material instability which can be related to the incremental behavior of the homogenized energy function without consideration of the fields outside the material.

Loss of ellipticity in finite-strain magnetoelasticity has only recently been studied in any detail; however a number of recent papers have addressed this issue. Kankanala and Triantafyllidis (2004) and Danas et al. (2012) discussed constitutive models for MREs while using the magnetization as the free variable and they give an expression for quasi-convexity with respect to those energy functions. This formulation can be related to the energy functions in this thesis by the appropriate Legendre transforms. Destrade and Ogden (2011) considered magneto-acoustic waves and provide a generalization of the strong ellipticity condition for incompressible magnetoelastic materials using the magnetic flux as the free variable. In the mathematically analogous elec-

troactive context, Rudykh and deBotton (2011) explored macroscopic instabilities in layered microstructures subjected to varying electromechanical loadings specializing the work of Destrade and Ogden (2011) to plane strain. Additionally, Bertoldi and Gei (2011) considered layered materials aligned with a pre-stretch direction and electric field normal to the layers and investigated microscopic instabilities and loss of ellipticity for that loading, extending the work of Triantafyllidis and Maker (1985).

In Chapter 4 a constitutive model is developed which characterizes the behavior of MREs. In the purely mechanical context this energy function may lose ellipticity and indeed the application of the magnetic field can affect the loss of ellipticity. Here we follow the work of Destrade and Ogden (2011), Bertoldi and Gei (2011), and Rudykh and deBotton (2011) who relate the formation of instabilities to the incremental magnetoelastic moduli tensors given by

$$\mathcal{L}^0_{ijkl} = \frac{\partial^2 W}{\partial F_{ij} \partial F_{kl}}, \quad \mathcal{M}^0_{ijk} = \frac{\partial^2 W}{\partial F_{ij} \partial B_k}, \quad \text{and} \quad \mathcal{B}^0_{ik} = \frac{\partial^2 W}{\partial B_i \partial B_k} \tag{3.25}$$

and W is the magnetoelastic energy function of a homogenous material. In our case it is the homogenized energy function for the MRE composite. In many contexts it is simpler to consider loss of ellipticity with respect to the current configuration (Bertoldi and Gei, 2011; Rudykh and deBotton, 2011) with the moduli given by

$$\mathcal{L}_{ijkl} = J^{-1} F_{ja} F_{lb} \mathcal{L}^0_{iakb} \quad \mathcal{M}_{ijk} = F_{ja} F^{-1}_{bk} \mathcal{M}^0_{iab}, \quad \text{and} \quad \mathcal{B}_{ik} = J F^{-1}_{ai} F^{-1}_{bk} \mathcal{B}^0_{ab}. \tag{3.26}$$

The previously mentioned authors relate these incremental moduli to the incremental equilibrium equations and derive the appropriate condition for loss of ellipticity. Following their procedure leads to expressions of the type used to compute loss of ellipticity in Chapter 4 for the two-dimensional case.

3.3 Homogenization estimates for MREs

In the previous section, we have determined that the homogenized magnetoelastic response of a composite is characterized by the homogenized energy-density function $\widetilde{W}$, as given by expression (3.5). Unfortunately, given the intrinsic nonlinearities of the problem, the exact solution of the variational problem defined by (3.5) is intractable in general. One possible way to make progress would be to take advantage

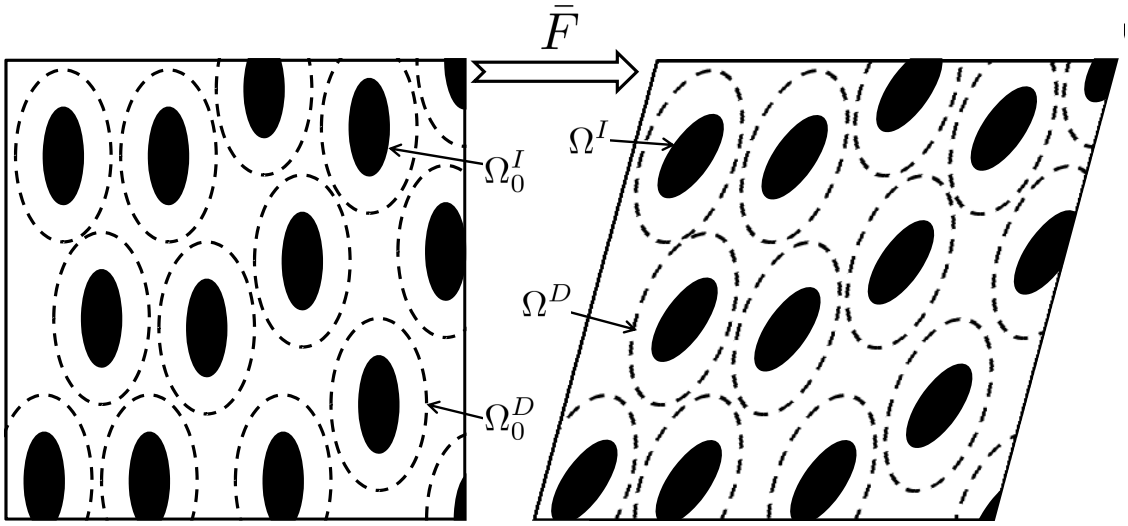

Figure 3.1: Schematic of the microstructure for the MRE showing the ellipsoidal particles (in black) and their ellipsoidal distribution (in dashed lines) in the undeformed and deformed configurations.

of an approximate method, such as the "linear comparison" variational methods that have been used with considerable success for the purely mechanical problem (Ponte Castañeda and Tiberio, 2000; Lopez-Pamies and Ponte Castañeda, 2006a,b). In this work, however, we will exploit the special properties of MREs to obtain more explicit estimates for these materials than would be possible by direct implementation of the linear comparison methods.

3.3.1 Initial microstructure

In Figure 3.1, we depict a specimen of the materials of interest consisting of randomly distributed, rigid, magnetic particles in an elastomeric matrix capable of finite strains. For simplicity, the ellipsoidal and magnetically anisotropic particles are assumed to be perfectly aligned (both magnetically and geometrically), and are distributed with "ellipsoidal symmetry" (Ponte Castañeda & Willis, 1995) in the reference configuration. More explicitly, we let the inclusions be described by an ellipsoid

$$\Omega_0^I = \left\{ \mathbf{X} \mid \mathbf{X} \cdot \left(\boldsymbol{Z}_0^I \right)^{-2} \mathbf{X} \leq 1 \right\}, \tag{3.27}$$

where $\boldsymbol{Z}_0^I$ is a symmetric, second-order tensor describing the shape and orientation of the particles. Then, defining the characteristic function Θ_0^I of such an ellipsoid,

such that $\Theta_0^I = 1$ if $\mathbf{X}$ is in Ω_0^I and zero otherwise, and letting $\mathbf{X}_\alpha$ denote the random positions of the ellipsoid centers in the elastomeric matrix, the characteristic function of the inclusion phase (labeled by a superscript 2) is given by

$$\Theta_0^{(2)}(\mathbf{X}) = \sum_{\alpha=1}^{n} \Theta_0^I(\mathbf{X} - \mathbf{X}_\alpha), \tag{3.28}$$

which can be rewritten in the form

$$\Theta_0^{(2)}(\mathbf{X}) = \int_{\Omega_0} \Theta_0^I(\mathbf{X} - \mathbf{Z})\Psi_0(\mathbf{Z})d\mathbf{Z}, \tag{3.29}$$

where

$$\Psi_0(\mathbf{Z}) = \sum_{\alpha=1}^{n} \delta(\mathbf{Z} - \mathbf{X}_\alpha) \tag{3.30}$$

is the random density field generated by the set of random points $\mathbf{X}_\alpha$ $(\alpha = 1, ..., n)$ describing the locations of the centers of the n inclusions in the specimen. The probability density functions for the particle's locations may then be determined from $\Psi_0(\mathbf{Z})$ via expressions of the form

$$p_0^I(\mathbf{Z}) = \langle\langle \Psi_0(\mathbf{Z}) \rangle\rangle_0 , \quad p_0^{II}(\mathbf{Z}, \mathbf{Z}') = \langle\langle \Psi_0(\mathbf{Z})\Psi_0(\mathbf{Z}') \rangle\rangle_0 - \langle\langle \Psi_0(\mathbf{Z}) \rangle\rangle_0 \, \delta(\mathbf{Z} - \mathbf{Z}'), \tag{3.31}$$

where the double triangular brackets denote ensemble averages over the reference configuration. Note that $p_0^I(\mathbf{Z})$ is the probability density for finding an inclusion centered at $\mathbf{Z}$, and $p_0^{II}(\mathbf{Z}, \mathbf{Z}')$ is the joint probability density for finding an inclusion centered at $\mathbf{Z}$ and a second inclusion at $\mathbf{Z}'$. Here, it will be assumed that the specimen of the composite is *statistically homogeneous* (see Milton (2001)), so that $p_0^I(\mathbf{Z}) = p_0^I$ (the number of inclusions per unit volume in the reference configuration) is constant, and the volume fraction of particles in the reference configuration is given by $c_0^I = p_0^I \times \text{Vol}(\Omega_0^I)$. Furthermore, $p_0^{II}(\mathbf{Z}, \mathbf{Z}') = p_0^{II}(\mathbf{Z} - \mathbf{Z}')$ is translation invariant and, as already stated earlier, the assumption will be made in this work that the particle centers are distributed with "ellipsoidal symmetry" (Ponte Castañeda and Willis, 1995), which corresponds to a generalization of statistical isotropy postulating that the joint probability density function p_0^{II} depends on $\mathbf{Z} - \mathbf{Z}'$ through the combination $|(\boldsymbol{Z}_0^D)^{-1}(\mathbf{Z} - \mathbf{Z}')|$, where $\boldsymbol{Z}_0^D$ is a symmetric, second-order tensor. It is also convenient for visualization purposes to define (following Ponte Castañeda and Willis (1995)) the

"distributional ellipsoid"

$$\Omega_0^D = \left\{ \mathbf{X} \mid \mathbf{X} \cdot \left(\boldsymbol{Z}_0^D \right)^{-2} \mathbf{X} \leq 1 \right\}, \tag{3.32}$$

which serves to characterize the "shape" and "orientation" of the random "ellipsoidal" distribution of the particle centers (see dashed lines around the ellipsoidal inclusions in Fig. 3.1). An ellipsoidal distribution implies a particular correlation between the angular and radial dependence of the two-point probability function. It can be thought of as an affine deformation of a random set of points from a *statistically isotropic* distribution, which corresponds to the special case where $\boldsymbol{Z}_0^D = \boldsymbol{I}$, so that p_0^{II} depends on $\mathbf{Z} - \mathbf{Z}'$ only through its magnitude $|\mathbf{Z} - \mathbf{Z}'|$. It should be emphasized that particle distributions need not be ellipsoidal and will in general exhibit independent angular and a radial dependences. However, if the microstructure can be approximated as being ellipsoidal, then simple analytical estimates may be given (see Ponte Castañeda and Willis (1995)) for the homogenized linear response depending only on the particle volume fraction c_0^I, the particle shape and orientation, as specified by $\boldsymbol{Z}_0^I$, and the distribution shape and orientation, as specified by $\boldsymbol{Z}_0^D$, and hence the motivation for adopting these microstructural hypotheses for the MREs of interest in this work.

3.3.2 Microstructure evolution

As illustrated in Fig. 3.1, the microstructure is expected to evolve as the deformation and magnetic fields are applied: the volume fraction of the particles (assuming that the matrix material can accommodate non-isochoric deformations), as well as the orientation and distribution of the particles, will change because of the applied mechanical and magnetic fields. However, the characterization of the evolution of this microstructure is a formidable problem which has not been resolved in full generality—even for purely mechanical constitutive behaviors. For dilute concentrations of deformable particles in a linearly viscous material, a theory is available from the work of Eshelby (1957). A generalization of this theory for viscoplastic composites with particulate microstructures, which is valid approximately beyond the dilute range, has been given in a sequence of papers by Ponte Castañeda and Zaidman (1994); Kailasam et al. (1997); Kailasam and Ponte Castañeda (1998). In the context of finite elasticity, the problem is even more difficult and exact solutions are not available even in the dilute limit. However, an approximate theory for moderate particle

concentrations has been given by Lopez-Pamies and Ponte Castañeda (2006a). This theory has been found to predict the microstructure evolution with good accuracy for dilute particle concentrations (Michel et al., 2010). In this subsection, an *approximate* theory is proposed for the evolution of the microstructure in MREs, building on the above-mentioned earlier works.

First of all, it is noted that, if the overall deformation includes a hydrostatic component ($\bar{J} \neq 1$), the particle number density p_0^I and the corresponding particle volume fraction c_0^I will change with the deformation. However, it follows from the mass conservation equation, and the fact that the particles are rigid and therefore incompressible, that the particle volume fraction in the deformed configuration will be given by $c^I = c_0^I/\bar{J}$.

Under the applied deformation $\bar{\boldsymbol{F}}$ and magnetic induction field $\overline{\mathbf{B}}$, the particles will also rotate and change relative positions, but they will not change their shape (or size), as they are rigid. Therefore, the microstructure in the deformed configuration can be described in terms of expressions of the form

$$\Theta^{(2)}(\mathbf{x}) = \int_{\Omega} \Theta^I(\mathbf{x}-\mathbf{z})\Psi(\mathbf{z})d\mathbf{z}, \tag{3.33}$$

where Θ^I is the characteristic function of the rotated inclusion, as defined by the rotated ellipsoid

$$\Omega^I = \left\{ \mathbf{x} \mid \mathbf{x} \cdot \left(\boldsymbol{Z}^{I^T} \boldsymbol{Z}^I \right)^{-1} \mathbf{x} \leq 1 \right\}, \tag{3.34}$$

where $\boldsymbol{Z}^I = \boldsymbol{Z}_0^I \boldsymbol{R}^{I^T}$ is a (non-symmetric) second-order tensor describing the (fixed) shape and (new) orientation of the inclusion, as described by the inclusion rotation $\boldsymbol{R}^I$ induced by the deformation field $\boldsymbol{F}$ (which in turn will depend on both the macroscopically applied deformation $\bar{\boldsymbol{F}}$ and magnetic induction field $\overline{\mathbf{B}}$). In this connection, it should be noted that all the fibers will be assumed to rotate with the same tensor $\boldsymbol{R}^I$, which will be identified further below with the average rotation of the particles as determined by the homogenization procedure. This is clearly an approximation that neglects possible near-neighbor inclusion interactions, and would be strictly valid only in the dilute limit (when the particles do not interact). However, in the spirit of a homogenization approach it is consistent to assume that "on the average" all the particles rotate with the average deformation in the inclusion phase. In addition, it should be noted that although, in principle, distributions of orientations can be easily

considered in the context of a more general analysis, in practice, having to keep track of multiple inclusion orientations would complicate the derivations to follow, and in this first treatment of the problem, we prefer to make the simplifying assumption of perfectly aligned inclusions.

In an analogous fashion, the random positions of the particle centers is expected to evolve with the deformation, which has implications for the above-defined, two-point, probability density functions, p_0^{II}, for the distribution of the particles. Thus, it is clear that, at least in the dilute limit, this function will change with the macroscopic deformation $\bar{\boldsymbol{F}}$, since the particles will be convected with the deformation (see Kailasam et al. (1997) for an analogous hypotheses for particle-reinforced viscoplastic solids). At concentrated volume fractions, once again, neighboring particles will interact with one another, both magnetically and mechanically, and the positions of the particles will not simply be convected with the deformation. Thus, in general, it is expected that the evolution of the two-point probability density functions may depend on higher-order statistics, and that the assumed "ellipsoidal" symmetry will almost certainly be broken down. This will of course lead to significant complications in the characterization of the microstructures and the associated computation of the homogenized response, even for linear response. For this reason, we will make here the approximation that the two-point probabilities remain ellipsoidal, and that the evolution of the shape and orientation of the distributional ellipsoid will be controlled entirely by the macroscopic deformation $\bar{\boldsymbol{F}}$. Again, this "closure" approximation is expected to be exact in the dilute limit, and probably not too bad for moderate particle concentrations, which is the main objective of this work in any case.

Therefore, it will be assumed here that the two-point probabilities $p^{II}(\mathbf{z}-\mathbf{z}')$ in the deformed configuration will also be ellipsoidal and depend on $\mathbf{z}-\mathbf{z}'$ through the combination $|(\boldsymbol{Z}^D)^{-T}(\mathbf{z}-\mathbf{z}')|$, where the distributional ellipsoid in the deformed configuration will be given by

$$\Omega^D = \left\{ \mathbf{x} \mid \mathbf{x} \cdot \left(\boldsymbol{Z}^{D^T} \boldsymbol{Z}^D \right)^{-1} \mathbf{x} \leq 1 \right\}, \tag{3.35}$$

with $\boldsymbol{Z}^D = \boldsymbol{Z}_0^D \bar{\boldsymbol{F}}^T$ describing the new shape and orientation of the distributional ellipsoid in the deformed configuration.

In summary, the microstructures for the MREs have been idealized in terms of a family of initially aligned ellipsoidal inclusions, as characterized by the tensor $\boldsymbol{Z}_0^I$,

and distributed with ellipsoidal symmetry, as specified by the tensor $\boldsymbol{Z}_0^D$. Under the applied deformation $\bar{\boldsymbol{F}}$ and magnetic induction field $\overline{\mathbf{B}}$, all the particles are assumed to rotate by identical amounts $\boldsymbol{R}^I$ to new orientations specified by tensors $\boldsymbol{Z}^I = \boldsymbol{Z}_0^I \boldsymbol{R}^{I^T}$, and to rearrange their distribution by the applied deformation $\bar{\boldsymbol{F}}$, as specified by new distributions tensors $\boldsymbol{Z}^D = \boldsymbol{Z}_0^D \bar{\boldsymbol{F}}^T$. In this connection, it is important to emphasize that while the macroscopic deformation $\bar{\boldsymbol{F}}$ is prescribed (and therefore known a priori), the particle rotations $\boldsymbol{R}^I$ need to be determined from the solution of the magnetoelastic problem in terms of the applied deformation $\bar{\boldsymbol{F}}$ and magnetic induction field $\overline{\mathbf{B}}$. This observation will play a key role in the next subsection, where we will identify certain special conditions for which the particle rotation may be determined without the need to solve the magnetoelastic problem in detail.

3.3.3 A partial decoupling approximation

As we have seen in the context of expressions (2.21) and (2.25), the magnetoelastic energy densities $W^{(r)}$ of the elastomeric matrix phase and the rigid, magnetically susceptible particles can be split into two separate contributions $W_{me}^{(r)}$ and $W_{mag}^{(r)}$. Following the corresponding definition for W in expression $(3.2)_2$, we introduce the notations

$$W_{me}(\mathbf{X}, \boldsymbol{F}) = \sum_{s=1}^{2} \Theta_0^{(s)}(\mathbf{X})\; W_{me}^{(s)}(\boldsymbol{F}), \tag{3.36}$$

and

$$W_{mag}(\mathbf{X}, \boldsymbol{F}, \mathbf{B}) = \sum_{s=1}^{2} \Theta_0^{(s)}(\mathbf{X})\; W_{mag}^{(s)}(\boldsymbol{F}, \mathbf{B}), \tag{3.37}$$

such that $W(\mathbf{X}, \boldsymbol{F}, \mathbf{B}) = W_{me}(\mathbf{X}, \boldsymbol{F}) + W_{mag}(\mathbf{X}, \boldsymbol{F}, \mathbf{B})$. Then, making use of the definition (3.5) of the homogenized magnetoelastic energy density for the composite, we have that

$$\widetilde{W}(\bar{\boldsymbol{F}}, \overline{\mathbf{B}}) = \inf_{\mathbf{F} \in \mathcal{K}(\overline{\mathbf{F}})} \inf_{\mathbf{B} \in \mathcal{B}_0(\overline{\mathbf{B}})} \left\{ \langle W_{me}(\mathbf{X}, \boldsymbol{F}) \rangle_0 + \langle W_{mag}(\mathbf{X}, \boldsymbol{F}, \mathbf{B}) \rangle_0 \right\}, \tag{3.38}$$

where it is recalled that the triangular brackets $\langle . \rangle_0$ denote volume averages over the composite in its reference configuration (Ω_0).

Noticing that the first term on the right of expression (3.38) is independent of $\mathbf{B}$,

we can rewrite this expression in the form

$$\widetilde{W}(\bar{\boldsymbol{F}},\overline{\mathbf{B}}) = \inf_{\mathbf{F}\in\mathcal{K}(\bar{\mathbf{F}})} \left\{ \langle W_{me}(\mathbf{X},\boldsymbol{F})\rangle_0 + \widetilde{W}_{mag}(\overline{\mathbf{B}};\boldsymbol{F}(\mathbf{X})) \right\}, \tag{3.39}$$

where

$$\widetilde{W}_{mag}(\overline{\mathbf{B}};\boldsymbol{F}(\mathbf{X})) = \inf_{\mathbf{B}\in\mathcal{B}_0(\overline{\mathbf{B}})} \langle W_{mag}(\mathbf{X},\boldsymbol{F},\mathbf{B})\rangle_0 \tag{3.40}$$

is the homogenized magnetic energy function associated with the local energy function potential $W_{mag}(\mathbf{X},\boldsymbol{F},\mathbf{B})$, defined above, for a given trial deformation field $\boldsymbol{F}(\mathbf{X})$. It is important to emphasize that both terms in expression (3.38) depend on the trial deformation field $\boldsymbol{F}(\mathbf{X})$, and therefore, the mechanical and magnetic energy terms are coupled together and cannot be separated in general. However, it is useful to rewrite the homogenized magnetic energy in the current configuration (see (3.14)), making use of expressions $(2.22)_2$ and (2.27) for the magnetic energy-density functions of the matrix and particles, respectively. Thus, we have that $\widetilde{W}_{mag}(\overline{\mathbf{B}};\boldsymbol{F}(\mathbf{X})) = \bar{J}\,\widetilde{w}_{mag}(\overline{\mathbf{b}};\boldsymbol{F}(\mathbf{X}))$, where $\bar{J} = \det\bar{\boldsymbol{F}}$ and

$$\widetilde{w}_{mag}(\overline{\mathbf{b}};\boldsymbol{F}(\mathbf{X})) = \inf_{\mathbf{b}\in\mathcal{B}(\overline{\mathbf{b}})} \left\langle \frac{1}{2\mu_0}\mathbf{b}\cdot\mathbf{b} + \rho_0^{(2)}\Theta^{(2)}(\mathbf{x})\varphi_{mag}^{(2)}(\overline{\boldsymbol{R}}^{(2)^T}\mathbf{b}) \right\rangle. \tag{3.41}$$

In this relation, $\Theta^{(2)}(\mathbf{x})$ describes the position and orientation of the particles in the deformed configuration, and the volume integral implied by the triangular brackets is now over the deformed configuration (Ω) of the composite. In addition, we have made use of the above-stated hypothesis that all the particles rotate by the same amount $\boldsymbol{R}^I$, which we have set equal to the average rotation $\overline{\boldsymbol{R}}^{(2)}$ of the particles, as determined by the solution of the homogenization problem (3.39) for the local deformation field $\boldsymbol{F}(\mathbf{X})$. Similarly, the characteristic function $\Theta^{(2)}(\mathbf{x})$ of the particles in the deformed configuration also depends on the current orientation of the particles $\boldsymbol{R}^I = \overline{\boldsymbol{R}}^{(2)}$, as described by relations (3.33) and (3.34) with $\boldsymbol{Z}^I = \boldsymbol{Z}_0^I\overline{\boldsymbol{R}}^{(2)^T}$, as well as on the macroscopic deformation $\bar{\boldsymbol{F}}$, as described by (3.35) with $\boldsymbol{Z}^D = \boldsymbol{Z}_0^D\bar{\boldsymbol{F}}^T$. It should be emphasized at this stage that writing the magnetic energy in its "more natural" Eulerian form (3.41) makes the explicit dependence on the deformation field $\boldsymbol{F}$ in the Lagrangian description (3.40) disappear.

Next, for reference in the development that will follow, we define the stored-energy

function of the "purely mechanical" problem via the expression

$$\widetilde{W}_{me}(\bar{\boldsymbol{F}}) = \inf_{\mathbf{F}\in\mathcal{K}(\bar{\mathbf{F}})} \langle W_{me}(\mathbf{X}, \boldsymbol{F})\rangle_0 \,, \tag{3.42}$$

and label $\boldsymbol{F}_m(\mathbf{X})$ the minimizing trial field (or solution) for this problem.

Indeed, the magnetic homogenization problem (3.41) for $\widetilde{w}_{mag}$ depends, in general, on the local deformation field $\boldsymbol{F}(\mathbf{X})$ (through the particle rotations $\boldsymbol{R}^I = \overline{\boldsymbol{R}}^{(2)}$), and $\widetilde{w}_{mag}$ cannot be taken out of the mechanical minimization problem (3.39). However, a variational estimate may be obtained by recognizing that the minimizing solution $\boldsymbol{F}_m(\mathbf{X})$ of the purely mechanical problem (3.42) is a perfectly acceptable trial field for the minimization problem (3.39). Then, using the fact (from (3.42)) that the first term in the right-hand side of expression (3.38) evaluated at $\boldsymbol{F}_m(\mathbf{X})$ is precisely $\widetilde{W}_{me}$, it is deduced that

$$\widetilde{W}(\bar{\boldsymbol{F}}, \overline{\mathbf{B}}) \leq \widetilde{W}_{me}(\bar{\boldsymbol{F}}) + \widetilde{W}_{mag}(\overline{\mathbf{B}}; \boldsymbol{F}_m(\mathbf{X})), \tag{3.43}$$

where $\widetilde{W}_{mag}(\overline{\mathbf{B}}; \boldsymbol{F}_m(\mathbf{X}))$ is given by (3.40) evaluated at $\boldsymbol{F} = \boldsymbol{F}_m$. Following the same procedure that led to expression (3.41) for the magnetic energy in the deformed configuration, but with the exact field $\boldsymbol{F}(\mathbf{X})$ replaced by the trial field $\boldsymbol{F}_m(\mathbf{X})$, the result (3.43) can also be rewritten in the form

$$\widetilde{W}(\bar{\boldsymbol{F}}, \overline{\mathbf{B}}) \leq \widetilde{W}_{me}(\bar{\boldsymbol{F}}) + \bar{J}\, \widetilde{w}_{mag}(\overline{\mathbf{b}}; \boldsymbol{F}_m(\mathbf{X})), \tag{3.44}$$

where

$$\widetilde{w}_{mag}(\overline{\mathbf{b}}; \boldsymbol{F}_m(\mathbf{X})) = \inf_{\mathbf{b}\in\mathcal{B}(\overline{\mathbf{b}})} \left\langle \frac{1}{2\mu_0}\mathbf{b}\cdot\mathbf{b} + \rho_0^{(2)}\Theta_m^{(2)}(\mathbf{x})\varphi_{mag}^{(2)}(\overline{\boldsymbol{R}}_m^{(2)^T}\mathbf{b}) \right\rangle. \tag{3.45}$$

In this last expression, $\overline{\boldsymbol{R}}_m^{(2)}$ refers to the particle rotations induced by the deformation $\boldsymbol{F}_m$ in the purely mechanical problem, and $\Theta_m^{(2)}(\mathbf{x})$ refers to the particle characteristic function defined by relations (3.33) and (3.34) with $\boldsymbol{Z}^I = \boldsymbol{Z}_0^I\overline{\boldsymbol{R}}_m^{(2)^T}$, as induced by the purely mechanical deformation field $\boldsymbol{F}_m$. The result also depends on the ellipsoidal shape of the distribution as determined by (3.35) with $\boldsymbol{Z}^D = \boldsymbol{Z}_0^D\bar{\boldsymbol{F}}^T$. A more detailed derivation of the partial decoupling approximation and the implications for the predicted energy is given in Appendix B.

It will be argued next that the estimates (3.43), or equivalently (3.44) with (3.45),

for $\widetilde{W}$ should be very accurate (exact to within the approximations already stated) for certain important special cases, including the cases where the material is completely isotropic (isotropic distribution of magnetically isotropic, spherical particles), as well as when the particle and distribution shapes, and the applied mechanical and magnetic loadings are all perfectly aligned.

Magnetically isotropic, spherical inclusions

When the rigid particles are magnetically isotropic and spherical, we expect the average particle rotation to be equal to the continuum rotation, i.e., $\boldsymbol{R}^I = \overline{\boldsymbol{R}}$. In this case, the dependence of the magnetic homogenization problem (3.41) for $\widetilde{w}_{mag}$ on the local deformation field $\boldsymbol{F}(\mathbf{X})$ would be only through its macroscopic average $\bar{\boldsymbol{F}}$. Therefore, since $\bar{\boldsymbol{F}}$ is fixed as far as the mechanical minimization problem (3.39) is concerned, the magnetic part of the energy may be taken out of the brackets to generate the "exact" (again to within the already stated approximations) result

$$\widetilde{W}(\bar{\boldsymbol{F}}, \overline{\mathbf{B}}) = \widetilde{W}_{me}(\bar{\boldsymbol{F}}) + \bar{J}\, \widetilde{w}_{mag}(\overline{\mathbf{b}}; \bar{\boldsymbol{F}}). \tag{3.46}$$

In this expression, $\widetilde{W}_{me}$ is the purely mechanical homogenized stored-energy function of the composite consisting of rigid spherical particles ($\boldsymbol{Z}^I = \boldsymbol{I}$) distributed isotropically (in the reference configuration) in an isotropic elastomeric matrix, as defined by relation (3.42), and correspondingly, $\widetilde{w}_{mag}(\overline{\mathbf{b}}; \bar{\boldsymbol{F}})$ is the purely magnetic energy-density function of a two-phase system consisting of a matrix with the magnetic susceptibly of vacuum and of magnetically isotropic, spherical particles distributed with ellipsoidal symmetry (in the deformed configuration), as determined by (3.35) with $\boldsymbol{Z}^D = \boldsymbol{Z}_0^D \bar{\boldsymbol{F}}^T$. It follows from (3.41) that

$$\widetilde{w}_{mag}(\overline{\mathbf{b}}; \bar{\boldsymbol{F}}) = \inf_{\mathbf{b} \in \mathcal{B}(\overline{\mathbf{b}})} \left\langle \frac{1}{2\mu_0} \mathbf{b} \cdot \mathbf{b} + \rho_0^{(2)} \Theta^{(2)}(\mathbf{x}) \varphi_{mag}^{(2)}(\mathbf{b}) \right\rangle, \tag{3.47}$$

where we have used the fact that $\varphi_{mag}^{(2)}(\overline{\boldsymbol{R}}^T \mathbf{b}) = \varphi_{mag}^{(2)}(\mathbf{b})$, when $\varphi_{mag}^{(2)}$ is isotropic.

Aligned, magnetically anisotropic, ellipsoidal inclusions

In this case, the inequality (approximation) in the expression (3.44) for the homogenized stored-energy function $\widetilde{W}$ of the magnetoelastic composite is also expected

to become an equality ("exact") when the magnetic induction and mechanical deformation fields are "perfectly aligned" with the magnetic and geometric axes of the particles, so that the particles remain fixed in orientation ($\overline{\boldsymbol{R}}^{(2)} = \boldsymbol{I}$), at least up to the possible development of bifurcation instabilities where the particles may abruptly change their orientation. More generally, the estimate (3.44) is expected to remain a good approximation in the "stiff matrix" limit when the energetic cost of rearrangements in the particle orientation from the mechanical equilibrium orientations is high compared with the energetic benefit of realigning the particles with the applied magnetic field. Attempts to account for the effect of particle reorientation due to a magnetically applied field have been carried out in the geometrically linear limit by Siboni and Ponte Castañeda (2012a), who find that the effect is indeed of higher order in the "stiff matrix" limit.

Finally, it is remarked that relation (3.44) (or (3.46) for the special case of isotropic composites, or "perfectly aligned" loading conditions), expresses the macroscopic energy-density function $\widetilde{W}$ of the magnetoelastic composite in terms of two complementary contributions. The first is the macroscopic stored-energy function $\widetilde{W}_{me}$ of the purely mechanical problem consisting of a composite with initial microstructure in the reference configuration as determined by ellipsoidal particles (3.27) with given $\boldsymbol{Z}_0^I$ distributed with ellipsoidal symmetry (3.32) with given $\boldsymbol{Z}_0^D$. The second part involves the macroscopic energy-density function $\widetilde{w}_{mag}$ of a purely magnetic problem in the deformed configuration, as specified by ellipsoidal particles with new orientation (3.34) given by $\boldsymbol{Z}^I = \boldsymbol{Z}_0^I \overline{\boldsymbol{R}}_m^{(2)^T}$ and new distribution (3.35) determined by $\boldsymbol{Z}^D = \boldsymbol{Z}_0^D \bar{\boldsymbol{F}}^T$. Although the mechanical and magnetic problems have been partially decoupled, it should be emphasized that the decoupling is not complete since $\widetilde{w}_{mag}$ still depends on the mechanical fields through $\overline{\boldsymbol{R}}_m^{(2)}$ and $\bar{\boldsymbol{F}}$. Moreover, both problems are still nonlinear and extremely difficult to solve. However, as already mentioned, "variational linear comparison" estimates have been provided by Ponte Castañeda and Tiberio (2000), as well as Lopez-Pamies and Ponte Castañeda (2006a), for the mechanical (hyperelastic) problem (3.42). In the next section, the deformation-dependent magnetic homogenization problem will be investigated first in the context of linear magnetic response for the particles using the theory of Ponte Castañeda and Willis (1995) for linear composites with particulate microstructures of the above-described type, and then corresponding estimates will be generated for the case of nonlinear (ferromagnetic) particles using the variational linear comparison theory of Ponte Castañeda (1992)

and Ponte Castañeda (2001) for nonlinear dielectric/conductor composites, which are mathematically analogous to the nonlinear magnetization composites described by (3.47).

3.4 MREs with linear and nonlinear magnetic particle response

3.4.1 Linear, anisotropic magnetic particle response

For magnetically linear behavior for the two phases in the deformed configuration (see $(2.22)_2$ and $(2.30)_1$), the homogenization problem (3.45) for $\widetilde{w}_{mag}$ reduces to

$$\widetilde{w}_{mag}(\bar{\mathbf{b}}; \boldsymbol{F}(\mathbf{X})) = \inf_{\mathbf{b}\in\mathcal{B}(\bar{\mathbf{b}})} \left(\frac{1}{2}\mathbf{b}\cdot\mu^{-1}(\mathbf{x})\mathbf{b}\right) = \frac{1}{2}\bar{\mathbf{b}}\cdot\tilde{\mu}^{-1}\bar{\mathbf{b}}, \tag{3.48}$$

where $\tilde{\boldsymbol{\mu}}$ is the homogenized permeability of the composite. In this expression, $\boldsymbol{\mu}(\mathbf{x})$ is the local magnetic permeability of the phases, given by

$$\boldsymbol{\mu}(\mathbf{x}) = \mu_0\boldsymbol{I} + \Theta_m^{(2)}(\mathbf{x})\left(\boldsymbol{\mu}^{(2)} - \mu_0\boldsymbol{I}\right), \quad \text{where} \qquad \boldsymbol{\mu}^{(2)} = \overline{\boldsymbol{R}}^{(2)}\boldsymbol{M}^{(2)}\overline{\boldsymbol{R}}^{(2)^T}, \tag{3.49}$$

with $\boldsymbol{M}^{(2)}$ a *fixed* (independent of the deformation) tensor corresponding to the magnetic permeability of the anisotropic rigid particles in the reference configuration.

Variational estimates for the effective magnetic permeability $\tilde{\boldsymbol{\mu}}$ of two-phase magnetostatic composite, defined by expression (3.48) with constitutive behavior described by (3.49) and "ellipsoidal microstructures," as defined by (3.34) and (3.35) with $\boldsymbol{Z}^I = \boldsymbol{Z}_0^I\overline{\boldsymbol{R}}^{(2)^T}$ and $\boldsymbol{Z}^D = \boldsymbol{Z}_0^D\bar{\boldsymbol{F}}^T$, may be obtained from the work of Ponte Castañeda and Willis (1995) as follows:

$$\tilde{\boldsymbol{\mu}} = \mu_0\boldsymbol{I} + c^I\left[\left(\boldsymbol{\mu}^{(2)} - \mu_0\boldsymbol{I}\right)^{-1} + \boldsymbol{P}^I - c^I\boldsymbol{P}^D\right]^{-1}, \tag{3.50}$$

where c^I is the (current) volume fraction of the particles, and $\boldsymbol{P}^I$ and $\boldsymbol{P}^D$ are microstructural tensors, related to the Eshelby tensor, serving to characterize the shape and orientation of the particles and distribution ellipsoids, respectively (see Ponte Castañeda and Willis (1995)). It should be noted here for later reference that these estimates have to satisfy certain geometric restrictions on the volume fraction and

the shape of the inclusions and distribution, ensuring that the particles do not interfere with each other's distributional ellipsoids, which would violate the ellipsoidal symmetry hypothesis (in the deformed configuration).

The second-order tensor $\boldsymbol{P}^I$ is symmetric and given by

$$\boldsymbol{P}^I = \frac{\det \boldsymbol{Z}^I}{4\pi\mu_0} \int\limits_{|\xi|=1} \xi \otimes \xi \, |\boldsymbol{Z}^I \xi|^{-3} \, dS(\xi), \tag{3.51}$$

while $\boldsymbol{P}^D$ is given by a completely analogous expression with $\boldsymbol{Z}^I$ replaced by $\boldsymbol{Z}^D$. Recalling the above-mentioned relations between $\boldsymbol{Z}^I$ and $\boldsymbol{Z}^I_0$, and between $\boldsymbol{Z}^D$ and $\boldsymbol{Z}^D_0$, it is remarked that

$$\boldsymbol{P}^I = \overline{\boldsymbol{R}}^{(2)} \boldsymbol{P}^I_0 \overline{\boldsymbol{R}}^{(2)^T}, \quad \text{and} \quad \boldsymbol{P}^D = \overline{\boldsymbol{R}} \boldsymbol{P}^D_0(\overline{\boldsymbol{U}}) \overline{\boldsymbol{R}}^T, \tag{3.52}$$

where $\boldsymbol{P}^I_0$ is the microstructural tensor of the particle evaluated in the reference configuration with $\boldsymbol{Z}^I$ replaced by the fixed tensor $\boldsymbol{Z}^I_0$ in expression (3.51), and $\boldsymbol{P}^D_0(\overline{\boldsymbol{U}})$ is given by

$$\boldsymbol{P}^D_0(\overline{\boldsymbol{U}}) = \frac{\bar{J} \det \boldsymbol{Z}^D_0}{4\pi\mu_0} \int\limits_{|\xi|=1} \xi \otimes \xi \, \left| \left(\boldsymbol{Z}^D_0 \overline{\boldsymbol{U}} \right) \xi \right|^{-3} \, dS(\xi), \tag{3.53}$$

which depends on the initial distribution tensor $\boldsymbol{Z}^D_0$, as well as on the macroscopic stretch $\overline{\boldsymbol{U}}$, but not on the macroscopic rotation $\overline{\boldsymbol{R}}$.

Next, for future convenience, it is noted that the expression (3.50) for $\tilde{\boldsymbol{\mu}}$ may be rewritten in terms of the effective magnetic susceptibility $\tilde{\boldsymbol{\chi}} = \boldsymbol{I} - \mu_0 \tilde{\boldsymbol{\mu}}^{-1}$ as

$$\tilde{\boldsymbol{\chi}} = c^I \left[\left(\boldsymbol{\chi}^{(2)} \right)^{-1} - \boldsymbol{I} + \mu_0 \boldsymbol{P}^I + c^I \left(\boldsymbol{I} - \mu_0 \boldsymbol{P}^D \right) \right]^{-1}, \tag{3.54}$$

where $\boldsymbol{\chi}^{(2)}$ is the magnetic susceptibility of the particles. It is noted that $\tilde{\boldsymbol{\chi}}$ is independent of μ_0, and symmetric, in view of the symmetry of $\boldsymbol{P}^I$ and $\boldsymbol{P}^D$, but clearly depends on $\bar{\boldsymbol{F}}$, because of relations (3.52).

Defining the particle rotation $\boldsymbol{R}^p$ relative to the macroscopic rotation $\overline{\boldsymbol{R}}$ via

$$\boldsymbol{R}^p = \overline{\boldsymbol{R}}^T \overline{\boldsymbol{R}}^{(2)}, \tag{3.55}$$

as well as the modified particle and distribution microstructural tensors

$$\hat{\boldsymbol{P}}_0^I = \mu_0 \boldsymbol{P}_0^I \quad \text{and} \quad \hat{\boldsymbol{P}}_0^D = \frac{\mu_0}{\bar{J}} \boldsymbol{P}_0^D, \tag{3.56}$$

and recalling that $\boldsymbol{\chi}^{(2)} = \overline{\boldsymbol{R}}^{(2)} \boldsymbol{X}^{(2)} \overline{\boldsymbol{R}}^{(2)^T}$, as well as expressions (3.52), it is noted that $\tilde{\boldsymbol{\chi}}$ can be written in the form

$$\tilde{\boldsymbol{\chi}}(\bar{\boldsymbol{F}}) = \overline{\boldsymbol{R}} \tilde{\boldsymbol{X}}(\overline{\boldsymbol{U}}) \overline{\boldsymbol{R}}^T, \tag{3.57}$$

where

$$\tilde{\boldsymbol{X}}(\overline{\boldsymbol{U}}) = \frac{c_0^I}{\bar{J}} \left[\boldsymbol{R}^p(\overline{\boldsymbol{U}}) \left(\boldsymbol{A}_0^I\right)^{-1} \boldsymbol{R}^{pT}(\overline{\boldsymbol{U}}) + \frac{c_0^I}{\bar{J}} \boldsymbol{I} - c_0^I \hat{\boldsymbol{P}}_0^D(\overline{\boldsymbol{U}}) \right]^{-1}. \tag{3.58}$$

In this expression, c_0^I is the prescribed initial (in the reference configuration) particle volume fraction, and

$$\boldsymbol{A}_0^I = \left[\left(\boldsymbol{X}^{(2)} \right)^{-1} - \boldsymbol{I} + \hat{\boldsymbol{P}}_0^I \right]^{-1} \tag{3.59}$$

is a fixed, symmetric second-order tensor, depending only on the initial shape and orientation of the particles. In addition, the dependence of the particle rotation $\boldsymbol{R}^p$ and of $\hat{\boldsymbol{P}}_0^D$ on the macroscopic stretch $\overline{\boldsymbol{U}}$ has been made explicit, to exhibit more clearly the dependence of the tensor $\tilde{\boldsymbol{X}}$ on $\overline{\boldsymbol{U}}$ (through $\bar{J}$, $\boldsymbol{R}^p$ and $\hat{\boldsymbol{P}}_0^D$). Note that $\tilde{\boldsymbol{X}}(\boldsymbol{I})$ is the macroscopic susceptibility in the reference configuration.

In conclusion, the expressions (3.57) and (3.58), together with $\tilde{\boldsymbol{\mu}}^{-1} = (\boldsymbol{I} - \tilde{\boldsymbol{\chi}})/\mu_0$ and (3.48), lead via (3.44) to the following (fully Lagrangian) estimate for the energy-density function of the magnetoelastic composite

$$\widetilde{W}_{DA}(\bar{\boldsymbol{F}}, \overline{\mathbf{B}}) = \widetilde{W}_{me}(\bar{\boldsymbol{F}}) + \frac{1}{2\mu_0 \bar{J}} \overline{\mathbf{B}} \cdot \overline{\boldsymbol{U}}^2 \overline{\mathbf{B}} - \frac{1}{2\mu_0 \bar{J}} \overline{\mathbf{B}} \cdot \left[\overline{\boldsymbol{U}} \tilde{\boldsymbol{X}}(\overline{\boldsymbol{U}}) \overline{\boldsymbol{U}} \right] \overline{\mathbf{B}}, \tag{3.60}$$

which obviously satisfies the objectivity requirement $\widetilde{W}_{DA}(\bar{\boldsymbol{F}}, \overline{\mathbf{B}}) = \widetilde{W}_{DA}(\overline{\boldsymbol{U}}, \overline{\mathbf{B}})$. Comparing this expression with the general expression (3.10), it follows that the effective specific free-energy function for the MRE is given by

$$\bar{\rho}_0 \widetilde{\Phi}_{DA}(\bar{\boldsymbol{F}}, \overline{\mathbf{B}}) = \widetilde{W}_{me}(\bar{\boldsymbol{F}}) - \frac{1}{2\mu_0 \bar{J}} \overline{\mathbf{B}} \cdot \left[\overline{\boldsymbol{U}} \tilde{\boldsymbol{X}}(\overline{\boldsymbol{U}}) \overline{\boldsymbol{U}} \right] \overline{\mathbf{B}}. \tag{3.61}$$

The macroscopic (Lagrangian) magnetic field $\overline{\mathbf{H}}$ and Piola-Kirchhoff stress $\bar{\boldsymbol{S}}$ may be computed in terms of the average deformation $\bar{\boldsymbol{F}}$ and magnetic induction field $\overline{\mathbf{B}}$ via expressions (3.11), and take the forms

$$\overline{\mathbf{H}} = \frac{1}{\mu_0 \bar{J}} \left[\overline{\boldsymbol{U}} \left(\boldsymbol{I} - \tilde{\boldsymbol{X}}(\overline{\boldsymbol{U}}) \right) \overline{\boldsymbol{U}} \right] \overline{\mathbf{B}}, \tag{3.62}$$

and

$$\bar{\boldsymbol{S}} = \bar{\boldsymbol{S}}^{M} + \bar{\boldsymbol{S}}^{me} + \bar{\boldsymbol{S}}^{ex}, \tag{3.63}$$

where $\bar{\boldsymbol{S}}^{M}$ is the Maxwell stress, as given by (3.12), $\bar{\boldsymbol{S}}^{me} = \partial \widetilde{W}_{me} / \partial \bar{\boldsymbol{F}}$ is the purely mechanical stress, and $\bar{\boldsymbol{S}}^{ex}$ is the "extra" stress corresponding to the additional stresses arising in the magnetoelastic composite, beyond the purely mechanical and vacuum magnetic contributions. Given the explicit dependence of the extra term in the free-energy function $\widetilde{\Phi}_{DA}$ on $\bar{\boldsymbol{U}}$, it is natural to make use of the chain rule and to write the extra stress $\bar{\boldsymbol{S}}^{ex}$ in terms of the corresponding "extra" Biot stress

$$\bar{\boldsymbol{T}}_{B}^{ex} = \frac{\partial \widetilde{\Phi}_{ex}}{\partial \bar{\boldsymbol{U}}}(\bar{\boldsymbol{U}}, \overline{\mathbf{B}}), \quad \text{where} \quad \widetilde{\Phi}_{ex}(\bar{\boldsymbol{U}}, \overline{\mathbf{B}}) = -\frac{1}{2\mu_0 \bar{J}} \overline{\mathbf{B}} \cdot \left[\overline{\boldsymbol{U}} \tilde{\boldsymbol{X}}(\overline{\boldsymbol{U}}) \overline{\boldsymbol{U}} \right] \overline{\mathbf{B}}, \tag{3.64}$$

via the expression (see Hoger (1993))

$$\begin{aligned} \bar{\boldsymbol{S}}^{ex} &= \bar{\boldsymbol{R}} \bar{\boldsymbol{T}}_{B}^{ex} + \frac{1}{\bar{I}\,\overline{II} - \bar{J}} \times \\ &\bar{\boldsymbol{R}} \left[\left(\bar{\boldsymbol{U}}^2 \bar{\boldsymbol{T}}_{B}^{ex} \bar{\boldsymbol{U}} - \bar{\boldsymbol{U}}\, \bar{\boldsymbol{T}}_{B}^{ex} \bar{\boldsymbol{U}}^2 \right) - \bar{I} \left(\bar{\boldsymbol{U}}^2 \bar{\boldsymbol{T}}_{B}^{ex} - \bar{\boldsymbol{T}}_{B}^{ex} \bar{\boldsymbol{U}}^2 \right) + \bar{I}^2 \left(\bar{\boldsymbol{U}}\, \bar{\boldsymbol{T}}_{B}^{ex} - \bar{\boldsymbol{T}}_{B}^{ex} \bar{\boldsymbol{U}} \right) \right], \end{aligned} \tag{3.65}$$

where the $\bar{I}, \overline{II}$ and $\bar{J}$ are the three principal invariants of $\bar{\boldsymbol{U}}$. In connection with this last expression, it should be noted that the terms in the second line add up to zero when the Biot extra stress (3.64) is coaxial with $\bar{\boldsymbol{U}}$. In addition, it is noted that in the evaluation of the expression (3.64) there will be a modified Maxwell-type stress arising from the derivatives with $\tilde{\boldsymbol{X}}$ held fixed, as well as additional contributions due to the macroscopic change in volume $\bar{J}$, the change in particle orientation $\boldsymbol{R}^{p}$, and the particle distribution $\boldsymbol{P}_{0}^{D}$, arising from the dependence of $\tilde{\boldsymbol{X}}$ on $\overline{\boldsymbol{U}}$ through these variables (see further below for a more detailed expression).

The corresponding expression for the Eulerian free-energy density function, de-

fined by (3.16), takes the form

$$\tilde{\phi}_{DA}(\bar{\boldsymbol{F}}, \overline{\mathbf{b}}) = \tilde{\phi}_{me}(\bar{\boldsymbol{F}}) - \frac{1}{2\mu_0 \bar{\rho}} \overline{\mathbf{b}} \cdot \tilde{\boldsymbol{\chi}}(\bar{\boldsymbol{F}}) \overline{\mathbf{b}}, \tag{3.66}$$

where $\tilde{\phi}_{me}(\bar{\boldsymbol{F}}) = \widetilde{W}_{me}(\bar{\boldsymbol{F}})/\bar{\rho}_0$ and $\tilde{\boldsymbol{\chi}}$ is given by expression (3.57) with (3.58). Using frame indifference (objectivity), the result can also be expressed in terms of $\tilde{\varphi}_{DA}(\bar{\boldsymbol{C}}, \overline{\boldsymbol{F}}^T \overline{\mathbf{b}}) = \tilde{\phi}_{DA}(\bar{\boldsymbol{F}}, \overline{\mathbf{b}})$, so that the average (Eulerian) magnetization $\bar{\mathbf{m}}$ and Cauchy stress $\bar{\boldsymbol{T}}$ may then be determined in terms of $\bar{\boldsymbol{F}}$ and $\overline{\mathbf{b}}$ via expressions (3.19). This involves taking derivatives of the above expression with respect to $\boldsymbol{C}$ (with the compound variable $\widehat{\mathbf{b}} = \overline{\boldsymbol{F}}^T \overline{\mathbf{b}}$ being held fixed), and in particular, obtaining the derivatives of $\overline{\boldsymbol{C}}^{1/2}$ with respect to $\bar{\boldsymbol{C}}$. However, we prefer here to compute the Eulerian version of the expressions (3.62) and (3.63) for the macroscopic magnetization and stress by converting them directly into the corresponding Eulerian variables by means of relations (3.13). The results can be put in the forms

$$\bar{\mathbf{m}} = \frac{1}{\mu_0} \tilde{\boldsymbol{\chi}}(\bar{\boldsymbol{F}}) \bar{\mathbf{b}}, \quad \text{and} \quad \bar{\boldsymbol{T}} = \bar{\boldsymbol{T}}^M + \bar{\boldsymbol{T}}^{me} + \bar{\boldsymbol{T}}^{ex}, \tag{3.67}$$

where $\tilde{\boldsymbol{\chi}}$ is again given by expressions (3.57) and (3.58), and where $\bar{\boldsymbol{T}}^M$ is the (true) Maxwell stress (2.14) in the composite, $\bar{\boldsymbol{T}}^{me}$ is the purely mechanical stress, and $\bar{\boldsymbol{T}}^{ex}$ is the extra stress given in terms of the Biot stress (3.64) via (Hoger, 1993)

$$\begin{aligned} \bar{\boldsymbol{T}}^{ex} = \frac{1}{\bar{J}\left(\bar{I}\,\overline{II} - \bar{J}\right)} \bar{\boldsymbol{R}} \Big[\bar{\boldsymbol{U}}^2 \bar{\boldsymbol{T}}_B^{ex} \bar{\boldsymbol{U}}^2 - \bar{I} \left(\bar{\boldsymbol{U}}^2 \bar{\boldsymbol{T}}_B^{ex} \bar{\boldsymbol{U}} + \bar{\boldsymbol{U}}\, \bar{\boldsymbol{T}}_B^{ex} \bar{\boldsymbol{U}}^2 \right) \\ + \left(\bar{I}^2 + \overline{II}\right) \left(\bar{\boldsymbol{U}}\, \bar{\boldsymbol{T}}_B^{ex} \bar{\boldsymbol{U}} \right) - \bar{J} \left(\bar{\boldsymbol{U}}\, \bar{\boldsymbol{T}}_B^{ex} + \bar{\boldsymbol{T}}_B^{ex} \bar{\boldsymbol{U}} \right) + \bar{I} \bar{J}\, \bar{\boldsymbol{T}}_B^{ex} \Big] \bar{\boldsymbol{R}}^T, \end{aligned} \tag{3.68}$$

which is seen to be symmetric. For the purposes of computing $\bar{\boldsymbol{T}}^{ex}$, it is convenient to write the Biot extra stress, as determined by (3.64), in the form

$$\begin{aligned} \bar{\boldsymbol{T}}_B^{ex} = \bar{J} \left(\overline{\mathbf{b}} \cdot \overline{\mathbf{m}} \right) \bar{\boldsymbol{U}}^{-1} - \bar{J} \left[\left(\overline{\boldsymbol{R}}^T \overline{\mathbf{m}} \right) \otimes_s \left(\bar{\boldsymbol{U}}^{-1} \bar{\boldsymbol{R}}^T \overline{\mathbf{b}} \right) \right] \\ + \frac{\mu_0 \bar{J}^2}{2 c_0^I} \frac{\partial}{\partial \bar{\boldsymbol{U}}} \left[(\overline{\boldsymbol{R}}^T \overline{\mathbf{m}}) \cdot \tilde{\boldsymbol{Y}} (\overline{\boldsymbol{R}}^T \overline{\mathbf{m}}) \right] \end{aligned} \tag{3.69}$$

where $\otimes_s$ stands for the symmetrized dyadic product. Also, the derivative of the last term in the square brackets is taken with the compound variable $\overline{\boldsymbol{R}}^T \overline{\mathbf{m}}$ being held

fixed, and

$$\tilde{\boldsymbol{Y}}(\overline{\boldsymbol{U}}) = \boldsymbol{R}^p(\overline{\boldsymbol{U}})\big(\boldsymbol{A}_0^I\big)^{-1}\boldsymbol{R}^{pT}(\overline{\boldsymbol{U}}) + \frac{c_0^I}{\bar{J}}\boldsymbol{I} - c_0^I\hat{\boldsymbol{P}}_0^D(\overline{\boldsymbol{U}}). \tag{3.70}$$

It is interesting to remark that the first term in expression (3.69) for the extra Biot stress corresponds exactly to the second term in expressions $(3.17)_1$ for the total Cauchy stress, while the second term in (3.69) is related the third term in $(3.17)_1$. Note that these two terms are proportional to the macroscopic magnetization, and therefore of order volume fraction c_0^I. On the other hand, it follows from (3.70) that the third term in expression (3.69) for the extra Biot stress is of order magnetization squared, and includes one contribution, due to the particle rotations, of order c_0^I, and two additional contributions, due to change in volume and particle distributions, of order $(c_0^I)^2$.

Magnetically isotropic, spherical inclusions

In this case, the particle susceptibility and microstructural tensor become isotropic, so that $\boldsymbol{A}_0^I = a_0^I\boldsymbol{I}$, where $a_0^I = d\chi^{(2)}/[\chi^{(2)} + d(1-\chi^{(2)})]$ ($d = 2$, or 3 is the dimension), and the tensor $\tilde{\boldsymbol{Y}}$ becomes independent of the particle rotation $\boldsymbol{R}^p$, such that

$$\tilde{\boldsymbol{Y}}(\overline{\boldsymbol{U}}) = \frac{1}{a_0^I}\boldsymbol{I} + \frac{c_0^I}{\bar{J}}\boldsymbol{I} - c_0^I\hat{\boldsymbol{P}}_0^D(\overline{\boldsymbol{U}}). \tag{3.71}$$

Then, the only contributions to the extra stress in expression (3.69) are through the change in volume fraction and distribution of the particles. Note however that, in general, the Biot extra stress is not coaxial with $\bar{\boldsymbol{U}}$, and the Cauchy stress still needs to be computed from expression (3.68).

Aligned, magnetically anisotropic, ellipsoidal inclusions

In this case, for general loading, the particles will rotate and no further simplifications are possible. However, when the loading axes are fixed ($\bar{\boldsymbol{R}} = \boldsymbol{I}$), and $\overline{\boldsymbol{U}}$ is coaxial with the particle axes, so that $\boldsymbol{R}^p = \boldsymbol{I}$, the expression for $\tilde{\boldsymbol{Y}}$ becomes

$$\tilde{\boldsymbol{Y}}(\overline{\boldsymbol{U}}) = \left(\boldsymbol{X}^{(2)}\right)^{-1} - \boldsymbol{I} + \hat{\boldsymbol{P}}_0^I + \frac{c_0^I}{\bar{J}}\boldsymbol{I} - c_0^I\hat{\boldsymbol{P}}_0^D(\overline{\boldsymbol{U}}). \tag{3.72}$$

Moreover, when the magnetic anisotropy tensor $\boldsymbol{X}^{(2)}$ is also coaxial with $\overline{\boldsymbol{U}}$ and the particle axes, the above expression for $\tilde{\boldsymbol{Y}}(\overline{\boldsymbol{U}})$ becomes coaxial with $\overline{\boldsymbol{U}}$. It follows that

if the magnetic induction field is aligned with one of these magnetic axis—that is, in the "perfectly aligned" case—only the component in that principal direction of $\boldsymbol{X}^{(2)}$ will be involved. In addition, it can be easily verified that the extra Biot stress $\bar{\boldsymbol{T}}_B^{ex}$, as given by (3.69), becomes coaxial with $\overline{\boldsymbol{U}}$, and therefore the extra Piola-Kirchhoff stress $\bar{\boldsymbol{S}}^{ex}$ reduces to the first term in (3.65). Then, the corresponding extra Cauchy stress $\bar{\boldsymbol{T}}^{ex}$ reduces to

$$\bar{\boldsymbol{T}}^{ex} = \left(\overline{\mathbf{m}} \cdot \overline{\mathbf{b}}\right) \boldsymbol{I} - \overline{\mathbf{m}} \otimes_s \overline{\mathbf{b}} - \frac{\mu_0}{2} \left(\overline{\mathbf{m}} \cdot \overline{\mathbf{m}}\right) \boldsymbol{I} - \frac{\mu_0}{2} \bar{J} \, \frac{\partial}{\partial \bar{\boldsymbol{U}}} \left[\overline{\mathbf{m}} \cdot \hat{\boldsymbol{P}}_0^D(\bar{\boldsymbol{U}}) \overline{\mathbf{m}}\right] \bar{\boldsymbol{U}} \tag{3.73}$$

where the derivative of the scalar-valued term in the square brackets is taken with $\overline{\mathbf{m}}$ being held fixed. This result, of course, also applies to the isotropic case provided that the magnetic field $\overline{\mathbf{m}}$ be aligned with one of the principal axes of the stretch $\bar{\boldsymbol{U}}$.

Dilute limit

For small particle concentrations ($c_0^I << 1$), it follows from expressions (3.58) and (3.59) for $\tilde{\boldsymbol{X}}$ and $\boldsymbol{A}_0^I$, respectively, that $\tilde{\boldsymbol{X}} \sim (c_0^I/\bar{J}) \boldsymbol{R}^p(\overline{\boldsymbol{U}}) \boldsymbol{A}_0^I \boldsymbol{R}^{pT}(\overline{\boldsymbol{U}})$. Therefore, in the dilute limit the effect of particle distributions disappears, as expected, and the above estimate (3.61) for $\bar{\rho}_0 \, \widetilde{\Phi}_{DA}$ simplifies to

$$\bar{\rho}_0 \widetilde{\Phi}_{DA}(\bar{\boldsymbol{F}}, \overline{\mathbf{B}}) \sim \widetilde{W}_{me}^{dil}(\bar{\boldsymbol{F}}) - \frac{c_0^I}{2\mu_0 \bar{J}^2} \overline{\mathbf{B}} \cdot \left[\overline{\boldsymbol{U}} \boldsymbol{R}^p(\overline{\boldsymbol{U}}) \boldsymbol{A}_0^I \boldsymbol{R}^{pT}(\overline{\boldsymbol{U}}) \overline{\boldsymbol{U}}\right] \overline{\mathbf{B}}, \tag{3.74}$$

where $\widetilde{W}_{me}^{dil}$ is the dilute estimate for the purely mechanical problem. Then, noting that the the magnetization in this case is given by

$$\bar{\mathbf{m}} = \frac{c_0^I}{\mu_0 \bar{J}} \bar{\boldsymbol{R}} \, \bar{\boldsymbol{R}}^p \boldsymbol{A}_0^I \boldsymbol{R}^{pT} \, \bar{\boldsymbol{R}}^T \bar{\mathbf{b}}, \tag{3.75}$$

the Biot extra stress (3.69) reduces to

$$\bar{\boldsymbol{T}}_B^{ex} = \bar{J} \left(\overline{\mathbf{b}} \cdot \overline{\mathbf{m}}\right) \bar{\boldsymbol{U}}^{-1} - \bar{J} \left[\left(\overline{\boldsymbol{R}}^T \overline{\mathbf{m}}\right) \otimes_s \left(\bar{\boldsymbol{U}}^{-1} \bar{\boldsymbol{R}}^T \overline{\mathbf{b}}\right)\right] - \bar{J} \, \mathbb{H}^p(\bar{\boldsymbol{U}}) \left[\left(\bar{\boldsymbol{R}}^T \overline{\mathbf{m}}\right) \otimes_a \left(\bar{\boldsymbol{R}}^T \overline{\mathbf{b}}\right)\right], \tag{3.76}$$

where $\otimes_a$ denotes the anti-symmetric dyadic product, and $\mathbb{H}^p(\bar{\boldsymbol{U}})$ is a fourth-order tensor function of $\bar{\boldsymbol{U}}$ with Cartesian components given by

$$H^p_{ijpq} = R^p_{pk} \frac{\partial R^p_{qk}}{\partial \overline{U}_{ij}}. \tag{3.77}$$

In this expression, it is recalled that $\boldsymbol{R}^p$ is the relative particle rotation, which is a function of $\bar{\boldsymbol{U}}$. Note that the tensor $\mathbb{H}^p$ satisfies the symmetries $H^p_{ijpq} = H^p_{jipq} = -H^p_{ijqp}$, and specializes for small strains to the combination $\mathbb{P}^{-1}\mathbb{R}^T$, where $\mathbb{P}$ and $\mathbb{R}$ are the well-known Eshelby tensors characterizing particle rotations in the context of small strains and rotations (see equations (15) and (19) in Kailasam and Ponte Castañeda (1998)). Moreover, it is also relevant to note that in the limit of *infinitesimal strains and rotations* the expression (3.76) for the extra stress simplifies to

$$\bar{\boldsymbol{T}}^{ex} = \left(\overline{\mathbf{b}} \cdot \overline{\mathbf{m}}\right) \boldsymbol{I} - \frac{1}{2}\left(\overline{\mathbf{m}} \otimes \overline{\mathbf{b}} + \overline{\mathbf{b}} \otimes \overline{\mathbf{m}}\right) - \frac{1}{2}\mathbb{P}^{-1}\mathbb{R}^T\left(\overline{\mathbf{m}} \otimes \overline{\mathbf{b}} - \overline{\mathbf{b}} \otimes \overline{\mathbf{m}}\right), \tag{3.78}$$

which agrees exactly with the dilute linearized deformation theory of Siboni and Ponte Castañeda (2012a) in the "stiff matrix" limit (i.e., in the limit as the dimensionless parameter $\kappa = \bar{b}^2/(2\mu_0 G) \to 0$, where G is the shear modulus of the elastomeric matrix).

If in addition, either the material is perfectly isotropic, or both the magnetic induction field and stretch are aligned with the particle axes and magnetic anisotropy (see earlier discussion), then the magnetization $\overline{\mathbf{m}}$ and the magnetic induction field $\overline{\mathbf{b}}$ are also aligned, and the result (3.76), when converted to Cauchy stress, further reduces to

$$\bar{\boldsymbol{T}}^{ex} = \left(\overline{\mathbf{b}} \cdot \overline{\mathbf{m}}\right) \boldsymbol{I} - \overline{\mathbf{m}} \otimes \overline{\mathbf{b}}, \tag{3.79}$$

which is consistent with expression (3.73), even for large strains, when terms of order $(c_0^I)^2$ are neglected. In this case, it can be shown, by applying the relevant jump conditions at the solid/empty space interface, that the Maxwell and extra stresses exactly cancel out with the induced stresses in the empty space immediately surrounding the boundary of the solid, leaving only the purely mechanical stresses in the body. In other words, when the concentration of the particles is small, and either the particles are spherical and isotropic, or perfectly aligned with the applied mechanical and magnetic fields, any magnetorheological effects will vanish (see Siboni and Ponte Castañeda (2012a); Galipeau and Ponte Castañeda (2012)). This conclusion

is, of course, consistent with the fact that in the dilute limit the particles do not interact with each other. In particular, for these isotropic or perfectly aligned cases, any magnetostrictive strain will be necessarily of order $(c_0^I)^2$. On the other hand, when the fields are not perfectly aligned, magnetostrictive strains will arise even for dilute concentration of non-spherical particles (i.e., the effect will be of order c_0^I), as a consequence of changes in the particle orientations in the last term in expression (3.76).

3.4.2 Nonlinear ferromagnetic particle response

As already mentioned, although the magnetization in the (soft) ferromagnetic particles can be described by the linear model (2.29) at low magnetic field intensities, at sufficiently large fields it is expected to saturate and the response becomes nonlinear. An example of such a nonlinear model was given by relations (2.31) for *isotropic* ferromagnetic particles. In this subsection, we will show how we can make use of the results of the previous subsection for magnetically linear behavior to generate corresponding results for magnetically nonlinear response. Thus, it will be assumed here that the magnetostatic energy density $w_{mag}^{(2)}$ is a general convex function of the magnetic field $\mathbf{b}$ with possibly anisotropic behavior. In addition, it is assumed that

$$w_{mag}^{(2)}(\boldsymbol{R}^{(2)}, \mathbf{b}) \sim \frac{1}{2}\mathbf{b} \cdot \boldsymbol{\mu}^{(2)^{-1}}\mathbf{b}, \quad \text{for} \quad b << 1, \quad \text{and} \quad \sim \frac{1}{2\mu_0}b^2, \quad \text{for} \quad b >> 1, \tag{3.80}$$

and that $w_{mag}^{(2)}$ is "strongly convex" in $\mathbf{b}$ in the sense that there exists a convex function $f^{(2)}$ in the space of symmetric second-order tensors, such that

$$w_{mag}^{(2)}(\boldsymbol{R}^{(2)}, \mathbf{b}) = f^{(2)}\left(\boldsymbol{R}^{(2)}, \frac{1}{2}\mathbf{b} \otimes \mathbf{b}\right). \tag{3.81}$$

This notion of strong convexity was introduced by Ponte Castañeda (1992) for isotropic energy functions (in the analogous context of nonlinear dielectrics), and generalized for anisotropic energy functions (in the context of viscoplasticity) by Ponte Castañeda and Suquet (1998). For example, the isotropic material model (2.31) is strongly convex and trivially satisfies the asymptotic conditions (3.80). Under these hypotheses,

it has been shown (see Idiart and Ponte Castañeda (2007)) that

$$w_{mag}^{(2)}(\boldsymbol{R}^{(2)},\mathbf{b}) = \sup_{\boldsymbol{\mu}_L^{(2)}} \left\{ \frac{1}{2}\mathbf{b}\cdot{\boldsymbol{\mu}_L^{(2)}}^{-1}\mathbf{b} - v^{(2)}(\boldsymbol{\mu}_L^{(2)}) \right\}, \tag{3.82}$$

where

$$v^{(2)}(\boldsymbol{\mu}_L^{(2)}) = \sup_{\mathbf{b}} \left\{ \frac{1}{2}\mathbf{b}\cdot{\boldsymbol{\mu}_L^{(2)}}^{-1}\mathbf{b} - w_{mag}^{(2)}(\boldsymbol{R}^{(2)},\mathbf{b}) \right\}. \tag{3.83}$$

These expressions provide generalizations to the fully anisotropic case of results first given in the context of *isotropic* nonlinear electrostatics by Ponte Castañeda (1992).

Making use of expression (3.82) in the expression for the homogenized magnetic energy (3.45), and interchanging the supremum and infimum, which is allowed by the appropriate Saddle Point Theorem, we arrive (see Idiart and Ponte Castañeda (2007) for analogous derivations in viscoplasticity) at the following estimate for the homogenized magnetic energy

$$\widetilde{w}_{mag}(\overline{\mathbf{b}};\boldsymbol{F}_m(\mathbf{X})) \geq \sup_{\boldsymbol{\mu}_L^{(2)}} \left\{ \frac{1}{2}\bar{\mathbf{b}}\cdot\tilde{\boldsymbol{\mu}}_L^{-1}\bar{\mathbf{b}} - c^I v^{(2)}(\boldsymbol{\mu}_L^{(2)}) \right\}, \tag{3.84}$$

where $\tilde{\boldsymbol{\mu}}_L$ is the effective magnetic permeability of a "linear comparison composite" (LCC) with the same matrix phase with magnetic permeability μ_0, but with the nonlinear particle phase replaced by a fictitious linear anisotropic phase with magnetic permeability $\boldsymbol{\mu}_L^{(2)}$. This means that an estimate for the effective energy $\widetilde{w}_{mag}$ of the material with nonlinear particles can be obtained in terms of the effective energy (3.48) of the material with linear, anisotropic particles, provided that the magnetic permeability $\boldsymbol{\mu}^{(2)}$ in (3.48) be identified with the solution of the optimization problem (3.84) for $\boldsymbol{\mu}_L^{(2)}$. Note that these optimized values of the variables $\boldsymbol{\mu}_L^{(2)}$, which will be labeled $\hat{\boldsymbol{\mu}}_L^{(2)}$, are functions of the magnetic field $\bar{\mathbf{b}}$ (and therefore no longer constant).

Next, introducing the magnetic susceptibility $\boldsymbol{\chi}_L^{(2)} = \boldsymbol{I} - \mu_0{\boldsymbol{\mu}_L^{(2)}}^{-1}$ of the particles in the LCC, it is noted that the nonlinear corrector function $v^{(2)}(\boldsymbol{\mu}_L^{(2)})$ may alternatively be written

$$v^{(2)}(\boldsymbol{\mu}_L^{(2)}) = \sup_{\mathbf{b}} \left\{ \frac{1}{2\mu_0}\mathbf{b}\cdot\boldsymbol{\chi}_L^{(2)}\mathbf{b} - \rho_0^{(2)}\varphi_{mag}^{(2)}({\overline{\boldsymbol{R}}^{(2)}}^T\mathbf{b}) \right\} = v_p^{(2)}(\boldsymbol{\chi}_L^{(2)}). \tag{3.85}$$

It then follows that the expression (3.84) may also be rewritten in the form

$$\widetilde{w}_{mag}(\overline{\mathbf{b}}; \boldsymbol{F}_m(\mathbf{X})) \geq \frac{1}{2\mu_0}\bar{b}^2 - \inf_{\boldsymbol{\chi}_L^{(2)}} \left\{ \frac{1}{2}\bar{\mathbf{b}} \cdot \tilde{\boldsymbol{\chi}}_L \bar{\mathbf{b}} + c^I v_p^{(2)}(\boldsymbol{\chi}_L^{(2)}) \right\}, \tag{3.86}$$

where $\tilde{\boldsymbol{\chi}}_L$ and $\boldsymbol{\chi}_L^{(2)}$ are related in the same way as $\tilde{\boldsymbol{\chi}}$ and $\boldsymbol{\chi}^{(2)}$ in expression (3.54).

Then, following parallel developments in the previous subsection for the linear, anisotropic particles, the particle rotation $\boldsymbol{R}^p$, relative to the macroscopic rotation $\overline{\boldsymbol{R}}$, is defined via $\boldsymbol{R}^p = \overline{\boldsymbol{R}}^T \overline{\boldsymbol{R}}^{(2)}$, so that letting $\boldsymbol{\chi}_L^{(2)} = \overline{\boldsymbol{R}}^{(2)} \boldsymbol{X}_L^{(2)} \overline{\boldsymbol{R}}^{(2)^T}$, it follows that $\tilde{\boldsymbol{\chi}}_L$ can also be written in the form

$$\tilde{\boldsymbol{\chi}}_L(\bar{\boldsymbol{F}}) = \overline{\boldsymbol{R}} \tilde{\boldsymbol{X}}_L(\overline{\boldsymbol{U}}; \boldsymbol{X}_L^{(2)}) \overline{\boldsymbol{R}}^T, \tag{3.87}$$

where $\tilde{\boldsymbol{X}}_L(\overline{\boldsymbol{U}}; \boldsymbol{X}_L^{(2)})$ is still given by expression (3.58), except that now

$$\boldsymbol{A}_0^I = \left[\left(\boldsymbol{X}_L^{(2)} \right)^{-1} - \boldsymbol{I} + \hat{\boldsymbol{P}}_0^I \right]^{-1}. \tag{3.88}$$

In these expressions, c_0^I is again the prescribed initial (in the reference configuration) particle volume fraction. Note that the dependence of $\tilde{\boldsymbol{X}}_L$ on $\overline{\boldsymbol{U}}$, through $\boldsymbol{R}^p$ and $\hat{\boldsymbol{P}}_0^D$, as well as on the magnetic susceptibility of the particles $\boldsymbol{X}_L^{(2)}$ in the LCC has been made explicit in these expressions, for clarity.

In addition, making use of the expression $\boldsymbol{\chi}_L^{(2)} = \overline{\boldsymbol{R}}^{(2)} \boldsymbol{X}_L^{(2)} \overline{\boldsymbol{R}}^{(2)^T}$, it follows from relation (3.85) for $v_p^{(2)}$ that

$$\begin{aligned} v_p^{(2)}(\boldsymbol{\chi}_L^{(2)}) &= \sup_{\mathbf{b}} \left\{ \frac{1}{2\mu_0} \mathbf{b} \cdot \left(\overline{\boldsymbol{R}}^{(2)} \boldsymbol{X}_L^{(2)} \overline{\boldsymbol{R}}^{(2)^T} \right) \mathbf{b} - \rho_0^{(2)} \varphi_{mag}^{(2)}(\overline{\boldsymbol{R}}^{(2)^T} \mathbf{b}) \right\} \\ &= \sup_{\mathbf{B}} \left\{ \frac{1}{2\mu_0} \mathbf{B} \cdot \boldsymbol{X}_L^{(2)} \mathbf{B} - \rho_0^{(2)} \Phi_{mag}^{(2)}(\mathbf{B}) \right\} = V^{(2)}(\boldsymbol{X}_L^{(2)}). \end{aligned} \tag{3.89}$$

Finally, substituting expressions (3.86), together with expressions (3.87) to (3.89), into expression (3.44), and subtracting the vacuum magnetic energy, we arrive at the (fully Lagrangian) estimate for the free-energy density of the nonlinear magnetoelastic

composite

$$\bar{\rho}_0\widetilde{\Phi}_{DA}(\bar{\boldsymbol{F}},\overline{\boldsymbol{U}}) = \widetilde{W}_{me}(\bar{\boldsymbol{F}}) - \inf_{\boldsymbol{X}_L^{(2)}} \left\{ \frac{1}{2\mu_0\bar{J}} \left(\overline{\boldsymbol{U}}\,\overline{\mathbf{B}}\right) \cdot \left[\tilde{\boldsymbol{X}}_L(\overline{\boldsymbol{U}};\boldsymbol{X}_L^{(2)})\right] \left(\overline{\boldsymbol{U}}\,\overline{\mathbf{B}}\right) + c_0^I V^{(2)}(\boldsymbol{X}_L^{(2)}) \right\}. \tag{3.90}$$

It should be pointed out in connection with this estimate that the inequalities in expressions (3.44) and (3.86) are inconsistent, and therefore the estimate is no longer a bound for $\widetilde{\Phi}_{DA}$ (although it should still be a very good stationary estimate).

On account of the convexity properties of expression (3.90), the optimality condition for the variables $\boldsymbol{X}_L^{(2)}$ in expression (3.90) is given by

$$-\frac{1}{2\mu_0 c_0^I \bar{J}} \frac{\partial}{\partial \boldsymbol{X}_L^{(2)}} \left[\left(\overline{\boldsymbol{U}}\,\overline{\mathbf{B}}\right) \cdot \tilde{\boldsymbol{X}}_L(\overline{\boldsymbol{U}};\hat{\boldsymbol{X}}_L^{(2)}) \left(\overline{\boldsymbol{U}}\,\overline{\mathbf{B}}\right) \right] \in \partial V^{(2)}(\hat{\boldsymbol{X}}^{(2)}), \tag{3.91}$$

where $\partial V^{(2)}$ denotes the subdifferential of the convex (but possibly non-smooth) function $V^{(2)}$ (see Idiart and Ponte Castañeda (2007)).

Given expression (3.90) for $\widetilde{\Phi}_{DA}$, the average Piola-Kirchhoff stress $\bar{\boldsymbol{S}}$ and Lagrangian magnetic field $\overline{\mathbf{H}}$ may then be computed in terms of the average deformation $\bar{\boldsymbol{F}}$ and magnetic induction field $\overline{\mathbf{B}}$ via expressions (3.11). However, it is important to note in this context that, in view of the optimality condition (3.91), the requisite derivatives of the expression (3.90) with respect to $\overline{\boldsymbol{F}}$ and $\overline{\mathbf{B}}$ may be evaluated with the variable $\boldsymbol{X}_L^{(2)}$ held fixed at its optimal value $\hat{\boldsymbol{X}}_L^{(2)}$, as determined by (3.91). Therefore, the expressions for the macroscopic Piola-Kirchhoff stress $\bar{\boldsymbol{S}}$ and Lagrangian magnetic field $\overline{\mathbf{H}}$ will still be given by the same expressions (3.62), and (3.63) to (3.65), as in the (magnetically) linear theory, except that now the variable $\boldsymbol{X}_L^{(2)}$ in these expressions should be replaced by $\hat{\boldsymbol{X}}_L^{(2)}$ (as determined by (3.91)), which is no longer constant and depends on the applied fields $\bar{\boldsymbol{F}}$ and $\overline{\mathbf{B}}$).

A corresponding Eulerian formulation may also be obtained starting from expression (3.86). The resulting expressions for the macroscopic Cauchy stress and (Eulerian) magnetization will still be given by expressions (3.67), together with (3.68) to (3.70), except that the variables $\boldsymbol{X}^{(2)}$ in these expressions must be substituted by the corresponding optimal values $\hat{\boldsymbol{X}}^{(2)}$, as determined by expression (3.91). In addition, the simplifications mentioned at the end of the previous section for isotropic, perfectly aligned and dilute systems with linear magnetic response also carry over for nonlinear magnetic behavior, with the appropriate reinterpretations.

3.4.3 Permanent magnetization particle response

It is possible that the rigid particles may exhibit some permanent magnetization within the composite. Recall from section 2.2.2 that in such a case the magnetization behavior of the rigid particles is characterized by a permanent magnetization $\mathbf{m}_0^{(2)}$ and a differential susceptibility $\boldsymbol{\chi}^{(2)}$, both of which depend on the rotation of the particles as well as a "specific heat" $\mathfrak{c}^{(2)}$

For the purposes of homogenization, we use the un-deformed un-magnetized state as the reference configuration. Then this composite is subjected to a large macroscopic magnetic field $\bar{\mathbf{b}}$ which causes the particles to become magnetized. For many inclusion materials the particles will retain their magnetization even when this applied field is removed. In this case the composite would also exhibit some permanent macroscopic magnetization $\tilde{\mathbf{m}}_0(\bar{\boldsymbol{F}})$ when $\bar{\mathbf{b}} = 0$. Additionally the magnetic field surrounding each particle will generate a corresponding stress field which may produce significant macroscopic magnetic stresses in the composite. After an MRE undergoes the previously mentioned magnetic loading cycle, we can use the partial decoupling approximation to determine the macroscopic stress and magnetization.

When the particles are described locally as having a constant (linear) differential susceptibility and permanent magnetization, as in equation (2.33), the composite also has a constant differential susceptibility. This allows us to use the linear homogenization framework in section 3.4.1 to compute the differential susceptibility of the composite based on the differential susceptibility of the constituent phases. We can also use Levin's relation for two-phase composites to determine the remnant magnetization of the composite $\tilde{\mathbf{m}}_0(\bar{\boldsymbol{F}})$ and the effective "specific heat" $\tilde{\mathfrak{c}}(\bar{\boldsymbol{F}})$.

Using the partial decoupling approximation, the magnetic homogenization produces an energy function of the form

$$\tilde{w}_{mag}(\bar{\boldsymbol{F}}, \bar{\mathbf{b}}) = \frac{1}{2\mu_0}\bar{\mathbf{b}} \cdot \bar{\mathbf{b}} - \frac{1}{2\mu_0}\bar{\mathbf{b}} \cdot \tilde{\boldsymbol{\chi}}(\bar{\boldsymbol{F}})\bar{\mathbf{b}} - \bar{\mathbf{b}} \cdot \tilde{\mathbf{m}}_0(\bar{\boldsymbol{F}}) - \frac{1}{2}\tilde{\mathfrak{c}}(\bar{\boldsymbol{F}}) \tag{3.92}$$

where

$$\tilde{\boldsymbol{\chi}}(\bar{\boldsymbol{F}}) = c^{\mathrm{I}}\left[\left(\boldsymbol{\chi}^{(2)}\right)^{-1} - \boldsymbol{I} + \mu_0 \boldsymbol{P}^{\mathrm{I}} + c^{\mathrm{I}}(\boldsymbol{I} - \mu_0 \boldsymbol{P}^{\mathrm{D}})\right]^{-1} \tag{3.93}$$

which is the same as equation (3.54). The corresponding permanent magnetization is given by

$$\tilde{\mathbf{m}}_0(\bar{\boldsymbol{F}}) = \tilde{\boldsymbol{\chi}}(\bar{\boldsymbol{F}})\left(\boldsymbol{\chi}^{(2)}\right)^{-1}\mathbf{m}_0^{(2)} \tag{3.94}$$

and the "specific heat"

$$\tilde{\mathfrak{c}}(\bar{\boldsymbol{F}}) = \mu_0 \mathbf{m}_0^{(2)} \cdot \left(\boldsymbol{\chi}^{(2)}\right)^{-1} \tilde{\boldsymbol{\chi}}(\bar{\boldsymbol{F}}) \left(\boldsymbol{\chi}^{(2)}\right)^{-1} \mathbf{m}_0^{(2)} - \mu_0 c^{\mathrm{I}} \mathbf{m}_0^{(2)} \cdot \left(\boldsymbol{\chi}^{(2)}\right)^{-1} \mathbf{m}_0^{(2)}. \tag{3.95}$$

In these expressions, we have assumed that $\mathfrak{c}^{(2)} = 0$. (If $\mathfrak{c}^{(2)} \neq 0$ it changes the total energy; however it produces no contribution to the stress or the magnetization). However $\tilde{\mathfrak{c}}(\bar{\boldsymbol{F}})$ depends on the macroscopic deformation and contributes to the stress so it cannot be ignored. We also recall that $\boldsymbol{\chi}^{(2)}$ and $\mathbf{m}_0^{(2)}$ depend on the rotation of the particles and therefore depend on the macroscopic deformation. These quantities can be related to the fixed Lagrangian counterparts via the relations $\mathbf{m}_0^{(2)} = \overline{\boldsymbol{R}}^{(2)} \mathbf{M}_0^{(2)}$ and $\boldsymbol{\chi}^{(2)} = \overline{\boldsymbol{R}}^{(2)} \boldsymbol{X}^{(2)} \overline{\boldsymbol{R}}^{(2)^T}$.

Using expressions (3.94) and (3.95), the energy given by expression (3.92) can be written as

$$\begin{aligned} \tilde{w}_{mag}(\bar{\boldsymbol{F}}, \bar{\mathbf{b}}) = {} & \frac{1}{2\mu_0} \bar{\mathbf{b}} \cdot \bar{\mathbf{b}} \\ & - \frac{1}{2\mu_0} \left(\bar{\mathbf{b}} + \left(\boldsymbol{\chi}^{(2)}\right)^{-1} \mu_0 \mathbf{m}_0^{(2)}\right) \cdot \tilde{\boldsymbol{\chi}}(\bar{\boldsymbol{F}}) \left(\bar{\mathbf{b}} + \left(\boldsymbol{\chi}^{(2)}\right)^{-1} \mu_0 \mathbf{m}_0^{(2)}\right) \\ & + \mu_0 c^{\mathrm{I}} \mathbf{m}_0^{(2)} \cdot \left(\boldsymbol{\chi}^{(2)}\right)^{-1} \mathbf{m}_0^{(2)}. \end{aligned} \tag{3.96}$$

The corresponding amended free-energy function for the composite is then given by

$$\begin{aligned} \tilde{W}_{mag}(\bar{\boldsymbol{F}}, \bar{\mathbf{B}}) = {} & \frac{1}{2\mu_0 \bar{J}} \bar{\mathbf{B}} \cdot \bar{\boldsymbol{U}}^2 \bar{\mathbf{B}} \\ & - \frac{\bar{J}}{2\mu_0} \left(\frac{\bar{\boldsymbol{U}} \bar{\mathbf{B}}}{\bar{J}} + \boldsymbol{R}^p(\bar{\boldsymbol{U}}) \left(\boldsymbol{X}^{(2)}\right)^{-1} \mathbf{M}_0^{(2)}\right) \cdot \tilde{\boldsymbol{X}} \left(\frac{\bar{\boldsymbol{U}} \bar{\mathbf{B}}}{\bar{J}} + \boldsymbol{R}^p(\bar{\boldsymbol{U}}) \left(\boldsymbol{X}^{(2)}\right)^{-1} \mathbf{M}_0^{(2)}\right) \\ & \frac{\mu_0 c_0^{\mathrm{I}}}{2} \mathbf{M}_0^{(2)} \cdot \left(\boldsymbol{X}^{(2)}\right)^{-1} \mathbf{M}_0^{(2)} \end{aligned} \tag{3.97}$$

with

$$\tilde{\boldsymbol{X}}(\bar{\boldsymbol{U}}) = \frac{c_0^{\mathrm{I}}}{\bar{J}} \left[\boldsymbol{R}^p(\bar{\boldsymbol{U}}) (\boldsymbol{A}_0^{\mathrm{I}})^{-1} \boldsymbol{R}^{p^{\mathrm{T}}}(\bar{\boldsymbol{U}}) + \frac{c_0^{\mathrm{I}}}{\bar{J}} \boldsymbol{I} - c_0^{\mathrm{I}} \hat{\boldsymbol{P}}_0^{\mathrm{D}}(\bar{\boldsymbol{U}})\right]^{-1}. \tag{3.98}$$

It is emphasized that $\mathbf{M}_0^{(2)}$ and $\boldsymbol{X}^{(2)}$ are constant.

The magnetic constitutive relation that results from the preceding homogenized

energy function is

$$\bar{\mathbf{m}} = \frac{1}{\mu_0}\tilde{\boldsymbol{\chi}}(\bar{\boldsymbol{F}})\bar{\mathbf{b}} + \tilde{\boldsymbol{\chi}}(\bar{\boldsymbol{F}})\left(\boldsymbol{\chi}^{(2)}\right)^{-1}\mathbf{m}_0^{(2)}. \tag{3.99}$$

The corresponding Biot stress is given by an expression of the form

$$\begin{aligned}\bar{\boldsymbol{T}}_{\mathrm{B}}^{\mathrm{ex}} &= \bar{J}(\bar{\mathbf{b}}\cdot\bar{\mathbf{m}})\bar{\boldsymbol{U}}^{-1} - \bar{J}\left[(\bar{\boldsymbol{R}}^{\mathrm{T}}\bar{\mathbf{m}})\otimes_{\mathrm{s}}(\bar{\boldsymbol{U}}^{-1}\bar{\boldsymbol{R}}^{\mathrm{T}}\bar{\mathbf{b}})\right] \\ &+ \frac{\mu_0\bar{J}^2}{2c_0^{\mathrm{I}}}\frac{\partial}{\partial\bar{\boldsymbol{U}}}\left[(\bar{\boldsymbol{R}}^{\mathrm{T}}\bar{\mathbf{m}})\cdot\tilde{\boldsymbol{Y}}(\bar{\boldsymbol{R}}^{\mathrm{T}}\bar{\mathbf{m}})\right] - \mu_0\bar{J}\frac{\partial}{\partial\bar{\boldsymbol{U}}}\left[(\bar{\boldsymbol{R}}^{\mathrm{T}}\bar{\mathbf{m}})\cdot\boldsymbol{R}^{p}(\bar{\boldsymbol{U}})\left(\boldsymbol{X}^{(2)}\right)^{-1}\mathbf{M}_0^{(2)}\right]\end{aligned} \tag{3.100}$$

with

$$\tilde{\boldsymbol{Y}}(\bar{\boldsymbol{U}}) = \frac{c_0^{\mathrm{I}}}{\bar{J}}\tilde{\boldsymbol{X}}^{-1} = \boldsymbol{R}^{p}(\bar{\boldsymbol{U}})(\boldsymbol{A}_0^{\mathrm{I}})^{-1}\boldsymbol{R}^{p^{\mathrm{T}}}(\bar{\boldsymbol{U}}) + \frac{c_0^{\mathrm{I}}}{\bar{J}}\boldsymbol{I} - c_0^{\mathrm{I}}\hat{\boldsymbol{P}}_0^{\mathrm{D}}. \tag{3.101}$$

Note that this expression is the same as equation (3.69) with the addition of the last term. We recall from before that derivatives with respect to $\bar{\boldsymbol{U}}$ are taken with $(\bar{\boldsymbol{R}}^{\mathrm{T}}\bar{\mathbf{m}})$ held fixed. It should be emphasized that this material has a magnetic stress even when the applied magnetic flux $\bar{\mathbf{b}} = 0$ because $\bar{\mathbf{m}} \neq 0$ due to the permanent magnetization.

No differential susceptibility, $\boldsymbol{X}^{(2)} = 0$

An important special case to consider is when the particles are permanent magnets with no differential susceptibility such that $\boldsymbol{X}^{(2)} = 0$. In this limit the energy functions reduce to

$$\begin{aligned}\tilde{w}_{mag}(\bar{\boldsymbol{F}},\bar{\mathbf{b}}) = \frac{1}{2\mu_0}\bar{\mathbf{b}}\cdot\bar{\mathbf{b}} - c^{\mathrm{I}}\bar{\mathbf{b}}\cdot\mathbf{m}_0^{(2)} \\ - \frac{\mu_0 c^{\mathrm{I}}}{2}\mathbf{m}_0^{(2)}\cdot\mathbf{m}_0^{(2)} + \frac{\mu_0 c^{\mathrm{I}}}{2}\mathbf{m}_0^{(2)}\cdot\mu_0\boldsymbol{P}^{\mathrm{I}}\mathbf{m}_0^{(2)} \\ + \frac{\mu_0(c^{\mathrm{I}})^2}{2}\mathbf{m}_0^{(2)}\cdot\mathbf{m}_0^{(2)} - \frac{\mu_0(c^{\mathrm{I}})^2}{2}\mathbf{m}_0^{(2)}\cdot\mu_0\boldsymbol{P}^{\mathrm{D}}\mathbf{m}_0^{(2)},\end{aligned} \tag{3.102}$$

while the amended free energy reduces to

$$\begin{aligned}\tilde{W}_{mag}(\bar{\boldsymbol{F}},\bar{\mathbf{B}}) = \frac{1}{2\mu_0\bar{J}}\bar{\mathbf{B}}\cdot\bar{\boldsymbol{U}}^2\bar{\mathbf{B}} - \frac{c_0^{\mathrm{I}}}{\bar{J}}\bar{\mathbf{B}}\cdot\bar{\boldsymbol{U}}\boldsymbol{R}^p(\bar{\boldsymbol{U}})\mathbf{M}_0^{(2)}. \\ - \frac{\mu_0 c_0^{\mathrm{I}}}{2}\mathbf{M}_0^{(2)}\cdot\mathbf{M}_0^{(2)} + \frac{\mu_0 c_0^{\mathrm{I}}}{2}\mathbf{M}_0^{(2)}\cdot\hat{\boldsymbol{P}}_0^{\mathrm{I}}\mathbf{M}_0^{(2)} \\ + \frac{\mu_0(c_0^{\mathrm{I}})^2}{2\bar{J}}\mathbf{M}_0^{(2)}\cdot\mathbf{M}_0^{(2)} - \frac{\mu_0(c_0^{\mathrm{I}})^2}{2}\boldsymbol{R}^p(\bar{\boldsymbol{U}})\mathbf{M}_0^{(2)}\cdot\hat{\boldsymbol{P}}_0^{\mathrm{D}}(\bar{\boldsymbol{U}})\boldsymbol{R}^p(\bar{\boldsymbol{U}})\mathbf{M}_0^{(2)}. \quad (3.103)\end{aligned}$$

On the other hand, the magnetic constitutive relation that results when $\boldsymbol{X}^{(2)} = 0$ becomes

$$\bar{\mathbf{m}} = \tilde{\mathbf{m}}_0 = \frac{c_0^{\mathrm{I}}}{\bar{J}}\bar{\boldsymbol{R}}\boldsymbol{R}^p(\bar{\boldsymbol{U}})\mathbf{M}_0^{(2)} = \frac{c_0^{\mathrm{I}}}{\bar{J}}\bar{\boldsymbol{R}}^{(2)}\mathbf{M}_0^{(2)}. \quad (3.104)$$

The corresponding Biot stress is given by the following expression

$$\begin{aligned}\bar{\boldsymbol{T}}_{\mathrm{B}}^{\mathrm{ex}} = \bar{J}(\bar{\mathbf{b}}\cdot\bar{\mathbf{m}})\bar{\boldsymbol{U}}^{-1} - \bar{J}\left[(\bar{\boldsymbol{R}}^{\mathrm{T}}\bar{\mathbf{m}})\otimes_{\mathrm{s}}(\bar{\boldsymbol{U}}^{-1}\bar{\boldsymbol{R}}^{\mathrm{T}}\bar{\mathbf{b}})\right] - \bar{J}\frac{\partial}{\partial\bar{\boldsymbol{U}}}\left[(\bar{\boldsymbol{R}}^{\mathrm{T}}\bar{\mathbf{b}})\cdot\boldsymbol{R}^p(\bar{\boldsymbol{U}})\mathbf{M}_0^{(2)}\right] \\ - \frac{\mu_0}{2}\bar{J}(\bar{\mathbf{m}}\cdot\bar{\mathbf{m}})\bar{\boldsymbol{U}}^{-1} - \frac{\mu_0}{2}\bar{J}^2\frac{\partial}{\partial\bar{\boldsymbol{U}}}\left[(\bar{\boldsymbol{R}}^{\mathrm{T}}\bar{\mathbf{m}})\cdot\hat{\boldsymbol{P}}_0^{\mathrm{D}}(\bar{\boldsymbol{U}})(\bar{\boldsymbol{R}}^{\mathrm{T}}\bar{\mathbf{m}})\right] \\ - \mu_0(c_0^{\mathrm{I}})^2\frac{\partial}{\partial\bar{\boldsymbol{U}}}\left[(\hat{\boldsymbol{P}}_0^{\mathrm{D}}\boldsymbol{R}^p\bar{\mathbf{m}})\cdot\boldsymbol{R}^p(\bar{\boldsymbol{U}})\mathbf{M}_0^{(2)}\right]. \quad (3.105)\end{aligned}$$

Note that when deriving this expression from the energy, the terms in the middle line of expression (3.103) are constant with respect to deformation and do not contribute to the total stress. We also point out that expression (3.105) is a specialization of expression (3.100). This can be shown directly by substituting expression (3.101) into expression (3.100) and taking the limit as $\boldsymbol{X}^{(2)} \to 0$.

New reference configuration for MREs with permanent magnet inclusions

In the previous section the un-magnetized un-deformed state was taken as the reference configuration. Once the composite exhibits a permanent magnetization, either through a change in temperature or a magnetic loading cycle, the overall composite will obtain the properties of a deformable permanent magnet. One effect is that the MRE will deform without the application of traction when free floating in the vacuum as a result of the magnetic stress in and around it. It may be tempting to define a new reference state based on this spontaneous deformation. Unfortunately, there are many ways to define the new reference state, each of which will produce different

results.

We could set either the macroscopic $\bar{\mathbf{b}} = 0$ or $\bar{\mathbf{h}} = 0$, and solve for the magnetostriction. However, the choice between $\bar{\mathbf{b}} = 0$ or $\bar{\mathbf{h}} = 0$ is arbitrary and the difference is non-trivial even in the simplest case. A different magnetostriction (and therefore a different reference configuration) will be determined for each definition. For these cases, the deformed state also depends on the orientation of the sample relative to the microstructure. This means that for each orientation a different reference configuration would be needed.

Another option is to solve for the deformation when the sample is free floating in vacuum and the far field vanishes. This represents the most realistic new reference state for the sample and it is a uniquely determined state which depends on the effective susceptibility and permanent magnetization. However this deformation is non-uniform and depends on the macroscopic shape and aspect ratio of the sample.

To the best of our knowledge there is no way around these inconsistencies and a new reference configuration as a material property cannot be defined. For these reasons the un-magnetized configuration will be taken as the reference state in this work.

3.5 Concluding remarks

The constitutive theory proposed in this work for MREs at finite strains is described by expressions (3.67) to (3.70), and requires the solution of the "purely mechanical" homogenization problem (3.42), together with corresponding estimates for the particle rotations. Such estimates for the mechanical problem may be generated by means of either the "tangent" (Ponte Castañeda and Tiberio, 2000), or the "generalized secant" (Lopez-Pamies and Ponte Castañeda, 2006a) nonlinear second-order homogenization methods, in terms of corresponding estimates for appropriately defined "linear comparison composites." These in turn may be obtained from the work of Ponte Castañeda and Willis (1995) for linear composites with particulate microstructures. This approach has already been implemented in this thesis and a companion paper, Galipeau and Ponte Castañeda (2013), where use is made of the general two-dimensional estimates of Lopez-Pamies and Ponte Castañeda (2006a) for reinforced elastomers with elliptical fibers to generate, via the above-described theory, explicit estimates for MREs. It incorporates the effects of particle concentration, shape, orien-

tation and distribution. On the other hand, estimates for the magnetostrictive strain in three-dimensional, aligned particle systems, subjected to aligned loading, will be given in Galipeau and Ponte Castañeda (2012) as well as this thesis. The results demonstrate the significant effect of particle shape and concentration on the magnetostrictive capabilities of these materials. At a more elementary level these models have the distinctive feature that they predict non-trivial magnetoelastic effects, even when neither constituent exhibits such coupled behaviors by itself.

Although in principle the "partial decoupling" approximation introduced in this work is not strictly necessary, as we have seen, it does simplify the homogenization problem considerably by reducing it to two simpler problems: a purely mechanical problem and a purely magnetic problem (in the deformed configuration). It was argued that this approximation should be very good at least for spherical particles as well as for aligned non-spherical particles, when the applied magnetic and mechanical fields are also aligned. Moreover Siboni and Ponte Castañeda (2012a) have shown in the small-deformation context that the decoupling approximation is of higher order in the "stiff matrix" limit (i.e., in the limit as $\kappa = \bar{b}^2/(2\mu_0 G) \to 0$). It is certainly our expectation, although this remains to be verified, that the decoupling approximation should also lead to accurate estimates in the stiff matrix limit for large deformations when the loading is not aligned with the particles and magnetic axes. However, independent of how accurate the model will turn out to be for specific cases, the model is already useful in identifying the basic mechanisms in these materials, which in turn can be of great help in the optimization of the microstructure for achieving the largest possible magnetostrictive strains.

The microstructure has been idealized to consist of perfectly aligned particles of identical shape in the first treatment of the problem. It should be emphasized that the approach is much more general and that it could be easily generalized to account for random distributions of orientations with a given texture as specified by an orientation distribution function. This would add some practical complications from the additional microstructural variables but the theory extends naturally. It is our expectation that the perfectly aligned systems that we have considered in this work would be fairly accurate for highly textured systems, at least away from any instabilities. In this connection, it should be noted that the theory could also be used to estimate the onset of macroscopic instabilities, as has already been done for purely elastic systems (Lopez-Pamies and Ponte Castañeda, 2006b; Michel et al., 2007). This exciting pos-

sibility will be taken up in future work. Another promising direction for future work would be to use more sophisticated theories to account for the ferromagnetic behavior of the particles, such as the "constrained theory" of micromagnetics of DeSimone and James (2002), which would also allow the incorporation of magnetostrictive behavior for the particles themselves.

Finally, it is also important to remark that the techniques that have been developed in this work in the context of MREs may be adapted/generalized to other types of active material systems, such as electroactive polymers. The general homogenization framework developed here could also be applied to electro- and magnetoelastic material systems with other types of microstructures, such as the granular microstructures observed in polycrystalline materials. Clearly, these and other homogenization techniques can be very useful in helping to characterize the constitutive response of electro- or magneto-active material systems, as they have been useful in helping to describe the purely mechanical behavior of many heterogenous material systems.

Chapter 4

2-D model including the effects of particle rotation

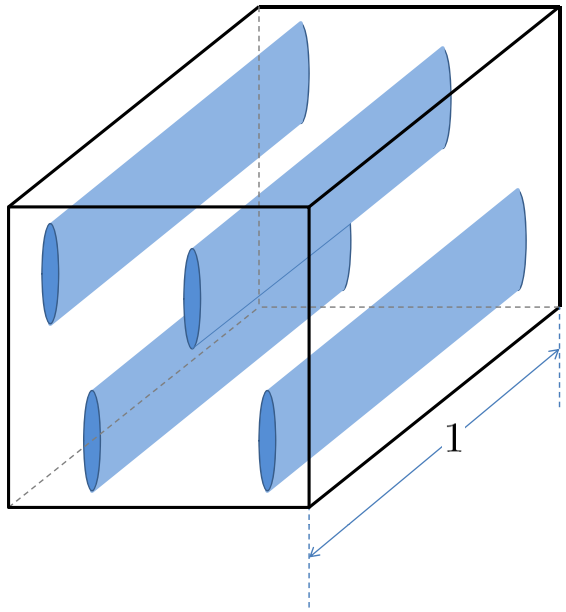

Figure 4.1: Graphical depiction of long cylindrical fibers with elliptical cross section, distributed randomly in a soft elastomer matrix.

In this chapter we will make use of the general results of Chapter 3 (Ponte Castañeda and Galipeau, 2011) to provide explicit expressions for the effective energy function $\widetilde{W}(\bar{\boldsymbol{F}}, \bar{\mathbf{B}})$ for a special class of MREs composed of aligned, rigid, magnetizable fibers of elliptical cross-section embedded in a soft magnetically insensitive matrix, as shown schematically in Figure 4.1. Note that the rigid fibers prevent stretch in the direction of their long axis, forcing all the deformation to take place in the transverse plane. The composite can only undergo a pure shear deformation because of the incompressibility of the matrix and fibers. This can be described in terms of the stretch and a loading angle. Furthermore, it should be noted that this two-dimensional microstructure may be expected to exhibit larger strains compared to 3D particles because of the enhanced magnetic interactions between the fibers and the externally applied magnetic field.

Chapter 3 applied the general homogenization framework to MREs and obtained estimates for the effective stored-energy function $\widetilde{W}$ for the class of magnetoelastic composites consisting of rigid, ellipsoidal particles with energy function (2.31) that are distributed randomly in an elastic matrix with energy function (2.21). This estimate made use of a certain "partial decoupling approximation" which is exact in the "stiff matrix" limit when the elasticity of the matrix is large compared to the magnetic

torques, but still small compared to the stiffness of the particles (see also Siboni and Ponte Castañeda (2012a)). The resulting estimate can be written in the form

$$\widetilde{W}(\bar{\boldsymbol{F}},\bar{\boldsymbol{B}}) = \widetilde{W}_{\rm me}(\bar{\boldsymbol{F}}) + \widetilde{W}_{\rm mag}(\bar{\boldsymbol{F}},\bar{\boldsymbol{B}}), \tag{4.1}$$

where $\widetilde{W}_{\rm me}$ is the effective stored-energy function of the "purely mechanical" problem (i.e., with $\bar{\boldsymbol{B}} = \boldsymbol{0}$). $\widetilde{W}_{\rm mag}$ corresponds to the effective magnetostatic energy of the composite in the current configuration, as determined by the purely mechanical problem. It is emphasized that the decomposition (4.1) of the effective magnetoelastic energy function of the composite in terms of a purely mechanical term and a second term containing the magnetoelastic interactions is not expected for more general magnetoelastic composites. It is however quite natural for the class of MRE composites of interest in this work. For this reason we will refer to the stress associated with the purely mechanical terms as the "mechanical" stress and to the rest as the "magnetic" stress. For example, we will refer to $\bar{\boldsymbol{S}}^{\rm me} = \partial\widetilde{W}_{\rm me}/\partial\bar{\boldsymbol{F}}$ and $\bar{\boldsymbol{S}}^{\rm mag} = \partial\widetilde{W}_{\rm mag}/\partial\bar{\boldsymbol{F}}$, such that $\bar{\boldsymbol{S}} = \bar{\boldsymbol{S}}^{\rm me} + \bar{\boldsymbol{S}}^{\rm mag}$, as the mechanical and magnetic parts of the total Piola-Kirchhoff stress $\bar{\boldsymbol{S}}$, respectively.

In this chapter we will use the *generalized* neo-Hookean model to represent the mechanical constitutive response of the incompressible rubber matrix. The mechanical stored-energy function of the matrix will be taken to be of the form $W^{(1)}_{me}(\boldsymbol{F}) = g^{(1)}(I)$, where $g^{(1)}$ is some appropriately constructed function of the first invariant $I = \operatorname{tr}\left(\boldsymbol{F}^{\rm T}\boldsymbol{F}\right)$. In particular we will provide explicit results for the Gent model (Gent, 1996). This model has two free parameters: G, the initial shear modulus of the composite, and J_m, the lockup parameter characterizing the limiting extensibility of the elastomer. It is given by the expression

$$W^{(1)}_{me}(\boldsymbol{F}) = g^{(1)}(I) = -\frac{GJ_{\rm m}}{2}\ln\left[1 - \frac{I-3}{J_{\rm m}}\right]. \tag{4.2}$$

Note that it reduces to the standard neo-Hookean material in the limit as $J_{\rm m} \to \infty$. The associated magnetoelastic energy function for the elastomer is given by

$$W^{(1)}(\boldsymbol{F},\mathbf{B}) = W^{(1)}_{me}(\boldsymbol{F}) + \frac{\boldsymbol{F}\mathbf{B}\cdot\boldsymbol{F}\mathbf{B}}{2J\mu_0}, \tag{4.3}$$

where the magnetic term in the right-hand side of this equation ensures that the non-magnetic rubber exhibits no magnetization or, in other words, has the same

magnetic constitutive response as vacuum. Because this term is at the origin of the Maxwell stress in a non-magnetic material, we refer to it as the Maxwell term in the magnetoelastic energy function.

On the other hand the constitutive response of the rigid magnetic particles is described by a function of the form

$$W^{(2)}(\boldsymbol{F}, \mathbf{B}) = W^{(2)}_{\text{me}}(\boldsymbol{F}) + \frac{\mathbf{B} \cdot \mathbf{B}}{2\mu_0} + \rho_0 \varphi^{(2)}_{\text{mag}}(\boldsymbol{R}^{(2)}\mathbf{B}) \tag{4.4}$$

where $W^{(2)}_{\text{me}}(\boldsymbol{F})$ is a mechanical energy function such that it is equal to zero if $\boldsymbol{F}$ is a pure rotation $\boldsymbol{R}^{(2)}$, and infinity otherwise, which serves to enforce the rigidity condition. $\varphi^{(2)}_{\text{mag}}$ characterizes the magnetic response of the particles. Note that $\boldsymbol{F}$ has been set equal to the rotation $\boldsymbol{R}^{(2)}$ in the second and third terms of the equation for W, corresponding to the vacuum and material contributions, respectively.

4.1 Composites with aligned, cylindrical fibers under in-plane loading

This section will provide more explicit results for the effective energy of the composite when these two materials are arranged as described in Figure 4.1. For simplicity, this section is broken up into subsections. Section 4.1.1 describes the relevant microstructural variables and evolution of the microstructure in the composite. Section 4.1.2 gives an expression for the purely mechanical energy function of the composite, and, in the process, provides an associated expression for the fiber rotations. This is also needed to determine the magnetostatic energy function of the composite. Section 4.1.3 gives an expression for the magnetic energy function, assuming that the microstructure in the deformed configuration is known. Section 4.1.4 provides some practical simplifications for computing magnetic constitutive relations from the given energy function and for dealing with the saturation phenomenon. Section 4.1.7 describes some possible extensions of the given model as well as some of the limitations.

4.1.1 Microstructural variables and evolution

Figure 4.2 shows a transverse cross-section of the fiber composite depicted in Figure 4.1 in its reference (left) and deformed (right) configurations. In this cross-section the

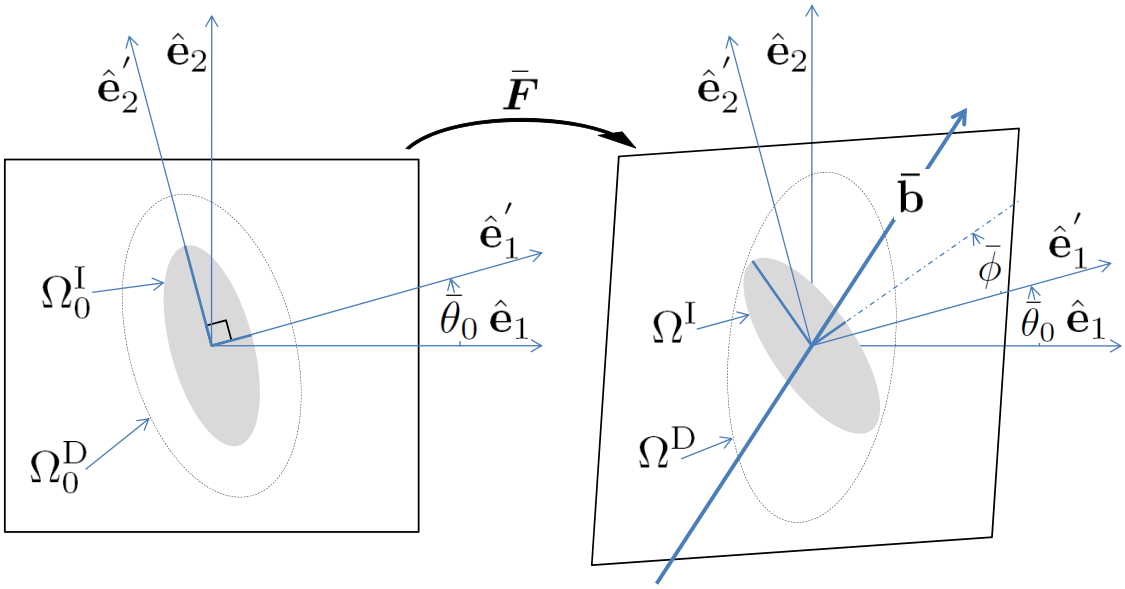

Figure 4.2: Cross-section of the MRE's microstructure in the reference (left) and current (right) configurations. The region Ω_0^{I} represents the initial region occupied by the inclusion material, while Ω_0^{D} represents the initial "shape" of the two-point correlation for the random distribution of the particle centers. Under the action of the deformation and the magnetic field, the regions Ω_0^{I} and Ω_0^{D} transform to new regions Ω^{I} and Ω^{D} in the current configuration. The fixed unit vectors $\hat{\mathbf{e}}_1'$ and $\hat{\mathbf{e}}_2'$ are aligned with the principal axes of the ellipses in the reference configuration, and are at an angle θ_0 relative to the laboratory frame, defined by the basis vectors $\hat{\mathbf{e}}_1$ and $\hat{\mathbf{e}}_2$.

composite can be considered a two-dimensional material consisting of elliptical inclusions, initially occupying regions $\Omega_0^{\rm I}$, in initial concentration $c_0^{\rm I}$, that are distributed randomly with "elliptical" symmetry (Willis, 1977) in the elastomeric matrix. As discussed by Ponte Castañeda and Willis (1995), elliptical symmetry in this context refers to the shape of the two-point probability function for the distribution of the particle centers. It can be described in terms of "distributional" ellipses $\Omega_0^{\rm D}$. The elliptical particles and distribution are in turn described in terms of shape tensors $\boldsymbol{Z}_0^{\rm I}$ and $\boldsymbol{Z}_0^{\rm D}$ by means of

$$\Omega_0^{\rm I} = \left\{ \mathbf{X} : \left| \left(\boldsymbol{Z}_0^{\rm I}\right)^{-T} \mathbf{X} \right| \leq 1 \right\} \quad \text{and} \quad \Omega_0^{\rm D} = \left\{ \mathbf{X} : \left| \left(\boldsymbol{Z}_0^{\rm D}\right)^{-T} \mathbf{X} \right| \leq 1 \right\}. \tag{4.5}$$

For simplicity it will be assumed that the *initial* shape and orientation of the particle and distributional ellipses are identical, with the same aspect ratio w and orientation θ_0 relative to the fixed laboratory frame.

Note that since $\boldsymbol{Z}_0^{\rm I}$ is a symmetric second-order tensor, it can be "diagonalized" such that

$$\boldsymbol{Z}_0^{\rm I} = \boldsymbol{R}_{\bar{\theta}_0} \boldsymbol{D}_0^{\rm I} \boldsymbol{R}_{\bar{\theta}_0}^{\rm T}, \tag{4.6}$$

where $\boldsymbol{R}_{\bar{\theta}_0}$ is an in-plane rotation by the angle $\bar{\theta}_0$ and $\boldsymbol{D}_0^{\rm I}$ defines the shape of the particle. They have Cartesian components relative to the laboratory frame:

$$\left[R_{\bar{\theta}_0}\right] = \begin{bmatrix} \cos\bar{\theta}_0 & -\sin\bar{\theta}_0 \\ \sin\bar{\theta}_0 & \cos\bar{\theta}_0 \end{bmatrix} \quad \text{and} \quad \left[D_0^{\rm I}\right] = \begin{bmatrix} 1 & 0 \\ 0 & w \end{bmatrix}. \tag{4.7}$$

Obviously, there is a completely analogous expression for the particle distribution tensor $\boldsymbol{Z}_0^{\rm D} = \boldsymbol{R}_{\bar{\theta}_0} \boldsymbol{D}_0^{\rm D} \boldsymbol{R}_{\bar{\theta}_0}^{\rm T}$.

As the deformation progresses, the microstructure evolves because the particles can rotate and move relative to one another, so that in the current configuration the microstructure is characterized by new regions $\Omega^{\rm I}$ and $\Omega^{\rm D}$ (Figure 4.2). The current concentration $c^{\rm I}$ is identical to its initial value ($c^{\rm I} = c_0^{\rm I}$) because of the assumed incompressibility of the matrix and rigidity of the fibers. Also, since the particles are rigid, they cannot deform and, following Ponte Castañeda and Galipeau (2011), they are all assumed to undergo (on the average) the same rotation $\boldsymbol{R}_{\bar{\phi}}$ (i.e., an in-plane rotation by an angle $\bar{\phi}$). As we will see below, this will be determined by the purely mechanical homogenization problem. In addition, the shape of the two-point probabilities is assumed to deform with the macroscopic deformation, as determined

by the average deformation gradient $\bar{\boldsymbol{F}} = \bar{\boldsymbol{R}}_{\bar{\psi}}\bar{\boldsymbol{U}}$, where the in-plane macroscopic rotation $\bar{\boldsymbol{R}}_{\bar{\psi}}$ is described by the angle $\bar{\psi}$. In summary, the regions in the deformed configuration also become ellipses, as defined by

$$\Omega^{\mathrm{I}} = \left\{\mathbf{x} : \left|\left(\boldsymbol{Z}^{\mathrm{I}}\right)^{-T}\mathbf{x}\right| \leq 1\right\} \quad \text{and} \quad \Omega^{\mathrm{D}} = \left\{\mathbf{x} : \left|\left(\boldsymbol{Z}^{\mathrm{D}}\right)^{-T}\mathbf{x}\right| \leq 1\right\}, \tag{4.8}$$

in terms of different shape tensors $\boldsymbol{Z}^{\mathrm{I}}$ and $\boldsymbol{Z}^{\mathrm{D}}$.

It is useful (Ponte Castañeda and Galipeau, 2011) to introduce the relative particle rotation $\bar{\boldsymbol{R}}_{\bar{\varphi}} = \bar{\boldsymbol{R}}_{\bar{\psi}}^{T}\,\bar{\boldsymbol{R}}_{\bar{\phi}}$, such that

$$\bar{\varphi} = \bar{\phi} - \bar{\psi}, \tag{4.9}$$

where it is recalled that $\bar{\psi}$ characterizes the in-plane macroscopic rotation. Recalling that the stretch tensor $\bar{\boldsymbol{U}}$ corresponds to a *pure shear* at an angle $\bar{\alpha}$, it is also useful to diagonalize $\bar{\boldsymbol{U}}$, such that $\bar{\boldsymbol{U}} = \boldsymbol{R}_{\bar{\alpha}}\bar{\boldsymbol{D}}\boldsymbol{R}_{\bar{\alpha}}^{\mathrm{T}}$, where $\bar{\boldsymbol{D}}$ is pure shear of magnitude $\bar{\lambda}$ relative to the laboratory frame, i.e.,

$$[D] = \begin{bmatrix} \bar{\lambda} & 0 \\ 0 & 1/\bar{\lambda} \end{bmatrix}. \tag{4.10}$$

On the other hand, $\bar{\alpha}$ characterizes the loading angle.

It then follows (Ponte Castañeda and Galipeau, 2011) from the hypotheses made that the inclusion and distribution shape tensors in the deformed configuration can be related to the corresponding reference shape tensors via

$$\boldsymbol{Z}^{\mathrm{I}} = \boldsymbol{Z}_0^{\mathrm{I}}\boldsymbol{R}_{\bar{\phi}}^{\mathrm{T}} = \boldsymbol{Z}_0^{\mathrm{I}}\boldsymbol{R}_{\bar{\varphi}}^{\mathrm{T}}\boldsymbol{R}_{\bar{\psi}}^{\mathrm{T}} \quad \text{and} \quad \boldsymbol{Z}^{\mathrm{D}} = \boldsymbol{Z}_0^{\mathrm{D}}\bar{\boldsymbol{F}}^{\mathrm{T}} = \boldsymbol{Z}_0^{\mathrm{D}}\bar{\boldsymbol{U}}\boldsymbol{R}_{\bar{\psi}}^{\mathrm{T}}. \tag{4.11}$$

It should be recalled that the above expression for the evolution of $\boldsymbol{Z}^{\mathrm{D}}$ is an approximation that should be reasonable provided that the particle volume fractions and strains are not too large.

4.1.2 Purely mechanical energy function

For the above-defined class of two-dimensional fibrous microstructures, Lopez-Pamies and Ponte Castañeda (2006b) have provided an analytical estimate for the effective

stored-energy function of the composite, which is given by

$$\widetilde{W}_{\rm me}(\bar{\boldsymbol{F}}) = \widehat{W}_{\rm me}(\bar{\lambda}, \bar{\alpha}) = (1 - c_0^I)\, g^{(1)}(\hat{I}^{(1)}), \tag{4.12}$$

where $g^{(1)}$ is given by expression (4.2) for the Gent material, and

$$\begin{aligned}\hat{I}^{(1)} = &\frac{c_0^I \left(1+\bar{\lambda}^2\right)^2 + \left[1 + 2\left(c_0^I - 2\right) c_0^I \bar{\lambda}^2 + \bar{\lambda}^4\right] + c_0^I \left(1+\bar{\lambda}^2\right)^2 w^2}{\left(1 - c_0^I\right)^2 \bar{\lambda}^2 w} \\ &- \frac{c_0^I \left(\bar{\lambda}^4 - 1\right)\left(w^2 - 1\right)}{\left(1 - c_0^I\right)^2 \bar{\lambda}^2 w} \sin(\bar{\varphi}) \sin\left[\bar{\varphi} - 2(\bar{\alpha} - \bar{\theta}_0)\right] - \frac{2 c_0^I \left(1+\bar{\lambda}^2\right)\left(1+w^2\right)}{\left(1 - c_0^I\right)^2 \bar{\lambda} w} \cos(\bar{\varphi}).\end{aligned} \tag{4.13}$$

In this last expression, c_0^I is the fiber volume fraction, w is the fiber aspect ratio, $\bar{\lambda}$ is the applied stretch, $\bar{\alpha}$ is the the loading angle, and $\bar{\theta}_0$ is the initial orientation of the fibers relative to the laboratory frame (see Figure 4.2). The relative fiber rotation $\bar{\varphi}$ satisfies the equation

$$2\bar{\lambda}\left(1 + w^2\right)\sin(\bar{\varphi}) - \left(\bar{\lambda}^2 - 1\right)\left(w^2 - 1\right)\sin[2(\bar{\varphi} - \bar{\alpha} + \bar{\theta}_0)] = 0, \tag{4.14}$$

which also depends on w, $\bar{\lambda}$, and $\bar{\alpha}$ but not on c_0^I. Note that the result is consistent with objectivity since the rigid body rotation, as defined by the angle $\bar{\psi}$, does not directly enter the result (see expression (4.9) for the variable $\bar{\varphi}$). Also, note that the replacement of $\bar{\theta}_0$ by $\bar{\theta}_0 - \pi$ does not affect the result, consistent with the material symmetry of the composite.

4.1.3 Magnetostatic energy function for particles with ferromagnetic particle response

As previously discussed the particles are taken to be magnetically isotropic, but nonlinear, and a Langevin-type function is a phenomenological model to describe the magnetic behavior of the inclusion material. Thus, the magnetic free-energy function of the particles depends on $b = |\mathbf{b}|$. It is defined by

$$\rho_0^{(2)} \varphi_{\rm mag}^{(2)}(\mathbf{b}) = -\frac{\mu_0 m_{\rm s}^2}{3\chi}\left[\ln\left(\sinh\left[\frac{3\chi b}{\mu_0 m_{\rm s}}\right]\right) - \ln\left(\frac{3\chi b}{\mu_0 m_{\rm s}}\right)\right], \tag{4.15}$$

where χ denotes the initial (linear) susceptibility and $m_{\rm s}$ is the saturation magnetization of the particle. The corresponding magnetization is then given by

$$\mathbf{m}(\mathbf{b}) = \frac{m_{\rm s}}{b}\left[\coth\left(\frac{3\chi b}{\mu_0 m_{\rm s}}\right) - \frac{\mu_0 m_{\rm s}}{3\chi b}\right]\mathbf{b}. \tag{4.16}$$

Other magnetic constitutive relations can be used; however, the Langevin model is sufficient to describe a wide range of materials such as magnetically soft iron.

When the magnetic behavior of the particles is *linear* with susceptibility χ (such that $\mathbf{m} = \chi\mathbf{b}/\mu_0$), Chapter 3 (Ponte Castañeda and Galipeau, 2011) made use of the linear homogenization estimates of Ponte Castañeda and Willis (1995) for the above-described *particulate* microstructures to obtain the following expression for the effective magnetic energy function for the composite

$$\widetilde{W}_{\rm mag}(\bar{\boldsymbol{F}}, \bar{\mathbf{B}}) = \frac{1}{2\mu_0}\left(\bar{\boldsymbol{U}}\bar{\mathbf{B}}\right)\cdot\left[\boldsymbol{I} - \tilde{\boldsymbol{X}}(\bar{\boldsymbol{U}}, \chi)\right]\left(\bar{\boldsymbol{U}}\bar{\mathbf{B}}\right), \tag{4.17}$$

where it is recalled that $\bar{J} = 1$ on account of the overall incompressibility of the composite. In this expression, $\tilde{\boldsymbol{X}}(\bar{\boldsymbol{U}}, \chi)$ is defined in terms of the effective magnetic susceptibility of the composite in the deformed configuration as determined by $\bar{\boldsymbol{F}} = \bar{\boldsymbol{R}}_{\bar{\psi}}\bar{\boldsymbol{U}}$ by means of the relation

$$\tilde{\boldsymbol{\chi}}(\bar{\boldsymbol{F}}, \chi) = \boldsymbol{R}_{\bar{\psi}}\tilde{\boldsymbol{X}}(\bar{\boldsymbol{U}}, \chi)\boldsymbol{R}_{\bar{\psi}}^{\rm T}, \tag{4.18}$$

and may be given the expression

$$\tilde{\boldsymbol{X}}(\bar{\boldsymbol{U}}, \chi) = c_0^I\left[\frac{1}{\chi}\boldsymbol{I} - (1-c_0^I)\boldsymbol{I} + \boldsymbol{P}(\boldsymbol{Z}_0^{\rm I}\boldsymbol{R}_{\bar{\varphi}}^{\rm T}) - c_0^I\boldsymbol{P}(\boldsymbol{Z}_0^{\rm D}\bar{\boldsymbol{U}})\right]^{-1}, \tag{4.19}$$

where $\boldsymbol{P}(\boldsymbol{Z}_0^{\rm I}\boldsymbol{R}_{\bar{\varphi}}^{\rm T})$ and $\boldsymbol{P}(\boldsymbol{Z}_0^{\rm D}\bar{\boldsymbol{U}})$ are microstructural tensors, respectively. They characterize the effects of the inclusions and distribution, as well as their evolution. In this connection it is useful to recall that the shape tensors $\boldsymbol{Z}_0^{\rm I}$ and $\boldsymbol{Z}_0^{\rm D}$ are given by expressions of the form (4.6), and that the rotation tensor $\boldsymbol{R}_{\bar{\varphi}}$ depending on $\bar{\varphi}$, as defined by expression (4.14), is a function of $\bar{\lambda}$ and $\bar{\alpha}$ through $\bar{\boldsymbol{U}}$. The microstructural tensors are defined in terms of the Eshelby-type expression

$$\boldsymbol{P}(\boldsymbol{Z}) = \frac{\det(\boldsymbol{Z})}{2\pi}\int_{|\xi|=1}|\boldsymbol{Z}\xi|^{-2}\xi\otimes\xi dS(\xi), \tag{4.20}$$

which can be computed analytically for general shape tensor $\boldsymbol{Z}$. Thus, its Cartesian components relative to the laboratory frame defined by $\hat{\mathbf{e}}_i$ (Figure 4.2) are given by

$$[P(\boldsymbol{Z})] = \begin{bmatrix} \frac{Z_{12}(Z_{12}-Z_{21})+Z_{22}(Z_{11}+Z_{22})}{(Z_{12}-Z_{21})^2+(Z_{11}+Z_{22})^2} & -\frac{Z_{11}Z_{12}+Z_{21}Z_{22}}{(Z_{12}-Z_{21})^2+(Z_{11}+Z_{22})^2} \\ -\frac{Z_{11}Z_{12}+Z_{21}Z_{22}}{(Z_{12}-Z_{21})^2+(Z_{11}+Z_{22})^2} & \frac{Z_{21}(Z_{21}-Z_{12})+Z_{11}(Z_{11}+Z_{22})}{(Z_{12}-Z_{21})^2+(Z_{11}+Z_{22})^2} \end{bmatrix}. \tag{4.21}$$

When the magnetic behavior of the particles is *nonlinear*, as specified by expressions (4.15) and (4.16), Chapter 3 (Ponte Castañeda and Galipeau, 2011) made use of the "linear comparison" homogenization theory of Ponte Castañeda (1992, 1998) to derive the following estimate for the effective magnetostatic energy function of the composite

$$\widetilde{W}_{\rm mag}(\bar{\boldsymbol{F}},\bar{\mathbf{B}}) = \frac{1}{2\mu_0}\left(\bar{\boldsymbol{U}}\bar{\mathbf{B}}\right)\cdot\left[\boldsymbol{I}-\tilde{\boldsymbol{X}}(\bar{\boldsymbol{U}},\chi_L)\right]\left(\bar{\boldsymbol{U}}\bar{\mathbf{B}}\right) + c_0^I\left[\chi_L\frac{\left(\hat{b}^{(2)}\right)^2}{2\mu_0}+\rho_0^{(2)}\varphi_{\rm mag}^{(2)}(\hat{b}^{(2)})\right] \tag{4.22}$$

where χ_L is the susceptibility of the inclusion phase in the "linear comparison composite" and $\hat{b}^{(2)}$ is the magnitude of the average of the corresponding magnetic induction field in the inclusions. They are determined as the solution of the coupled nonlinear algebraic relations

$$\hat{b}^{(2)} = \frac{\mu_0 m_{\rm s}}{\chi_L}\left[\coth\left(\frac{3\chi\hat{b}^{(2)}}{\mu_0 m_{\rm s}}\right)-\frac{\mu_0 m_{\rm s}}{3\chi\hat{b}^{(2)}}\right] \tag{4.23}$$

and

$$\hat{b}^{(2)} = \frac{1}{\chi_L c_0^{\rm I}}\left|\tilde{\boldsymbol{\chi}}(\bar{\boldsymbol{F}},\chi_L)\bar{\mathbf{b}}\right| = \frac{1}{\chi_L c_0^{\rm I}}\left|\tilde{\boldsymbol{X}}(\bar{\boldsymbol{U}},\chi_L)\,\bar{\boldsymbol{U}}\bar{\mathbf{B}}\right|. \tag{4.24}$$

Therefore, the effective magnetostatic energy function $\widetilde{W}_{\rm mag}$ of the nonlinear composite is computed as a function of $\bar{\boldsymbol{F}}$ and $\bar{\mathbf{B}}$ by first solving equations (4.23) and (4.24) for the variables χ_L and $\hat{b}^{(2)}$, and then substituting the result into equation (4.22).

4.1.4 Constitutive relations

Having obtained expressions (4.12), together with (4.13) and (4.14) for the mechanical energy function $\widetilde{W}_{\rm me}$, and expression (4.22), together with (4.23) and (4.24) for the corresponding magnetostatic energy function $\widetilde{W}_{\rm mag}$, the total magnetoelastic energy

function $\widetilde{W}$ for the nonlinear MRE is obtained from expression (4.1). The macroscopic constitutive relations for the composite may be determined by means of expression (3.9). It is important to recall that the magnetic energy $\widetilde{W}_{\rm mag}$, and in particular $\tilde{\boldsymbol{X}}(\bar{\boldsymbol{U}}, \chi_L)$, depend on χ_L which is a function of both the magnetic and mechanical fields. In principle, we would need to account for variations in χ_L when taking derivatives of $\widetilde{W}_{\rm mag}$; however, as pointed out by Ponte Castañeda and Galipeau (2011), the *stationarity* condition used to determine χ_L implies that the derivatives with respect to χ_L do not contribute, so that the macroscopic magnetization can be shown to be given by

$$\bar{\mathbf{m}} = \frac{1}{\mu_0}\tilde{\boldsymbol{\chi}}(\bar{\boldsymbol{F}}, \chi_L)\bar{\mathbf{b}} = \frac{1}{\mu_0}\boldsymbol{R}_{\bar{\psi}}\tilde{\boldsymbol{X}}(\bar{\boldsymbol{U}}, \chi_L)\bar{\boldsymbol{U}}\bar{\mathbf{B}}. \tag{4.25}$$

It is emphasized that χ_L must still be obtained from the solution of equations (4.23) and (4.24), as a function of $\bar{\boldsymbol{F}}$ and $\bar{\mathbf{B}}$, so that, in particular, it depends nonlinearly on $\bar{\mathbf{b}}$. Therefore the dependence of $\bar{\mathbf{m}}$ on $\bar{\mathbf{b}}$ is also nonlinear, as would be expected.

Similarly, when computing the "magnetic" stresses by differentiation with respect to the deformation, the variable χ_L can be treated as a constant in the process. For example the magnetic part of the Biot stress (see Ponte Castañeda and Galipeau (2011)) is given by

$$\bar{\boldsymbol{T}}_{\rm B}^{\rm mag} = \frac{\partial\widetilde{W}_{\rm mag}}{\partial\bar{\boldsymbol{U}}} = \frac{1}{2\mu_0}\frac{\partial}{\partial\bar{\boldsymbol{U}}}\left(\bar{\boldsymbol{U}}\bar{\mathbf{B}}\cdot\bar{\boldsymbol{U}}\bar{\mathbf{B}} - \bar{\boldsymbol{U}}\bar{\mathbf{B}}\cdot\tilde{\boldsymbol{X}}(\bar{\boldsymbol{U}}, \chi_L)\bar{\boldsymbol{U}}\bar{\mathbf{B}}\right), \tag{4.26}$$

where the derivative is taken with χ_L held fixed.

Recalling that the composite is incompressible, the corresponding mechanical Biot stress can be obtained from

$$\bar{\boldsymbol{T}}_{\rm B}^{\rm me} = \frac{\partial\widetilde{W}_{\rm me}}{\partial\bar{\boldsymbol{U}}} - p\,\bar{\boldsymbol{U}}^{-1}, \tag{4.27}$$

where p is an arbitrary hydrostatic pressure. After converting the mechanical and magnetic Biot stresses to the corresponding Cauchy-type stresses (see Ponte Castañeda and Galipeau (2011)), the total Cauchy stress is found via the relation

$$\bar{\boldsymbol{T}} = \bar{\boldsymbol{T}}^{\rm me} + \bar{\boldsymbol{T}}^{\rm mag}. \tag{4.28}$$

4.1.5 Saturation

As previously discussed the magnetization of the particles is expected to reach a saturation value as the magnitude of the magnetic field $\bar{b} = |\bar{\mathbf{b}}|$ is increased, and the Langevin model (4.16) for the particles exhibits this important feature. It is expected that certain macroscopic variables for the composite will also saturate because of this, and we use the expression

$$[A]_{\text{sat}} = \lim_{\bar{b}\to\infty} A \tag{4.29}$$

to denote the saturation value of a quantity A. It should be noted, however, that the saturation value of a given quantity may depend on the direction of the applied field $\bar{\mathbf{b}}$.

Since the magnetization of the (isotropic) particles has been assumed to reach a saturation state of magnitude m_s, it is expected in particular that the macroscopic magnetization of the composite will also saturate. It is indeed found from expression (4.25) that

$$[\bar{\mathbf{m}}]_{\text{sat}} = c_0^{\text{I}} m_s \frac{\bar{\mathbf{b}}}{|\bar{\mathbf{b}}|}, \tag{4.30}$$

where $\bar{\mathbf{b}}/|\bar{\mathbf{b}}|$ is the unit vector in the direction of the applied field. It is emphasized that this relation is valid even for anisotropic microstructures. It implies that the magnitude of the magnetization vector $\bar{\mathbf{m}}$ will reach the saturation value $c_0^{\text{I}} m_s$, and, in addition, $\bar{\mathbf{m}}$ will tend to align itself with the applied field $\bar{\mathbf{b}}$ for sufficiently large $\bar{b}$.

As will be seen later in the applications section, the result (4.30) has implications for certain important quantities, such as the magnetic torque on a given MRE sample when the particles are not aligned with the applied magnetic field. We remark here, for later reference, that the quantity $\bar{\mathbf{m}} \times \bar{\mathbf{b}}$ which, as will be shown below, is related to the macroscopic torques, also saturates. Although $\bar{\mathbf{b}}$ continues to increase, because $\bar{\mathbf{m}}$ also tends to align itself with the applied field $\bar{\mathbf{b}}$, the cross product of these two quantities actually tends to a non-zero saturation value. The value depends on the direction of $\bar{\mathbf{b}}$ relative to the microstructure in the deformed configuration, as determined by the quantity

$$\tilde{\boldsymbol{\eta}}(\bar{\boldsymbol{F}}) = \boldsymbol{R}_{\bar{\psi}} \left[(1 - c_0^I)\boldsymbol{I} - \boldsymbol{P}(\boldsymbol{Z}_0^{\text{I}} \boldsymbol{R}_{\bar{\varphi}}^{\text{T}}) + c_0^I \boldsymbol{P}(\boldsymbol{Z}_0^{\text{D}} \bar{\boldsymbol{U}}) \right] \boldsymbol{R}_{\bar{\psi}}^{\text{T}}. \tag{4.31}$$

In terms of this quantity, the saturation value of $\bar{\mathbf{m}} \times \bar{\mathbf{b}}$ is given by

$$\left[\bar{\mathbf{m}} \times \bar{\mathbf{b}}\right]_{\text{sat}} = -c_0^{\text{I}} m_s^2 \frac{\sin(2\gamma)}{2} \left(\xi_2(\tilde{\boldsymbol{\eta}}(\bar{\boldsymbol{F}})) - \xi_1(\tilde{\boldsymbol{\eta}}(\bar{\boldsymbol{F}})),\right) \tag{4.32}$$

where $\xi_2(\tilde{\boldsymbol{\eta}}(\bar{\boldsymbol{F}}))$ and $\xi_1(\tilde{\boldsymbol{\eta}}(\bar{\boldsymbol{F}}))$ denote the largest and smallest eigenvalues of $\tilde{\boldsymbol{\eta}}(\bar{\boldsymbol{F}})$, while γ is the counterclockwise angle from the eigenvector associated with $\xi_1(\tilde{\boldsymbol{\eta}}(\bar{\boldsymbol{F}}))$ to the applied field. Note that $\left[\bar{\mathbf{m}} \times \bar{\mathbf{b}}\right]_{\text{sat}}$ is a function of deformation through $\tilde{\boldsymbol{\eta}}(\bar{\boldsymbol{F}})$. As will be seen further below, the saturation of $\bar{\mathbf{m}} \times \bar{\mathbf{b}}$ is consistent with the physical expectation that the magnetic torques on a sample of the MRE should also saturate.

4.1.6 Loss of ellipticity for 2-D loadings

As shown by Lopez-Pamies and Ponte Castañeda (2006a), the purely mechanical energy function may lose strong ellipticity at sufficiently large stretches when the reinforced elastomer is loaded in compression along the long axis of the fibers. Therefore, a fully coupled stability analysis would need to be considered for these magnetoelastic composites as it is expected that the magnetic field can have a significant impact on the stability and loss of ellipticity. For most of this chapter we will ignore the loss of ellipticity and focus on the effect of the magnetic fields on the coupled magnetoelastic behavior. However in section 4.2.4 we consider the effect of the magnetic field on loss of ellipticity under aligned loading.

As discussed in section 3.2 the composite may lose ellipticity under certain loading conditions. The onset of instability is characterized by the incremental magnetoelastic moduli $\mathcal{L}$, $\mathcal{M}$, and $\mathcal{B}$ as defined by equations (3.25) and (3.26). Following the work of Rudykh and deBotton (2011) when specialized to 2-D incompressible materials and assuming $\mathcal{B}$ is invertible, we can show that the loss of ellipticity occurs when the polynomial

$$\Gamma_6\xi^6 + \Gamma_5\xi^5 + \Gamma_4\xi^4 + \Gamma_3\xi^3 + \Gamma_2\xi^2 + \Gamma_1\xi + \Gamma_0 = 0 \tag{4.33}$$

admits at least one real solution ξ. The polynomial coefficients Γ_i are given in terms

of the magnetoelastic moduli as

$$
\begin{aligned}
\Gamma_0 =& \mathcal{M}_{122}^2 - \mathcal{L}_{2121}\mathcal{B}_{22}, \\
\Gamma_1 =& 2\left(\mathcal{L}_{2121}\mathcal{B}_{12} + \left(\mathcal{L}_{1121} - \mathcal{L}_{2122}\right)\mathcal{B}_{22} - \mathcal{M}_{122}\left(\mathcal{M}_{112} + \mathcal{M}_{121} - \mathcal{M}_{222}\right)\right), \\
\Gamma_2 =& -\mathcal{L}_{2121}\mathcal{B}_{11} - 4\left(\mathcal{L}_{1121} - \mathcal{L}_{2122}\right)\mathcal{B}_{12} - \left(\mathcal{L}_{1111} - 2\mathcal{L}_{1122} - 2\mathcal{L}_{1221} + \mathcal{L}_{2222}\right)\mathcal{B}_{22} \\
& + 2\mathcal{M}_{122}\left(\mathcal{M}_{111} - \mathcal{M}_{122} - \mathcal{M}_{221}\right) + \left(\mathcal{M}_{112} + \mathcal{M}_{121} - \mathcal{M}_{222}\right)^2, \\
\Gamma_3 =& 2((\mathcal{L}_{1121} - \mathcal{L}_{2122})\mathcal{B}_{11} + (\mathcal{L}_{1222} - \mathcal{L}_{1112})\mathcal{B}_{22} \\
& + (\mathcal{L}_{1111} - 2\mathcal{L}_{1122} - 2\mathcal{L}_{1221} + \mathcal{L}_{2222})\mathcal{B}_{12} \\
& + (\mathcal{M}_{121}\mathcal{M}_{122} - (\mathcal{M}_{111} - \mathcal{M}_{122} - \mathcal{M}_{221})(\mathcal{M}_{112} + \mathcal{M}_{121} - \mathcal{M}_{222}))), \\
\Gamma_4 =& -\left(\mathcal{L}_{1111} - 2\mathcal{L}_{1122} - 2\mathcal{L}_{1221} + \mathcal{L}_{2222}\right)\mathcal{B}_{11} + 4\left(\mathcal{L}_{1112} - \mathcal{L}_{1222}\right)\mathcal{B}_{12} \\
& - \mathcal{L}_{1212}\mathcal{B}_{22} + \left(\mathcal{M}_{122} + \mathcal{M}_{221} - \mathcal{M}_{111}\right)^2 - 2\mathcal{M}_{121}\left(\mathcal{M}_{112} + \mathcal{M}_{121} - \mathcal{M}_{222}\right), \\
\Gamma_5 =& 2\left(\left(\mathcal{L}_{1222} - \mathcal{L}_{1112}\right)\mathcal{B}_{11} + \mathcal{L}_{1212}\mathcal{B}_{12} + \mathcal{M}_{121}(\mathcal{M}_{111} - \mathcal{M}_{122} - \mathcal{M}_{221})\right), \\
\Gamma_6 =& \mathcal{M}_{121}^2 - \mathcal{L}_{1212}\mathcal{B}_{11}.
\end{aligned}
\tag{4.34}
$$

This can be specialized further when the magnetic and mechanical loading are aligned along the material symmetry axis. In such a case many of the magnetoelastic moduli vanish due to symmetry and the non-zero coefficients are

$$
\begin{aligned}
\Gamma_0 =& \mathcal{M}_{122}^2 - \mathcal{L}_{2121}\mathcal{B}_{22}, \\
\Gamma_2 =& -\mathcal{L}_{2121}\mathcal{B}_{11} - \left(\mathcal{L}_{1111} - 2\mathcal{L}_{1122} - 2\mathcal{L}_{1221} + \mathcal{L}_{2222}\right)\mathcal{B}_{22} \\
& + 2\mathcal{M}_{122}\left(\mathcal{M}_{111} - \mathcal{M}_{122} - \mathcal{M}_{221}\right) + \left(\mathcal{M}_{112} + \mathcal{M}_{121} - \mathcal{M}_{222}\right)^2, \\
\Gamma_4 =& -\mathcal{L}_{1212}\mathcal{B}_{22} - \left(\mathcal{L}_{1111} - 2\mathcal{L}_{1122} - 2\mathcal{L}_{1221} + \mathcal{L}_{2222}\right)\mathcal{B}_{11} \\
& + \left(\mathcal{M}_{122} + \mathcal{M}_{221} - \mathcal{M}_{111}\right)^2 - 2\mathcal{M}_{121}\left(\mathcal{M}_{112} + \mathcal{M}_{121} - \mathcal{M}_{222}\right), \\
\Gamma_6 =& \mathcal{M}_{121}^2 - \mathcal{L}_{1212}\mathcal{B}_{11}.
\end{aligned}
\tag{4.35}
$$

The loss of ellipticity can be detected at critical combinations of $\bar{\lambda}$ and $\bar{b}$ which we label $\bar{\lambda}^c$ and $\bar{b}^c$.

4.1.7 Limitations of the model

It should be noted that the microstructure evolution equations (4.11) for $\boldsymbol{Z}^{\mathrm{I}}$ and $\boldsymbol{Z}^{\mathrm{D}}$ may, under certain conditions, lead to microstructures that are inconsistent with the estimates (4.18) and (4.19) that have been used to estimate the effective magnetic

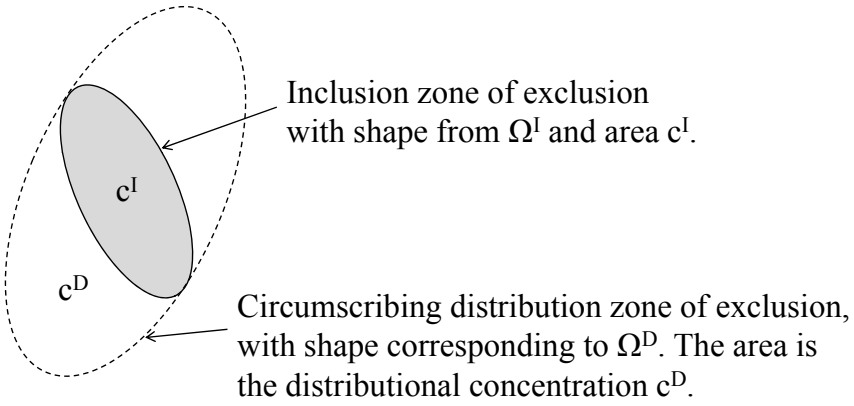

Figure 4.3: The dashed line represents the boundary of a distributional ellipse defined as the smallest ellipse circumscribing the inclusion (with shapes and orientations described by $\boldsymbol{Z}^{\mathrm{D}}$ and $\boldsymbol{Z}^{\mathrm{D}}$, respectively).

susceptibility of the composite in the current configuration, especially if the volume fraction of the particles is large. This is because the estimates (4.18) and (4.19) for the effective susceptibility of the composite have the implicit restriction that the volume fraction of the fibers cannot be such that the fibers penetrate each others' "exclusion" regions, as defined by the smallest distributional ellipses surrounding the fibers. Mathematically, the condition requires that the concentration of such "distributional" ellipses be such that $c^{\mathrm{D}} < 1$ (Ponte Castañeda and Willis, 1995). The distributional concentration c^{D} is a function of $\boldsymbol{Z}^{\mathrm{D}}$, $\boldsymbol{Z}^{\mathrm{I}}$, and c_0^{I}, and corresponds to the volume fraction of the exclusion ellipses surrounding the actual particles, as depicted in Figure 4.3. Clearly, when the aspect ratios of the distributional ellipses and particles differ, and/or when the corresponding principal axes are not aligned, the maximum particle concentration c_0^{I} has to be strictly less than 1. Since $\boldsymbol{Z}^{\mathrm{I}}$ and $\boldsymbol{Z}^{\mathrm{D}}$ depend on the deformation in a complicated manner, the above condition on c^{D} may not be satisfied for all deformations, especially if the volume fraction and aspect ratio of the particles are large. In this work the particle volume fraction will be assumed to be relatively small ($c_0^{\mathrm{I}} < 0.5$), and the exclusion condition will be verified numerically.

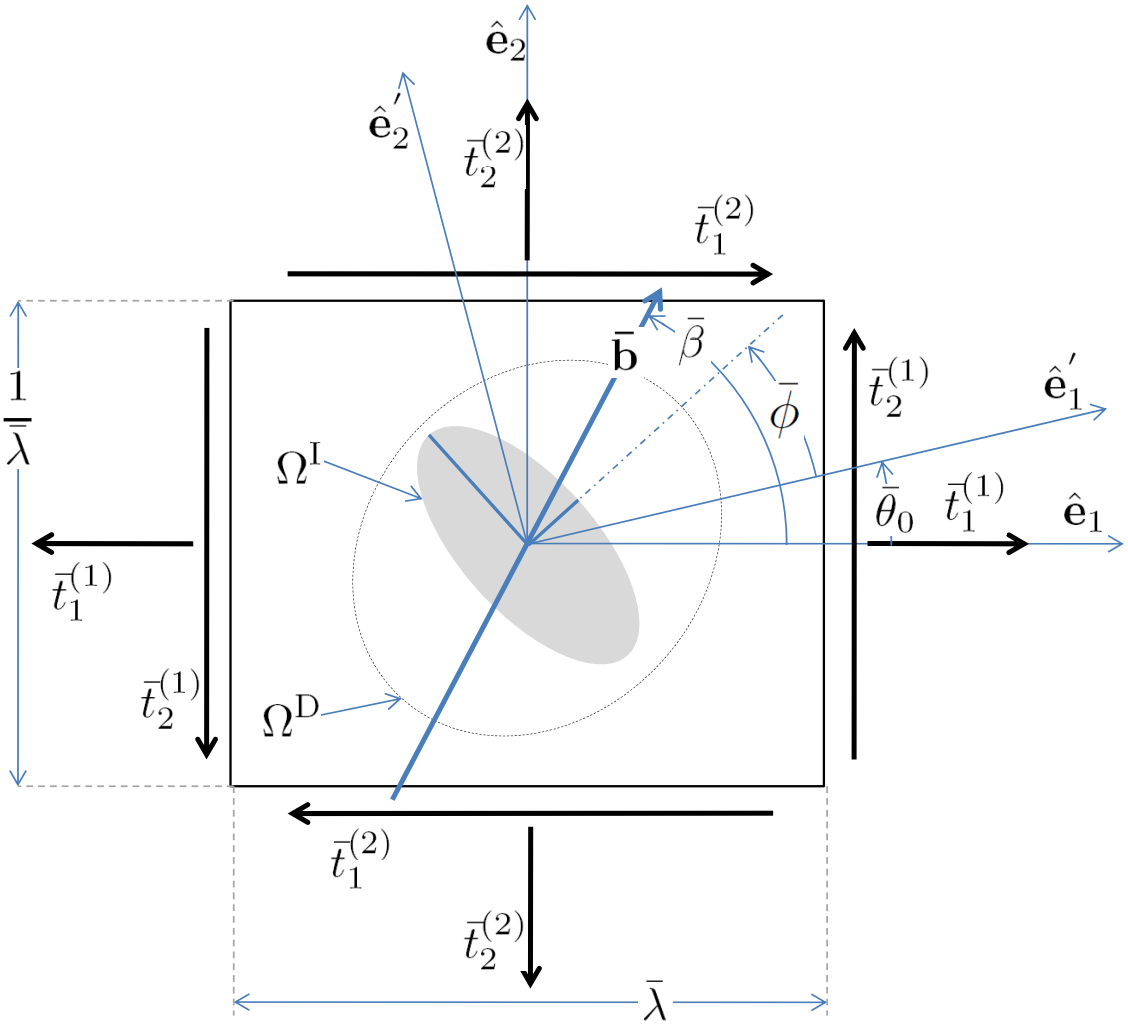

Figure 4.4: A sample of MRE with particles that are initially oriented at an angle $\bar{\theta}_0$ relative to the $\hat{\mathbf{e}}_1$ axis is subjected to a uniform stretch $\bar{\lambda}$ along the $\hat{\mathbf{e}}_1$ axis and a magnetic field $\bar{\mathbf{b}}$ at an angle $\bar{\beta}$, resulting in reorientation $\bar{\phi}$ of the particles in the current configuration. The tractions on the exposed surfaces $\bar{t}_1^{(1)}$, $\bar{t}_2^{(2)}$, $\bar{t}_1^{(2)}$ and $\bar{t}_2^{(1)}$ are calculated assuming that the magnetic fields in the vacuum surrounding the sample are such that the stress $\bar{\boldsymbol{T}}$ and magnetic field $\bar{\mathbf{b}}$ are macroscopically uniform inside the sample.

4.2 Results for MREs subjected to non-aligned magnetoelastic loadings with ferromagnetic response

In this section we consider a rectangular sample of the MRE described in the prior section such that the sides of the sample are parallel to the fixed laboratory axes $\hat{\mathbf{e}}_i$, and the particles are initially aligned with the material axes $\hat{\mathbf{e}}'_i$ at an angle $\bar{\theta}_0$ relative to the laboratory frame. As depicted in Figure 4.4, the sample is subjected to a *pure shear* with stretch of magnitude $\bar{\lambda}$ that is aligned with the laboratory axes, such that $\bar{\alpha} = \bar{\psi} = 0$. In the deformed configuration the particles have undergone a rotation $\bar{\varphi} = \bar{\phi}$, and magnetic fields are applied to the sample such that the average magnetic induction field $\bar{\mathbf{b}}$ in the sample has magnitude $\bar{b}$ and is oriented at an angle $\bar{\beta}$ relative to the lab frame. Under this loading the components of the deformation gradient $\bar{\boldsymbol{F}}$ and of the Lagrangian magnetic induction field $\bar{\mathbf{B}}$ with respect to the $\hat{\mathbf{e}}_i$ basis are given by

$$\big[\bar{F}\big] = \big[\bar{U}\big] = \begin{bmatrix} \bar{\lambda} & 0 \\ 0 & 1/\bar{\lambda} \end{bmatrix} \quad \text{and} \quad \big\{\bar{B}\big\} = \begin{Bmatrix} \bar{B}_1 \\ \bar{B}_2 \end{Bmatrix} = \begin{Bmatrix} \big(\bar{b}/\bar{\lambda}\big)\cos\bar{\beta} \\ \bar{b}\bar{\lambda}\sin\bar{\beta} \end{Bmatrix} \tag{4.36}$$

The magnetoelastic stored-energy function for the MRE is obtained from expressions (4.1), together with (4.12) and (4.22), in the form $\widetilde{W}(\bar{\boldsymbol{F}}, \bar{\mathbf{B}}) = \widehat{W}(\bar{\lambda}, \bar{\alpha}, \bar{B}_1, \bar{B}_2)$. On the other hand the derivatives with respect to $\bar{\boldsymbol{U}}$ needed in the computation of the magnetic and mechanical stresses, as defined by (4.26) and (4.27), can be related to derivatives with respect to $\bar{\lambda}$ and $\bar{\alpha}$ by means of the chain rule. Thereby the components of the total Cauchy stress $\bar{\boldsymbol{T}}$ relative to the $\hat{\mathbf{e}}_i$ basis can then be expressed in the form

$$\bar{T}_{11} - \bar{T}_{22} = \bar{\lambda}\frac{\partial\widehat{W}}{\partial\bar{\lambda}} \quad \text{and} \quad \bar{T}_{12} = \bar{T}_{21} = \frac{\bar{\lambda}^2}{\bar{\lambda}^4 - 1}\frac{\partial\widehat{W}}{\partial\bar{\alpha}}, \tag{4.37}$$

where the partial derivatives are taken with the components of the Lagrangian magnetic induction field $\bar{B}_1$ and $\bar{B}_2$ held fixed. Nevertheless, the magnetic constitutive relation is most easily obtained directly from expression (4.25) for $\bar{\mathbf{m}}$ via expression (4.19).

As previously discussed, the actual traction that would need to be applied on the boundary of the sample to maintain this deformation will depend on the magnetic fields surrounding the sample. From expression (2.38) it can also be seen that the mechanical tractions depend on the boundary normals. The normals to the surfaces

remain the same and are given by $\hat{\mathbf{e}}_1$ and $\hat{\mathbf{e}}_2$ for this deformation. Assuming that the external magnetic fields are such that the macroscopic deformation gradient $\bar{\boldsymbol{U}}$ and stress $\bar{\boldsymbol{T}}$, as well as the magnetic fields $\bar{\mathbf{b}}$ and $\bar{\mathbf{h}}$, remain uniform inside the sample, the tractions on the exposed surfaces (see Figure 4.4) satisfy the conditions

$$\bar{t}_1^{(1)} - \bar{t}_2^{(2)} = \bar{T}_{11} - \bar{T}_{22} - \bar{h}_1\bar{b}_1 + \bar{h}_2\bar{b}_2 - \frac{\mu_0\left(\bar{m}_1\right)^2}{2} + \frac{\mu_0\left(\bar{m}_2\right)^2}{2}, \tag{4.38}$$

$$\bar{t}_2^{(1)} = \bar{T}_{12} - \bar{h}_2\bar{b}_1 \quad \text{and} \quad \bar{t}_1^{(2)} = \bar{T}_{12} - \bar{h}_1\bar{b}_2, \tag{4.39}$$

where the superscripts correspond to the direction normals to the surface on which the tractions act, while the subscripts correspond to the components relative to the laboratory coordinates, as defined by the unit vectors $\hat{\mathbf{e}}_i$.

Significantly when the sample is magnetically insensitive (for example when $c_0^{\mathrm{I}} = 0$), the magnetic stresses inside and outside the sample will still be non-zero. However these magnetic stresses will be self-equilibrated and the traction components in expressions (4.38) to (4.39) will depend only on the mechanical stress in the usual fashion. In addition when the sample is magnetically susceptible ($c_0^{\mathrm{I}} \neq 0$), the total stress components $\bar{T}_{ij}$ will continue to increase with an increasing applied magnetic field $\bar{\mathbf{b}}$. They will do so in such a way that the traction components $\bar{t}_i^{(j)}$ will saturate with the magnetization $\bar{\mathbf{m}}$, as expected on physical grounds.

We emphasize that while the total stress $\bar{\boldsymbol{T}}$ is symmetric, the shear tractions on the sample need not be equal (i.e., $\bar{t}_2^{(1)} \neq \bar{t}_1^{(2)}$ in general). In fact the difference in the shear tractions corresponds to the net torque acting on the sample. Such macroscopic torques are a direct consequence of the microscopic torques that develop on the particles in the sample when the magnetic field is not aligned with the particle axes. Additional magnetic torques arise when the distribution of the particles is not isotropic and the magnetic field is not aligned with the axes of the "distributional" ellipse. For these reasons in the discussions to follow, we will consider the "torque" and "distortional" shear stress, as given by

$$\frac{1}{2}\left(\bar{t}_2^{(1)} - \bar{t}_1^{(2)}\right) = -\frac{1}{2}\,\bar{\mathbf{m}} \times \bar{\mathbf{b}} \quad \text{and} \quad \frac{1}{2}\left(\bar{t}_2^{(1)} + \bar{t}_1^{(2)}\right) = \bar{T}_{12} - \frac{1}{2}\left(\bar{h}_2\bar{b}_1 + \bar{h}_1\bar{b}_2\right), \tag{4.40}$$

respectively (instead of $\bar{t}_2^{(1)}$ and $\bar{t}_1^{(2)}$ separately).

Finally, the results below will be presented in dimensionless form. Recalling that

μ_0 is the permeability of vacuum, G is the shear modulus of the matrix, and m_s is the saturation magnetization of the particles, we define the dimensionless magnetic induction, magnetization and traction via

$$\frac{\bar{b}}{\mu_0 m_s}, \quad \frac{\bar{m}}{m_s}, \quad \frac{\bar{t}_i^{(j)}}{G} = \frac{\bar{t}_i^{(j)\mathrm{me}}}{G} + \kappa \frac{\bar{t}_i^{(j)\mathrm{mag}}}{\mu_0 m_s^2}, \tag{4.41}$$

where $\bar{t}_i^{(j)\mathrm{me}}$ corresponds to the contributions of the purely mechanical stresses and $\bar{t}_i^{(j)\mathrm{mag}}$ to the remaining magnetic terms (4.28). and where

$$\kappa = \mu_0 m_s^2 / G \tag{4.42}$$

is a dimensionless group serving to characterize (Galipeau and Ponte Castañeda, 2012) the relative importance of the magnetic versus mechanical contributions in the tractions. Typical values of κ for various magnetic particle/elastomer matrix combinations have been given in Table 7.1; κ can reach values into the hundreds for very soft rubbers. The choice of κ would depend on the specific application. While higher values of κ may be useful in achieving large magnetostriction, smaller values may be necessary to produce large tractions with no deformation.

4.2.1 Magnetization response

Figure 4.5 shows normalized plots for the magnitude $\bar{m}$ of the magnetization $\bar{\mathbf{m}}$ and of its cross product with $\bar{\mathbf{b}}$ for an unstrained sample ($\bar{\lambda} = 1$) with elliptical particles of initial orientation $\bar{\theta}_0 = 0°$, aspect ratio $w = 4$, magnetic susceptibility $\chi = 0.95$ and concentration $c_0^I = 0.4$, subjected to non-aligned magnetic fields of magnitude $\bar{b}$ at various angles $\bar{\beta}$ (refer to Figure 4.4). Figure 4.5a shows that the magnitude of the magnetization depends initially on the loading angle. However it tends to the same saturation value for large values of $\bar{b}$ which is consistent with expression (4.30). It is found in Figure 4.5b that while ($\bar{\beta} \neq 0, 90°$) $\bar{\mathbf{m}}$ is initially not aligned with $\bar{\mathbf{b}}$ for non-aligned loadings, it does tend to align itself with $\bar{\mathbf{b}}$, again in agreement with expression (4.30). In spite of this fact, Figure 4.5c shows that the cross product of $\bar{\mathbf{m}}$ with $\bar{\mathbf{b}}$ actually tends to a finite, non-zero value as $\bar{\mathbf{b}}$ continues to increase. This result, which is consistent with the observations in connection with expression (4.32) for the saturation value of $\bar{\mathbf{m}} \times \bar{\mathbf{b}}$, is significant because, as indicated by expression

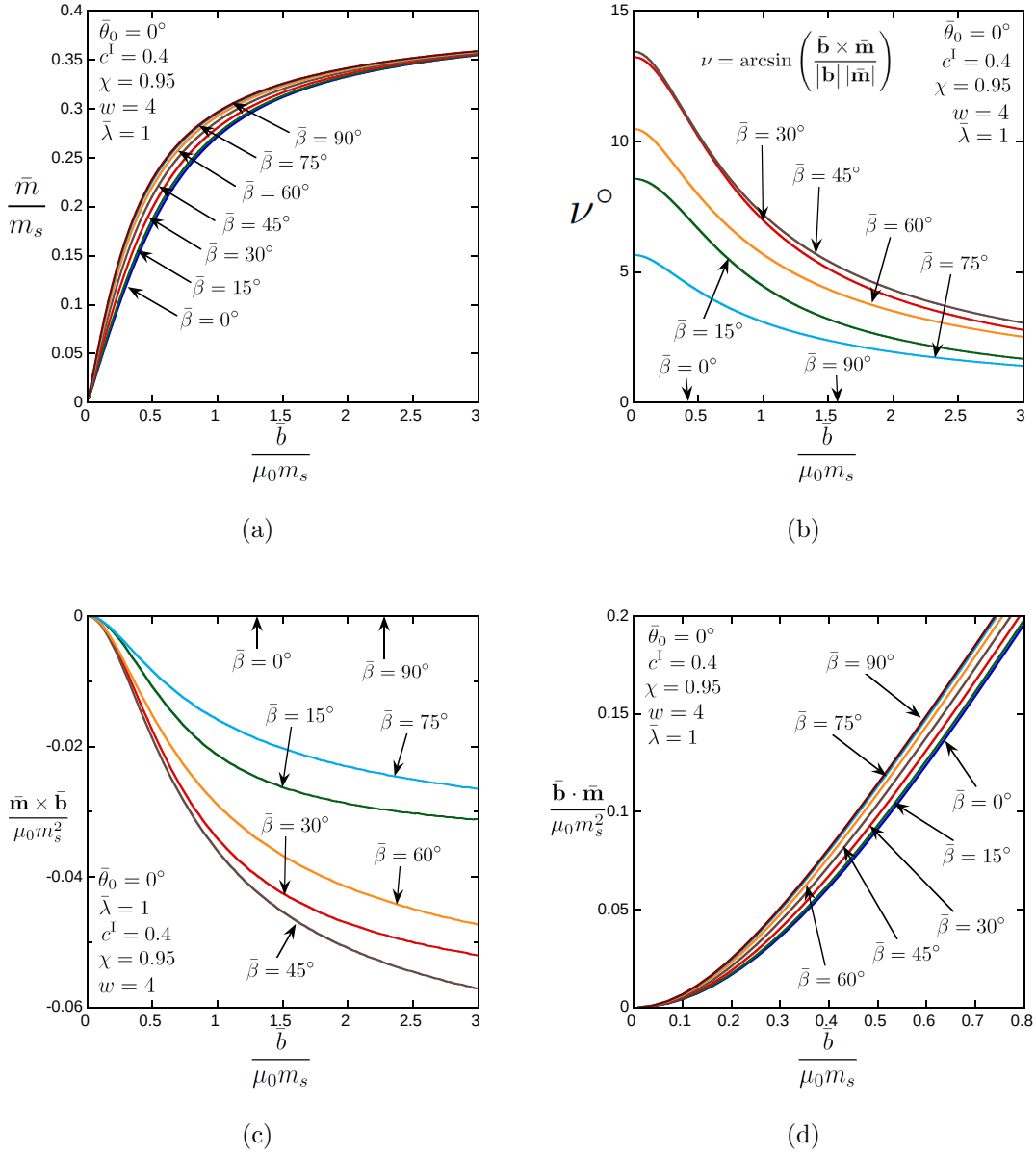

Figure 4.5: Macroscopic magnetization $\bar{m}$ as a function of the magnetic induction $\bar{b}$ for MRE samples with elliptical fibers ($w = 4$) subjected to different magnetic field angles $\bar{\beta}$. (a) The magnitude of the magnetization. (b) The angle between the $\bar{\mathbf{m}}$ field and the $\bar{\mathbf{b}}$. (b) The cross product of $\bar{\mathbf{m}}$ and $\bar{\mathbf{b}}$ (corresponding to the negative of the macroscopic torque in the MRE sample in Fig. 4.7). (d) The dot product of the $\bar{\mathbf{m}}$ field and the $\bar{\mathbf{b}}$ field.

$(4.40)_1$, the macroscopic torque on the sample is proportional to $\bar{\mathbf{m}} \times \bar{\mathbf{b}}$. The results of Figure 4.5c confirm that the torque on the sample indeed tends to saturate with increasing applied magnetic field $\bar{b}$. Note that the saturation value $\bar{\mathbf{m}} \times \bar{\mathbf{b}}$ depends on the angle $\bar{\beta}$ since $\gamma = \bar{\beta}$ in expression (4.32). Figure 4.5d shows that the dot product of $\bar{\mathbf{m}}$ and $\bar{\mathbf{b}}$ grows linearly as the applied field becomes large after quadratic initial growth. By considering the curves as a whole, it is clear that the composite behaves differently for small magnetic fields (the linear regime) as compared to the behavior at saturation (Galipeau and Ponte Castañeda, 2012). It also emphasized that although the saturation values for the different loading angles are the same ($\bar{\beta} = 15$ and $\bar{\beta} = 75$ for example), their behavior for small fields is significantly different.

The magnetization depends on the applied stretch $\bar{\lambda}$ through the particle rotation and the change in shape of the distribution tensor as can be deduced from expression (4.19). For brevity results will not be shown here for this dependence. Instead, results will be shown below for the magnetic tractions, which arise in part due to the dependence of the magnetic susceptibility on the applied stretch, as evident from expression (4.26). Note, however, that expression (4.30) shows that the saturation values of $\bar{\mathbf{m}}$ are independent of $\bar{\lambda}$, while expression (4.32) shows that the saturation value of $\bar{\mathbf{m}} \times \bar{\mathbf{b}}$ depends on $\bar{\lambda}$.

4.2.2 Actuation traction

In this subsection a magnetic induction of magnitude $\bar{b}$ is applied at some given angle $\bar{\beta}$ to the rectangular MRE samples with circular ($w = 1$) and elliptical particles ($w = 4$) of magnetic susceptibility $\chi = 0.95$ and concentration $c_0^I = 0.4$, at various orientation angles $\bar{\theta}_0$ (refer to Figure 4.4). Then, the tractions needed to prevent any deformation ($\bar{\lambda} = 1$) are determined and plotted as functions of the magnetic induction $\bar{b}$ and other parameters. We refer to such tractions as "actuation" tractions, because they would correspond to the tractions that would be exerted by the sample if it were constrained externally. It should be emphasized that while the results of this subsection are independent of κ, it is implicitly assumed that the matrix is stiff enough (i.e., κ small enough) so that the magnetic torques on the particles are directly transmitted to the elastic matrix without any appreciable particle rotations, which would tend to lessen the effect.

Figure 4.6 shows the actuation tractions as functions of $\bar{b}$ for MRE samples with

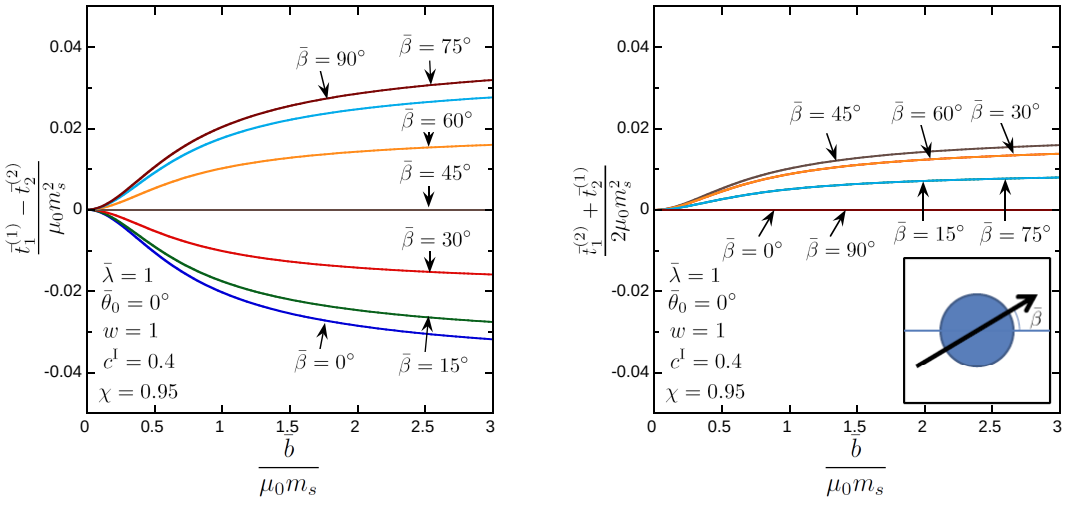

(a) (b)

Figure 4.6: The actuation tractions versus $\bar{b}$ for MRE samples with circular particles ($w = 1$). Plots are shown for magnetic field applied at various angles $\bar{\beta}$ relative to the sample. (a) The normal tractions. (b) The distortional shear tractions. (The magnetic torques vanish for all loading angles in this case.)

circular particles ($w = 1$) loaded magnetically at various angles $\bar{\beta}$. The mechanical contribution to the tractions and to the total stresses are zero in this case because the macroscopic deformation vanishes and the required tractions are solely the result of the magnetic field. The resulting tractions exhibit an initial regime of quadratic growth for all loading angles $\bar{\beta}$, which transitions to a saturation regime as the magnetic field becomes large. As shown in Figure 4.6a, the normal tractions that are required to maintain the deformation can be compressive or tensile depending on the direction of the magnetic field. They are largest when the field is aligned with the sides of the sample ($\bar{\beta} = 0$, or $90°$). In this case the initial shape and distribution of the particles are circular and the overall configuration is magnetically isotropic implying that the macroscopic torque on the composite vanishes (not shown). However, the magnetic field still produces shear (distortional) tractions when the field is not aligned with the specimen. These distortional tractions are maximal for $\bar{\beta} = 45°$, as shown in Figure 4.6b, when the normal tractions vanish.

Figure 4.7 shows the actuation tractions as functions of $\bar{b}$ for MRE samples with elliptical fibers ($w = 4$) that are initially aligned with the laboratory axes ($\bar{\theta}_0 = 0$) and

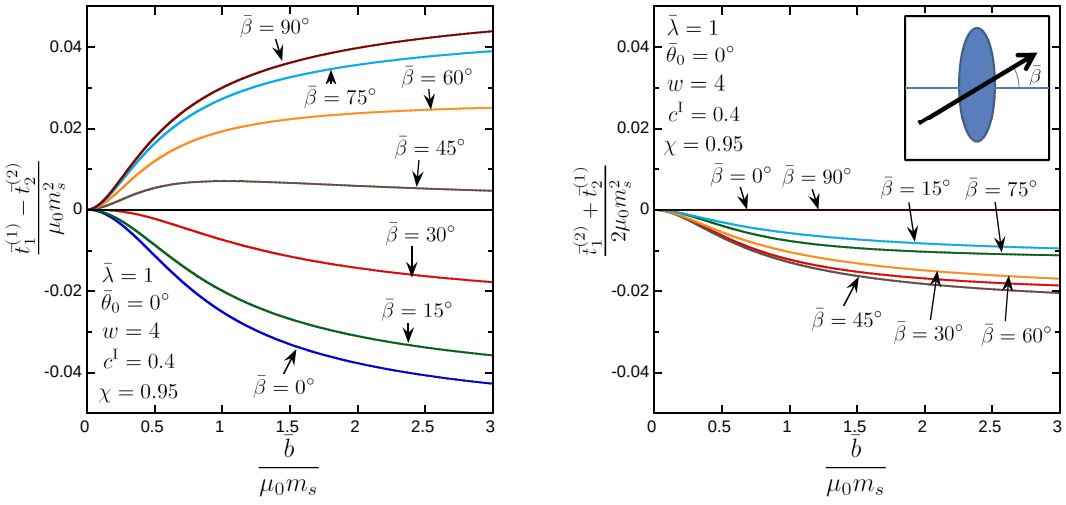

(a) (b)

Figure 4.7: The actuation tractions versus $\bar{b}$ for MRE samples with elliptical particles ($w = 4$). Plots are shown for the magnetic field applied at various angles $\bar{\beta}$ relative to the sample. (a) The normal tractions. (b) The distortional shear tractions.

loaded at various angles $\bar{\beta}$. The normal tractions are similar to those for the case with circular particles; however, the elliptical particles tend to have larger magnetizations, leading to somewhat larger normal tractions. The elliptical shape of the particles also breaks the symmetry about $\bar{\beta} = 45°$, causing the curves to shift slightly upward. In this case, the shear tractions on the horizontal and vertical sides of the sample are no longer equal, except for $\bar{\beta} = 0, 90°$. The actuation torques, which correspond to minus one half of the plots for $\bar{\mathbf{m}} \times \bar{\mathbf{b}}$ (shown in Figure 4.5c), are non-zero in general because of this. As expected, the macroscopic torque of the tractions is positive (CCW) since the particles tend to align the geometric axes with the applied field, leading to a negative magnetic torque. This must be balanced by the applied tractions to prevent macroscopic rotation of the sample. On the other hand, the distortional contribution of the shear tractions has the opposite sign as for the circular particle case. Thus, it can be seen that the shape of the particles can have significant effects on the response of the MRE samples.

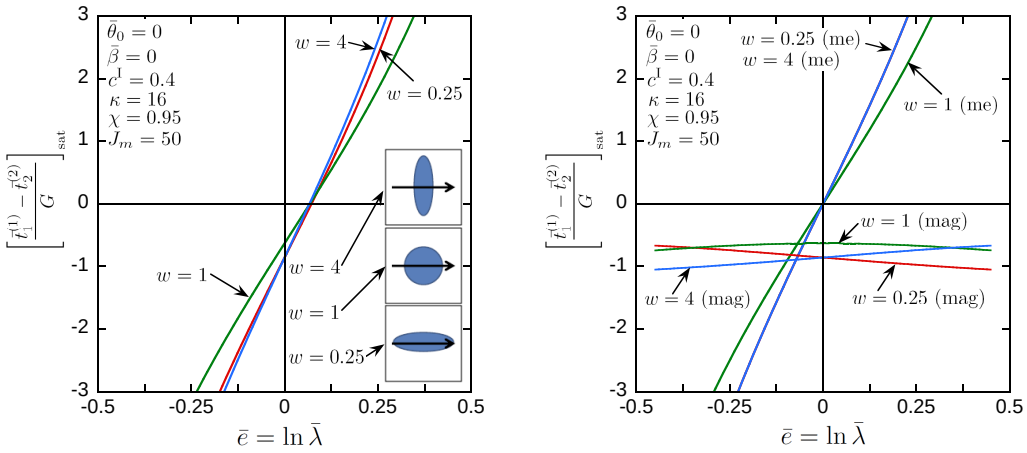

(a) (b)

Figure 4.8: The normal traction versus the strain $\bar{e} = \ln \bar{\lambda}$ for MRE samples subject to aligned loading for various aspect ratios ($w = 0.25, 1, 4$). (a) The total normal traction. (b) The purely mechanical and magnetoelastic contributions to the tractions.

4.2.3 Traction-stretch relations

We investigate the effect of the magnetic field on the traction-strain relations in this subsection for the MRE samples described earlier (see Figure 4.4). The MRE samples have circular ($w = 1$) or elliptical particles ($w = 4$) of magnetic susceptibility $\chi = 0.95$, in concentration $c_0^I = 0.4$ and varying initial orientations $\bar{\theta}_0$. The matrix is of the Gent type with $J_m = 50$ and elastic modulus G, such that the dimensionless parameter $\kappa = 16$. (This value of $\kappa = 16$ was also used in Chapter 7 (Galipeau and Ponte Castañeda, 2012) for MRE samples with aligned spheroidal particles.) For simplicity, we will only show results here for MRE samples at magnetic saturation ($\bar{b} \to \infty$), although the effect of the magnetic orientation $\bar{\beta}$ will also be explored.

Figure 4.8 shows plots of the tractions versus the applied logarithmic strain $\bar{e} = \ln \bar{\lambda}$ for particles of different aspect ratios ($w = 0.25, 1$ and 4) that are initially aligned with the mechanical and magnetic loading axes ($\bar{\theta}_0 = \bar{\beta} = 0$). The particles do not rotate and shear tractions are not generated in this case because of the symmetries of this configuration. However, it should be noted that the $w = 4$ and $w = 0.25$ configurations may become unstable at sufficiently large tensile and

compressive strains, respectively. This is further discussed in the context of Figure 4.11 below.) Figure 4.8a shows the results at magnetic saturation, while Figure 4.8b depicts separately the purely mechanical (labelled "me") and magnetic (labelled "mag") responses of the sample. Thus, it is seen that the response of the MRE sample under combined magnetic and mechanical loadings basically corresponds to a downward shift of the purely mechanical response of the sample. This result, which is consistent with earlier findings by Galipeau and Ponte Castañeda (2012) for samples with aligned 3-D ellipsoidal particles, is a consequence of the overall tendency of the sample to stretch along the direction of the applied magnetic field. Although the contribution of the magnetic fields to the tractions is a function of the strain, and depends on the aspect ratio of the particles, this contribution is relatively weak. As expected, the mechanical response of the sample with elliptical fibers is stiffer than that of the sample with circular particles. The mechanical responses of the $w = 0.25$ and $w = 4$ particles are identical due to the two-dimensional character of the problem (Lopez-Pamies and Ponte Castañeda (2006b).) However, the magneto-mechanical response of the sample with the $w = 4$ particles is slightly stiffer overall due to the slight stiffening behavior of the magnetic traction for the $w = 4$ case, as opposed to the slight softening for $w = 0.25$.

Consistent with the results of the previous subsection for the actuation tractions, a compressive normal traction is required to prevent the sample from deforming when an aligned magnetic field is applied ($\bar{\theta}_0 = \bar{\beta} = 0$). Therefore the vertical downward shift at $\bar{e} = 0$ in the traction-strain curves depicted in Figure 4.8b corresponds to the actuation tractions. On the other hand the horizontal shift in the curves along the zero traction axis corresponds to the magnetostrictive strain. In addition the slopes of the curves at zero strain and zero traction could be used to define magnetoelastic moduli for the MRE sample, which evidently would be affected by the application of the magnetic field. A more in-depth analysis for MRE samples with ellipsoidal particles subjected to aligned loading conditions has already been given in Chapter 7 (Galipeau and Ponte Castañeda, 2012). For this reason we will not discuss any further the aligned loading cases here, except as special limiting cases of more general situations with non-aligned loading conditions leading to the rotation of the particles. As we will show below, particle rotations can lead to significant additional magnetoelastic effects, as initially suggested in Chapter 3 (Ponte Castañeda and Galipeau, 2011).

Next, in Figure 4.9, we consider the case where the particles are still initially

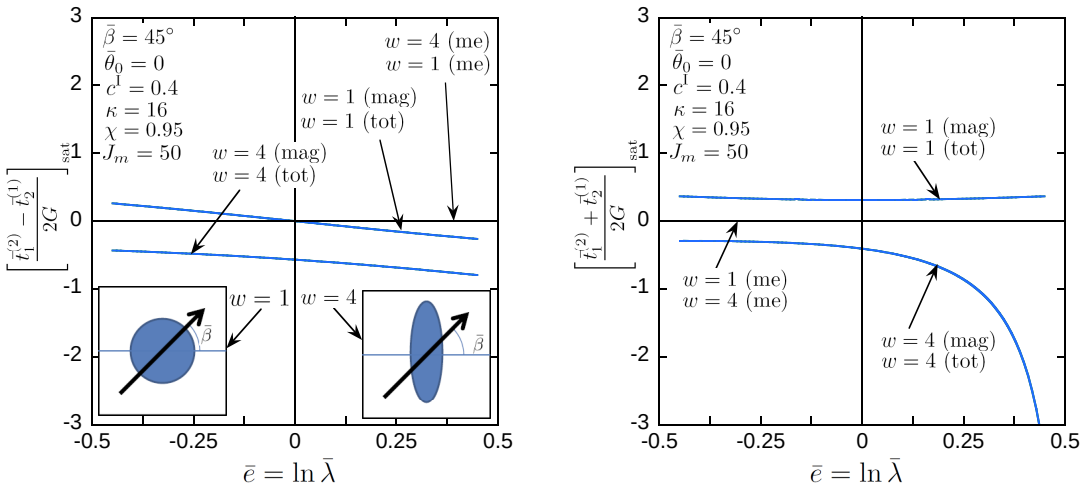

(a) (b)

Figure 4.9: The traction-strain relations for MRE samples with circular ($w = 1$) and elliptical ($w = 4$) particles. The total traction for the composite (tot) is broken into its purely mechanical contribution (me) and its magnetic part (mag). Plots are shown for a magnetic field being applied at an angle to the mechanical loading ($\bar{\beta} = 45°$). (a) The applied torque. (b) The distortional shear traction. (The normal tractions are the same as the mechanical tractions in Figure 4.8b for $w = 1, 4$.)

aligned with the mechanical loading axes ($\bar{\theta}_0 = 0$), but the magnetic field is applied at an angle ($\bar{\beta} = 45°$). In this case, the magnetic fields are not sufficiently strong to reorient the particles (recall that the theory holds in the stiff matrix limit), but macroscopic torques develop in the sample as a consequence of the microscopic torques imposed by the magnetic field on the particles. The magnetic contribution to the normal tractions vanishes in the saturation limit as suggested by the curves for $\bar{\beta} = 45°$ in Figures 4.6a and 4.7a. For this reason, the normal tractions in this case are identical to the purely mechanical tractions shown in Figure 4.8b, and will not be repeated here. However, as shown in Figure 4.9, torques and distortional shear tractions develop in the sample which are purely magnetic in origin. Considering first the samples with circular particles ($w = 1$) shown in Figure 4.9b, we can see that the distortional shear traction is relatively independent of the deformation. However the torque, shown in Figure 4.9a, varies with the deformation, vanishing only when $\bar{e} = 0$. Since the torque is given by $-\bar{\mathbf{m}} \times \bar{\mathbf{b}}/2$, this indicates that the magnetization can become misaligned with the applied magnetic field as a result of the deformation, *even* in an initially isotropic MRE sample. This is because the deformation changes the distribution of the particles, and as a result, $\tilde{\boldsymbol{X}}(\bar{\boldsymbol{U}})$ in equation (4.19) becomes anisotropic with the deformation. However, this effect is of second order in the concentration because it is the result of changes in the distribution of the particles. For elliptical particles ($w = 4$) the particles still do not rotate, but a magnetic torque is generated in the sample, even when no deformation is applied. In addition, it should be noted that the elliptical ($w = 4$) particle configuration may become unstable for $\bar{e} > 0$, provided that sufficiently large compression is generated along the long axis of the particles.

Figure 4.10 illustrates the case of ellipsoidal particles when both the magnetic and mechanical loading are 35 degrees to the initial orientation of the particles. This is a representative example showing the full complexity of magnetoelastic traction-strain relations. First, by looking at the purely mechanical traction, we can see how this composite would behave if no magnetic field were applied. As expected, normal tractions develop as well as equal shear tractions, consistent with the purely elastic problem. However maintaining a particular state of deformation in the presence of a magnetic field requires additional tractions at all states of deformation. It should be noted that the particles undergo a rotation as the composite stretches so the particles do not remain 35 degrees to the applied magnetic field. Subsequently the

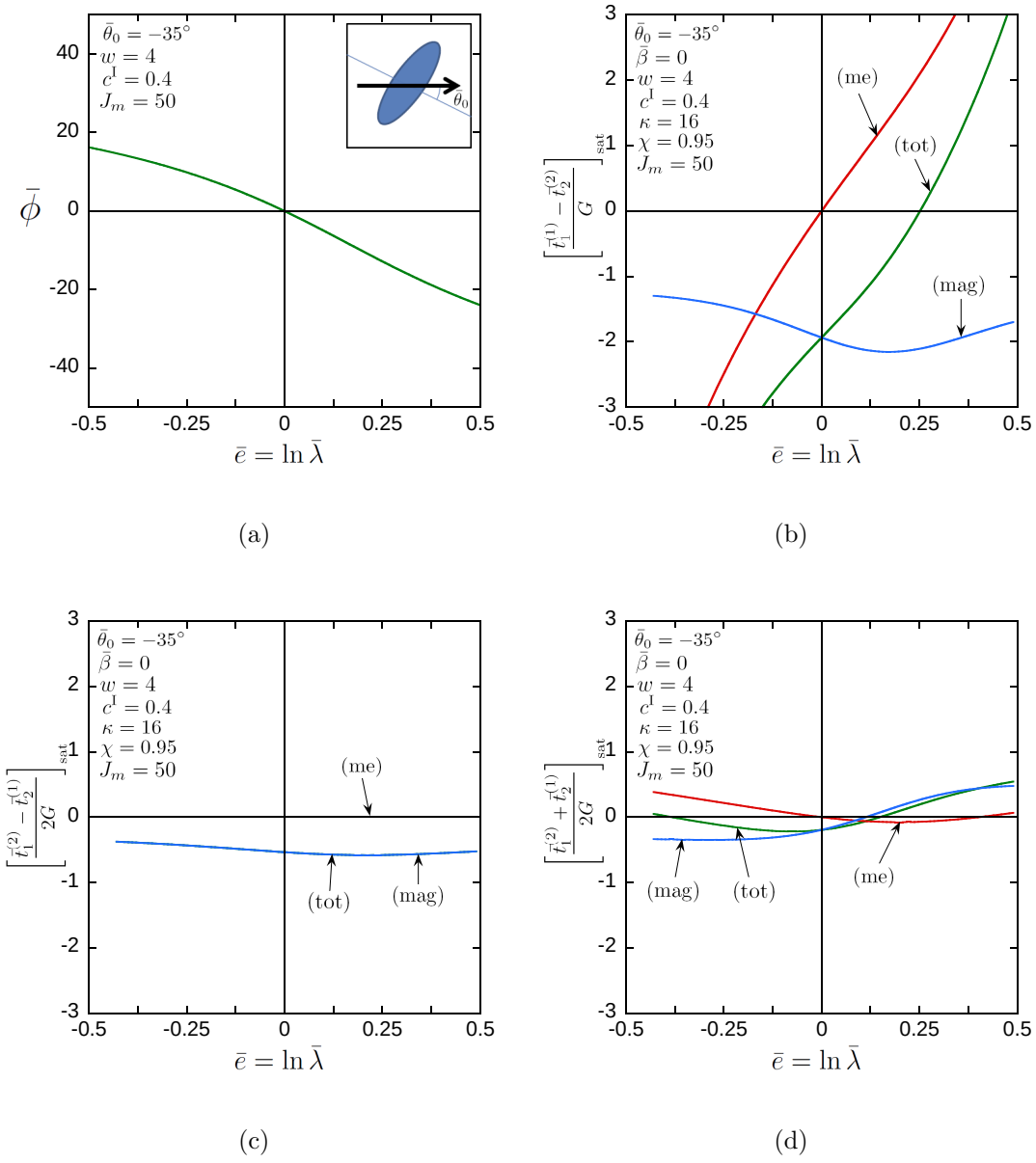

Figure 4.10: The particle rotation and tractions as functions of the strain $\bar{e} = \ln \bar{\lambda}$ for MRE samples with elliptical particles that are initially misaligned with the stretch directions ($\bar{\theta}_0 = -35^\circ$) and the magnetic field ($\bar{\beta} = 0$). The total traction for the composite (tot) is broken into its purely mechanical contribution (me) and its magnetic part (mag). (a) The particle rotation. (b) The normal tractions. (c) The applied torque. (d) The distortional shear traction.

maximum torque is obtained when the particles are roughly 45 degrees to the applied magnetic field. Some torque can be related to distributional effects. These results show that in general the magnetoelastic problem requires four independent tractions versus three in the purely mechanical case (in 2D). Also the complexity of the applied traction makes effects such as magnetostriction difficult to evaluate. If no traction were applied to this sample it would experience a torque aligning it with the magnetic field. The equilibrium shape of the specimen would no longer be a rectangle even if the appropriate torque were applied.

Finally we consider the case when elliptical ($w = 4$) particles are initially oriented at variable angles $\bar{\theta}_0$ to the stretching axis, while the magnetic field is aligned with the stretching axis ($\bar{\beta} = 0$). Thus, Figure 4.11 depicts plots of the particle rotation angle $\bar{\varphi} = \bar{\phi}$, as well as the normal tractions, torque and distortional tractions, as functions of the strain $\bar{e}$, for several values of $\bar{\theta}_0$ ranging between 0 and $-90°$. First of all, it is noted that the cases of $\bar{\theta}_0 = 0$ and $-90°$ correspond respectively to the results shown in Figure 4.8a for $w = 4$ and $w = 0.25$. The second case corresponds exactly to a rotation by $-90°$ of the first because of the 2-D character of the problem. There are no particle rotations and the macroscopic torque and distortional tractions vanish identically in these cases, which are shown for reference. As can be seen in Figure 4.11a for other choices of $\bar{\theta}_0$, the particles undergo significant rotations, depending on the amount and direction of the strain. More specifically, the smallest values (in magnitude) of $\bar{\theta}_0$ tend to produce the largest rotations for tensile strains, while the opposite is true for compressive strains. In particular this means that a slight perturbation of the $\bar{\theta}_0 = 0$ and $90°$ cases would lead to rotation of the particles for tensile and compressive strains, respectively. However, the results are not shown in the figure. Also, as can be seen in Figure 4.11b these particle rotations have a significant impact on the normal tractions. The normal traction curves are shifted quite significantly to the right for particles with $\bar{\theta}_0 = -11.25, -22.5$ and $-33.75°$ and tensile strains, relative to the perfectly aligned cases ($\bar{\theta}_0 = 0$ and $-90°$). As will be discussed in more detail in Chapter 6, this shift has important implications for the generation of much larger magnetostrictive strains than would be possible with either circular particles, or for aligned loadings of elliptical fibers. Similarly, it can be seen from Figure 4.11b that an initial misorientation angle of $\bar{\theta}_0 = -45°$ leads to the largest shift downward at $\bar{\lambda} = 1$, which translates into much enhanced actuation tractions relative to the aligned cases. We can also see that the particle rotations have

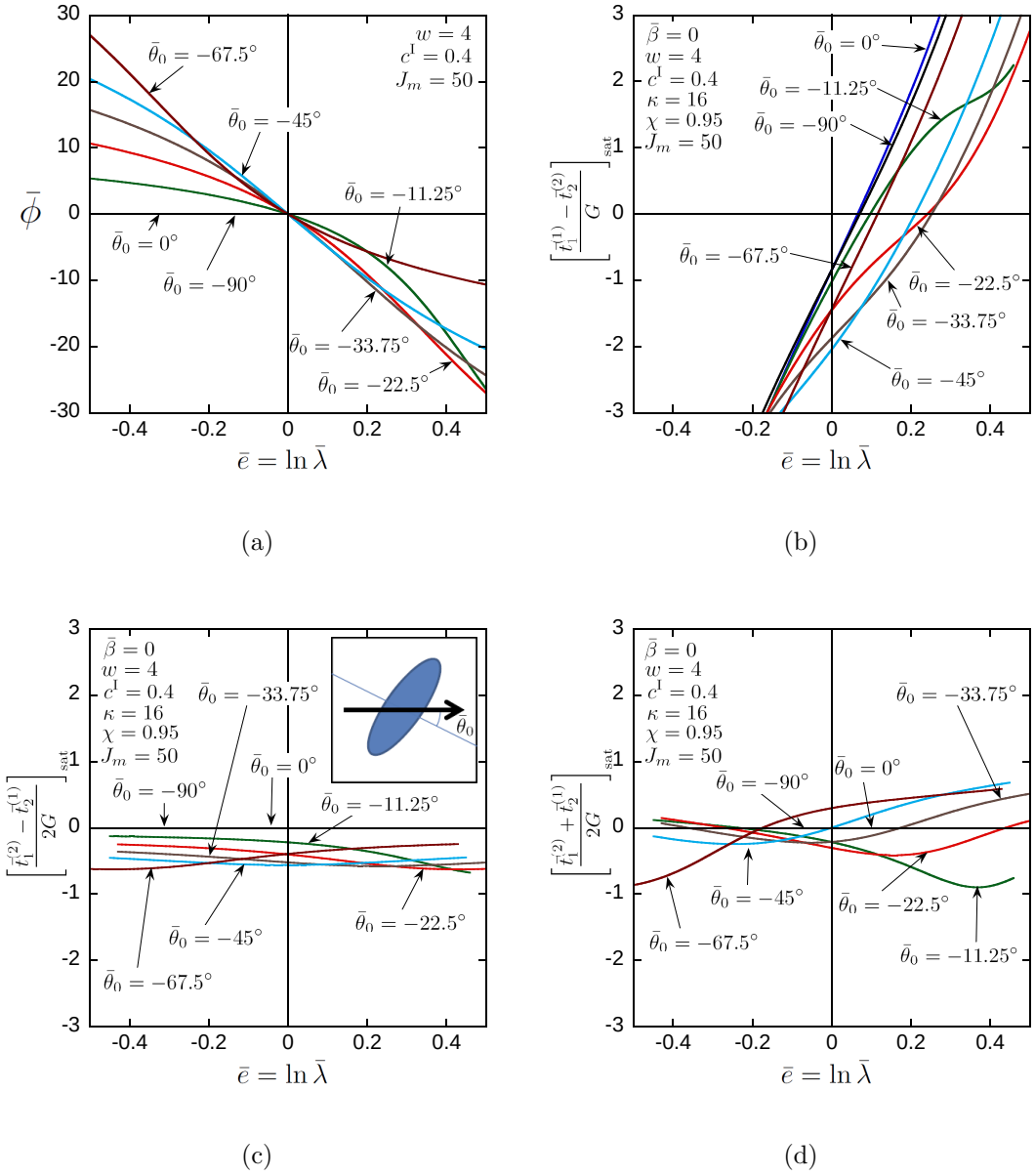

Figure 4.11: The particle rotation and tractions as functions of the strain $\bar{e} = \ln \bar{\lambda}$ for MRE samples with elliptical ($w = 4$) particles that are initially misaligned with the stretch directions (variable $\bar{\theta}_0$) and the magnetic field ($\bar{\beta} = 0$). (a) The particle rotation. (b) The normal tractions. (c) The applied torque. (d) The distortional shear traction.

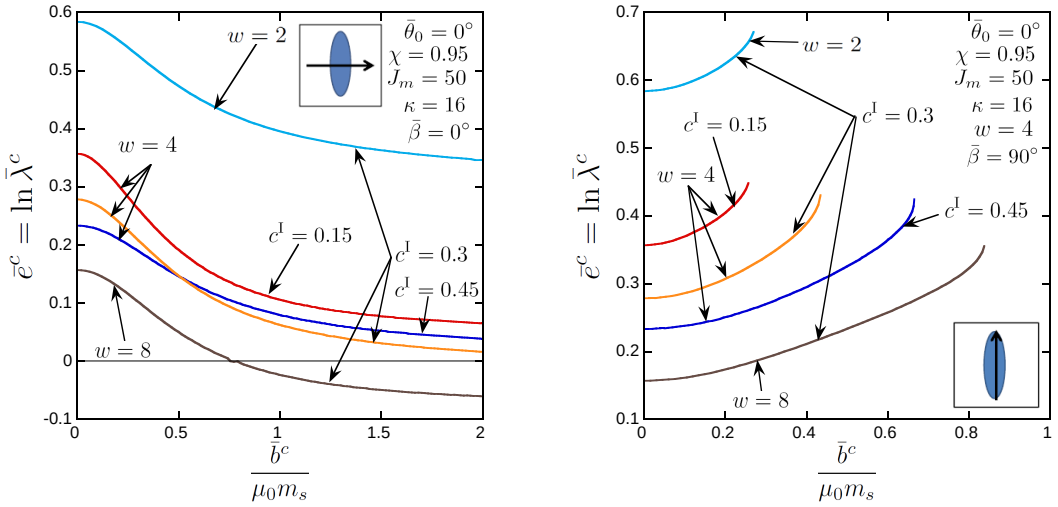

(a) (b)

Figure 4.12: Critical loadings $(\bar{b}^c, \bar{\lambda}^c)$ at which the composite loses ellipticity. The composite maintains ellipticity below the respective curves. (a) Magnetic field applied transverse to the particles' long axis, along the mechanical loading direction. (b) Magnetic field applied along the particles' long axis, transverse to the mechanical loading direction.

important consequences for the (various) magnetoelastic moduli of the MRE samples. In addition as shown in Figures 4.11c and d, the particle rotations for the non-aligned cases can lead to the development of macroscopic torques and distortional tractions in the MRE samples, which although small in comparison to the normal tractions, are significantly affected by the strain $\bar{e}$ and initial orientation angle $\bar{\theta}_0$.

4.2.4 Loss of ellipticity of the 2-D model under aligned loading

Figure 4.12 shows the critical loadings $(\bar{b}^c, \bar{\lambda}^c)$ for various microstructures computed using expression (4.35). Figure 4.12a depicts $\bar{\beta} = 0°$, aligned along the loading direction and along the short axis of the particles, while Figure 4.12b describes $\bar{\beta} = 90°$, transverse to the loading direction and along the long axis of the particles. In both cases $\bar{\lambda} > 1$ compresses the composite along the long axis of the fibers which is known to cause instability in the purely mechanical case (Lopez-Pamies and Ponte

Castañeda, 2006a). The elliptic region is characterized by the space under the curves, with the curves representing the boundary where ellipticity is lost. These can also be interpreted as illustrating how the critical stretch varies with the magnetic field or the critical magnetic field varies with the stretch. Note that for $\bar{b}^c = 0$ the critical stretch corresponds to loss of ellipticity in the purely mechanical case. Depending on how the magnetic field is applied, the magnetic field either stabilizes the composite or destabilizes it. When the magnetic field is applied at $\bar{\beta} = 90°$ the magnetic field stabilizes the composite and the stretch needed to lose ellipticity increases. The composite will become stable for all stretch for a relatively small value of $\bar{b}$. When the magnetic field is applied at $\bar{\beta} = 0°$, the magnetic field destabilizes the composite and the composite loses ellipticity for a smaller value of stretch. The magnetic field can even cause the composite to lose ellipticity in the reference configuration when $w = 8$. In such a case an additional compressive stretch would be required to maintain ellipticity. In all of the cases investigated here loss of ellipticity occurs when $\Gamma_6 \to 0$ in expression (4.35). Note that Γ_6 represents a magnetoelastic shear modulus in the direction transverse to the compressive load.

Figure 4.13 shows the traction as a function of the strain and indicates the point at which the homogenized energy function loses ellipticity (denoted by a circle in the figures). Figure 4.13a has $\bar{\beta} = 0°$ aligned along the loading direction and along the short axis of the particles, while Figure 4.13b has $\bar{\beta} = 90°$ transverse to the loading direction and along the long axis of the particles. The dashed lines depict the principal solution after the energy function loses ellipticity and the validity of the principal solution becomes questionable. The results show that for $\bar{\beta} = 0°$ the composite loses ellipticity for smaller values of the stretch and for $\bar{\beta} = 90°$ a larger stretch is required. For $\bar{\beta} = 90°$ if the magnetic field $\bar{b}/\mu_0 m_s \gtrsim 0.43$, loss of ellipticity is not found within the model's range of validity. A post-bifurcation analysis would need to be performed to evaluate the behavior of the composite after loss of ellipticity which is not included in this thesis.

4.3 Extension to permanent magnetization

The analysis of section 4.1 can also be applied when the particles exhibit some permanent magnetization. As laid out in section 3.4.3, we assume that the particles have a constant differential susceptibility $\boldsymbol{X}$ and no longer saturate. In the two-dimensional

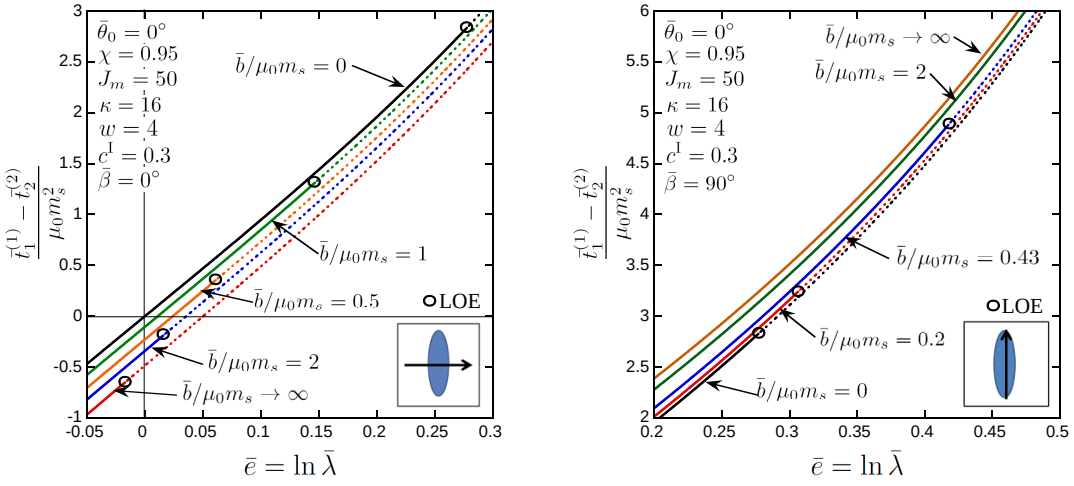

(a) (b)

Figure 4.13: The normal traction versus the strain $\bar{e} = \ln \bar{\lambda}$ for MRE samples showing the loss of ellipticity. The lines are dashed where the homogenized energy function is not elliptic. (a) Magnetic field applied transverse to the particles' long axis, along the mechanical loading direction. (b) Magnetic field applied along the particles' long axis, transverse to the mechanical loading direction.

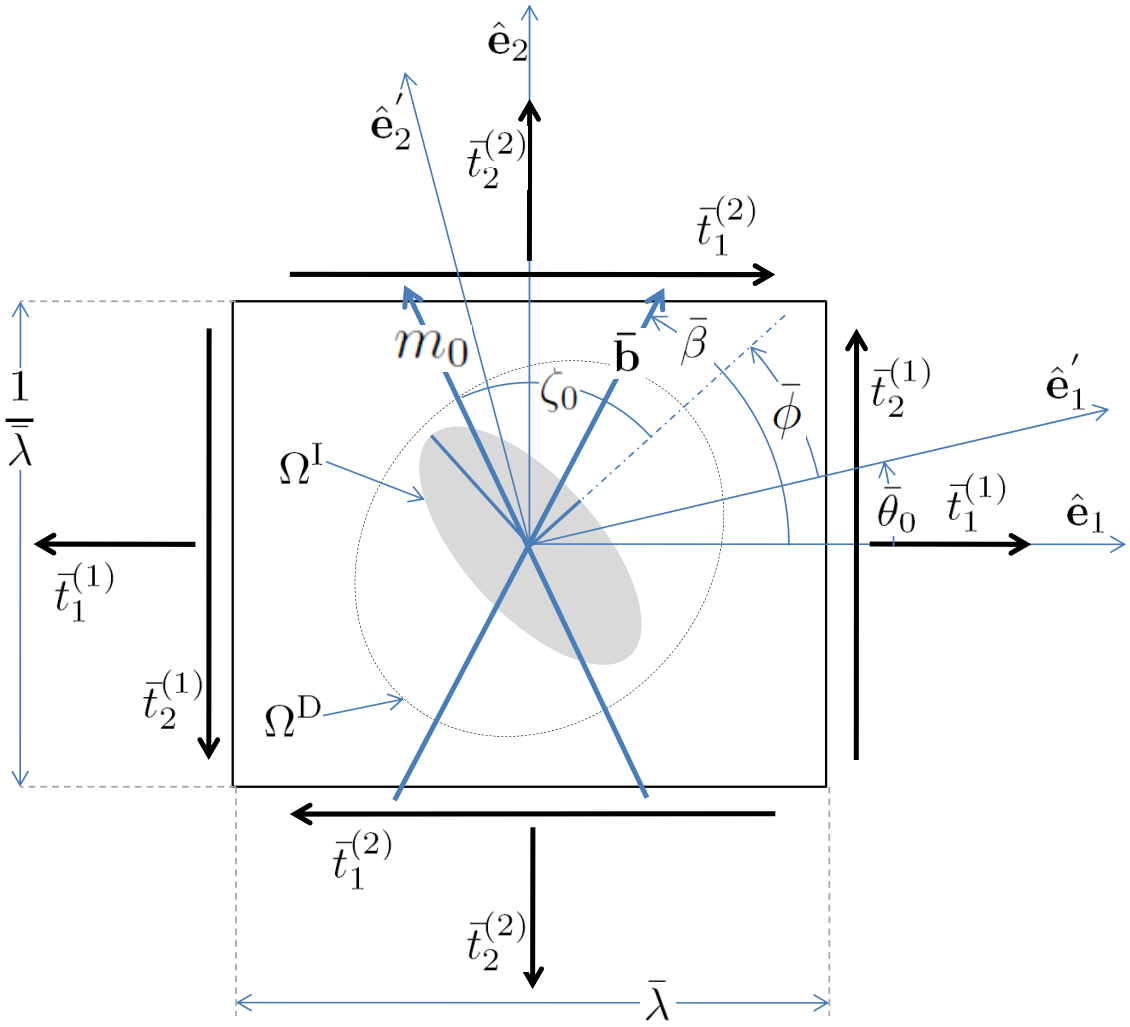

Figure 4.14: Magnetoelastic loading conditions. A sample of MRE is subject to stretch along the $\hat{\mathbf{e}}_1$ axis and a magnetic field $\bar{\mathbf{b}}$ specified in the current configuration. The tractions on the exposed surface $\bar{t}_1^{(1)}$, $\bar{t}_2^{(2)}$, $\bar{t}_1^{(2)}$ and $\bar{t}_2^{(1)}$ are calculated assuming the magnetic field is approximately uniform inside the sample and a non-magnetizable material (vacuum) surrounds the sample.

case the permanent magnetization is characterized by a reference permanent magnetization $\mathbf{M}_0$ which has magnitude M_0 and is at an angle ζ_0 relative to the $\hat{\mathbf{e}}_1'$ axis. This implies that the magnetization of the particles in the current configuration $\mathbf{m}_0$ has magnitude $m_0 = M_0$ and is at an angle ζ_0 relative to their short axis when $w > 1$, as depicted in Figure 4.14.

In this section we take the differential susceptibility of the particles to be isotropic such that the susceptibilities $\boldsymbol{X} = \boldsymbol{\chi} = \chi \boldsymbol{I}$. The magnetic part of the amended free-energy function for the composite specialized from equation (3.100) reduces to

$$\tilde{W}_{mag}(\bar{\boldsymbol{F}}, \bar{\mathbf{B}}) = \frac{1}{2\mu_0 \bar{J}} \bar{\mathbf{B}} \cdot \bar{\boldsymbol{U}}^2 \bar{\mathbf{B}} - \frac{\bar{J}}{2\mu_0} \left(\frac{\bar{\boldsymbol{U}} \bar{\mathbf{B}}}{\bar{J}} + \frac{\bar{\boldsymbol{R}}_{\bar{\phi}} \mathbf{M}_0}{\chi} \right) \cdot \tilde{\boldsymbol{X}} \left(\frac{\bar{\boldsymbol{U}} \bar{\mathbf{B}}}{\bar{J}} + \frac{\bar{\boldsymbol{R}}_{\bar{\phi}} \mathbf{M}_0}{\chi} \right) + \frac{\mu_0 c_0^{\mathrm{I}}}{2\chi} \mathbf{M}_0 \cdot \mathbf{M}_0 \quad (4.43)$$

with

$$\tilde{\boldsymbol{X}}(\bar{\boldsymbol{U}}) = c_0^I \left[\frac{1}{\chi} \boldsymbol{I} - (1 - c_0^I) \boldsymbol{I} + \boldsymbol{P}(\boldsymbol{Z}_0^{\mathrm{I}} \boldsymbol{R}_{\bar{\varphi}}^{\mathrm{T}}) - c_0^I \boldsymbol{P}(\boldsymbol{Z}_0^{\mathrm{D}} \bar{\boldsymbol{U}}) \right]^{-1} \quad (4.44)$$

in this case. The magnetization can also be derived from equation (3.99) as

$$\bar{\mathbf{m}} = \frac{1}{\mu_0} \tilde{\boldsymbol{\chi}}(\bar{\boldsymbol{F}}, \chi) \bar{\mathbf{b}} + \frac{\tilde{\boldsymbol{\chi}}}{\chi} \bar{\boldsymbol{R}}_{\bar{\phi}} \mathbf{M}_0. \quad (4.45)$$

These expressions can be used along with the expressions and variables from section 4.1 to predict and evaluate the constitutive behavior of MREs with permanent magnetization.

Since there is no magnetic saturation for this model we normalize with respect to the magnitude of the permanent magnetization M_0 instead such that

$$\frac{\bar{b}}{\mu_0 M_0}, \quad \frac{\bar{m}}{M_0}, \quad \frac{\bar{t}_i^{(j)}}{G} = \frac{\bar{t}_i^{(j)\mathrm{me}}}{G} + \kappa \frac{\bar{t}_i^{(j)\mathrm{mag}}}{\mu_0 M_0^2}, \quad (4.46)$$

where $\bar{t}_i^{(j)\mathrm{me}}$ corresponds to the contributions of the purely mechanical stresses and $\bar{t}_i^{(j)\mathrm{mag}}$ to the remaining magnetic terms (see equation (4.28)). Similarly the dimensionless parameter

$$\kappa = \mu_0 M_0 / G \quad (4.47)$$

is the appropriate dimensionless group for MREs with permanent magnetization. In the results presented, we only consider the actuation tractions such that κ is not truly

needed, as was the case in section 4.2.2.

4.3.1 Actuation traction for MREs with permanent magnet inclusions.

As discussed in section 3.4.3, the un-deformed un-magnetized state is taken as the reference configuration. From this stress-free state, the material is subjected to some large magnetic field which induces permanent magnetization. Then the applied field is removed and there is some stress and magnetization remaining in the material. The figures in this subsection consider the actuation traction for such a material and can be interpreted as the traction necessary to restore the reference configuration after the permanent magnetization has been induced. In general, this depends on the shape and orientation of the sample relative to the microstructure and applied magnetic field.

For the plots, we consider the material is being held in the reference configuration and the magnetic field is held fixed relative to microstructure by holding $\bar{\beta} - \bar{\theta}_0$ fixed, even as we vary $\bar{\theta}_0$. This implies that the total stress in the material is the same for all loading angles $\bar{\theta}_0$ and the material is just rotating within the laboratory frame. We then consider the traction, which results from the total stress inside the material and the Maxwell stress in the surrounding vacuum, as a function of the material orientation $\bar{\theta}_0$. The actuation traction considered as a function of the loading angle represents the material rotating in the laboratory fixed frame and can be interpreted as evaluating the traction on different rectangular specimens relative to the material microstructure. These figures provide us with a general picture of the surface traction that will be generated by the distribution of magnetic particles in a given configuration.

Actuation traction in the absence of magnetic flux

Figure 4.15 shows the actuation traction when no magnetic field is applied ($\bar{b} = 0$), the particle susceptibility is zero ($\chi = 0$), and the permanent magnetization is aligned along the particles' axis ($\zeta_0 = 0$). For $\bar{\theta}_0 = 0$ the magnetization seeks to extend the sample in the direction of the magnetization such that a compressive traction is necessary, similiar to the case of ferromagnetic materials. When the microstructure is rotated, a combination of normal and distortional shear tractions are needed to

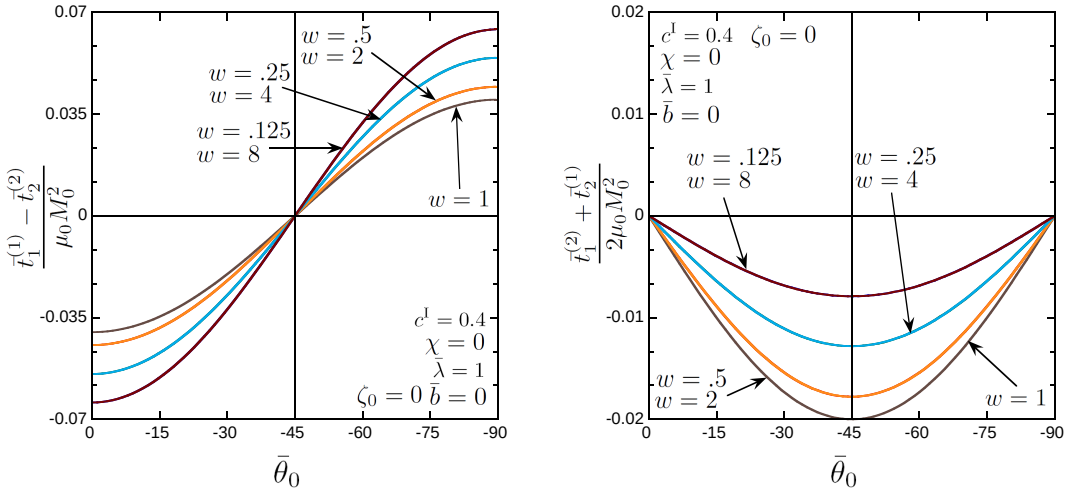

(a) (b)

Figure 4.15: Actuation traction as a function of loading angle for different particle aspect ratios. The permanent magnetization is aligned along the particle axis $\zeta_0 = 0$, the applied flux $\bar{\mathbf{b}} = 0$, and the differential susceptibility $\chi = 0$. (a) The normal traction (b) The distortional shear traction.

maintain the configuration. When $\bar{\theta}_0 = 45°$, only shear tractions are required as the symmetry implies the normal tractions must vanish. It is also interesting that aspect ratios of w and $1/w$ produce exactly the same result in this case, even though the distribution of the magnetization is different. These plots are periodic with respect to $\bar{\theta}_0$ with a complete cycle taking 180°. It is important to note the phase and amplitude of these plots, as these are the primary features which change with the microstructure and material variables we consider in this section. We also point out that there is no shear torque in this case because $\bar{b} = 0$.

Figure 4.16 shows the actuation traction when no magnetic field is applied ($\bar{b} = 0$) and the particles are differentially susceptible ($\chi = 0.99$). The permanent magnetization is aligned along the particles' axis ($\zeta_0 = 0$). The magnetization seeks to extend the sample in the direction of the magnetization as in the previous case ($\chi = 0$) except that here the effect is larger because the differential susceptibility of the particles allows the composite to become more magnetized, indicating that the magnetization reinforces itself. The effect occurs in the dilute limit because the permanent magnetization and vacuum surrounding the particle interact so that the local $\mathbf{b}$ field in

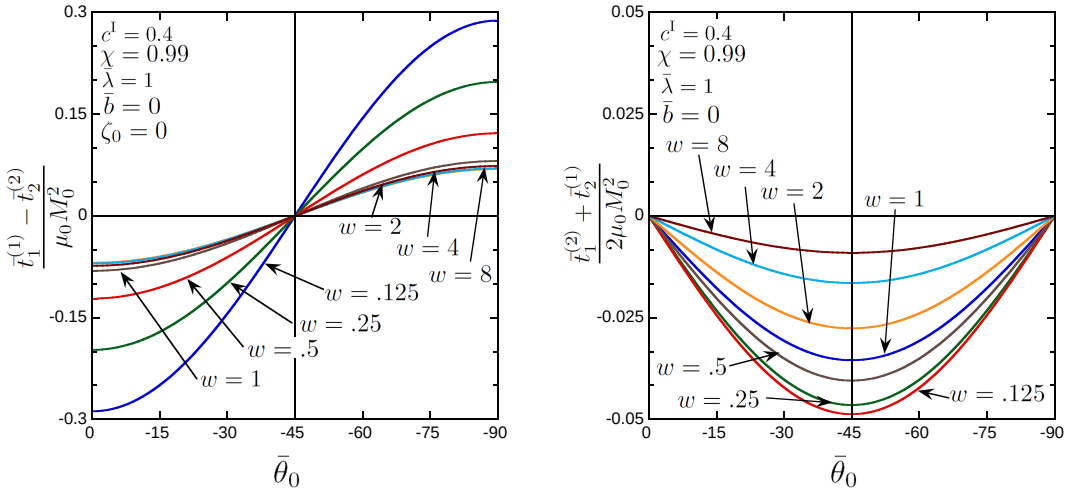

Figure 4.16: Actuation traction as a function of loading angle for different particle aspect ratios. The permanent magnetization is aligned along the particle axis $\zeta_0 = 0$, the applied flux $\bar{\mathbf{b}} = 0$, and the differential susceptibility $\chi = 0.99$. (a) The normal traction (b) The distortional shear traction.

each particle is not zero even though the macroscopic field $\bar{\mathbf{b}} = 0$. Since the particles are differentially susceptible this changes the magnetization of the particles and in all cases they exhibit a magnetization greater than M_0. This effect depends on the shape of the particles which accounts for the difference between aspect ratios of w and $1/w$. Combining these effects together determines the effective remnant magnetization of the composite. This additional magnetization increases the total magnetization and increases the amplitude of the coupling effects.

Figure 4.17 shows the actuation traction when no magnetic field is applied ($\bar{b} = 0$) and no susceptibility ($\chi = 0$) but with permanent magnetization not aligned along a particle axis ($\zeta_0 = 45°$). The primary effect here can be regarded as a phase shift with respect to the plots in Figure 4.15 due to the rotated magnetization. Additionally there is a change in magnitude of the curves because the distribution of the particles and the magnetization direction are not aligned. Figure 4.18 shows the same case with a non-zero particle susceptibility ($\chi = 0.99$). In this case the particles interact with the surrounding vacuum and their susceptibility such that they come to a new magnetization which is not aligned with the remnant magnetization. The angle of the

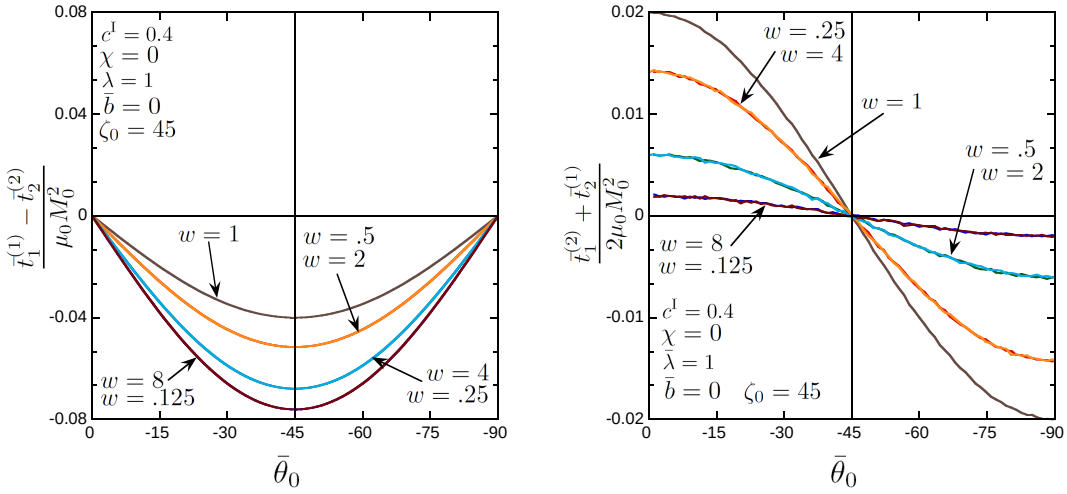

(a) (b)

Figure 4.17: Actuation traction as a function of loading angle for different particle aspect ratios. The permanent magnetization is aligned relative to the particle axis at $\zeta_0 = 45°$, the applied flux $\bar{\mathbf{b}} = 0$, and the differential susceptibility $\chi = 0$. (a) The normal traction (b) The distortional shear traction.

magnetization is different for each aspect ratio. This magnetization angle contributes a phase shift to the plots while the magnitude change modifies the amplitude.

Actuation traction in the presence of magnetic flux

The applied magnetic field has an impact on the actuation tractions. However, for aligned loadings the results reduce to plots already given. If there is no susceptibility ($\chi = 0$), the magnetization is along the particle axis ($\zeta_0 = 0$), and the magnetic field is applied along or perpendicular to the permanent magnetization ($\bar{\beta} - \bar{\theta}_0 = 0°$ or $\bar{\beta} - \bar{\theta}_0 = 90°$), the applied magnetic field has no effect on the tractions and the results coincide with Figure 4.15. This makes sense because the magnetization of the composite is fixed and the tractions only depend on the magnetization. If we consider the case where the particles are susceptible ($\chi \neq 0$) but the loadings are still aligned, as previously suggested, the plots are very similar to Figure 4.16 with different magnitudes.

Figure 4.19 shows the actuation traction when a magnetic field is applied ($\bar{b} = \mu_0 M_0$) at an angle $\bar{\beta} - \bar{\theta}_0 = 20°$, the particle susceptibility is zero ($\chi = 0$), and the

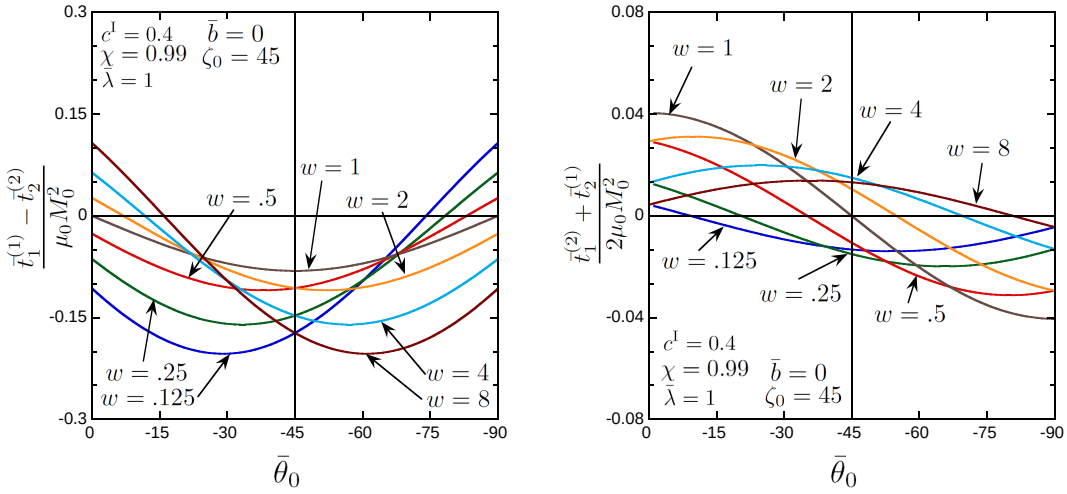

(a) (b)

Figure 4.18: Actuation traction as a function of loading angle for different particle aspect ratios. The permanent magnetization is aligned relative to the particle axis at $\zeta_0 = 45°$, the applied flux $\bar{\mathbf{b}} = 0$, and the differential susceptibility $\chi = 0.99$. (a) The normal traction (b) The distortional shear traction.

permanent magnetization is aligned along the particles' axis ($\zeta_0 = 0°$). Fixing $\bar{\beta} - \bar{\theta}_0$ holds the magnetic field fixed at an angle relative to the microstructure so that the total stress in the material remains fixed and rotates within the laboratory frame. There is a shear torque in this case (not shown) but it is constant with respect to θ_0 because the magnetization and the magnetic flux rotate together. There are two distinct effects enhancing the normal and the distortional shear tractions shown here. The first effect can be understood by considering the case with $w = 1$ which shows the same traction as Figure 4.15. For this case the circular particles do not rotate with respect to the stretch so deformation cannot lower the energy of the particles. Consequently no additional traction develops and the normal traction curve follows the same path as when $\bar{b} = 0$. For all other cases, where $w \neq 1$, the particles rotate with respect to the macroscopic stretch. This means that lower energy can be obtained by deforming the composite such that the permanent magnetization aligns itself with the applied magnetic field. The additional normal and shear stresses correlate to aligning the magnetization with the applied field. The applied field causes a torque on the particles because the energy is lower if the permanent magnetization axis aligns

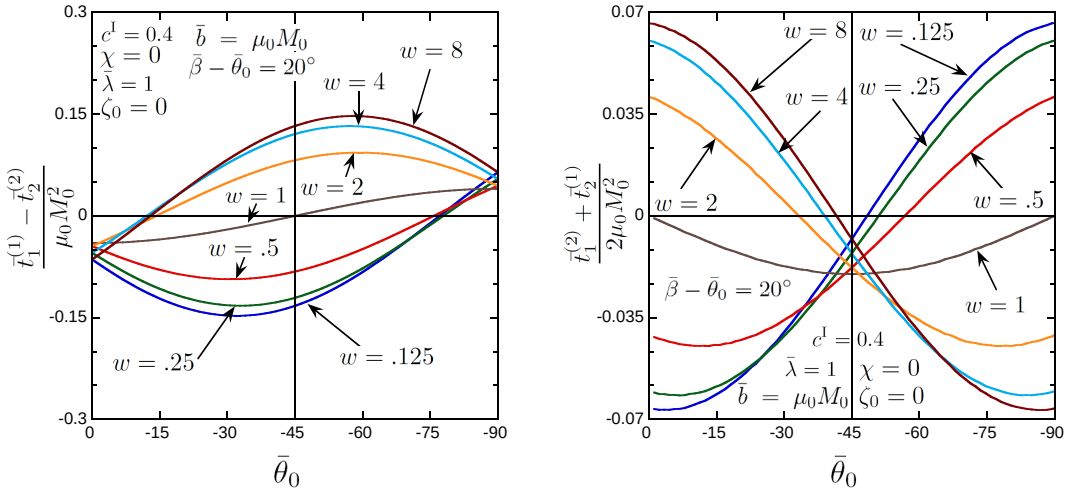

Figure 4.19: Actuation traction as a function of loading angle for different particle aspect ratios. The permanent magnetization is aligned relative to the particle axis at $\zeta_0 = 0°$, the differential susceptibility $\chi = 0$, and the applied flux $\bar{b} = \mu_0 M_0$ at an angle $\bar{\beta} - \bar{\theta}_0 = 20°$.(a) The normal traction (b) The distortional shear traction.

itself with the applied field. The magnitude of this torque can be directly related to the effect on the tractions. In this sense the exact angle of the misalignment does not qualitatively change the result, it merely changes the magnitude of the shear torque and the additional tractions that it produces. Note that all these effects contribute to the magnitude and phase of the traction curves.

Figure 4.20 shows the same case as Figure 4.19 but the particles are also susceptible ($\chi = 0.50$). The susceptibility changes the magnitude and the phase of the traction curves as the particle shape, the susceptibility, and the applied magnetic field interact with vacuum outside the particles to determine a new magnetization for the particles. Then all the previously discussed effects combine together to generate this complicated material behavior.

We have not considered plots as a function of strain in this section. Under the action of a mechanical load, the microstructure in these composites would evolve but this amounts to changing the orientation and distribution of the particles. Here we have considered the effect of microstructure on the tractions; therefore these results can provide a general picture of the magnetic contribution to the tractions even when

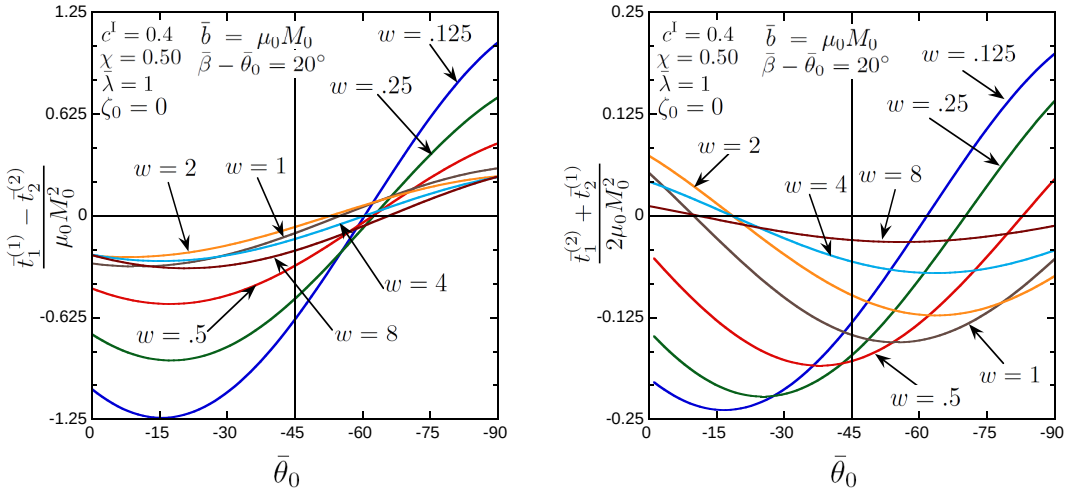

(a) (b)

Figure 4.20: Actuation traction as a function of loading angle for different particle aspect ratios. The permanent magnetization is aligned relative to the particle axis at $\zeta_0 = 0°$, the differential susceptibility $\chi = 0.50$, and the applied flux $\bar{b} = \mu_0 M_0$ at an angle $\bar{\beta} - \bar{\theta}_0 = 20°$. (a) The normal traction (b) The distortional shear traction.

the composite is deformed.

4.4 Concluding remarks

In this work we have developed constitutive models for a special class of magnetorheological elastomers (MREs) consisting of aligned fibers with elliptical cross-section of a soft magnetic material distributed randomly in an elastomeric matrix phase. The model was obtained by means of the magnetoelastic homogenization framework of Chapter 3 (Ponte Castañeda and Galipeau, 2011) via the corresponding purely mechanical model of Lopez-Pamies and Ponte Castañeda (2006b). It is valid for finite deformations and arbitrary values of the applied magnetic field. The model can account for relatively general magnetic behavior, including the initial susceptibility and magnetic saturation of the particles, as well as for the initial microstructure of the MRE and its evolution under finite deformations. Thus, for non-aligned loadings (in the transverse plane), the magnetic field generates torques on individual particles (or groups of particles) which in turn leads to macroscopic torques on a given sample

of the MRE. These effects are found to be of first order in the fiber concentration, and can have a significant impact on the constitutive behavior of the MRE even for small concentrations, as opposed to dipole-type interactions which are of order volume fraction squared and have negligible effects for dilute concentrations (Galipeau and Ponte Castañeda, 2012).

Another important feature of the model is its ability to deal consistently with magnetic saturation effects. Given that the magnetization of the fibers saturates for sufficiently high values of the magnetic field, and that the matrix phase is itself magnetically insensitive, it is expected that the effects of the applied magnetic field on a given MRE sample should also saturate at sufficiently high values of the field. Indeed, our results show that although the total stresses inside the sample continue to increase with increasing values of the magnetic field, the macroscopic traction-strain response of the sample tends to saturate. This is a consequence of the magnetic fields surrounding the given sample, which must be accounted for by the implementation of the appropriate jump conditions on the boundary of the specimen, leading to the cancelation of the unbounded contributions of the magnetic fields to the total stresses. Because of this, it is found that all coupled magnetoelastic effects, such as the actuation tractions (including macroscopic torques), magnetostrictive strains and magnetoelastic moduli tend to saturate at sufficiently high values of the applied magnetic field. It is therefore crucial to account for these saturation effects in the accurate estimation of these magnetoelastic properties.

We have also investigated materials when the particles exhibit permanent magnetic composites by considering the actuation stresses in the reference configuration. We see that the permanent magnetization of the composite does have an impact on the constitutive behavior of the composite. However these models are somewhat limited to a small range of applied fields because large magnetic field would change the permanent magnetization of the materials and at present we have no simple means to include hysteresis behavior.

Chapter 5

Comparison with FEM results

In this chapter the effective behavior of magnetorheological elastomers (MREs) with random and periodic distribution of the particles is studied. We analyze the role of microstructure, concentration, and particle shape on the coupled behavior of these composites. We apply the model for MREs with random distributions of particles developed in Chapter 4 (Galipeau and Ponte Castañeda, 2012), to a pure shear loading in the presence of a magnetic field and we obtain a closed form expression for the MREs' response. To study the behavior of MREs with periodic microstructures, we develop a finite element-based code and obtain the effective properties of the periodic MREs with rectangular and quasi-hexagonal microstructures.

We demonstrate that the governing parameter of the magnetomechanical coupling is not the magnetic susceptibility but its derivative with respect to deformation. This parameter is directly related to magnetostriction, actuation stress, and the magnetoelastic Young's modulus in a uniaxial tension test. We reveal that the magnetoelastic effects are rather different even for microstructures that have the same effective susceptibility. By evaluating the magnetomechanical coupling parameter for random as well as periodic quasi-hexagonal and rectangular microstructures, we show that the magnetoelastic effects are of second order in the concentration. This implies that the coupled behavior is primarily the result of the interaction between inclusions. We evaluate the magnetostriction as a function of the concentrations and aspect ratio to provide the guidance for the optimal microstructures of MREs.

The concise homogenization framework to determine the total magnetoelastic stress within the composite material was introduced in Chapter 3 and it was shown that significant simplifications of expressions describing the effective behavior of MREs can be obtained for the composites with nearly rigid inclusions. For the particular case of layered microstructures, the homogenization is available through the exact solution of the boundary value problem as it was shown by Rudykh and deBotton (2011) for the analogous case of electroactive laminates. However, the set of microstructures for which exact solutions can be obtained is rather limited, and the effective behavior of MREs should be estimated via homogenization. By application of the theoretical framework for MREs with random distribution of the particles, important characteristics such as magnetostriction, actuation stress, and magnetoelastic moduli are determined (Galipeau and Ponte Castañeda, 2012, 2013). In this work we make use of these results to further compare them to MREs with periodic microstructures.

In general seeking an exact solution for periodic materials subjected to finite deformations is a daunting task even for purely mechanical problem. Therefore the finite element (FE) method is usually employed to tackle such problems (Rudykh and deBotton, 2012). Consequently we develop a FE-based code for solving the magnetomechanical problem in finite deformation and periodic boundary conditions. Specifically we examine periodic MREs with *(i) rectangular* and *(ii) quasi-hexagonal* periodicity and obtain the effective properties of the composites by averaging the local fields under the unit cell domains.

We define the parameters that govern the coupled magnetomechanical behavior of MREs. These parameters are directly related to the applied traction measured on the surface of the material while accounting for the magnetic stresses outside the material. The governing parameters of the magnetomechanical coupling are evaluated for MREs with random, quasi-hexagonal, and rectangular periodic microstructures over a wide range of concentrations and particle aspect ratios. Moreover, we find that linearly magnetic materials with the same susceptibilities can have rather different magnetoelastic coupling.

5.1 Homogenization of periodic and randomly structured MREs

Consider MREs made with rigid, linearly magnetizable particles and a magnetically non-susceptible, incompressible elastic matrix. Depending on the microstructure, the composite may exhibit significantly different macroscopic responses. To obtain the effective properties of the composite we follow the work in Chapter 3 (Ponte Castañeda and Galipeau, 2011) and make use of the scale-separation assumptions; in particular, we assume that the characteristic size of the sample is significantly larger than the characteristic length of the microstructure, such that boundary effects can be neglected.

The response of the composite can be characterized by considering the behavior of a representative volume element which can be identified with Ω_0. Due to the magnetomechanical loading, the occupied region transforms into a new region Ω. The effective constitutive behavior of the composite is then characterized as the relationship between the volume averaged field quantities denoted with barred quantities (Ponte

Castañeda and Galipeau, 2011). Note that barred values for Lagrangian quantities such as $\boldsymbol{F}$, $\boldsymbol{S}$, $\mathbf{B}$, and $\mathbf{H}$ are averaged over the reference region Ω_0; for example,

$$\bar{\boldsymbol{F}} = \frac{1}{|\Omega_0|}\int_{\Omega_0} \boldsymbol{F} dV, \tag{5.1}$$

while the Eulerian quantities, $\boldsymbol{T}$, $\mathbf{b}$, $\mathbf{h}$, and $\mathbf{m}$, are averaged over the deformed configuration,

$$\bar{\boldsymbol{T}} = \frac{1}{|\Omega|}\int_{\Omega} \boldsymbol{T} dv. \tag{5.2}$$

with $|\Omega_0|$ and $|\Omega|$ denoting the volume of the undeformed and deformed regions respectively.

Additionally when the local phases are characterized by energy functions, the overall composite can be characterized by a homogenized energy function $\tilde{W}(\bar{\boldsymbol{F}}, \bar{\mathbf{B}})$ or, alternatively, $\tilde{\phi}(\bar{\boldsymbol{F}}, \bar{\mathbf{b}})$. The Lagrangian energy function $\tilde{W}(\bar{\boldsymbol{F}}, \bar{\mathbf{B}})$ is found by averaging the local energy over the reference configuration consistent with the homogenization approach of Ponte Castañeda and Galipeau (2011). This Lagrangian energy is then used to define the Eulerian energy function via equation (2.11).

In this chapter we consider the effective behavior of MREs with random and periodic distributions of the magnetoactive particles in the soft matrix. For composites with random distributions, the homogenization is performed by considering the response of a representative volume element to fields $\bar{\boldsymbol{F}}$ and $\bar{\mathbf{B}}$ applied on the boundary of the composite. In this case the microstructure is not specified exactly and we make use of estimates which take advantage of two-point statistics to approximate the magnetoelastic energy function of the composite.

For periodic media the initial microstructure is fully determined once the unit cell has been specified. The effective properties can be found by evaluating the response of the primitive unit cell under periodic boundary conditions. Once again, we assume that the material occupies a sufficiently large domain and the influence of the boundary effects can be neglected. This applies up to the onset of instabilities at which the periodicity scale can spontaneously change and become larger than the single unit cell. This corresponds to the onset of long wavelength instabilities and loss of ellipticity. Consideration of these effects is beyond the scope of this chapter and will not be considered here.

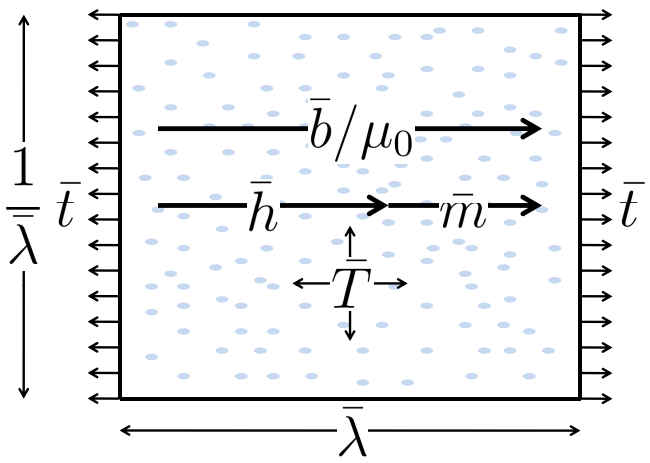

Figure 5.1: The schematic of the experiment on a MRE sample. The sample is excited by applying a $\bar{b}$ field and a stretch $\bar{\lambda}$ and the system responds by determining a $\bar{m}$, $\bar{h}$, $\bar{t}$ and $\bar{T}$.

5.2 Theoretical analysis of 2-D aligned loadings

5.2.1 Magnetomechanical loading conditions

Homogenization of the MREs under general loading conditions can be rather complicated. Additionally even if the homogenization can be carried out, analyzing the results for completely general loading can be quite daunting so in this chapter we consider only the response of 2-dimensional incompressible MREs subjected to magnetomechanical loadings aligned along the symmetry axis of the material, $\hat{\mathbf{e}}_1$ and $\hat{\mathbf{e}}_2$. The loading is defined via the average deformation gradient

$$\bar{\boldsymbol{F}} = \hat{\mathbf{e}}_1 \otimes \hat{\mathbf{e}}_1 \bar{\lambda} + \hat{\mathbf{e}}_2 \otimes \hat{\mathbf{e}}_2 \bar{\lambda}^{-1}, \tag{5.3}$$

and mean magnetic field

$$\bar{\mathbf{b}} = \bar{b}\hat{\mathbf{e}}_1, \tag{5.4}$$

as it is schematically depicted in Figure 5.1. We consider MREs with particles distributed such that their ellipticity axes are aligned with $\hat{\mathbf{e}}_1$ and $\hat{\mathbf{e}}_2$. Thus the general material response is characterized by the magnetization $\bar{m}$, the magnetic intensity $\bar{h}$ along the $\hat{\mathbf{e}}_1$ direction. Clearly the stress tensor $\bar{\boldsymbol{T}}$ has components along both axes. However by eliminating the Lagrange multiplier associated with the incompressibility

constraint we define the specifiable component as

$$\bar{T} = \bar{T}_{11} - \bar{T}_{22}. \tag{5.5}$$

This implies that only one traction $\bar{t}$ in the $\hat{\mathbf{e}}_1$ direction is necessary to achieve the specified deformation (alternatively, $\bar{t}$ can also be defined to be the difference between the traction on the two surfaces). Note that these loading conditions can produce motion in a line such that they have potential uses as "linear actuators." We emphasize that the non-linearity of constitutive relationships, finite deformations, and the non-linearity due to magneto-mechanical coupling are indeed taken into account.

5.2.2 The parameters governing MRE performance

Clearly the particles move with respect to one another as a result of the deformation; we refer to this change as microstructure evolution. Since the loading is aligned along a symmetry axis of the material, it can be assumed that the particles do not rotate with respect to the magnetic field and the material symmetry axes remain unchanged. This condition holds true for periodic composites up to the onset of bifurcations and should remain a good assumption for MREs with random microstructures.

The effective energy for these composites under uniaxial tension was shown by Ponte Castañeda and Siboni (2011) to be

$$\tilde{\phi}(\bar{\lambda}, \bar{b}) = \tilde{\phi}_{\mathrm{me}}(\bar{\lambda}) - \tilde{\chi}(\bar{\lambda})\frac{\bar{b}^2}{2\bar{\rho}\mu_0}, \tag{5.6}$$

where $\tilde{\phi}_{\mathrm{me}}(\bar{\lambda})$ is a function of the stretch only. Note that considering $\bar{b} = 0$, $\tilde{\phi}_{\mathrm{me}}(\bar{\lambda})$ is the mechanical energy function for the composite in the absence of the magnetic field. This form of the energy is appropriate as long as the magnetic field does not cause rotation of the particles when $\bar{\lambda}$ is held fixed. Consequently, the macroscopic magnetic relations for the composite can be written as

$$\bar{m} = \tilde{\chi}(\bar{\lambda})\frac{\bar{b}}{\mu_0} \qquad \text{or} \qquad \bar{h} = (1 - \tilde{\chi}(\bar{\lambda}))\frac{\bar{b}}{\mu_0} \tag{5.7}$$

where $\tilde{\chi}(\bar{\lambda})$ is the magnetic susceptibility of the composite and is a function of the macroscopic stretch.

The energy form (5.6), the overall incompressibility, and equations (5.3), (5.4)

(2.13) and (5.5) yield

$$\bar{T} = \bar{\rho}\frac{\partial\tilde{\phi}(\bar{\lambda},\bar{b})}{\partial\bar{\lambda}}\bar{\lambda} + \frac{\bar{b}^2}{\mu_0} - \bar{m}\bar{b} = \bar{T}_{me}(\bar{\lambda}) + \mu_0\bar{m}^2\frac{\partial\tilde{\chi}^{-1}(\bar{\lambda})}{\partial\bar{\lambda}}\frac{\bar{\lambda}}{2} + \frac{\bar{b}^2}{\mu_0} - \bar{m}\bar{b}, \tag{5.8}$$

where $\bar{T}_{me}(\bar{\lambda}) = \bar{\rho}\frac{\partial\tilde{\phi}_{\mathrm{me}}(\bar{\lambda})}{\partial\bar{\lambda}}\bar{\lambda}$ represents the "purely mechanical" stress.

Additionally, accounting for the boundary effects of the magnetic field via equation (2.38), we find that the applied traction is

$$\bar{t} = \bar{T}_{me}(\bar{\lambda}) + \tilde{\Upsilon}(\bar{\lambda})\mu_0\bar{m}^2, \tag{5.9}$$

where the "magnetoelastic coefficient" is given by

$$\tilde{\Upsilon}(\bar{\lambda}) = \left(\frac{\partial\tilde{\chi}^{-1}(\bar{\lambda})}{\partial\bar{\lambda}}\frac{\bar{\lambda}}{2} - \frac{1}{2}\right). \tag{5.10}$$

It is easy to see that the magnetoelastic effects are related to the derivative of the susceptibility $\tilde{\chi}$ and are quadratic in the magnetization from equation (5.9).

This analysis emphasizes the importance of $\tilde{\Upsilon}$ for magnetoelastic materials. In particular the "magnetoelastic coefficient" can be directly related to the actuation stress and the magnetostriction. The actuation stress $\bar{t}^{(0)}$ is defined as the traction when no macroscopic stretch is applied. Since the mechanical stress vanishes when $\bar{\lambda} = 1$, the actuation stress is purely magnetic in nature and is given by

$$\bar{t}^{(0)} = \bar{t}|_{\bar{\lambda}=1} = \mu_0\bar{m}^2\tilde{\Upsilon}(\bar{\lambda} = 1). \tag{5.11}$$

Similarly the magnetostriction is defined as the stretch when no mechanical load is applied. The magnetostrictive stretch $\bar{\lambda}_{\mathrm{m}}$ can be determined by solving the following equation

$$-\bar{T}_{me}(\bar{\lambda}_{\mathrm{m}}) = \mu_0\bar{m}^2\tilde{\Upsilon}(\bar{\lambda}_{\mathrm{m}}). \tag{5.12}$$

Note that $\bar{m}$ is a function of $\bar{\lambda}$ if $\bar{b}$ or $\bar{h}$ is chosen to be the independent variable.

Furthermore, the magnetoelastic coefficient determines how the magnetic field changes the effective stiffness. The associated effective magnetoelastic Young's modulus is measured with respect to the applied traction such that we define the effective modulus to be the derivative of the traction with respect to the logarithmic strain

$\bar{e} = \ln \bar{\lambda}$

$$\tilde{E} \equiv \frac{\partial \bar{t}}{\partial \bar{e}}. \tag{5.13}$$

For the considered magnetomechanical loadings the effective Young's modulus is

$$\tilde{E} = \tilde{E}_{me}(\bar{\lambda}) + \frac{\partial \tilde{\Upsilon}(\bar{\lambda})}{\partial \bar{\lambda}} \mu_0 \bar{m}^2 \bar{\lambda} + 2\tilde{\Upsilon}(\bar{\lambda}) \mu_0 \bar{m} \frac{\partial \bar{m}}{\partial \bar{\lambda}} \bar{\lambda}, \tag{5.14}$$

where $\tilde{E}_{me}(\bar{\lambda}) = \frac{\partial \bar{T}_{me}(\bar{\lambda})}{\partial \bar{\lambda}} \bar{\lambda}$ is the purely mechanical Young's modulus which, indeed, reduces to the linear Young's modulus for the composite in the small-strain limit.

In general the relation between the magnetization and the stretch is controlled by the experimental conditions; for instance we could hold $\bar{b}$ fixed with respect to $\bar{\lambda}$ or hold $\bar{h}$ fixed with respect to $\bar{\lambda}$. Here, for convenience, we will consider the case where the magnetization $\bar{m}$ is held fixed with respect to deformation and define the magnetoelastic part of the modulus

$$\tilde{E}_{mag}(\bar{\lambda}) = \frac{\partial \tilde{\Upsilon}(\bar{\lambda})}{\partial \bar{\lambda}} \bar{\lambda} \mu_0 \bar{m}^2 = \left[\frac{\partial^2 \tilde{\chi}^{-1}(\bar{\lambda})}{\partial \bar{\lambda}^2} \frac{\bar{\lambda}^2}{2} + \frac{\partial \tilde{\chi}^{-1}(\bar{\lambda})}{\partial \bar{\lambda}} \frac{\bar{\lambda}}{2} \right] \mu_0 \bar{m}^2. \tag{5.15}$$

Note that the sign of $\tilde{E}$ determines whether the magnetic field stiffens or softens the composite. Clearly, since $\bar{\lambda}$, $\bar{m}^2$, and μ_0 can take only positive values, the sign of $\tilde{E}$ is determined by $\frac{\partial \tilde{\Upsilon}(\bar{\lambda})}{\partial \bar{\lambda}}$, which in general is a function of deformation.

Equations (5.10) and (5.15) show that the critical parameter for determining magnetoelastic effects is not the susceptibility $\tilde{\chi}$ but its derivative with respect to deformation. Moreover, in general, MREs with different microstructures may be characterized by the same susceptibility while having significantly different magnetoelastic coefficients. Consequently the magnetomechanical behavior of the MREs with the same constituents and similar volume fractions may be significantly different. Remarkably the magnetic field may either stiffen or soften the composites depending on microstructure. We further examine MREs with different microstructures described in the next section to illustrate these effects.

5.2.3 The mechanical reinforcement

Effects such as magnetostriction also depend on the mechanical stiffness in the composite. To evaluate the mechanical reinforcement in the dilute limit we define the

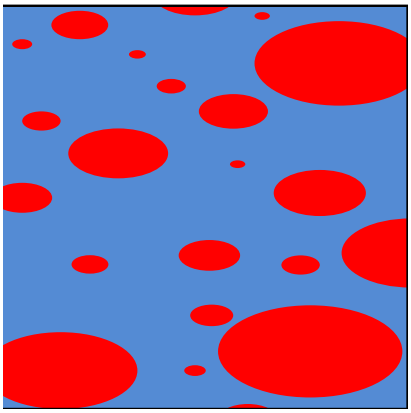

Figure 5.2: Random distribution of magnetoactive particles in soft matrix.

normalized mechanical stress polarization $\tilde{N}$ such that

$$\bar{T}_{me} = T_{me}^{(1)}(\bar{\lambda}) + \tilde{N}Gc\ln(\bar{\lambda}) \tag{5.16}$$

where $T_{me}^{(1)}(\bar{\lambda})$ is the purely mechanical stress in the homogenous matrix material subject to stretch $\bar{\lambda}$, G is the small-strain shear modulus of the matrix, and c is the concentration of rigid inclusions. The superscript (1) denotes the matrix phase. It is important to consider the mechanical stiffening because the magnetostriction depends on the relation between the mechanical stiffness and magnetoelastic forces. Additionally, when considering the magnetoelastic modulus, it is desirable that the magnetic field causes a large change in the modulus relative to the underlying mechanical stiffness. The underlying mechanical stiffness of the composite depends on the reinforcement effect of the particles and it is different for each microstructure.

5.3 Macroscopic responses of MREs with different microstructures

5.3.1 Constituent energy functions

Recalling that the matrix is magnetically inactive, we assume that its behavior can be described by a neo-Hookean model. Consequently, the material energy function reduces to

$$\phi^{(1)}(\boldsymbol{F}) = \frac{G}{2\rho_0^{(1)}}\left[\mathrm{tr}(\boldsymbol{F}^{\mathrm{T}}\boldsymbol{F}) - 2\right], \tag{5.17}$$

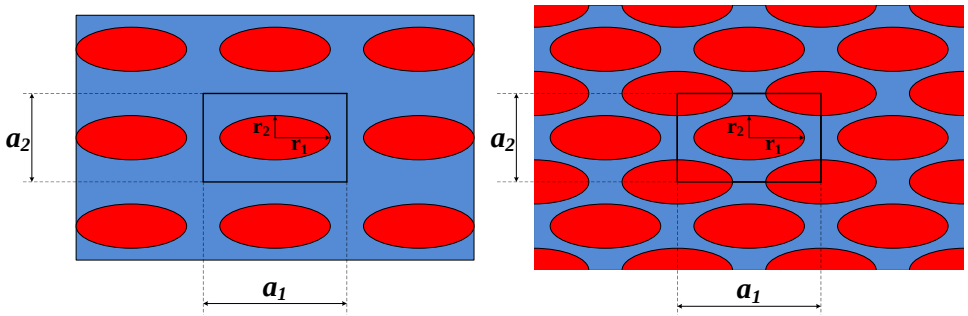

(a) (b)

Figure 5.3: A schematic representation of MREs with rectangular (a) and hexagonal (b) periodic microstructures.

where G is the shear modulus of the matrix phase. The total stress tensor in the matrix phase which is given by expression (2.13) includes the magnetic Maxwell stress tensor and, consequently, depends on the local magnetic field.

Assuming linear magnetic behavior for the particles, their response is characterized by

$$\phi^{(2)}(\boldsymbol{F}, \mathbf{b}) = \phi^{(2)}_{\text{me}}(\boldsymbol{F}) - \chi \frac{\mathbf{b} \cdot \mathbf{b}}{2\rho^{(2)}\mu_0}, \tag{5.18}$$

where χ is the magnetic susceptibility, and the superscript (2) denotes the inclusion phase. The rigidity of the particles is enforced by assuming that $\phi^{(2)}_{\text{me}}(\boldsymbol{F})$ is equal to zero if $\boldsymbol{F}$ is a pure rotation and infinity otherwise.

As described previously these two phases can be combined in different microstructures which will result in different magnetoelastic properties. In this work we examine the responses of MREs with three different microstructures: *(i)* MREs with *random* distribution of the magnetoactive particles (Figure 5.2); *(ii)* MREs with *periodic rectangular* microstructure (Figure 5.3a); *(iii)* MREs with *periodic quasi-hexagonal* microstructure (Figure 5.3b).

5.3.2 Random microstructures

The energy of the MREs with the random microstructure is characterized by the concentration c and aspect ratio w of the particles and their relative distributions. The particles are also assumed to be distributed randomly with "ellipsoidal" symmetry (Willis, 1977) with an initial aspect ratio which for this work we take to be w, the same shape as the particles. The distributional ellipsoid characterizes the average

distance between the particles in different directions.

Specializing the work of (Lopez-Pamies and Ponte Castañeda, 2006b) to uniaxial loading along the fiber direction, the homogenized mechanical energy is given by

$$\tilde{\phi}_{\text{me}}^{(\text{ran})}(\bar{\lambda}) = \frac{G}{2\bar{\rho}_0}(1-c)\left(\frac{\left[1+2\left(c-2\right)c\bar{\lambda}^2+\bar{\lambda}^4\right]w+c\left(1-\bar{\lambda}^4\right)\left(1+w^2\right)}{\left(1-c\right)^2\bar{\lambda}^2 w}-2\right). \tag{5.19}$$

Similarly specializing the results of Chapter 4 (Galipeau and Ponte Castañeda, 2013) to uniaxial loading along the fiber direction, we write the effective susceptibility $\tilde{\chi}(\bar{\lambda})$ for the aligned loading in the form of

$$\tilde{\chi}^{(\text{ran})}(\bar{\lambda}) = c\left[\frac{1}{\chi}-\frac{w}{w+1}+c\frac{w\bar{\lambda}^2}{w\bar{\lambda}^2+1}\right]^{-1}. \tag{5.20}$$

$w\bar{\lambda}^2$ represents the aspect ratios of the distributional ellipsoid in the deformed configuration consistent with the partial decoupling approximation (Galipeau and Ponte Castañeda, 2012, 2013).

From expressions (5.20) and (5.10) the magnetoelastic coefficient can be determined explicitly as

$$\tilde{\Upsilon}^{(\text{ran})}(\bar{\lambda}) = \frac{w\bar{\lambda}^2}{\left(1+w\bar{\lambda}^2\right)^2}-\frac{1}{2}. \tag{5.21}$$

Equation (5.15) yields the explicit expression for the effective elastic modulus, namely

$$\frac{\tilde{E}_{mag}}{\mu_0\bar{m}^2} = \frac{2w\bar{\lambda}^2\left(1-w\bar{\lambda}^2\right)}{\left(1+w\bar{\lambda}^2\right)^3}. \tag{5.22}$$

5.3.3 MREs with rectangular and quasi-hexagonal periodic microstructures.

We develop a finite element (FE) based model to analyze the behavior of the MREs with periodic microstructures. We examine periodic MREs with two main unit cells, rectangular and quasi-hexagonal (see Figure 5.3). Within each of these unit cells the microstructure can be varied further by varying the aspect ratio of the unit cell, the aspect ratio of the inclusions, and the concentration.

To prevent the particles from extending past the unit cell and to maintain parity with the random microstructures, the aspect ratio of the unit cells are varied with

the aspect ratio of the particles. For the rectangular unit cell the ratio between the lengths of vertical and horizontal faces (a_1 and a_2 respectively) varies with the inclusion ellipticity ratio such that

$$a_1^{(rec)}/a_2^{(rec)} = w, \tag{5.23}$$

while the ratio between the lengths of vertical and horizontal sides of the hexagonal unit cell is

$$a_1^{(hex)}/a_2^{(hex)} = \sqrt{3}w. \tag{5.24}$$

We set the origin of the coordinate system to be the center of one of the particles for convenience, implying that

$$-\frac{a_1}{2} \leq X_1 \leq \frac{a_1}{2}, \qquad -\frac{a_2}{2} \leq X_2 \leq \frac{a_2}{2}, \tag{5.25}$$

for each unit cell, respectively. The regions define the reference domain Ω_0.

The radii of the inclusions is defined via the inclusion volume fraction and representative volume element (RVE) geometry parameters

$$r_2^{(rec)} = \left(\frac{c}{\pi}\right)^{1/2} a_2 \quad \text{and} \quad r_2^{(hex)} = \left(\frac{\sqrt{3}c}{2\pi}\right)^{1/2} a_2, \quad \text{and} \quad r_1 = wr_2. \tag{5.26}$$

The magnetomechanical loading is implemented by applying periodic boundary conditions for both displacement (Rudykh and deBotton, 2012) and magnetic field. This is accomplished by specifying the deformation and magnetostatic potential on the boundary of the composite. (Since Curl $\mathbf{H} = 0$, there exists a scalar field, the magnetostatic potential φ, such that $\mathbf{H} = -\text{Grad}\,\varphi$.) On the top $\left(X_2 = \frac{a_2}{2}\right)$ and bottom $\left(X_2 = -\frac{a_2}{2}\right)$ boundaries, the deformation and magnetostatic potential are

$$\begin{cases} x_1^{(T)} = x_1^{(B)} \\ x_2^{(T)} = x_2^{(B)} + \frac{1}{\lambda} a_2 \\ \varphi^{(T)} = \varphi^{(B)} \end{cases}, \tag{5.27}$$

while the on right $\left(X_1 = \frac{a_1}{2}\right)$ and left $\left(X_1 = -\frac{a_1}{2}\right)$ boundaries, the deformation and

magnetostatic potential are related via

$$\begin{cases} x_1^{(L)} = x_1^{(R)} + \bar{\lambda} a_1 \\ x_2^{(L)} = x_2^{(R)} \\ \varphi^{(L)} = \varphi^{(R)} + \bar{H} b \end{cases} . \tag{5.28}$$

We use the magnetic intensity $\mathbf{H}$ as the independent variable for the finite element solution. The boundary value problems are solved by means of commercial FE code COMSOL Multiphysics. Once the local fields are determined via the FEM, the material response is measured by integrating the local field over the relevant domain.

For the purposes of the FE simulations, the shear modulus of the matrix is set to $G = 1$ MPa. Additionally since the rigid inclusions must be "deformable" for the FEM simulations, their mechanical behavior is taken to be the same as the matrix with a stiffness of $G^{(2)} = 1$GPa, i.e. $\phi_{me}^{(2)} = 1000\phi_{me}^{(1)}$. This is consistent with the fact that the inclusions are stiff and the matrix accommodates the deformation along the load path. In general, the finite element simulation would need to be performed for each combination of $\bar{\lambda}$ and $\bar{H}$. However for each value of $\bar{\lambda}$ we can perform the FE simulations at $\bar{H} = 0$ and a non-zero $\bar{H}$ and extrapolate to all other values of the magnetic field based on the analysis in section 5.2. For this work we set

$$\bar{H} = \sqrt{\frac{G}{\mu_0}} \tag{5.29}$$

so that the magnetoelastic stresses are of comparable magnitude to the purely mechanical stresses.

From data obtained for $\bar{\mathbf{B}}$, $\bar{\mathbf{H}}$, $\bar{\boldsymbol{F}}$, $\bar{\boldsymbol{T}}$, and $\bar{\boldsymbol{T}}_{\text{me}}$ as a function of λ, the corresponding $\bar{b}$, $\bar{h}$, $\bar{m}$, $\bar{T}$, and $\bar{T}_{\text{me}}$ are computed. The corresponding magnetoelastic parameters are calculated directly without computing the energy. In this regard we note that there are two distinct ways to evaluate the magnetoelastic coefficient from the fundamental quantities directly evaluated or input into the FE code. Considering that $\bar{b}$, $\bar{h}$, $\bar{m}$, $\bar{\lambda}$, $\bar{T}$, and $\bar{T}_{\text{me}}$ are defined, the first way to compute the magnetoelastic coefficient is to use the total stress

$$\tilde{\Upsilon}^{(\mathrm{T})}(\bar{\lambda}) = \frac{\bar{T} - \left(\bar{T}_{\text{me}} + \bar{b}^2/\mu_0 - \bar{m}\bar{b}\right)}{\mu_0 \bar{m}^2} - \frac{1}{2}. \tag{5.30}$$

The second way is to determine the susceptibility from $\bar{b}$ and $\bar{m}$ and consider the incremental change in the quantity to determine the magnetoelastic coefficient as

$$\tilde{\Upsilon}^{(\chi)}(\bar{\lambda}) = \frac{1}{\mu_0}\frac{\partial\left(\bar{b}/\bar{m}\right)}{\partial\bar{\lambda}}\frac{\bar{\lambda}}{2} - \frac{1}{2}. \tag{5.31}$$

These two quantities should be the same if the assumptions are correct and the FE code is sufficiently accurate. For the results we present in this work, these quantities coincide.

5.4 Results and discussion

To highlight the underlying magnetoelastic mechanisms in these different microstructures, we present the sophisticated picture in terms of the following parameters:

- $\tilde{\Upsilon}$, the magnetoelastic coupling coefficient given by equation (5.10) which provides information about the magnetic contribution to the traction;
- $\tilde{\chi}/c$, the effective susceptibility normalized by the concentration which describes the magnetization behavior of the composite;
- $\tilde{E}_{mag}(\bar{\lambda})/(\mu_0\bar{m}^2)$ the normalized magnetoelastic modulus, where $\tilde{E}$ is given by equation (5.15); this quantity captures the variable stiffness of the composite;
- $\tilde{N}$ the mechanical stress polarization in the inclusion; a measure of the purely mechanical reinforcement of the composite due to the heterogeneity given by equation (5.16).

5.4.1 Magnetoelastic properties as a function of the stretch

Figure 5.4 displays the effective properties of the composite with the aspect ratio $w = 1$ and volume fraction $c = 0.1$ as a function of the logarithmic strain $\bar{e} = \ln\bar{\lambda}$. Consistent with Eshelby's result for dilute magnetic composites (Eshelby, 1957), the susceptibility $\tilde{\chi}$ for these materials differs only by terms of order concentration. Note that as the composite is compressed, the particles get closer together in the magnetic field direction and the susceptibility goes up. This is consistent with more magnetic interactions between the particles. The mechanical reenforcement for these

three composites is quite similar in the reference configuration but behaves quite differently for large stretch. The fact that $\tilde{N}$ changes with the deformation indicates the nonlinearity in the mechanical reinforcement with respect to strain which must be accounted for when considering large magnetostriction.

However these materials show very different magnetoelastic coupling. The magnetoelastic coefficient $\tilde{\Upsilon}$ can be both positive and negative. Thus the magnetostriction can be extension or compression along the applied field. For random distributions this value is relatively independent of the stretch whereas for rectangular and quasi-hexagonal microstructures the effect depends strongly on the stretch. In particular for hexagonal microstructures the effect can be both positive or negative depending on the stretch indicating a change in the dominant mechanisms responsible for the magnetoelastic coupling.

The modulus effect for MREs with random microstructures is weak; for MREs with periodic rectangular and quasi-hexagonal microstructure there is a more significant modulus effect. For rectangular periodic microstructures the effect is close to zero at the undeformed state ($\bar{e} = 0$) but becomes negative or positive when subjected to compression or tension, respectively. The magnetic field softens the composites even at the undeformed configuration ($\bar{e} = 0$) when applied to MREs with hexagonal microstructure. This effect is preserved with an increase of compressive load. In contrast, tensile loading leads to an increase in the value of the magnetoelastic modulus, and at some level of the tensile load, the value of the modulus switches the sign and becomes positive, indicating the stiffening effect of the magnetic field. The variability in these effects with respect to deformation shows the sensitivity to microstructure of magnetoelastic effects.

We observe that the magnetoelastic coupling is significantly stronger in periodic materials as compared with random materials. This is because for periodic materials the magnetic interactions between particles are all the same in each unit cell such that their attraction or repulsion combine together to give a significant effect. For random systems the particles have many different interactions, some attractive and some repulsive, such that the average effect is usually smaller and less sensitive to deformation. This also illustrates that these differences in microstructure can produce totally different magnetoelastic effects.

Figure 5.5 shows the magnetoelastic properties as a function of the stretch for the composites with particle aspect ratios $w = 1/4$ and $w = 4$. Note that the

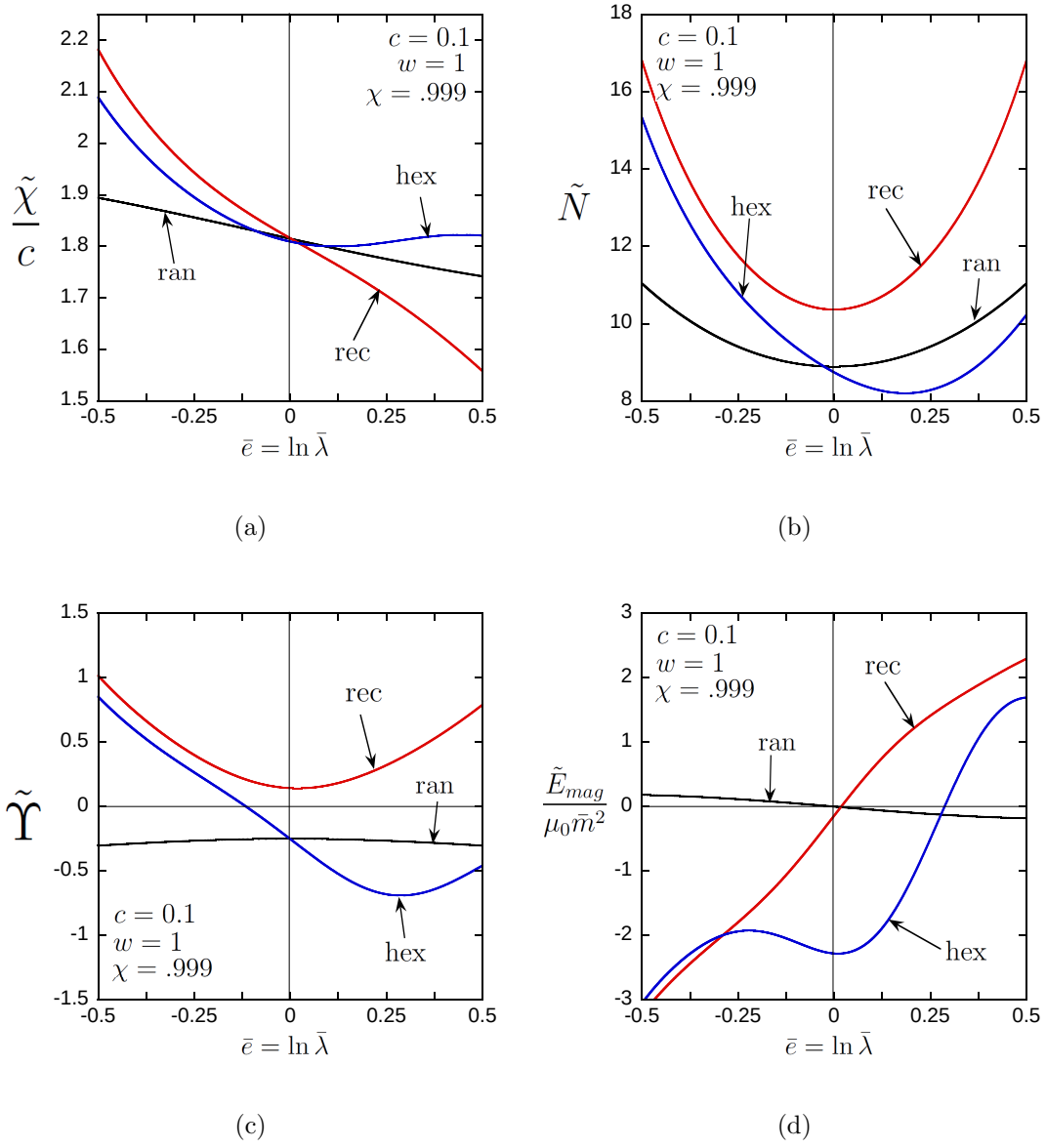

Figure 5.4: Magnetoelastic properties as a function of strain for $w = 1$ and $c = 0.1$. (a) Normalized composite susceptibility. (b) The normalized mechanical stress concentration. (c) The magnetoelastic coupling coefficient. (d) The magnetoelastic Young's modulus.

plots terminate when the FEM model failed to converge to a solution. The effective susceptibility of the composites strongly depends on the particle shape. In particular, the composites with particles elongated in the direction of the magnetic field $w = 4$ produce a much more susceptible composite than those with particles of $w = 1/4$. The difference is due to the fact that the particles are more easily magnetized when their long axis is aligned with the applied field. Additionally the susceptibility for composites with $w = 4$ shows a stronger dependence on deformation than composites with aspect ratio $w = 1/4$.

The aspect ratio also affects the mechanical reenforcement of the composite. Indeed the mechanical reinforcement also depends on the particle shape. However the influence of the particle shape on the mechanical reinforcement is rather different in MREs with random and periodic distributions of the particles. Whereas the mechanical reenforcement is the same for both aspect ratios for random microstructures, the periodic microstructures with $w = 4$ and $w = 1/4$ show different mechanical reenforcement. These effects are important because while some microstructures produce stronger magnetic effects, they also may generate more mechanical stiffening and may therefore be less desirable.

The shape of the particles has a large impact on the coupling coefficient and and its dependence on deformation. For random microstructures the effect is small and continues to be relatively independent of deformation. For periodic microstructures the change is much more dramatic both in its magnitude and its dependence on deformation. For $w = 1/4$ the positive slope indicates that the magnetic fields stiffens the composite while for $w = 4$ the negative slope indicates that the magnetic field softens the composite. This is made more explicit in Figure 5.5d which shows a negligible change in stiffness for random composites and a large change in periodic medium. Note that the stiffening or softening is independent of the direction of magnetostriction.

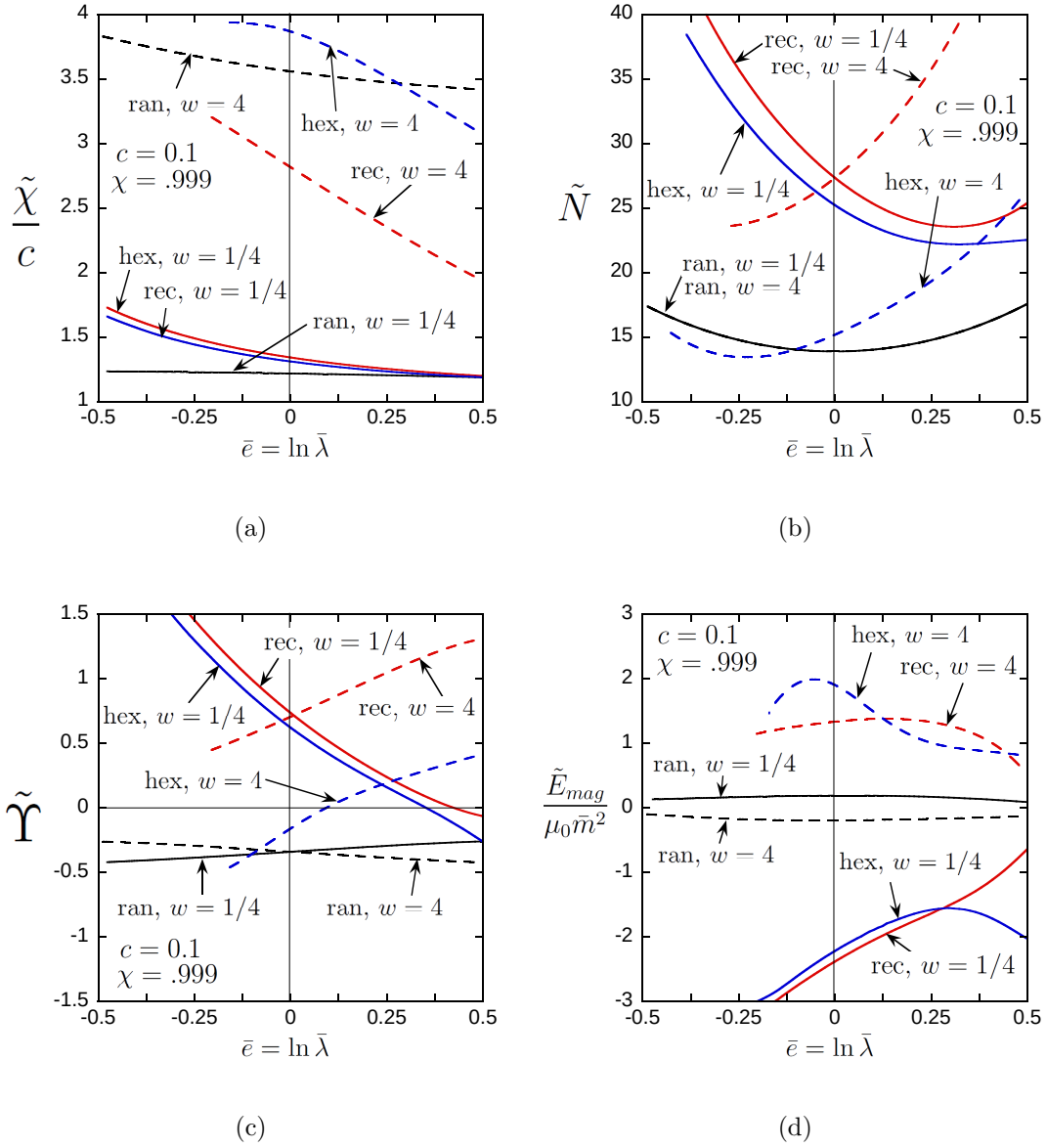

Figure 5.5: Magnetoelastic properties as a function of strain for $c = 0.1$. (a) Normalized composite susceptibility. (b) The normalized mechanical stress concentration. (c) The magnetoelastic coupling coefficient. (d) The magnetoelastic Young's modulus.

5.4.2 Magnetoelastic parameters as a function of the concentration.

Figure 5.6 shows the effective properties of the composite as a function of the concentration c. We can see that the mechanical polarizations and the susceptibilities tend to the same value for each microstructure in the small concentration limit consistent with Eshelby's result for dilute composites. However the magnetoelastic properties of these microstructures are very different in this limit. To highlight this phenomenon, consider the expansion of the susceptibility for small concentrations such that

$$\tilde{\chi} = \tilde{\chi}_0 c + \tilde{\chi}_1 c^2 + o(c^3). \tag{5.32}$$

The dilute result for particulate composites guarantees that $\tilde{\chi}_0$ only depends on the shape of the particle so that this term is the same for each microstructure if w is the same, specifically

$$\tilde{\chi}_0 = \frac{\chi(w+1)}{1+w(1-\chi)}. \tag{5.33}$$

Therefore $\tilde{\chi}_0$ is independent of deformation because the particles are rigid and do not change shape and volume fractions do not change for incompressible materials. Then the magnetoelastic coefficient (5.10) is determined to leading order by $\tilde{\chi}_1$. This term is expected to be different for each microstructure because it depends on how the particles interact with each other which depends on their positions with respect to one another. This information is specified by the microstructure. A similar result governs the mechanical stiffness in the dilute, small-strain limit which implies that $\tilde{N}$ is the same for different microstructures when the aspect ratio is the same.

At this point it is useful to consider the total stress including the Maxwell stresses so we can understand how it relates to the magnetoelastic coupling. To this end Figures 5.7a and 5.7b show the total magnetic stress normalized by the magnetic flux

$$\frac{\mu_0 \bar{T}^{\text{mag}}}{\bar{b}^2} = 1 - \tilde{\chi} + \tilde{\chi}^2 \frac{\partial \tilde{\chi}^{-1}(\bar{\lambda})}{\partial \bar{\lambda}} \frac{\bar{\lambda}}{2} \tag{5.34}$$

and the total stress, with detracted contribution of the "Maxwell stress", normalized by the magnetization and the magnetic flux

$$\frac{\bar{T}^{\text{mag}} - \bar{b}^2/\mu_0}{\bar{m}\bar{b}} = -1 + \tilde{\chi} \frac{\partial \tilde{\chi}^{-1}(\bar{\lambda})}{\partial \bar{\lambda}} \frac{\bar{\lambda}}{2}. \tag{5.35}$$

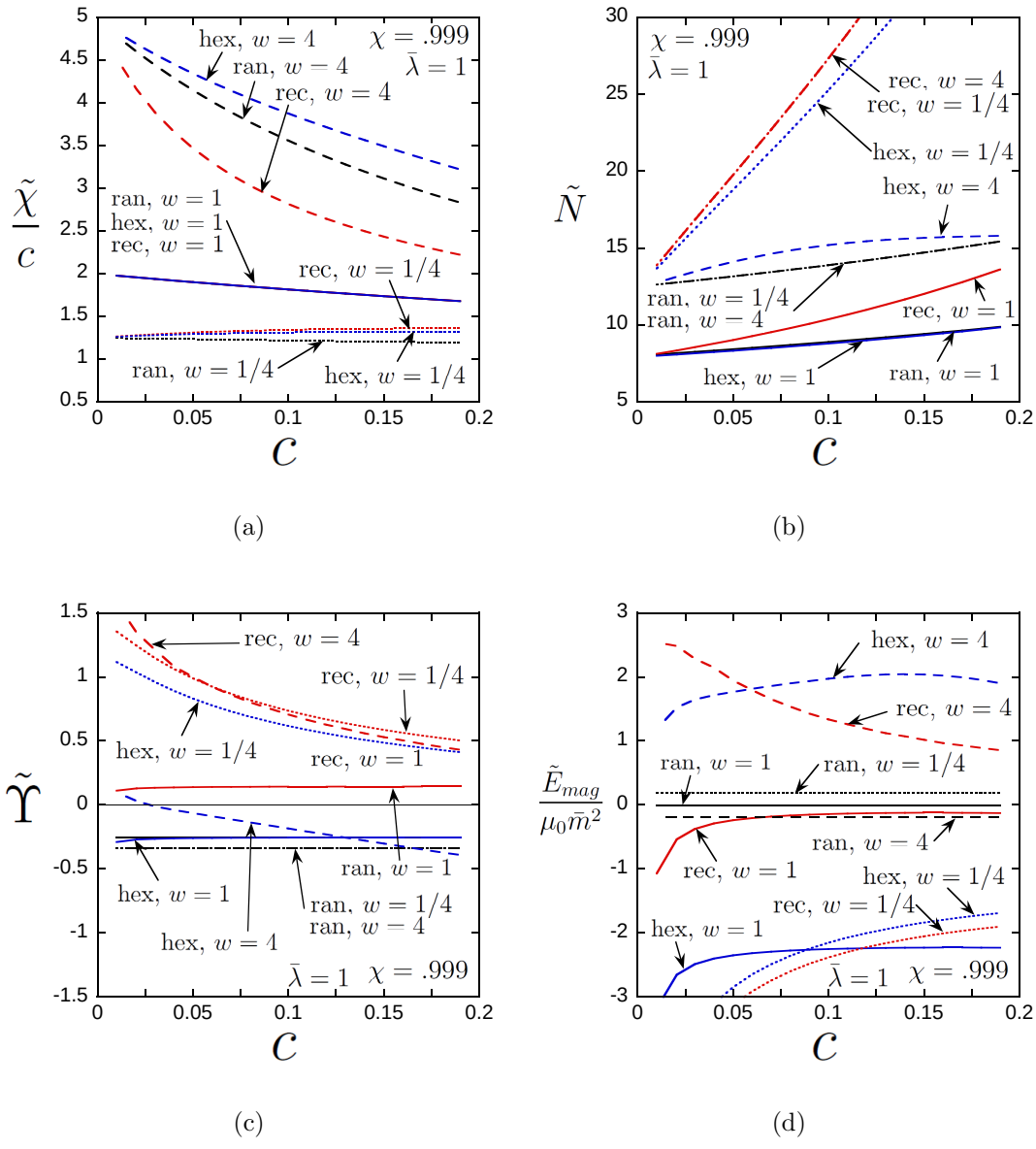

Figure 5.6: Magnetoelastic properties as a function of concentration. (a) Normalized composite susceptibility. (b) The normalized mechanical stress concentration. (c) The magnetoelastic coupling coefficient. (d) The magnetoelastic Young's modulus.

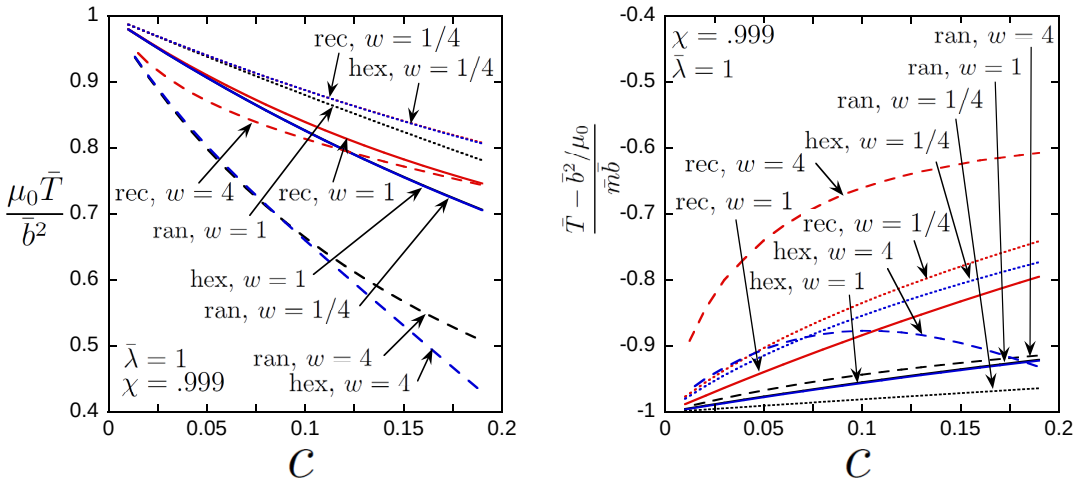

(a) (b)

Figure 5.7: Magnetoelastic properties as a function of concentration. (a) The normalized total stress. (b) The normalized total stress minus the "Maxwell" contribution.

Since $\tilde{\chi}$ is the same to first order in the concentration for all microstructures, we observe that the absolute difference in the magnetic part of the total stress for these composites is vanishingly small, in particular, of order c^2. Moreover, the difference in the stress, once the Maxwell stress is removed, is still rather small, in particular, of order c. However, when we consider the magnetoelastic coefficient, the differences between these materials become apparent. The difference in the magnetoelastic coefficient is what remains of the total stress after the boundary conditions are accounted for, and it is a very small correction (of order c^2) to the total stress. Thus, a high degree of accuracy is necessary to extract the relevant information from the total stress since it is the coupling coefficient which provides information about the magnetoelastic behavior.

5.4.3 Magnetoelastic parameters as a function of the aspect ratio.

To highlight the influence of the particle shape on the magnetomechanical coupling, we now present the parameters as a function of particles' aspect ratio. Although the results are presented in Figure 5.8 for composites with the volume fraction $c = 0.1$,

we note that the dependency almost does not change with respect to volume fraction. More specifically, we studied the dependency of the parameters on the aspect ratio in the range of $0.01 \leq c \leq 0.2$ and report a weak dependence of the corresponding curves on the volume fraction.

Note the qualitative similarities between varying the aspect ratio, as shown in Figure 5.7, and varying the stretch, as shown in Figure 5.4. This likeness can be explained as follows. The relative positions of the particles are similar when $w = 1, \bar{\lambda} = 1.2$ or $w = 1.44, \bar{\lambda} = 1$. For random microstructures this connection is explicit because $\tilde{\Upsilon}$ depends only on the quantity $w\bar{\lambda}^2$. Our conjecture is that a similar situation exists for periodic media because the unit cell takes on a new aspect ratio as a result of stretch. The aspect ratio of the unit cell in the deformed configuration is $w\bar{\lambda}^2$. When two periodic composites have the same unit cell aspect ratio in the current configuration, the magnetoelastic coefficient for the two materials is similar. The particles in these unit cells will be of different shape but their relative positions will be the same. This provides further evidence that the magnetoelastic effects are controlled by the distribution of the particles and, to a lesser extent, the shape of the inclusions.

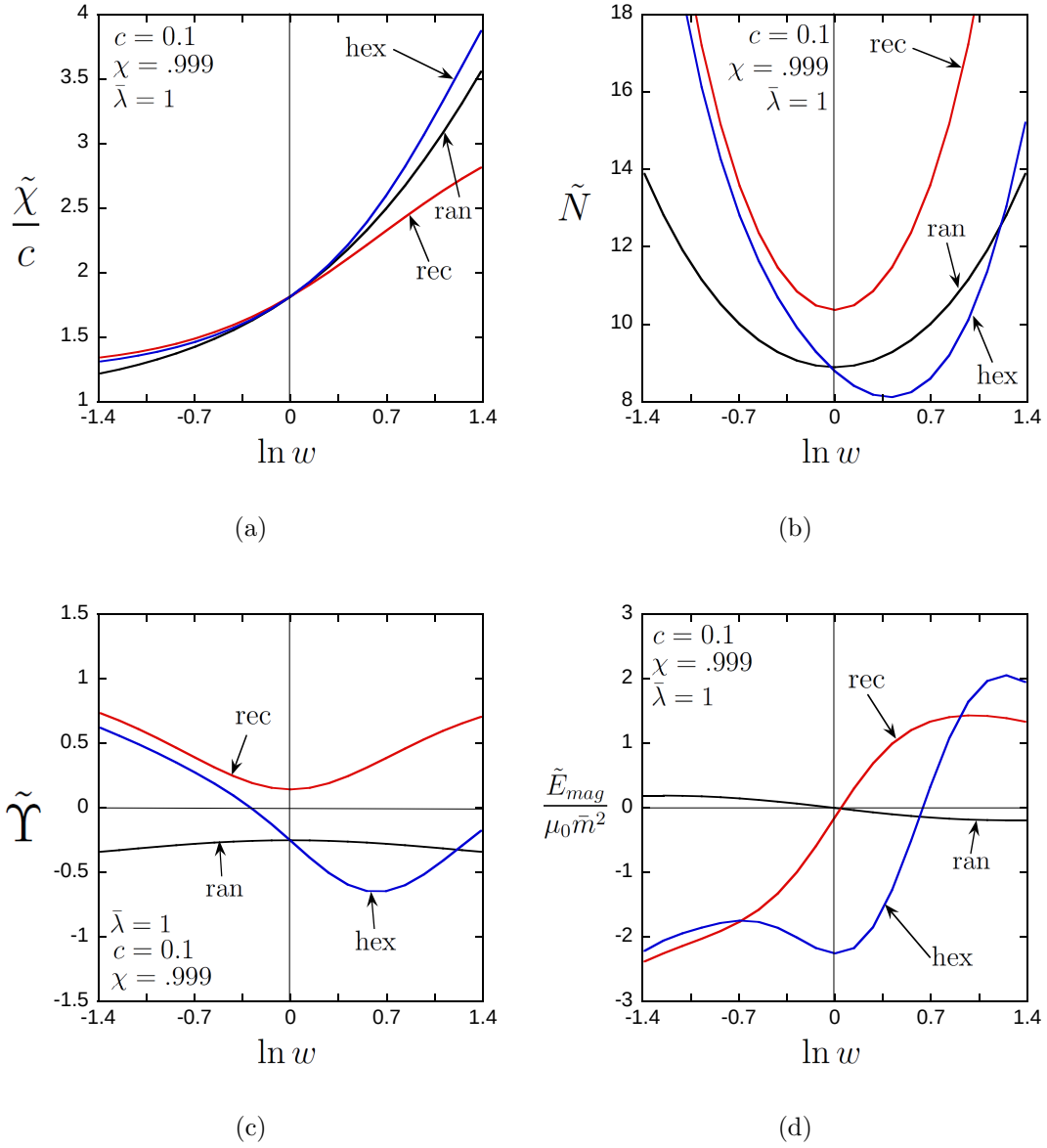

Figure 5.8: Magnetoelastic properties as a function of aspect ratio for $c = 0.1$. (a) Normalized composite susceptibility. (b) The normalized mechanical stress concentration. (c) The magnetoelastic coupling coefficient. (d) The magnetoelastic Young's modulus.

5.4.4 Magnetostriction as a function of the microstructure

Figure 5.9 shows the magnetostriction as a function of the concentration (a) and aspect ratio (b) for the three different microstructures. Consider first the influence of the concentration on the MREs' magnetostriction. The magnetostriction is quadratic to leading order with respect to the concentration; however, as the concentration becomes large enough it is expected that the composites mechanically lock-up. This effect can already be seen for rectangular microstructures with $w = 4$ at concentrations of 15% as the maximum magnetostriction has already been passed. This mechanical stiffening limits the magnetostriction despite the increasing magnetic stresses. More generally for the composites examined here, the ones with $w = 4$ exhibit the highest magnetostriction for all three microstructures; however there is a significant difference between the random, rectangular, and hexagonal microstructures.

To highlight the influence of particle shape on the magnetostriction, consider the magnetostrictive strain as a function of aspect ratio w in Figure 5.9b. For all microstructures larger aspect ratios lead to larger magnetostriction. We expect that eventually the composites will become mechanically rigid as w gets large which will limit the magnetostriction. This can be seen for quasi-hexagonal microstructures. For rectangular and random microstructures the optimal microstructure is beyond the available data. Also note that for hexagonal microstructures the magnetostriction can be positive or negative depending on the initial aspect ratio.

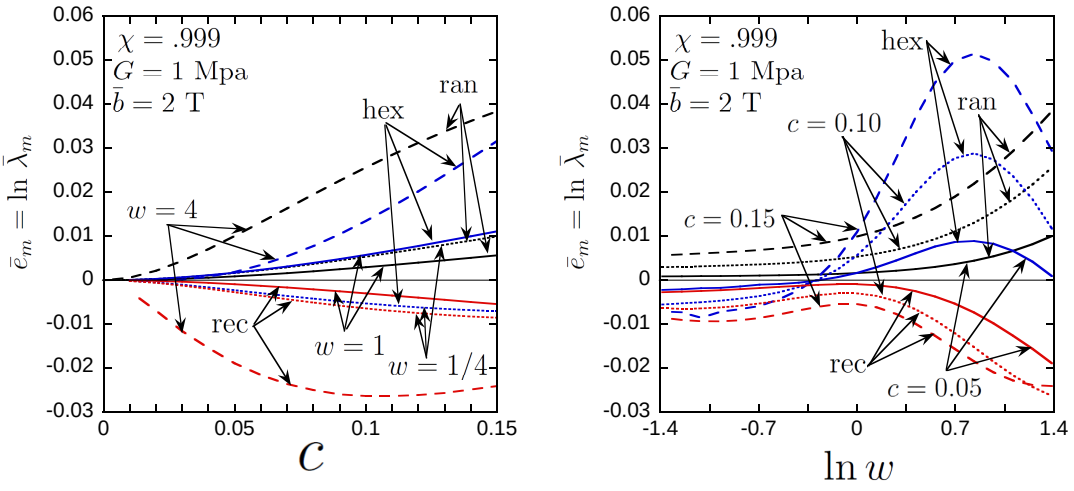

(a) (b)

Figure 5.9: Magnetostriction as a function of the microstructure. (a) The magnetostriction as a function of the concentration. (b) The magnetostriction as a function of the aspect ratio.

5.5 Concluding remarks

We examined the effective behavior of magnetorheological elastomers with random and periodic distribution of the particles. We analyzed the role of the concentration, distribution and shape of the particles on the magnetomechanical response of the composites. In particular, the random and periodic rectangular and quasi-hexagonal microstructures with varying concentrations and shape of the particles were considered. Motivated by the potential applications for "linear actuators," we specifically examined the materials subjected to uniaxial loading in the presence of a magnetic field. Note that we accounted for the Maxwell stress outside the material in calculation of the traction measured on the surface of the material. We introduced specific parameters that control the magnetomechanical performance of the MREs. These parameters, including the key magnetoelastic coupling coefficient, are further used in the analysis of the magnetoactive composites.

To characterize the behavior of the MREs with random microstructures we employed a recently developed theoretical framework for MRE homogenization (Galipeau and Ponte Castañeda, 2012) and specified the results for the considered uniaxial

magnetomechanical loading. Thus, the closed form expression for the MREs response was obtained. To study the behavior of MREs with periodic microstructures, we developed a finite element-based code and obtained the effective properties of the periodic MREs with rectangular and quasi-hexagonal microstructures.

Throughout the analysis, we observed that the periodic media exhibit significantly stronger magnetoelastic effects than MREs with randomly distributed particles. This is due to the fact that the magnetoelastic interactions in periodic media act cooperatively to produce stronger effects, whereas the effect of the magnetoelastic local interactions is weakened when averaged over a large domain.

Although an increase of the concentration results in higher magnetic stresses in the materials, at some critical concentration the material locks-up mechanically. This effect limits the ability to increase magnetostriction by an increase of the particle concentration. The mechanical locking of the material is the general effect; however, we note the critical lock-up concentration value strongly depends on the microstructure type and the particle shape. By evaluating the magnetomechanical coupling parameter for random, periodic quasi-hexagonal, and rectangular microstructures, we show that the magnetoelastic effects are of second order in the concentration. This implies that the coupled behavior is primarily the result of the interaction between inclusions. We evaluate the magnetostriction as a function of the concentrations and aspect ratio, and find that the magnetostriction can be enhanced by using the composites with highly elliptical inclusions aligned in the magnetic field.

By varying the aspect ratio of the particles, we found that the effective susceptibility increases with the aspect ratio as particles elongated along the magnetic field direction are magnetized more effectively. However, the magnetomechanical coupling can still be lower in these materials. In this regard throughout the analysis we demonstrate that the governing parameter of the magnetomechanical coupling is not the magnetic susceptibility but its derivative with respect to deformation as defined by the magnetoelastic coupling coefficient. This parameter is directly related to magnetostriction, actuation stress, and the magnetoelastic Young's modulus in a uniaxial tension test. In this regard microstructure is the key to optimizing magnetoelastic performance of MREs.

Chapter 6

Homogenization of multi-scale laminated composites

This chapter is devoted to developing designer MREs capable of enhanced magnetoelastic effect. Specifically we look at the role of microstructure in multi-scale composites to develop materials with large magnetostriction, actuation stress, and changes in modulus. All the composites considered here have the necessary symmetry such that they can be used as linear actuators and vibration dampers. It is anticipated that these results will provide direction for experimental development of MREs.

6.1 Analysis for laminated composites

As we have seen in Chapter 4, when the magnetic fields are not aligned with the geometric axes of the particles in the MRE samples, the resulting magnetic torques on the particles can have significant effects on the macroscopic magnetoelastic response of the samples. In fact, as argued in Chapter 3 (Ponte Castañeda and Galipeau, 2011), these effects (which are of order volume fraction) should be stronger than the corresponding effects of dipole interactions between the particles (which are of order volume fraction squared). On the other hand, when the applied magnetic fields are not aligned, it is necessary to enforce complex boundary conditions—including the application of tractions with a resulting torque—on the MRE sample to maintain equilibrium. In an effort to keep the boundary conditions simple while still being able to favorably exploit the potential of the magnetic torques on the particles, we propose to consider more symmetric laminated samples consisting of layers of the MREs of Chapter 4 with alternating fiber orientations.

6.1.1 Magnetic field applied along the lamination direction

We consider a two-phase laminate with the normal to the lamination layers $\mathbf{N} = \hat{\mathbf{e}}_1$, as depicted schematically in Figure 6.1. The two phases in this laminate consist of the same material considered in Chapter 4, but with fiber orientations defined by $+\bar{\theta}_0$ and $-\bar{\theta}_0$. These two phases, which will be referred to as the $(+)$ and the $(-)$ phase, respectively, will be taken in 50% volume fraction, so that the $\mathbf{N} = \hat{\mathbf{e}}_1$ direction will be a symmetry axis for the laminated MRE sample. The sample is loaded by applying a pure shear deformation with axial stretch $\bar{\lambda}$ and a magnetic induction field of magnitude $\bar{b}$, both of which are aligned with the symmetry axis defined by $\hat{\mathbf{e}}_1$, as

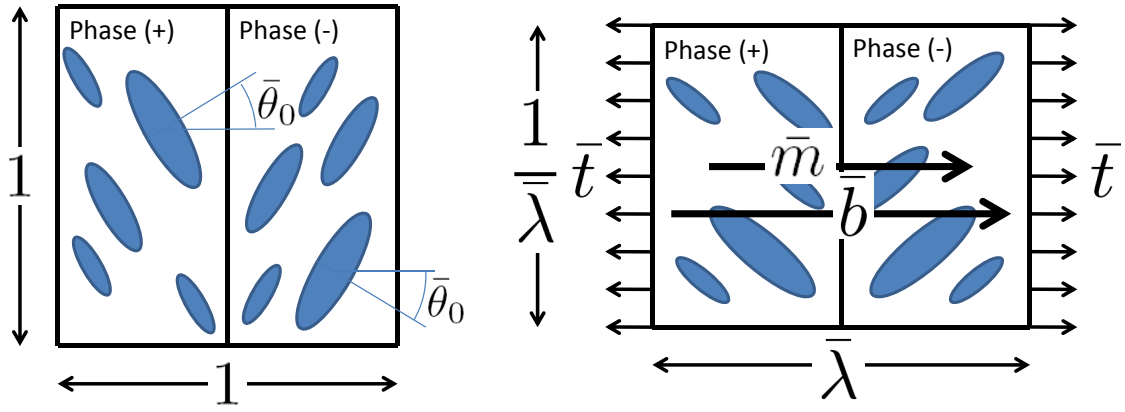

Figure 6.1: Schematic representation of the laminated MRE sample in the reference and deformed configurations (before and after application of mechanical and/or magnetic loading), with the macroscopic magnetic field aligned to the layers' normal direction. The two phases, which are in equal proportions and are labelled the $(+)$ and the $(-)$ phases, are defined by the fiber orientation angles $+\bar{\theta}_0$ and $-\bar{\theta}_0$, respectively. Upon application of a macroscopic stretch $\bar{\lambda}$ and magnetic flux $\bar{b}$, the macroscopic magnetoelastic response of the sample is aligned with the applied stretch and magnetic induction field, and can be described by the applied traction $\bar{t}$ and macroscopic magnetization $\bar{m}$.

shown in Figure 6.1. The material response can then be characterized by the normal traction difference $\bar{t} = \bar{t}_1^{(1)} - \bar{t}_2^{(2)}$ (recall that the materials are incompressible) and the macroscopic magnetization $\bar{m}$. In this case, the Lagrangian magnetic induction is also aligned with $\hat{\mathbf{e}}_1$, and its magnitude is $\bar{B} = \bar{b}/\bar{\lambda}$.

To obtain the macroscopic response of the laminated MRE, it will be assumed that the size of the layers is small compared to that of the laminated sample, but still large compared to the size of the elliptical fibers, so that we can make use of iterated homogenization (Braides and Defrancheschi, 1998). It is then possible to obtain the macroscopic stored-energy function for the MRE laminate by making use of the results of Chapter 4 for MREs with elliptical fibers in given initial orientations $\pm\bar{\theta}_0$, together with the general homogenization result of Ponte Castañeda and Galipeau (2011) for the laminate. As is well-known (see deBotton (2006) and Lopez-Pamies and Ponte Castañeda (2009), for the purely mechanical problem), the fields in a laminated composite are piecewise constant—at least up to the possible onset of an instability. Then, making use of the appropriate jump and average conditions, the components of the deformation gradient in the two phases of the laminate may be expressed in

the form (relative to the laboratory frame)

$$\left[\bar{F}^{(+)}\right] = \begin{bmatrix} \bar{\lambda} & 0 \\ F_{21} & 1/\bar{\lambda} \end{bmatrix} \qquad \text{and} \qquad \left[\bar{F}^{(-)}\right] = \begin{bmatrix} \bar{\lambda} & 0 \\ -F_{21} & 1/\bar{\lambda} \end{bmatrix}, \tag{6.1}$$

where $\pm F_{21}$ are the unknown shears in phases $(\pm)$. Similarly, the corresponding components of the magnetic induction field in the two phases of the laminate may be written in the form

$$\left\{\bar{B}^{(+)}\right\} = \begin{Bmatrix} \bar{B} \\ B_2 \end{Bmatrix} \qquad \text{and} \qquad \left\{\bar{B}^{(-)}\right\} = \begin{Bmatrix} \bar{B} \\ -B_2 \end{Bmatrix}, \tag{6.2}$$

where $\pm B_2$ are the unknown transverse components of the magnetic field in the $(\pm)$ phases.

The macroscopic stored-energy function for the MRE laminate may then be expressed in the form

$$\widehat{W}^{aligned}(\bar{\lambda}, \bar{B}) = \min_{F_{21}} \min_{B_2} \frac{1}{2} \left[\widetilde{W}_{+\bar{\theta}_0}(\bar{\boldsymbol{F}}^{(+)}, \bar{\mathbf{B}}^{(+)}) + \widetilde{W}_{-\bar{\theta}_0}(\bar{\boldsymbol{F}}^{(-)}, \bar{\mathbf{B}}^{(-)}) \right], \tag{6.3}$$

where $\widetilde{W}_{\pm\bar{\theta}_0}$ correspond to the stored-energy functions for the MREs with aligned elliptical fibers in directions $\pm\bar{\theta}_0$, respectively, as defined in Chapter 4. Note that simplified expressions for $\widetilde{W}_{\pm\bar{\theta}_0}$ can be obtained as in section 4.2 by using the polar decomposition theorem and diagonalizing the deformation gradients (6.1) in the phases.

In terms of the homogenized energy function for the laminate $\widehat{W}(\bar{\lambda}, \bar{B})$, the macroscopic magnetization is given by

$$\bar{m} = \frac{\bar{b}}{\mu_0} - \frac{1}{\bar{\lambda}} \frac{\partial \widehat{W}}{\partial \bar{B}}(\bar{\lambda}, \bar{B}), \tag{6.4}$$

while the macroscopic normal traction difference is given by

$$\bar{t} = \bar{\lambda} \frac{\partial \widehat{W}}{\partial \bar{\lambda}}(\bar{\lambda}, \bar{B}) - \frac{\bar{b}^2}{\mu_0} + \bar{b}\,\bar{m} - \frac{\mu_0 \left(\bar{m}\right)^2}{2}. \tag{6.5}$$

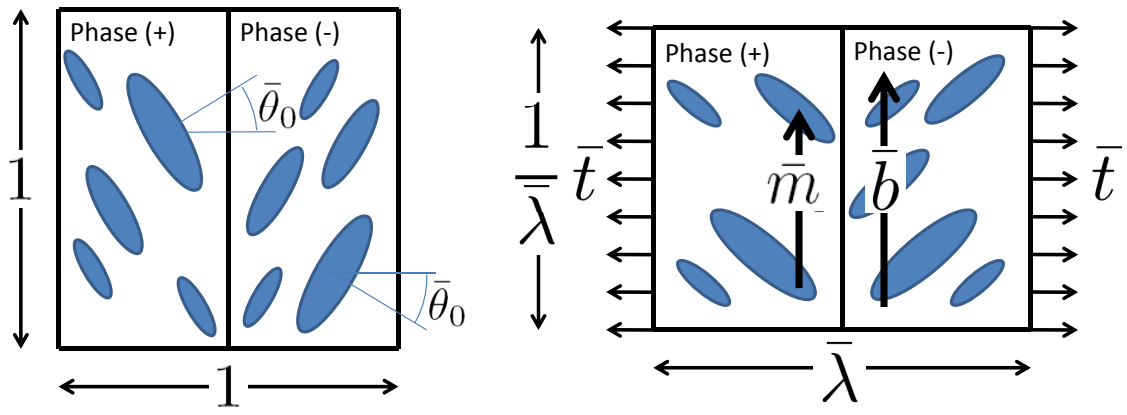

Figure 6.2: Schematic representation of the laminated MRE sample in the reference and deformed configurations (before and after application of mechanical and/or magnetic loading), with the macroscopic magnetic field applied transverse to the layers' normal direction. The two phases, which are in equal proportions and are labelled the $(+)$ and the $(-)$ phases, are defined by the fiber orientation angles $+\bar{\theta}_0$ and $-\bar{\theta}_0$, respectively. Upon application of a macroscopic stretch $\bar{\lambda}$ and magnetic flux $\bar{b}$, the macroscopic magnetoelastic response of the sample is aligned with the applied stretch and magnetic induction field, and can be described by the applied traction $\bar{t}$ and macroscopic magnetization $\bar{m}$.

6.1.2 Magnetic field applied transverse to the lamination direction

We can also consider the same laminated composite with a magnetic field applied transverse to the direction of the layers of the normals as shown in Figure 6.2. The sample is loaded by applying a pure shear deformation with axial stretch $\bar{\lambda}$ and a magnetic induction field of magnitude $\bar{b}$. In this case the shear is still applied along the $\hat{\mathbf{e}}_1$ direction but the magnetic field is applied along the transverse $\hat{\mathbf{e}}_2$ direction, as shown in Figure 6.2. The material response can then be characterized by the normal traction difference $\bar{t} = \bar{t}_1^{(1)} - \bar{t}_2^{(2)}$ (recall that the materials are incompressible) and the macroscopic magnetization $\bar{m}$ which is also aligned along the $\hat{\mathbf{e}}_2$ direction. In this case the Lagrangian magnetic induction is also aligned with $\hat{\mathbf{e}}_2$, and its magnitude is $\bar{B} = \bar{b}\bar{\lambda}$.

When the magnetic field is applied in the $\hat{\mathbf{e}}_2$ direction, the symmetries provide

additional simplifications so that

$$\bar{\mathbf{B}}^{(+)} = \begin{Bmatrix} 0 \\ \bar{B} \end{Bmatrix} \qquad \text{and} \qquad \bar{\mathbf{B}}^{(-)} = \begin{Bmatrix} 0 \\ \bar{B} \end{Bmatrix} \tag{6.6}$$

with the deformation gradients still given by expression (6.1). The energy function for the transverse case is

$$\widehat{W}^{trans}(\bar{\lambda}, \bar{B}) = \min_{F_{12}} \frac{1}{2} \left[\widetilde{W}_{+\bar{\theta}_0}(\bar{\boldsymbol{F}}^{(+)}, \bar{\mathbf{B}}^{(+)}) + \widetilde{W}_{-\bar{\theta}_0}(\bar{\boldsymbol{F}}^{(-)}, \bar{\mathbf{B}}^{(-)}) \right]. \tag{6.7}$$

The macroscopic magnetization is given in terms of the homogenized energy function for the laminate $\widehat{W}(\bar{\lambda}, \bar{B})$ by

$$\bar{m} = \frac{\bar{b}}{\mu_0} - \bar{\lambda} \frac{\partial \widehat{W}}{\partial \bar{B}}(\bar{\lambda}, \bar{B}), \tag{6.8}$$

while the macroscopic normal traction difference is

$$\bar{t} = \bar{\lambda} \, \frac{\partial \widehat{W}}{\partial \bar{\lambda}}(\bar{\lambda}, \bar{B}) + \frac{\bar{b}^2}{\mu_0} - \bar{b} \, \bar{m} + \frac{\mu_0 \, (\bar{m})^2}{2}. \tag{6.9}$$

6.1.3 Actuation traction and magnetostriction

These laminated composites can be evaluated by considering the actuation traction and the magnetostrictive strain because they have the necessary symmetry. The actuation traction $\bar{t}_a$ is obtained from expression (6.5) or (6.9) for $\bar{t}$ by setting $\bar{\lambda} = 1$. Similarly the magnetostrictive strain is obtained from expression (6.5) or (6.9) by setting $\bar{t} = 0$, solving for the resulting stretch $\bar{\lambda}_m$, and using $\bar{e}_m = \ln \bar{\lambda}_m$. Note that the actuation traction $\bar{t}_a$ and magnetostrictive strain $\bar{e}_m$ are both functions of the applied magnetic induction field $\bar{b}$, and they tend to saturate as $\bar{b}$ becomes large.

Moreover, it is useful to define a magnetoelastic Young's modulus for the MRE laminated sample. Because of the effects of the magnetic fields external to the sample, it makes sense to define the magnetoelastic Young's modulus in terms of the tractions and not directly from the stresses. Therefore we define

$$\tilde{E} = \frac{\partial \bar{t}}{\partial \bar{e}} = \bar{\lambda} \frac{\partial \bar{t}}{\partial \bar{\lambda}}, \tag{6.10}$$

where the derivatives are taken with the magnetic induction field $\bar{b}$ held fixed. This quantity has the advantage that it is easier to relate to experimental results, since the stresses are more difficult to measure experimentally than the tractions on the sample. Notice that, like other magnetoelastic effects, the Young's modulus is a function of the magnetic field $\bar{b}$, but it also saturates for large values of $\bar{b}$. In addition, it should be noted that the above-defined modulus is also a function of the stretch $\bar{\lambda}$. Here, we will consider two special cases. The first is the modulus in the undeformed configuration ($\bar{\lambda} = 1$), which we will refer to as the actuation Young's modulus. It is given by

$$\tilde{E}_{\mathrm{a}} = \tilde{E}\Big|_{\bar{\lambda}=1}. \tag{6.11}$$

The second is the modulus at the magnetostricted deformation ($\bar{\lambda} = \bar{\lambda}_m$), which we will refer to as the magnetostricted Young's modulus and define via

$$\tilde{E}_{\mathrm{m}} = \tilde{E}\Big|_{\bar{\lambda}=\bar{\lambda}_{\mathrm{m}}}. \tag{6.12}$$

These two moduli can be quite different when the magnetostriction is large as will be seen below.

6.1.4 Spontaneous formation of shear bands in the homogenous limit

The homogenization for the laminated composites will naturally reveal certain types of instabilities with respect to the homogenous material used to characterise the (+) and (−) phases, which in our case corresponds to the material derived in Chapter 4. In the limit when $\bar{\theta}_0 \to 0$ or $\bar{\theta}_0 \to 90$, the laminated composite shown in Figure 6.1 and Figure 6.2 becomes homogenous as the (+) and (−) layers become identical. For these cases, one equilibrium solution is that the deformation remains homogenous throughout the composite such that $F_{21} = 0$ (and $B_2 = 0$ for the aligned case) and fields within the (+) and (−) phases are the same. This solution leads to constitutive behavior for the "laminate" which is identical to the principal solution of the model given in Chapter 4. However the minimizations in equation (6.3) or (6.7) may find the global minimum such that $F_{21} \neq 0$. This indicates that the homogenous material has spontaneously formed shear bands and some stability limit for the homogenous material has been passed. These effects are important for the laminated composite

because when we consider the limits as $\bar{\theta}_0 \to 0$ or $\bar{\theta}_0 \to 90$, the behavior of the composite may not converge to the principal behavior of the homogenous material and instead may converge to the solution with shear bands.

In the homogeneous limit just described, there is a significant connection between the formation of shear bands and the loss of ellipticity of the material in Chapter 4. Indeed, these "laminated" microstructures also suggest one possible post-bifurcation solution for the homogenous material after loss of ellipticity. If there is no instability in the homogenous material, the behavior of the composite converges to the principal solution for the homogenous material in the limit as $\bar{\theta}_0 \to 0$ or $\bar{\theta}_0 \to 90$. The stretch and magnetic flux ($\bar{\lambda}$ and $\bar{b}$) at which the principal solution and the limiting solution differ frequently corresponds to loss of ellipticity for the homogenous material but a non-homogenous solution may also be detected without loss of ellipticity. Both of these effects have been observed in conjunction with this work and a full investigation of magnetoelastic instabilities for the MRE model derived in Chapter 4 is currently underway.

The formation of these shear bands is primarily driven by particle rotations in both the purely mechanical and magnetoelastic case. For the purely mechanical case this is discussed in Lopez-Pamies and Ponte Castañeda (2006a). Considering the magnetoelastic contribution to this effect, the magnetic energy of the particles is lowest when their long axis is aligned with the applied field direction and highest when their long axis is transverse to the field direction. Since the formation of shear bands is associated with particle rotations within the layers, the magnetic field can have a strong influence on the stability of the composite. However it is essential that the shear band direction allows for sufficient particle rotation if this effect is to be observed. For this section w will always be taken to be greater than 1. When $\bar{\theta}_0 = 0$ and $w > 1$, the particles would undergo significant rotation when the material shears in the F_{12} direction. This is not captured by the energy minimization. Shear along the F_{21} direction when $\bar{\theta}_0 = 0$ and $w > 1$ does not allow sufficient particle rotation to provide a lower energy solution and as such, we never observe instability for these cases even though the homogenous material will lose ellipticity and become unstable. When $\bar{\theta}_0 = 90^\circ$ and $w > 1$, the long axis of the particles is along the layer normal $\hat{\mathbf{e}}_1$ and shear in the F_{21} direction can cause large particle rotation. This implies that the energy minimization may detect shear band formation under some circumstances. It should be noted that while the minimization does not detect instabilities when

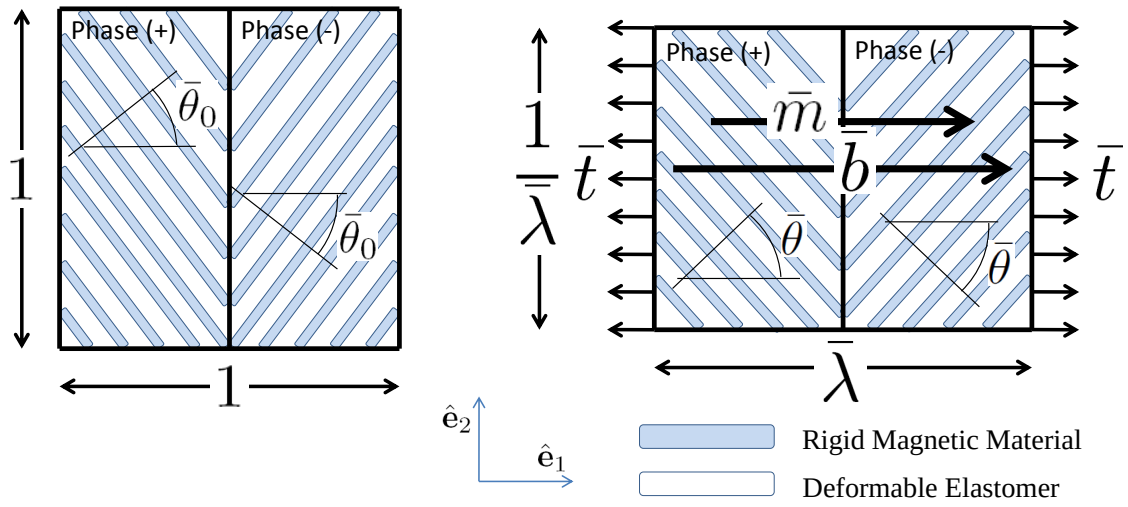

Figure 6.3: Schematic representation of the rank 2 laminated MRE in the reference and deformed configurations. The phases in the rank 2 laminate, labeled (+) and (−), have equal concentrations and each consists of a rank 1 laminate. The orientations of the rank 1 laminates within the (+) and (−) phases are defined by the angles $+\bar{\theta}_0$ and $-\bar{\theta}_0$, respectively. Upon the application of the magnetoelastic loading the orientations of the rank 1 laminates within the (+) and (−) phases become $+\bar{\theta}$ and $-\bar{\theta}$, respectively.

$\bar{\theta}_0 = 0$, it can be related to the case when $\bar{\theta}_0 = 90°$ by interchanging the appropriate variables.

6.1.5 Magnetoelastic properties of a rank-2 laminate

We can also consider an MRE where a rigid phase, magnetic material and a nonmagnetic, incompressible elastomer material are combined together into a rank-2 laminate shown in Figure 6.3. This represents a limiting case of the laminates given in section 6.1.1 where the particle aspect ratio $w \to \infty$. The composite is loaded with stretch $\bar{\lambda}$ and magnetic flux $\bar{b}$ along the symmetry axis and the composite will respond with some traction on the surface $\bar{t}$ and some magnetization $\bar{m}$. Composites of this type have the advantage that we can determine this relationship exactly even for large strain based on the properties of the magnetic and elastomer phase.

The composite is characterized by the same microstructural and material parameters as in section 6.1.1 except without w. In this section $\bar{\theta}_0$ and $\bar{\theta}$ are reinterpreted as the direction normal to the rigid and elastomer layers in the reference and deformed

configuration as shown in Figure 6.3. The concentration of the rigid layers is c instead of c^I (They are no inclusions in this case). For the material properties we take the behavior of the matrix to be the Gent model described by equation (4.2) and the magnetization behavior of the particles is given by equations (4.15) and (4.16).

For the rank-2 laminate composites the energy can be expressed in the decoupled form

$$\widehat{W}^{rank2}(\bar{\boldsymbol{F}}, \bar{\boldsymbol{B}}) = \widetilde{W}^{rank2}_{\text{me}}(\bar{\boldsymbol{F}}) + \widetilde{W}^{rank2}_{\text{mag}}(\bar{\boldsymbol{F}}, \bar{\boldsymbol{B}}). \tag{6.13}$$

For the rank-2 laminate the microstructure in the current configuration is entirely determined by the macroscopic stretch (as we will see). This means that the magnetic field does not change the microstructure and assumptions of the partial decoupling approximation are satisfied exactly. Then the magnetic energy is found from the solution of a rank-2 laminate homogenization problem which can be performed exactly with no need to consider microstructure evolution. This leads to an energy of form (6.13).

This is different than the particulate/laminate composite described in section 6.1.1 where the energy could not be decoupled exactly. The homogenized energy of the particulate (+) and (−) phases indeed uses the partial decoupling approximation and the energy for each phase is decoupled. However the homogenization at the lamination level can be done exactly without resorting to any approximations. This involves minimizations with respect to the shear in the layers and associated particles' rotations even when the macroscopic stretch is held fixed. This violates the assumptions of the partial decoupling approximation and hence an energy of form (6.13) is not expected.

Mechanical energy

We must compute the local fields in each phase which will allow us to calculate the total energy in the composite. Based on the symmetry between the (+) and (−) phase, the average deformation gradient in the (+) and (−) must be

$$\left[\bar{F}^{(+)}\right] = \begin{bmatrix} \bar{\lambda} & 0 \\ F_{21} & 1/\bar{\lambda} \end{bmatrix} \qquad \text{and} \qquad \left[\bar{F}^{(-)}\right] = \begin{bmatrix} \bar{\lambda} & 0 \\ -F_{21} & 1/\bar{\lambda} \end{bmatrix}. \tag{6.14}$$

The (+) phase is inextensible along the rigid layer direction providing the con-

straint

$$\left|\bar{\boldsymbol{F}}^{(+)}\mathbf{q}\right| = 1 \quad \text{where} \qquad \mathbf{q} = \left\{ \begin{array}{c} \sin\bar{\theta}_0 \\ -\cos\bar{\theta}_0 \end{array} \right\}. \tag{6.15}$$

This constraint implies that

$$F_{21} = \frac{\cot\theta_0}{\bar{\lambda}} - \sqrt{\frac{1}{\sin^2\theta_0} - \bar{\lambda}^2}. \tag{6.16}$$

Note that F_{21} must be a real number so

$$\bar{\lambda} \leq \frac{1}{\sin\theta_0}, \tag{6.17}$$

providing the limit of extensibility due to the presence of the rigid phase. We also note that based on the geometric constraints of the rigid magnetic layers, their orientation with respect to the laboratory frame changes to give

$$\bar{\theta} = \arcsin\left(\bar{\lambda}\sin\bar{\theta}_0\right). \tag{6.18}$$

For future use we consider $\Delta\bar{\theta} = \bar{\theta} - \bar{\theta}_0$ as the rotation of the rigid phase. This implies directly that the deformation gradient in the magnetic material is

$$\left[\boldsymbol{F}^{(2+)}\right] = \begin{bmatrix} \cos\Delta\bar{\theta} & \sin\Delta\bar{\theta} \\ -\sin\Delta\bar{\theta} & \cos\Delta\bar{\theta} \end{bmatrix} \quad \text{and} \quad \left[\boldsymbol{F}^{(2-)}\right] = \begin{bmatrix} \cos\Delta\bar{\theta} & -\sin\Delta\bar{\theta} \\ \sin\Delta\bar{\theta} & \cos\Delta\bar{\theta} \end{bmatrix} \tag{6.19}$$

where the superscripts $(2+)$ and $(2-)$ indicate the magnetic material in the $(+)$ and $(-)$ phases, respectively. The volume average of the layers in the $(+)$ phase must be $\bar{\boldsymbol{F}}^{(+)}$ with the same result for the $(-)$ phase. This implies the deformation gradients in the elastomer phase are

$$\bar{\boldsymbol{F}}^{(1+)} = \frac{\bar{\boldsymbol{F}}^{(+)} - c\boldsymbol{F}^{(2+)}}{(1-c)} \quad \text{and} \quad \bar{\boldsymbol{F}}^{(1-)} = \frac{\bar{\boldsymbol{F}}^{(+)} - c\boldsymbol{F}^{(2-)}}{(1-c)}. \tag{6.20}$$

The first invariant of the deformation in the matrix is the same throughout the composite because the deformation in the $(+)$ and $(-)$ phases are symmetric. It is given by

$$I^{(1)}(\bar{\lambda}) = \mathrm{tr}(\bar{\boldsymbol{F}}^{(1+)\mathrm{T}}\bar{\boldsymbol{F}}^{(1+)}) = \mathrm{tr}(\bar{\boldsymbol{F}}^{(1-)\mathrm{T}}\bar{\boldsymbol{F}}^{(1-)}). \tag{6.21}$$

Given that the other layer is rigid and the matrix consists of a Gent material, the

effective mechanical energy for the system reduces to

$$\widehat{W}_{me}^{rank2}(\bar{\lambda}) = (1-c) - \frac{GJ_{\mathrm{m}}}{2}\ln\left[1 - \frac{I^{(1)}(\bar{\lambda})-3}{J_{\mathrm{m}}}\right]. \tag{6.22}$$

Magnetic energy

The microstructure in the deformed configuration can be determined exactly based solely on the macroscopic stretch $\bar{\lambda}$ because of the constraints of the mechanical problem. All that remains is to solve a magnetic problem described in the current configuration. The critical parameter for the magnetic homogenization is the orientation of the laminated layers $\bar{\theta}$ which defines the normal to the layers within the $(+)$ and $(-)$ phases. The system has 4 different phases denoted $(2+)$, $(1+)$, $(2-)$, and $(1-)$ with the number denoting the matrix or the rigid phase and sign denoting the $(+)$ or $(-)$ layer. We also use just the superscripts $(+)$ and $(-)$ to denote the average fields in the respective layers.

The system is inherently non-linear because of the non-linear magnetic behavior in the rigid phase; however the equations can be simplified to have two unknown variables, the Cartesian components of $\bar{\mathbf{b}}^{(2+)}$ (or $\bar{\mathbf{b}}^{(2-)}$) with respect to the laboratory frame. For simplicity we will derive the conditions for the $(+)$ phase even though a redundant set of equations can be derived for the $(-)$ phase.

The fields satisfy the averaging conditions $(1-c)\bar{\mathbf{b}}^{(1+)} + c\bar{\mathbf{b}}^{(2+)} = \bar{\mathbf{b}}^{(+)}$ and $\bar{b}_1^{(+)} + \bar{b}_1^{(+)} = \bar{b}$ consistent with homogenization. This implies that

$$(1-c)\bar{b}_1^{(1+)} + c\bar{b}_1^{(2+)} = \bar{b}. \tag{6.23}$$

The symmetry of the $(+)$ and $(-)$ phases, the jump condition on the $\mathbf{h}$ field between the $(+)$ and $(-)$ phases implies that $\bar{h}_2^{(+)} = \bar{h}_2^{(-)} = 0$. The averaging condition on $(1+)$ and $(2+)$ in conjunction with that equation yields $(1-c)\bar{h}_2^{(1+)} + c\bar{h}_2^{(2+)} = 0$. Writing this condition in terms of the $\mathbf{b}$ field components in each phase and $\mathbf{m}(\mathbf{b})$, the magnetization function for the rigid layers, we arrive at the equation

$$(1-c)\bar{b}_2^{(1+)} + c\bar{b}_2^{(2+)} + c\mu_0\bar{m}_2(\bar{\mathbf{b}}^{(2+)}) = 0. \tag{6.24}$$

The fields must also satisfy the jump conditions in between the rigid and elastomer

layers. The jump condition $[\bar{\mathbf{b}}^{(1+)} - \bar{\mathbf{b}}^{(2+)}] \cdot \mathbf{n} = 0$ field gives

$$\bar{b}_1^{(1+)} \cos\bar{\theta} + \bar{b}_2^{(1+)} \sin\bar{\theta} = \bar{b}_1^{(2+)} \cos\bar{\theta} + \bar{b}_2^{(2+)} \sin\bar{\theta}. \tag{6.25}$$

Similarly the jump condition $[\bar{\mathbf{h}}^{(1+)} - \bar{\mathbf{h}}^{(2+)}] \times \mathbf{n} = 0$ yields the equation

$$\begin{aligned} &\bar{b}_1^{(1+)} \sin\bar{\theta} - \bar{b}_2^{(1+)} \cos\bar{\theta} \\ &\qquad = \bar{b}_1^{(2+)} \sin\bar{\theta} - \bar{b}_2^{(2+)} \cos\bar{\theta} + \bar{m}_1^{(2+)}(\bar{\mathbf{b}}^{(2+)}) \sin\bar{\theta} - \bar{m}_2(\bar{\mathbf{b}}^{(2+)}) \cos\bar{\theta} \end{aligned} \tag{6.26}$$

when written in terms of the components of $\bar{\mathbf{b}}$.

Removing the components of the $\mathbf{b}^{(1+)}$ from equations (6.23), (6.24), (6.25), and (6.26) yields the equations

$$\bar{b} = \bar{b}_1^{(2+)} + (1-c)\left[\mu_0 m_1(\bar{\mathbf{b}}^{(2+)}) \sin\bar{\theta} - \mu_0 m_2(\bar{\mathbf{b}}^{(2+)}) \cos\bar{\theta}\right] \tag{6.27}$$

and

$$\bar{b}_1^{(2+)} \cos\bar{\theta} - \bar{b} \cos\bar{\theta} + \bar{b}_2^{(2+)} \sin\bar{\theta} + c\mu_0 m_2(\bar{\mathbf{b}}^{(2+)}) \sin\bar{\theta} = 0. \tag{6.28}$$

These two equations can be solved for the components of $\bar{\mathbf{b}}^{(2+)}$.

The fields in the matrix phase are then given by

$$\bar{b}_1^{(1+)} = \frac{\bar{b} - c\bar{b}_1^{(2+)}}{1-c} \tag{6.29}$$

and

$$\bar{b}_2^{(1+)} = \frac{-\bar{b} + \bar{b}_1^{(2+)}}{1-c} \cot\bar{\theta} + \bar{b}_2^{(2+)}. \tag{6.30}$$

It is easily verified that the solution of this equation satisfies the necessary jump conditions, symmetry requirement, and volume averaging conditions such that it represents a solution of the magnetic problem.

Noting that $\bar{B} = \bar{b}/\bar{\lambda}$ the energy in the composite can be given by

$$\widehat{W}_{mag}^{rank2}(\bar{\lambda}, \bar{B}) = c\rho^{(2)}\varphi_{\text{mag}}^{(2)}(\bar{\mathbf{b}}^{(2+)}) + (1-c)\frac{\bar{\mathbf{b}}^{(1+)} \cdot \bar{\mathbf{b}}^{(1+)}}{2\mu_0} + c\frac{\bar{\mathbf{b}}^{(2+)} \cdot \bar{\mathbf{b}}^{(2+)}}{2\mu_0}. \tag{6.31}$$

Given the expressions for the magnetic and mechanical parts of the energy, the total magnetoelastic energy $\widehat{W}^{rank2}$ is given by expression (6.13) while the traction and magnetization are given by expressions (6.5) and (6.4) respectively.

6.2 Results for laminated composites

In this section we investigate the effect of the magnetic induction field on the macroscopic magnetization and traction for the laminated MRE samples described earlier (see Figure 6.1 and 6.2). The matrix is of the Gent type with $J_m = 50$ and elastic modulus G. The magnetic susceptibility of the particles $\chi = 0.95$ and the saturation magnetization $m_{\rm s}$ is chosen such that the dimensionless parameter $\kappa = 16$. The results shown reflect the same values of the material parameters as in Chapter 4. The magnetoelastic effects are considered for different values of the strain $\bar{e} = \ln \bar{\lambda}$, applied magnetic field $\bar{b}$, and initial orientations of the fibers θ_0.

We present results for the traction-strain relationship for these laminated composites when the magnetic field is applied normal and transverse to the layers' normal direction. Then we build on those results to provide more specific results for the effect of the magnetic field $\bar{b}$ on the actuation traction $\bar{t}_a$, magnetostrictive strain $\bar{e}_m$ and Young's moduli $\tilde{E}_a$ and $\tilde{E}_m$ of the laminated MRE samples with varying fiber orientations $\bar{\theta}_0$ for magnetic field.

With the objective of optimizing the microstructure of the laminated MRE samples, we then provide results for the saturation values of the actuation traction $\bar{t}_a$ and the magnetostrictive strain $\bar{e}_m$ (at saturation) for various particle concentrations ($c^I = 0.15, 0.3$ and 0.45) and aspect ratios ($w = 1, 4$ and 8), as functions of the initial fiber orientation $\bar{\theta}_0$. In addition, we also consider the effect of $\bar{\theta}_0$ on the Young's moduli $\tilde{E}_a$ and $\tilde{E}_m$ (at saturation) for the laminated samples with various particle concentrations ($c^I = 0.15, 0.3$ and 0.45) and aspect ratio $w = 4$.

The final subsection briefly shows the effect of the magnetic field on the instability to provide motivation for a fully-coupled stability analysis for MREs.

6.2.1 Results for laminated composites in the absence of the magnetic field

Figure 6.4 represents the mechanical response of the laminated composite. Figure 6.4a shows the traction strain relation for various $\bar{\theta}_0$ and Figure 6.4b shows particle rotations in the respective phases as a function of deformation. The stretch of the composite generates particle rotations. In all cases the particle rotation vanishes when $\bar{\lambda} = 1$. This plot also shows the onset of instability when $\bar{\theta}_0 = 90^\circ$ and the composite is compressed. In this case the material is homogenous since the $(+)$ and $(-)$ phase

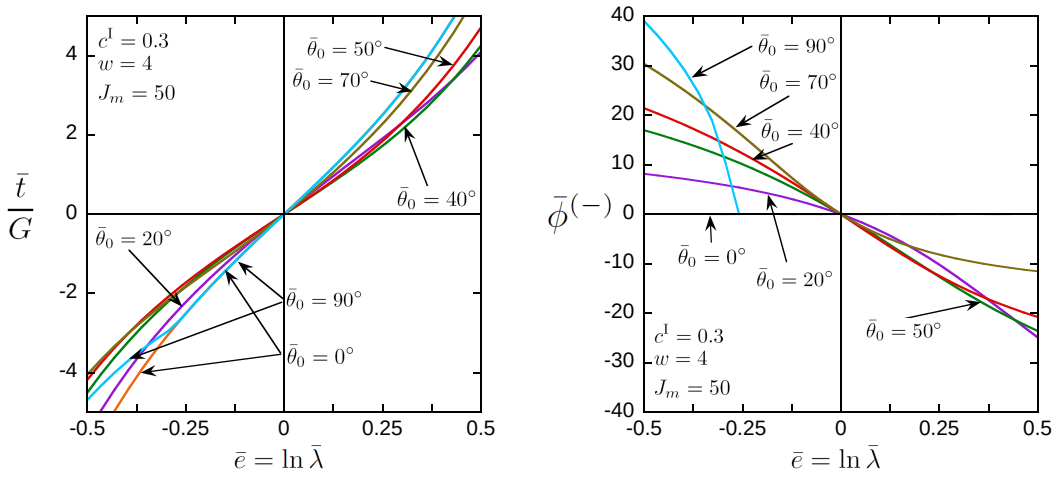

(a) (b)

Figure 6.4: Traction $\bar{t}$ as functions of the strain $\bar{e}$ in a laminated MRE sample with elliptical fibers ($w = 4$) for different initial orientation. (a) The mechanical shear traction. (b) The particle rotation in phase $(-)$.

are identical. The material is symmetric about the loading axis so the particles do not rotate until the composite is compressed enough to activate the unstable mode. At that point the $(+)$ and $(-)$ phases undergo equal and opposite deformations. This instability also occurs when $\bar{\theta}_0 = 0$ when the composite is stretched. However the correct shear band corresponds to phase deformation in the F_{12} direction which is not captured by the minimizations in equation (6.3) and (6.7).

6.2.2 Results for aligned magnetic loading

Magnetization and traction as functions of the strain for aligned loading

Figure 6.5 shows plots of the macroscopic magnetization $\bar{m}$ and traction $\bar{t}$ as functions of the applied strain $\bar{e}$ in the laminated MRE samples for increasing values of the applied magnetic induction $\bar{b}$ applied along the layers' normal direction. Figure 6.5a shows that the magnetization in the laminate samples increases with the applied magnetic induction until reaching the saturation level, but the dependence on the applied strain is relatively weak and disappears altogether at saturation consistent with the earlier results for the MRE samples of section 4.2 (see Figure 4.5a). On the other

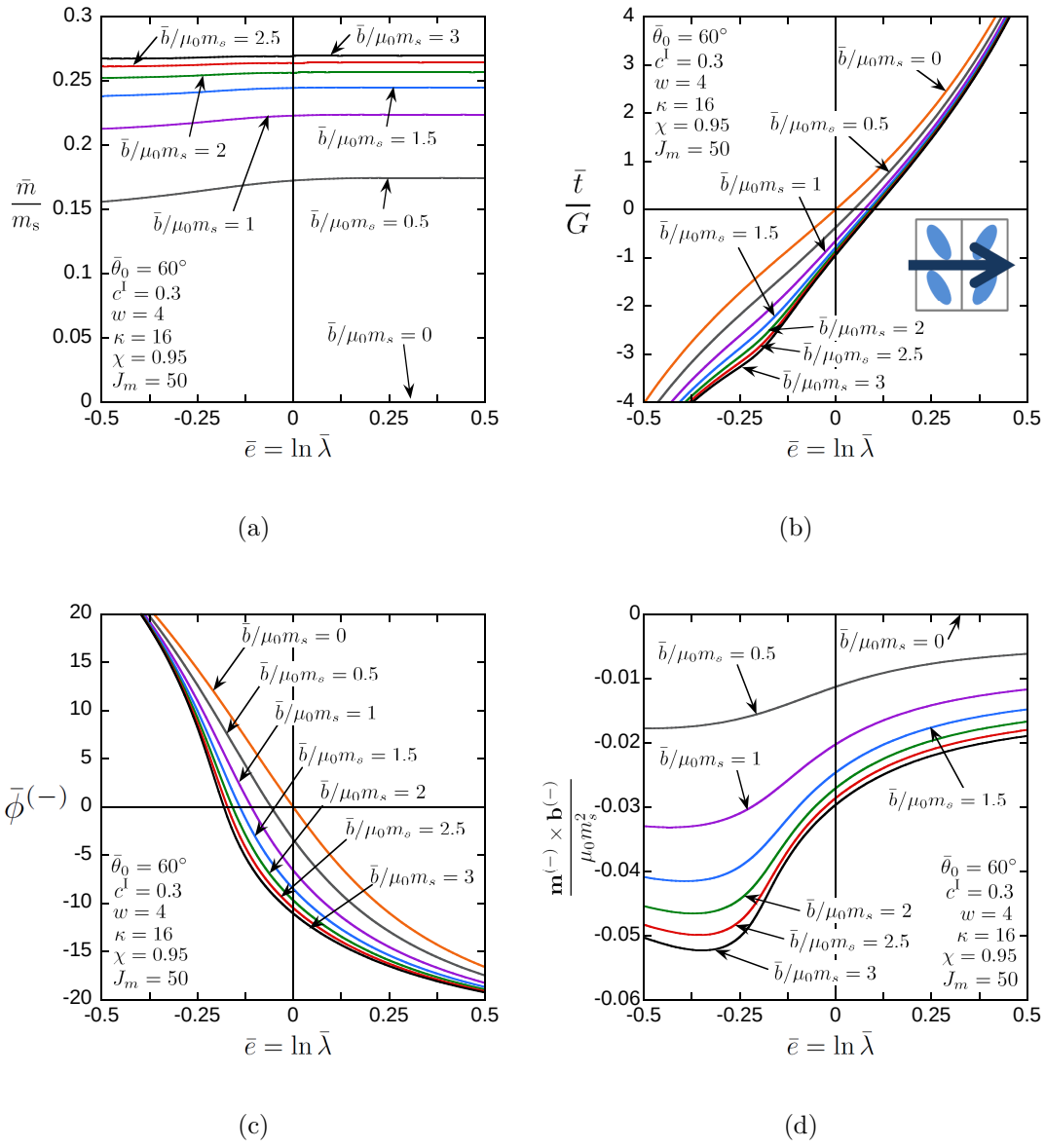

Figure 6.5: The magnetization $\bar{m}$ and traction $\bar{t}$ as functions of the strain $\bar{e}$ in a laminated MRE sample with elliptical fibers ($w = 4$) and orientation $\bar{\theta}_0 = 60°$, for increasing values of the applied magnetic induction $\bar{b}$. The magnetic field is applied along the layers' normal direction. (a) The normalized magnetization-strain relation. (b) The normalized traction-strain relation. (c) The particle rotation in phase $(-)$. (d) The torque $\bar{\mathbf{m}} \times \bar{\mathbf{b}}$ in phase $(-)$.

hand, Figure 6.5b shows that the magnetic induction field has a more pronounced effect on the traction-strain curves for the MRE laminated samples. Although the effect also tends to saturate, the shapes of the curves change quite significantly with increasing magnetic induction. These effects may be understood in terms of the concomitant effects on the evolution with the deformation of the particle rotations, shown in Figure 6.5c, and the magnetic torque, shown in Figure 6.5d, in the two phases of the laminate (the results in phase (+) are the negatives of the results in phase (−)). Indeed, the application of the magnetic induction has a different effect on the particle rotation and magnetic torques for tension and compression, which translates into significant differences in the traction-strain curves for tension and compression. Globally, however, the effect on the macroscopic traction-strain curves is similar to earlier results for the non-aligned particle samples, with the traction-strain curves shifting to the right and downward. However, for the laminated samples, the magnetic field can produce particle rotations in the layers, even when no macroscopic deformation is allowed ($\bar{e} = 0$). As we will see below, this extra "degree of freedom" in the laminated samples, which can be controlled by appropriate selection of the initial particle orientation angles $\bar{\theta}_0$, will have significant implications for the actuation tractions, magnetostrictive strains, and moduli for the laminated samples.

Actuation, magnetostriction, and Young's moduli as functions of the magnetic field for aligned loading

Figure 6.6 shows the actuation traction and associated magnetoelastic effects as a function of magnetic flux $\bar{b}$ for various initial orientation angles $\bar{\theta}_0$ when the magnetic field is applied along the layers' normal direction. In all cases the actuation stress is initially quadratic in the applied magnetic field then reaches a saturation as the magnetic field becomes large. The macroscopic magnetization develops similarly for all microstructures with the primary difference being a small change in the initial slope of the magnetization curve. There is also a mesoscale magnetic response which is not shown. In each case the magnetization in each phase will align with the loading direction in the limit of large applied field, but we still observe the saturation of $\bar{\mathbf{m}} \times \bar{\mathbf{b}}$ in each phase. It can also be seen that even though the macroscopic deformation is being held fixed at $\bar{\lambda} = 1$ the particles rotate depending on the applied magnetic field (along with meso-scale shear). In this sense the magnetic field will advance the microstructure even without a change in the macroscopic deformation. In general the

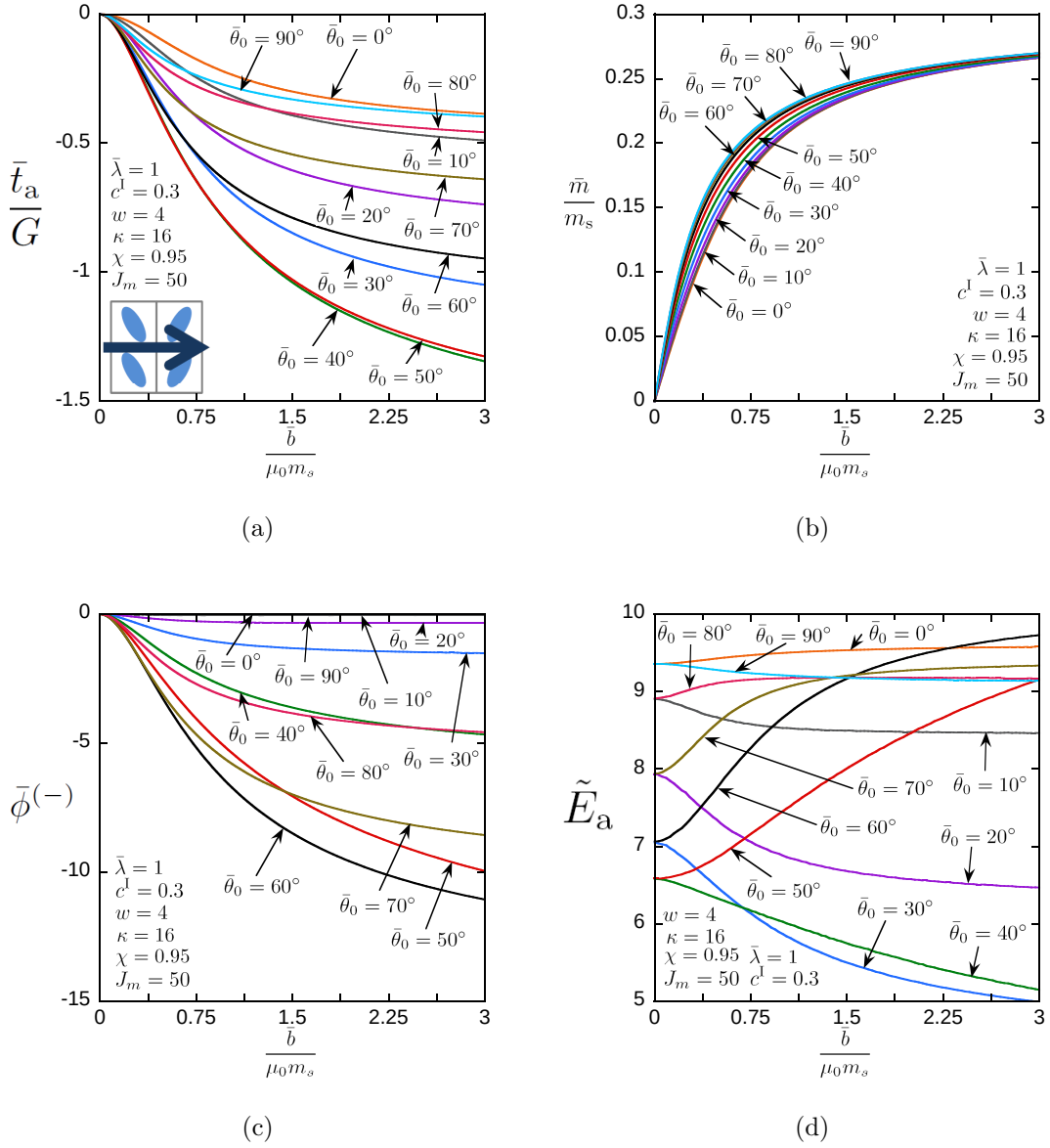

Figure 6.6: Actuation traction of the laminated MRE samples with elliptical fibers ($w = 4$) as functions of the magnetic induction $\bar{b}$ for different microstructural angles $\bar{\theta}_0$ with the magnetic field applied along the layers' normal direction. (a) The actuation stress. (b) The composite magnetization. (c) The particle rotation in phase (-). (d) The magnetoelastic Young's modulus evaluated at the reference stretch.

particles tend to align themselves with the applied magnetic field and the amount of rotation increases with the applied magnetic field. The particle rotations tend to produce an elongation of the sample in the direction of the applied field, which either requires the application of a compressive traction—the actuation traction is negative—or results in an overall tensile strain if no tractions are imposed on the sample—the magnetostrictive strains are positive. The results show that initial fiber orientations near 45° are most effective at producing actuation tractions. These effects are the weakest for the perfectly aligned cases ($\bar{\theta}_0 = 0$ and 90°).

Figure 6.7 illustrates the magnetostriction and associated magnetoelastic effects as a function of $\bar{b}$ for various particle angles. Figure 6.7a shows that the magnetic field elongates the composite in the direction of the applied field. This effect depends strongly on the initial angle of the particles although each magnetostriction curve has initially quadratic growth then saturates as the field becomes large. As a response to the applied field the composite develops macroscopic magnetization as well as mesoscopic magnetic and mechanical effects. The macroscopic magnetization develops similarly for all microstructures, with the primary difference being a small change in the initial slope of the magnetization curve. In all cases the particles align their long axis with the applied magnetic field; however the magnitude of the mesoscale evolution is very different for the various microstructures. We also display the magnetoelastic modulus evaluated at the magnetostriction state $\tilde{E}_{\mathrm{m}}$. Even though initial quadratic dependence followed by saturation is observed, the effect is not necessarily monotonic as shown by $\bar{\theta}_0 = 30°$. This effect is the result of a complicated interaction between the magnetic field and macroscopic stretch, both of which cause the microstructure to evolve.

Together Figures 6.7d and 6.6d show plots of the magnetoelastic Young's moduli in the reference ($\tilde{E}_{\mathrm{a}}$) and stricted ($\tilde{E}_{\mathrm{m}}$) configurations, respectively, as functions of the magnetic induction $\bar{b}$ for various initial fiber orientation angles $\bar{\theta}_0$. The values for $\bar{b} = 0$ correspond to the purely mechanical moduli in the reference configuration. Because of the incompressibility and two-dimensional symmetry of the fiber-reinforced elastomers, it is known (Lopez-Pamies and Ponte Castañeda, 2006b) that the moduli of complementary angles (e.g. $\bar{\theta}_0 = 40$ and 50°) have exactly the same modulus, with $\bar{\theta}_0 = 45°$ yielding the softest response, and the perfectly aligned cases ($\bar{\theta}_0 = 0$ and 90°), the stiffest. On application of the magnetic field, an initial quadratic regime is observed that quickly transitions into the saturation regime. It is also remarked that,

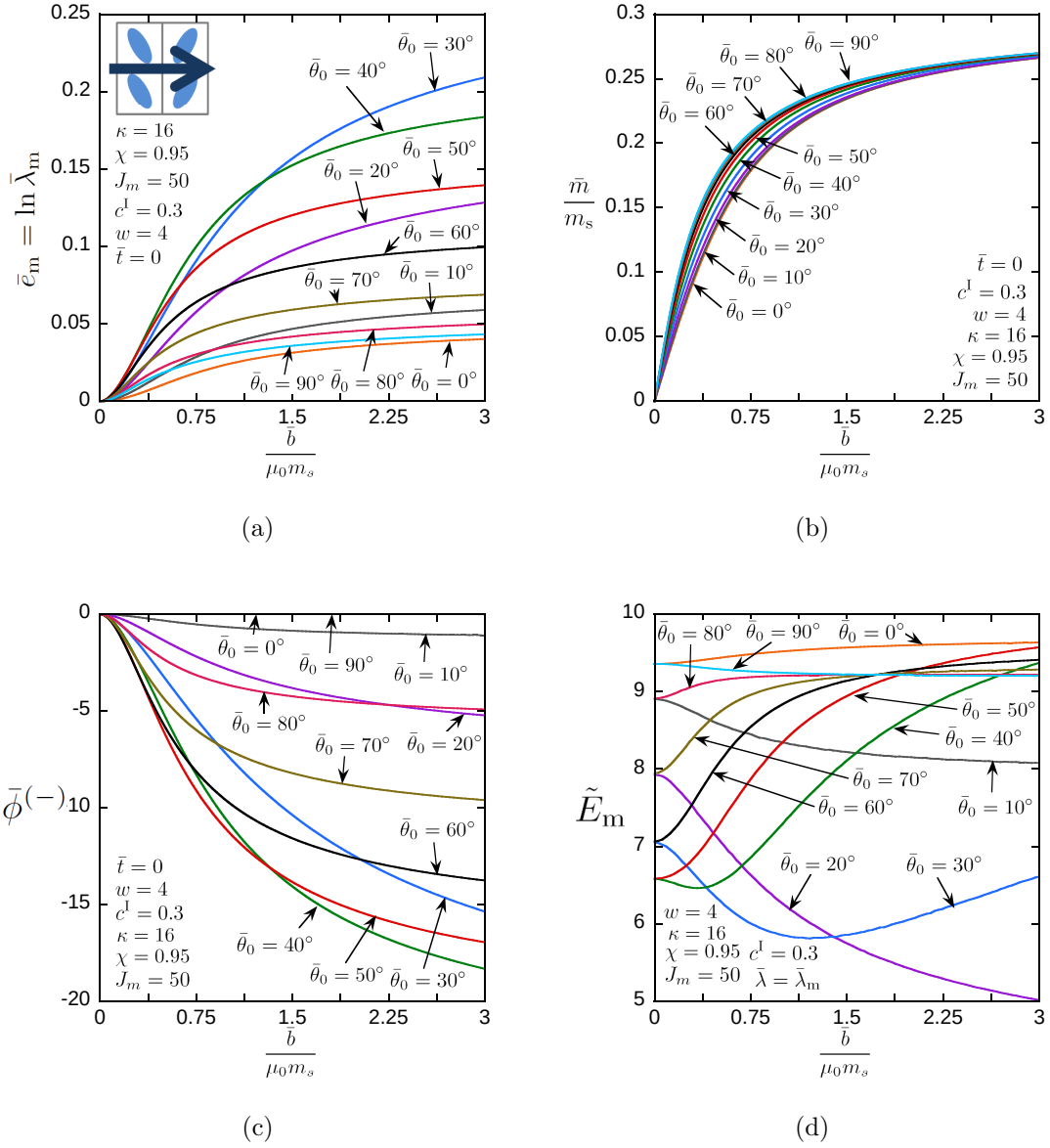

Figure 6.7: Magnetostriction of the laminated MRE samples with elliptical fibers ($w = 4$) as functions of the magnetic induction $\bar{b}$ for different microstructural angles $\bar{\theta}_0$ with the magnetic field applied along the layers' normal direction. (a) The magnetostriction. (b) The composite magnetization. (c) The particle rotation in phase (-). (d) The magnetoelastic Young's modulus evaluated at the magnetostricted stretch.

while the initial moduli of complementary angles are identical, the magnetic field has opposite effects on the two angles. This is because the configuration with initial orientation that is most closely aligned with the field ($\bar{\theta}_0 > 45°$) tends to become even more aligned, and therefore stiffer, while the one with initial orientation that is most misaligned ($\bar{\theta}_0 < 45°$) tends to increase (toward 45°), leading to a more compliant response. Finally, it should also be noted that since the particle rotations are larger for the magnetostricted state, this may lead to a stiffening effect even for the initially more misaligned ($\bar{\theta}_0 < 45°$) configurations, since the angle can go significantly beyond 45°, which would lead eventually to a stiffening behavior.

Optimal microstructures for the actuation, magnetostriction and Young's moduli for aligned loading

Figures 6.8a and b show plots for the actuation traction and magnetostrictive strain at saturation when the magnetic field is aligned with the layers' normal direction, as functions of the initial fiber orientation $\bar{\theta}_0$. It can be seen from these figures that a significant enhancement in the actuation traction and magnetostrictive strain can be achieved for the laminated samples with elliptical fibers when the initial fiber orientation $\bar{\theta}_0$ is appropriately selected. Selection depends on the particle volume fraction and aspect ratio. Thus, for the laminated samples with $c^I = 0.45$ and $w = 8$, for example, we can see that it is possible to enhance the activation traction by over 350% relative to an MRE sample with an isotropic distribution of circular particles ($w = 1$) with the same volume fraction ($c^I = 0.45$) by selecting $\bar{\theta}_0$ to be approximately equal to 50°. On the other hand, the magnetostriction can be correspondingly improved by over 400% for the same MRE samples by selecting $\bar{\theta}_0 \approx 25°$. In this context, it should be re-emphasized that the much larger enhancement in the actuation traction and magnetostrictive strain for the nonaligned elliptical fiber cases (relative to the perfectly aligned cases) is due to the particle rotations, as predicted by the general theory of Ponte Castañeda and Galipeau (2011).

We have ignored the possible development of instabilities in this figure because the lamination direction does not correspond to the correct unstable mode. Indeed, it is known from the work of Lopez-Pamies and Ponte Castañeda (2006a) for the purely mechanical case that long wavelength bifurcation instabilities are expected when the composite is loaded in compression along the long axis of the fibers, corresponding in this case to values of $\bar{\theta}_0$ near 0°. For this reason, it is possible that the traction

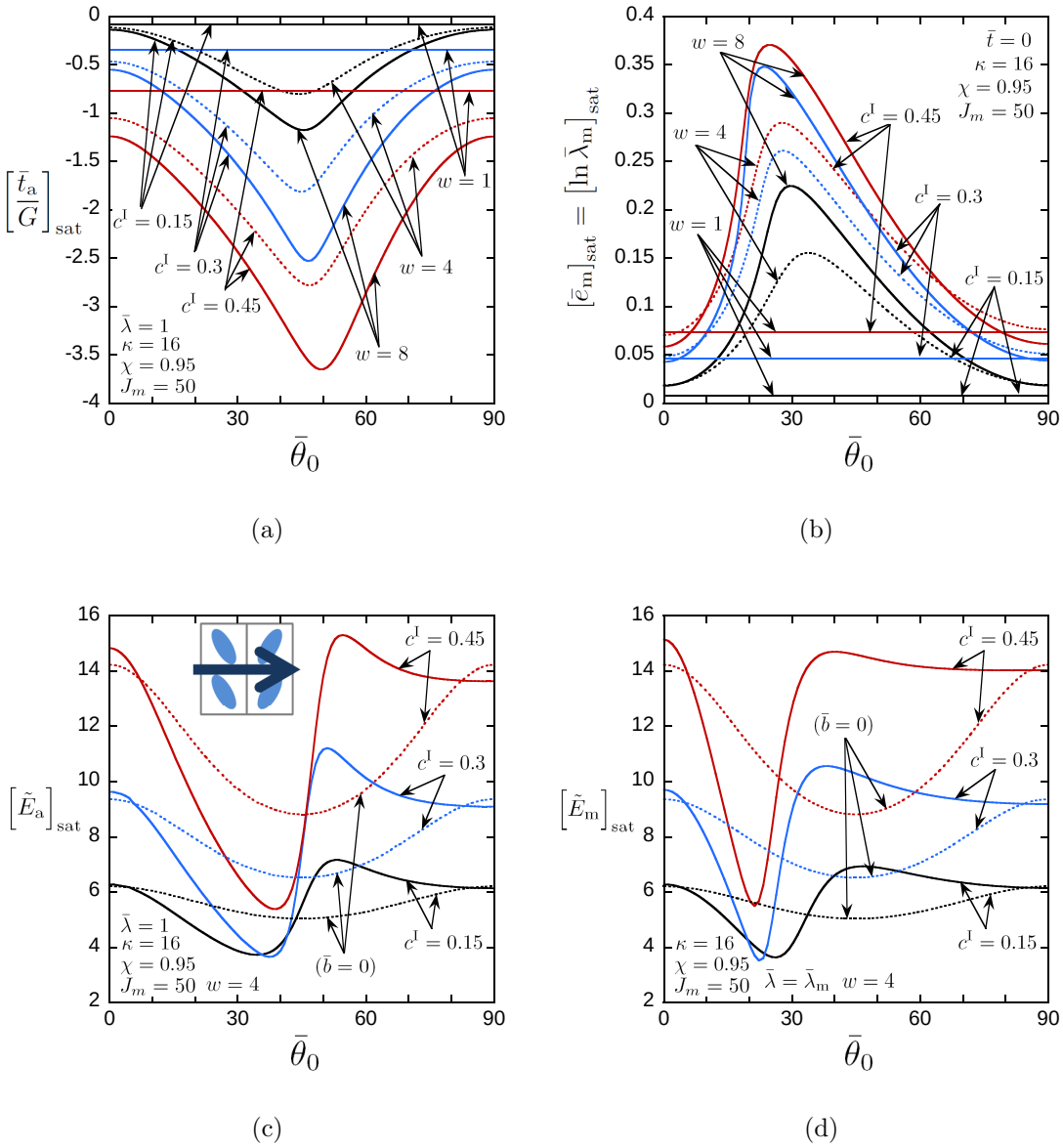

Figure 6.8: Magnetoelastic properties of the laminated MRE samples at saturation, as functions of the microstructural angle $\bar{\theta}_0$ for several values of the particle volume fraction ($c^I = 0.15, 0.3$ and 0.45) and aspect ratio ($w = 1, 4$ and 8). The magnetic field is applied along the layers' normal direction. (a) The actuation stress. (b) The magnetostrictive strain. (c) The magnetoelastic Young's modulus evaluated in the undeformed configuration. (d) The magnetoelastic Young's modulus evaluated at the magnetostricted strain. (Results for the mechanical moduli are also given for comparison in the last 2 figures.)

values in Figure 6.8a would not actually be achieved for values of $\bar{\theta}_0 \approx 0°$. However, instabilities would not be expected for the larger values of $\bar{\theta}_0$, and therefore it is unlikely that the possible onset of instabilities would affect the optimal values of the actuation tractions which occur for $\bar{\theta}_0 \approx 50°$. On the other hand, instabilities may also be expected to affect the magnetostriction results for values of $\bar{\theta}_0 \approx 0$. However, once again, these instabilities would not be expected to affect the optimal values of the magnetostriction, which take place for values of $\bar{\theta}_0 \approx 25°$.

Finally, Figures 6.8c and d show plots of the magnetoelastic Young's moduli $\tilde{E}_a$ and $\tilde{E}_m$ at magnetic saturation for the laminated samples with fiber aspect ratio $w = 4$ at various particle concentrations ($c^I = 0.15, 0.3$ and 0.45). In addition, the corresponding results for the magnetically unloaded samples ($\bar{b} = 0$) are also shown for comparison purposes. Recalling that the results for $\bar{\theta}_0 = 0$ and $90°$ correspond to microstructures with perfectly aligned fibers, it is seen that the effect of the magnetic field on the moduli is quite small in this case, consistent with the finding of Galipeau and Ponte Castañeda (2012) for perfectly aligned loadings. The effect on the moduli is entirely due to the changes in the shape of the distribution of the particle centers for these cases where particle rotations are not observed, which is an effect of order volume fraction squared. On the other hand, it can be seen that very significant changes can be achieved in the magnetoelastic moduli $\tilde{E}_a$ and $\tilde{E}_m$ for initial particle orientations near 45 and 30°, respectively. These results can be attributed to the particle rotations and are of order volume fraction, and therefore expected to be larger than the effects due to changes in the distribution of the particle centers. Thus when $10° \lesssim \bar{\theta}_0 \lesssim 45°$, the magnetic field tends to make the laminated sample more compliant in the reference configuration (i.e., $\tilde{E}_a$ drops with application of the magnetic field). This is because of two effects: one is that the magnetic field causes the particles to rotate closer to 45° from the lamination direction which is a softer mechanical mode. The second is that the rotational force on the particles is increasing and attains its maximum around 45° (consider the actuation traction in Figure 6.8a). Since the magnetic field makes the composite mechanically softer, and the magnetic torques tend to increase with deformation, the overall effect is a decrease in the modulus. However these two effects are interdependent and there is no simple way to separate the effects into "purely mechanical" and "magnetoelastic." For $\bar{\theta}_0 \gtrsim 45°$ both effects work in opposite directions and the magnetic field drives the particles into alignment of their long axis with the lamination direction where the composite is mechanically

stiffer, but the magnetic torques decrease because the stretch also tends to align the particles with the applied magnetic field. The upshot is that the magnetically loaded samples are stiffer than the unloaded samples for $45° \lesssim \bar{\theta}_0 \lesssim 80°$. The magnetostricted modulus $\tilde{E}_m$, shown in Figure 6.8d, is controlled by the same effects with the additional consideration of the macroscopic deformation that is induced by the magnetic field. Since the elongation tends to stiffen the composite by rotating the particles toward alignment of their long axes with the applied stretch and magnetic field, the overall composite becomes stiffer for smaller values of $\bar{\theta}_0$.

6.2.3 Results for transverse magnetic loading.

Magnetization and traction as functions of the strain for transverse loading

Figure 6.9 shows plots of the macroscopic magnetization $\bar{m}$ and traction $\bar{t}$ as functions of the applied strain $\bar{e}$ in the laminated MRE samples. They are for increasing values of the applied magnetic induction $\bar{b}$ when the magnetic field is applied transverse to the lamination direction. The transverse magnetic loading is different than aligned loading because many of the effects reverse direction; however the underlying mechanisms are similar. Most notably the magnetic field causes the composite to contract in the mechanical loading direction as opposed to extend as in the aligned case. This can be observed in Figure 6.9b because the magnetic field shifts the traction-deformation curve upward instead of down. Similarly the magnetic field causes the particles to rotate in the opposite direction when the deformation is the same.

Actuation, magnetostriction and Young's moduli as functions of the magnetic field for transverse loading

Figure 6.10 shows the actuation traction and associated magnetoelastic effects as a function of magnetic flux $\bar{b}$ for various initial orientation angles $\bar{\theta}_0$ when the magnetic field is applied transverse to the normal direction. In all cases the actuation stress is initially quadratic in the applied magnetic field then reaches a saturation as the magnetic field becomes large. This is very similar to the aligned loading plots in Figure 6.6 except that the traction and spin have changed sign. The modulus effects are also reversed such that, generally speaking, the transverse field stiffens the composite if the aligned field softened it and vice versa. In this sense altering the orientation of the magnetic field can reverse the modulus effects.

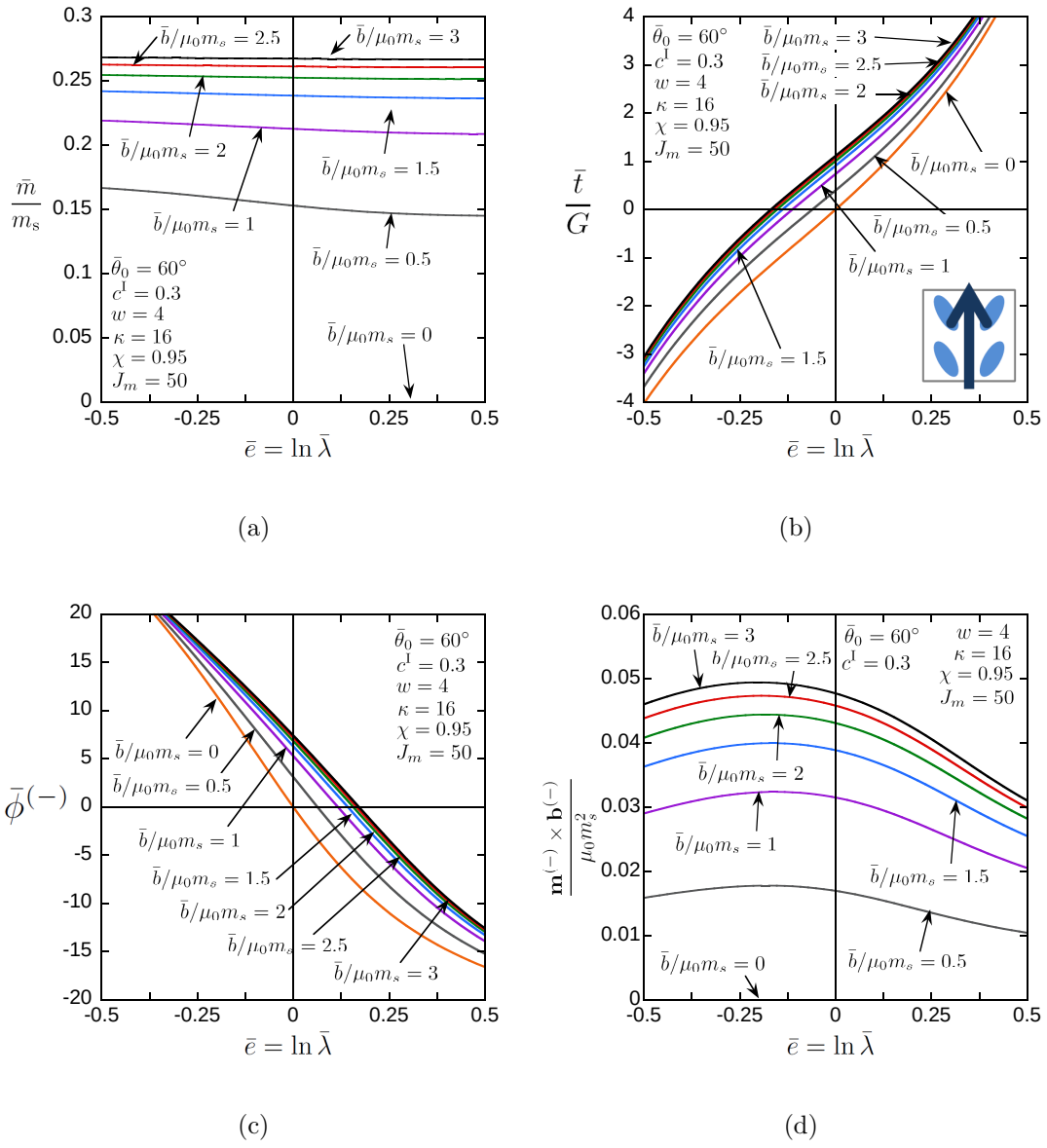

Figure 6.9: The magnetization $\bar{m}$ and traction $\bar{t}$ as functions of the strain $\bar{e}$ in a laminated MRE sample with elliptical fibers ($w = 4$) and orientation $\bar{\theta}_0 = 60°$, for increasing values of the applied magnetic induction $\bar{b}$. The magnetic field is applied transverse to the layers' normal direction. (a) The normalized magnetization-strain relation. (b) The normalized traction-strain relation. (c) The particle rotation in phase $(-)$. (d) The torque $\bar{\mathbf{m}} \times \bar{\mathbf{b}}$ in phase $(-)$.

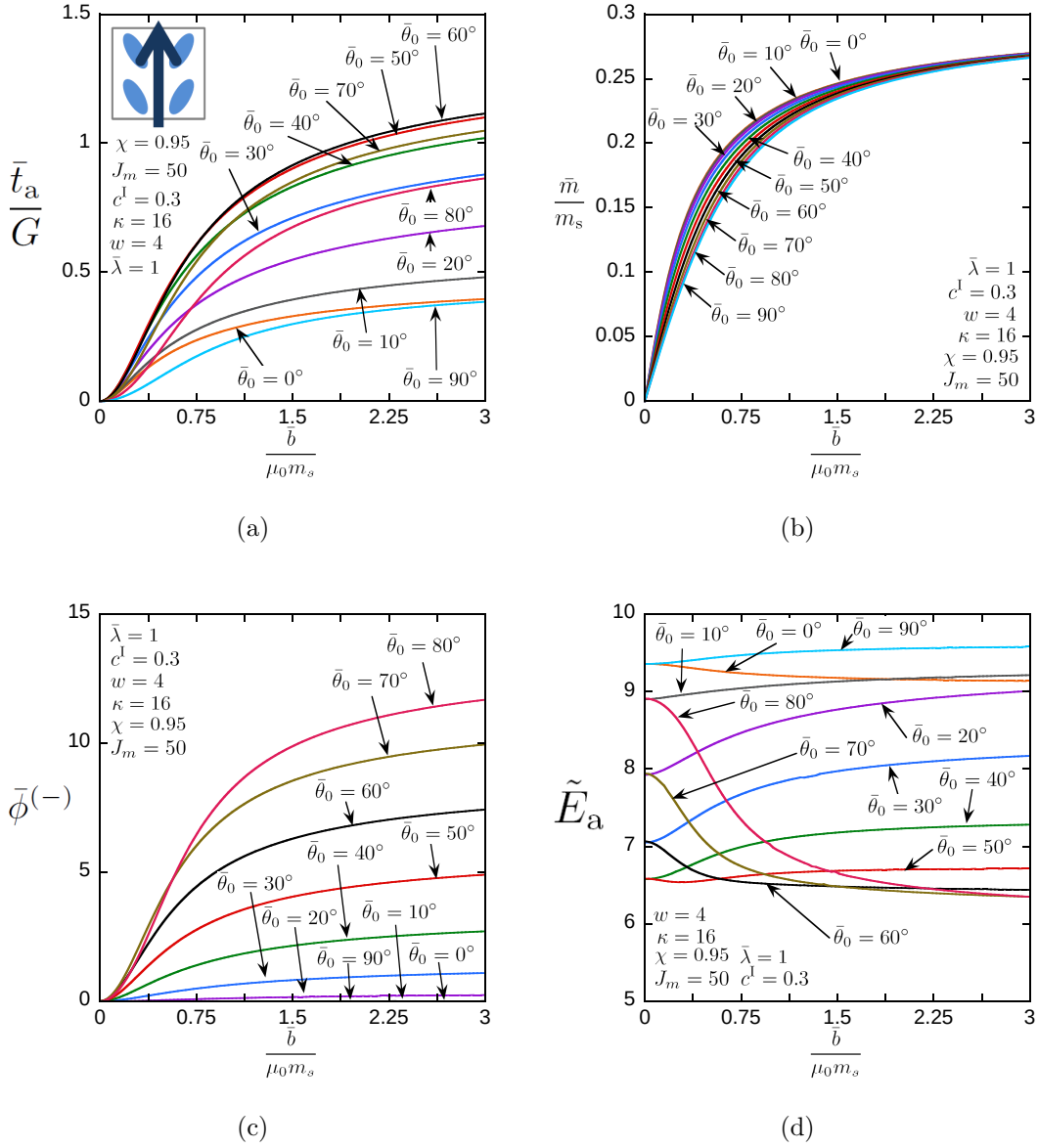

Figure 6.10: Actuation traction of the laminated MRE samples with elliptical fibers ($w = 4$) as functions of the magnetic induction $\bar{b}$ for different microstructural angles $\bar{\theta}_0$ with the magnetic field applied transverse to the layers' normal direction. (a) The actuation stress. (b) The composite magnetization. (c) The particle rotation in phase $(-)$. (d) The magnetoelastic Young's modulus evaluated at the reference stretch.

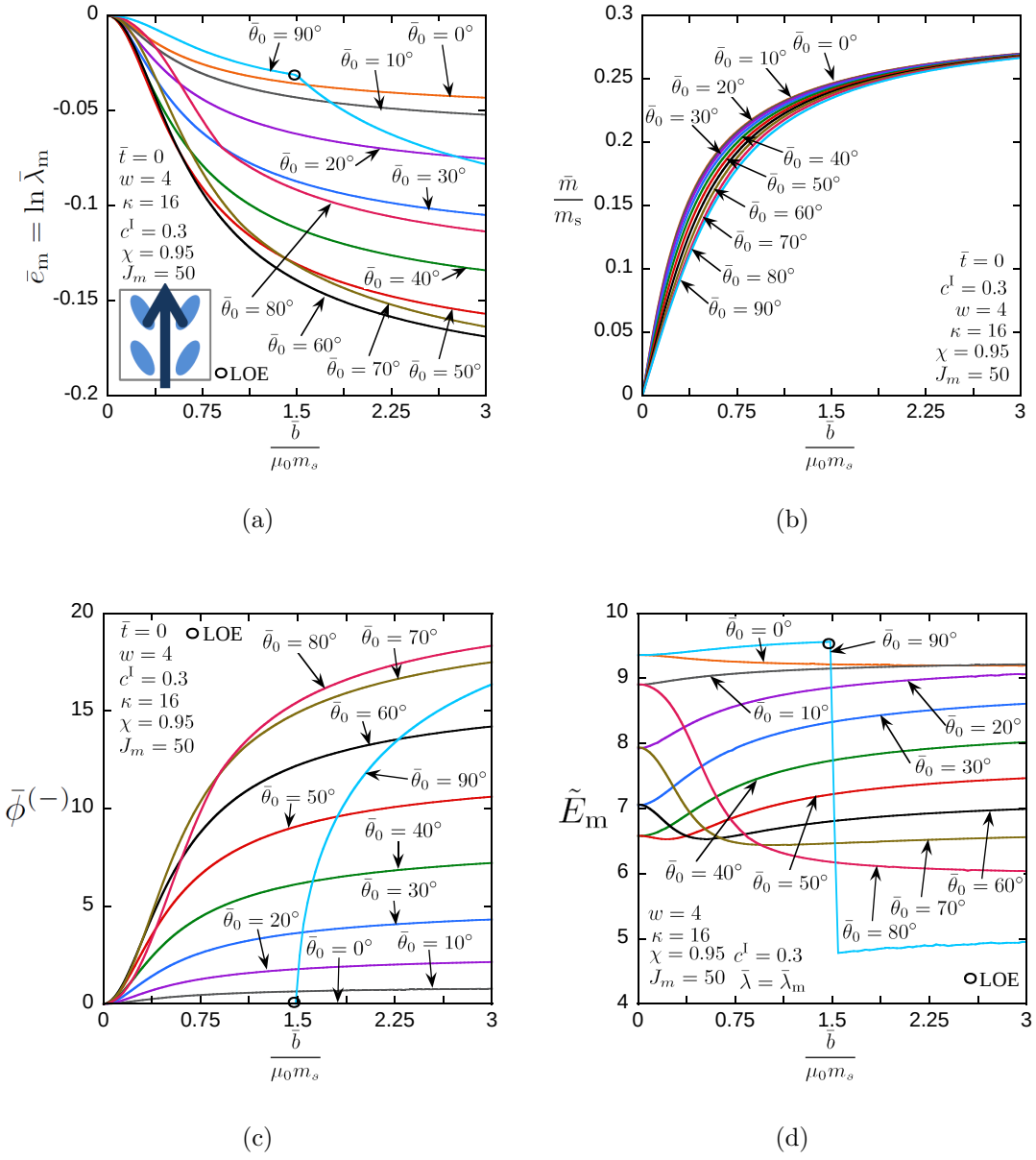

Figure 6.11: Magnetostriction of the laminated MRE samples with elliptical fibers ($w = 4$) as functions of the magnetic induction $\bar{b}$ for different microstructural angles $\bar{\theta}_0$ with the magnetic field applied transverse to the layers' normal direction. LOE indicates loss of ellipticity for the homogenous composite. (a) The magnetostriction. (b) The composite magnetization. (c) The particle rotation in phase $(-)$. (d) The magnetoelastic Young's modulus evaluated at the magnetostricted stretch.

Figure 6.11 shows the magnetostriction and associated magnetoelastic effects as a function of $\bar{b}$ for various initial orientation angles $\bar{\theta}_0$ when the magnetic field is applied transverse to the normal direction. This transverse loading is very similar to the aligned case with the same reversals observed in the actuation stress plots. This case does show the presence of the instability when $\bar{\theta}_0 = 90°$. The magnetostriction compresses the composite along the long axis of the particles and when a critical value is reached, the solution bifurcates and the instability is observed. This appears in Figure 6.11a where we observe discontinuous slope in the magnetostriction curve. The nature of the effect becomes obvious when we look at the particle rotation in Figure 6.11c. The particles undergo a large spontaneous spin at the critical magnetic field. This instability also causes the discontinuity in the modulus as shown in Figure 6.11d.

Optimal microstructures for the actuation, magnetostriction and Young's moduli for transverse loading

Figures 6.12a and b show the actuation traction and magnetostrictive strain at saturation when the magnetic field is applied transverse to the layers' normal direction, as functions of the initial fiber orientation $\bar{\theta}_0$. Applying the magnetic field transverse to the layers' normal direction produces similar effects to aligned loading except that the signs of the traction and magnetostriction are reversed. The major difference here is that the effect of instabilities becomes apparent since $\bar{\theta}_0 = 0°$ and $\bar{\theta}_0 = 90°$ show different actuation traction and magnetostriction. This is because the unstable mode has been activated at $\bar{\theta}_0 = 90°$.

Figures 6.12c and d show plots of the magnetoelastic Young's moduli $\tilde{E}_a$ and $\tilde{E}_m$ at magnetic saturation for the laminated samples with fiber aspect ratio $w = 4$ at various particle concentrations ($c^I = 0.15, 0.3$ and 0.45) when the magnetic field is applied transverse to the layers' normal direction. In addition the corresponding results for the magnetically unloaded samples ($\bar{b} = 0$) are shown for comparison purposes. The same mechanisms that were discussed in the context of aligned loading occur here except that the magnetic torques are in the opposite direction which causes the stiffening or softening to reverse. Additionally the effect of the instability is very apparent at $\bar{\theta}_0 \approx 90°$ where the magnetic field cause a large rotation of the particles. This holds the composite in a significantly softer mode causing a large drop in modulus.

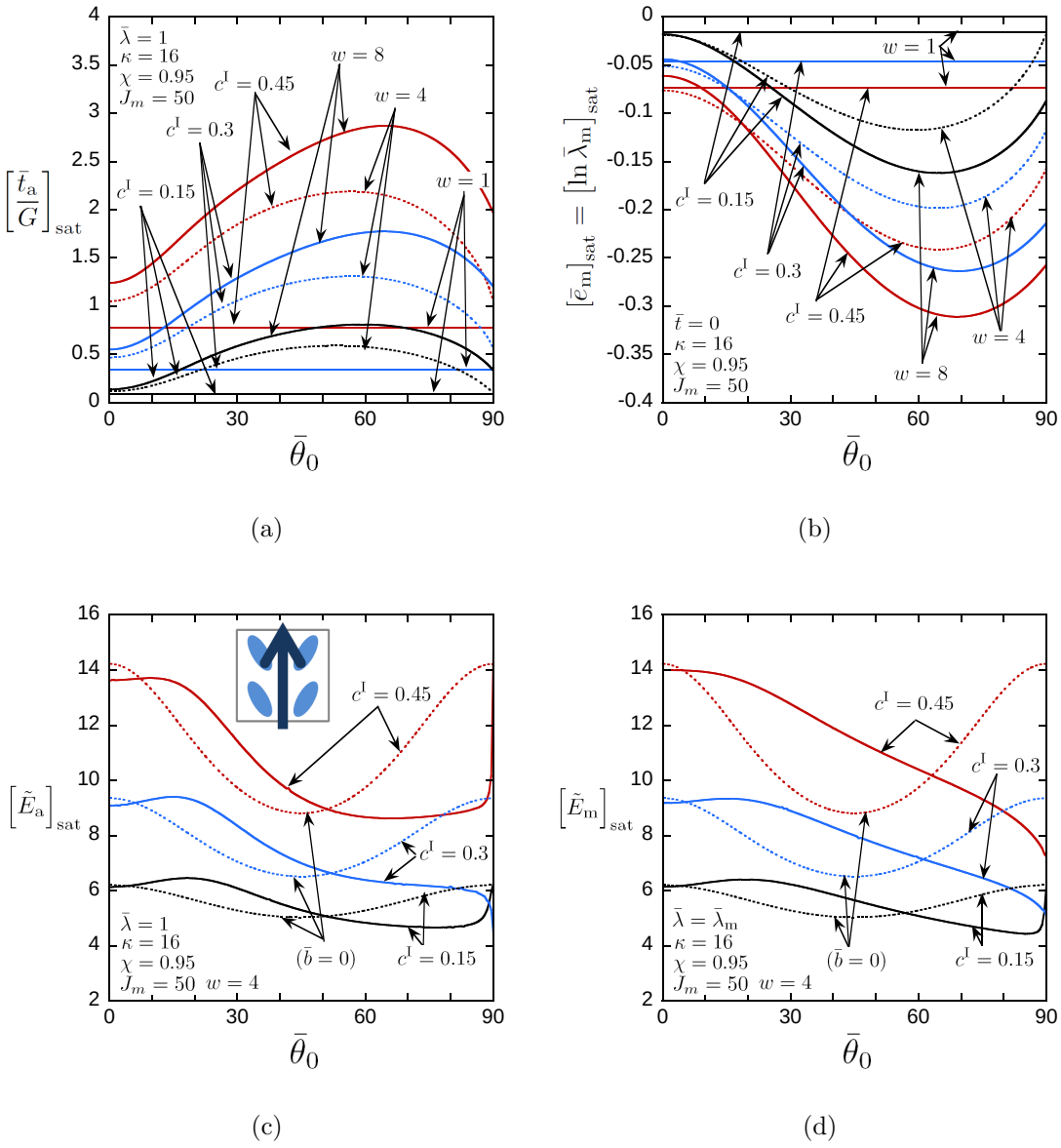

Figure 6.12: Magnetoelastic properties of the laminated MRE samples at saturation, as functions of the microstructural angle $\bar{\theta}_0$ for several values of the particle volume fraction ($c^I = 0.15, 0.3$ and 0.45) and aspect ratio ($w = 1, 4$ and 8). (a) The actuation stress. (b) The magnetostrictive strain. (c) The magnetoelastic Young's modulus evaluated in the undeformed configuration. (d) The magnetoelastic Young's modulus evaluated at the magnetostricted strain. (Results for the mechanical moduli are also given for comparison in the last 2 figures.)

6.2.4 Results for rank-2 laminate

Figure 6.13 shows the magnetoelastic properties of the rank 2 laminated MRE as functions of the magnetic induction $\bar{b}$ for different microstructural angles $\bar{\theta}_0$. The plots show various values of the initial orientation angle, $\bar{\theta}_0$, each for a concentration, $c = 0.30$. Figure 6.13d displays the magnetization of the composite at the magnetostricted state as a function of the magnetic flux, $\bar{b}$. The magnetization behavior of the composite exhibits the expected saturation behavior. Since the concentration of the rigid phase is the same for each curve and constant with respect to deformation, the saturation magnetization of the composite is always the same. The initial susceptibility of the composite is characterized by the slope of the curves at $\bar{b} = 0$. This quantity depends on the initial orientation of the rigid layers. Figure 6.13b illustrates the magnetostriction of the composite as a function of the magnetic flux, $\bar{b}$. The model predicts that the magnetostriction will behave quadratically for small magnetic fluxes then saturate as the field becomes large. The magnetostriction is strongly influenced by the initial orientation angle with $\bar{\theta}_0 = 20^\circ - 60^\circ$ producing the largest effect. Notice that the magnetostrictive effect vanishes as $\bar{\theta}_0 \to 0^\circ$ and $\bar{\theta}_0 \to 90^\circ$ because the composite becomes rigid with respect to the strain direction in those limits. Figure 6.13c shows the normalized magnetoelastic Young's modulus, $\frac{\tilde{E}_m}{\tilde{E}_{me}}$ as a function of the magnetic flux, $\bar{b}$. It is important to note that each plot considers the modulus for a different value of the initial orientation angle $\bar{\theta}_0$ so the reference mechanical stiffness for each curve is different. Also the reference modulus is evaluated at the undeformed configuration and is not the mechanical part of the modulus at the magnetostrictive state. The plots show the relative change in modulus that could be obtained with application of the magnetic field. Results predict that for $\bar{\theta}_0 = 50^\circ - 90^\circ$ the magnetic field can stiffen the composite by a factor of 2 to 4. The magnetic field can soften the composite to 75% of its original value for $\bar{\theta}_0 = 30^\circ$. This indicates that the magnetic field can significantly modulate composite stiffness for this class of microstructures.

Figure 6.14 shows the saturation magnetostriction as functions of the microstructure. Figure 6.14a shows the magnetostriction as functions of the concentration c. The magnetostriction depends linearly on the concentration in the dilute limit for all initial microstructural angles. Then for moderate concentration the magnetic effects continue to increase. However the composite is becoming mechanically stiffer such that the magnetostriction reaches a maximum value. For large concentrations where

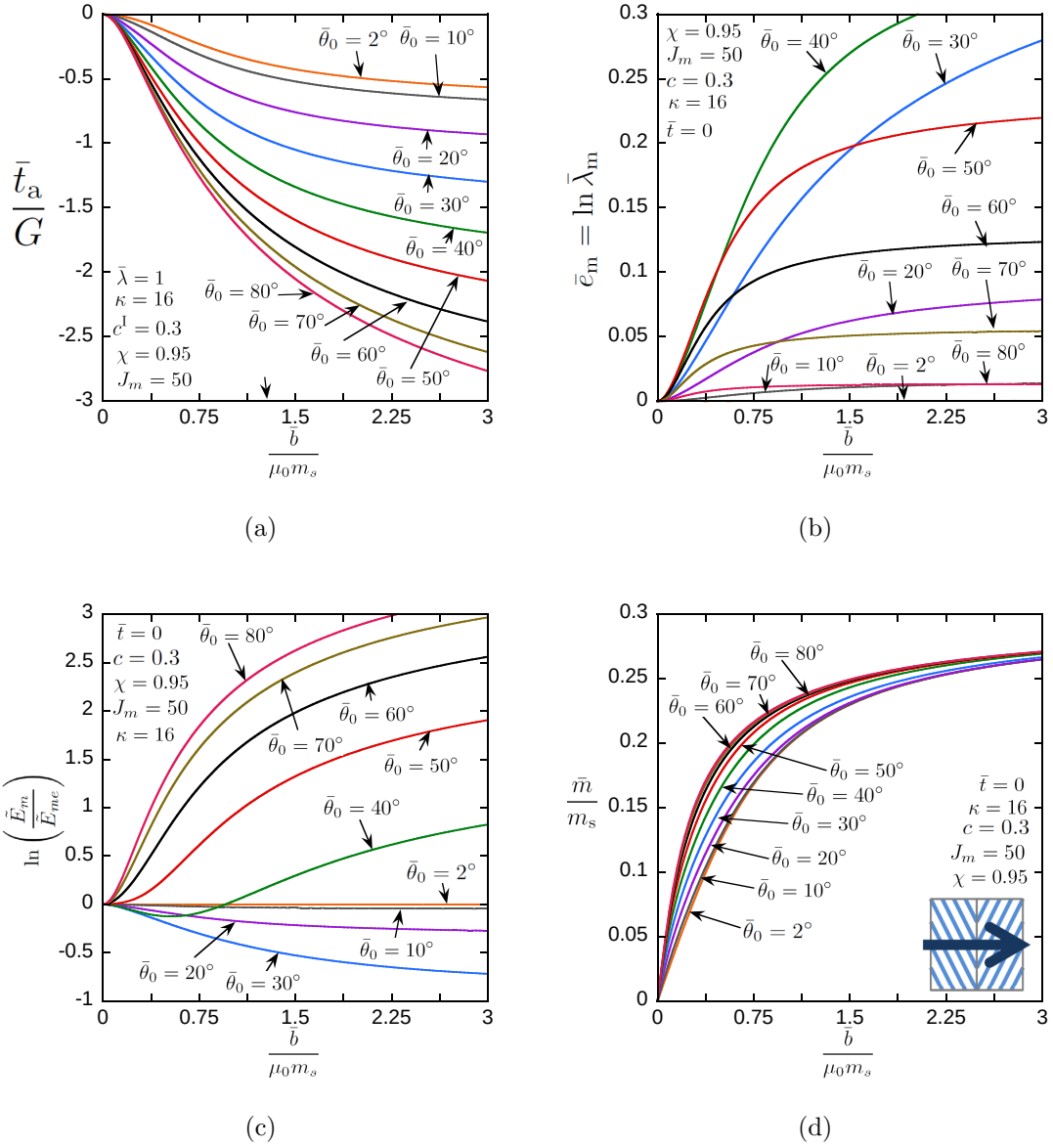

Figure 6.13: Magnetoelastic properties of the rank 2 laminated MRE as functions of the magnetic induction $\bar{b}$ for different microstructural angles $\bar{\theta}_0$. (a) The actuation traction. (b) The magnetostriction. (c) The magnetoelastic Young's modulus evaluated at the magnetostrictive strain normalized by the purely mechanical modulus measured at the reference configuration. (d) The composite magnetization.

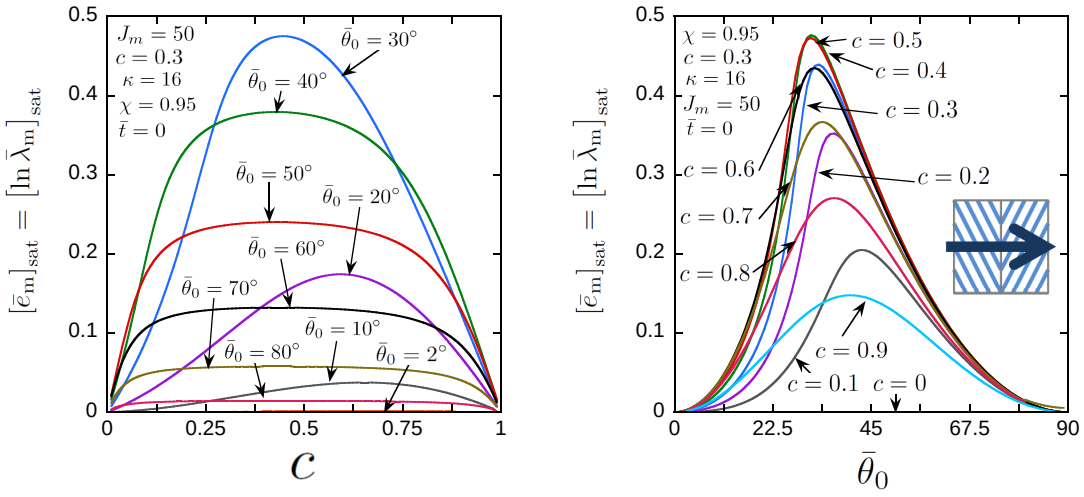

(a) (b)

Figure 6.14: The saturation magnetostriction of the rank 2 laminate as functions of the microstructure. (a) The magnetostriction as a function of the concentration for various microstructural angles. (b) The magnetostriction as a function of the microstructural angle for various concentrations.

$c \to 1$ the composite becomes rigid such that the magnetostriction vanishes in all cases. The optimal concentration depends on the initial orientation angle $\bar{\theta}_0$ as well as the non-dimensional parameter κ (not shown in the plots). Figure 6.14b shows the magnetostriction as functions of the initial orientation angles $\bar{\theta}_0$. The composite becomes mechanically rigid for $\bar{\theta}_0 \to 0$ and $\bar{\theta}_0 \to 90$ which limits the magnetostriction. The magnetostriction reaches a maximum which depends on the concentration for moderate values of the microstructural angle. Taken together Figures 6.14a and 6.14b suggest that the magnetostriction is optimized for $\bar{\theta}_0 \approx 30°$ and $c \approx 0.5$, with the precise result depending on κ.

Comparison of the fiber laminates and the rank-2 laminate

Figure 6.15 shows the actuation traction and magnetostriction for different values of w including the rank-2 laminate results when $w \to \infty$. In Figure 6.15a we consider the actuation traction for different aspect ratios. Results are relatively consistent as the initial orientation angle is increased, but past $\bar{\theta}_0 = 45°$ the results for the rank-2 laminate and the fiber composite with high aspect ratio diverge. In the limit as the

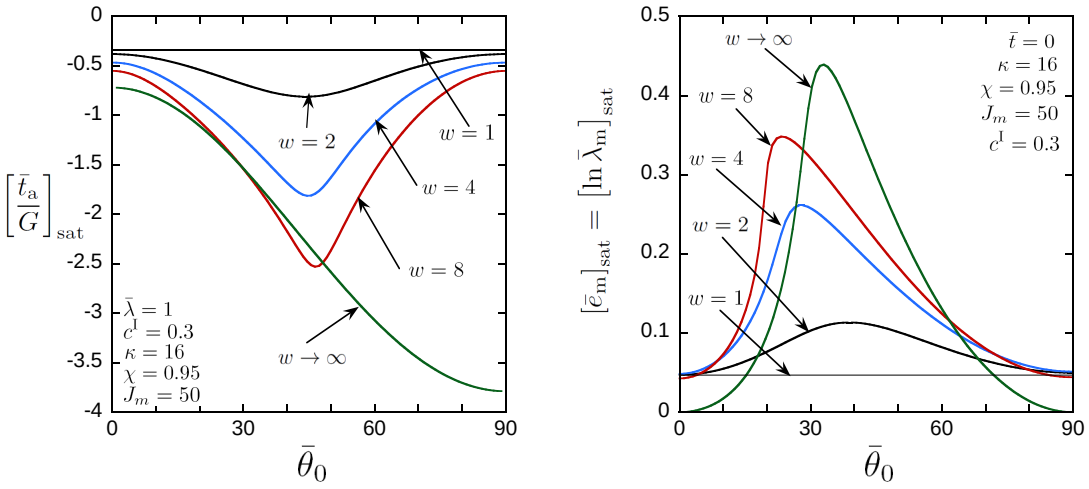

(a) (b)

Figure 6.15: The actuation traction and magnetostriction as functions of the microstructural angle $\bar{\theta}_0$ and aspect ratio $w = 1, 4, 8$ and $w \to \infty$. (a) The actuation stress. (b) The magnetostrictive strain.

initial orientation angle $\bar{\theta}_0 \to 90°$ the composite is becoming mechanically rigid. For those cases where the composite becomes rigid the actuation stress depends on how the limit is reached. For instance letting $w \to \infty$ then letting $\bar{\theta}_0 \to 90°$ is expected to produce a different result than taking the limits in reverse order. Another way to achieve a composite with this configuration is to allow the magnetic layers to be deformable and take the limit as they become rigid, which will again produce a different result for the actuation traction. The fact that this limit does not exist suggests that it may be not physical to consider the actuation stress along directions where the material becomes rigid. Figure 6.15b depicts the magnetostriction for the same material parameters. In this case the magnetostriction vanishes in the limits $\bar{\theta}_0 \to 90°$ and $\bar{\theta}_0 \to 0$, which is consistent with the material becoming mechanically rigid. Even though the actuation stress may be not physical in those limits, magnetostriction accounts for the mechanical stiffening which leads to the expected physical result.

6.3 Concluding remarks

In this section we have demonstrated how simple MRE laminates made of layers of the elliptical fiber MREs with alternating orientations can be used to enhance the effect of the applied magnetic field on the magnetostriction, actuation tractions, and magnetoelastic moduli, by exploiting the synergetic effects of the particle rotations. The quantitative understanding of these microscopic effects is crucial for the successful design of MREs with optimal magnetoelastic properties. Our results for the laminated MRE samples show that it is possible to produce 3 to 4 fold increases in the magnetostriction and actuation stress, and generate over 50% changes in the magnetoelastic moduli upon the application of the magnetic field, by suitable choices of the shape and orientation of the fibers relative to the loading and layering directions.

We have also considered the limit where the aspect ratio of the fibers becomes large and the composite tends to a rank two laminate. In this case the microstructure evolution can be characterized entirely by the macroscopic deformations such that the partial decoupling approximation applies fully. This example also allowed us to solve the homogenization problem exactly without the need for approximation. The results are in agreement with the previous cases, confirming the validity of our approach. The rank 2 laminates are also a realizable microstructure for enhanced magnetoelastic effects which should be relatively simple to produce.

Chapter 7

Application of PDCA to aligned loads in 3D

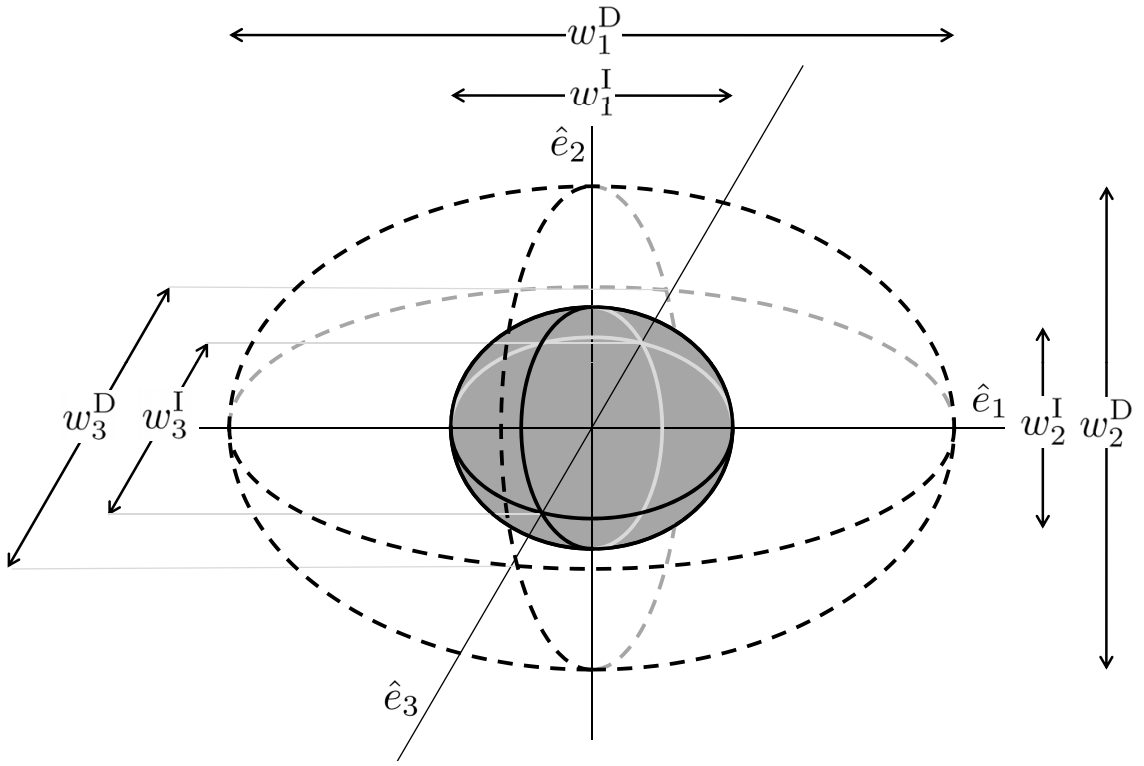

Figure 7.1: A general ellipsoidal inclusion surrounded by its distributional ellipsoid. The principal axes of both ellipses are aligned with the coordinate system and have lengths w_i^{I} and w_i^{D}, respectively.

In this chapter we employ the partial decoupling approximation for 3D aligned loadings at small-strain. The model most closely resembles the MREs which have been produced experimentally and we present some comparisons with experimental results. It is important to note that this chapter does make use of information about the evolution of the distribution from the full finite strain theory, even though the final result focuses on small-strain.

7.1 Aligned loading constitutive response

In this section, we will specialize the general results of Chapter 3 (Ponte Castañeda and Galipeau, 2011) for situations when the magnetic and mechanical loadings are aligned with the microstructure of the MRE. It is recalled from that work that the MREs are modeled as elastic materials containing random distributions of aligned particles. The particles are taken to have ellipsoidal shape and to be distributed

randomly with "ellipsoidal" symmetry (Willis, 1977). Particulate microstructures of this type can be visualized, as shown in Figure 7.1, as having ellipsoidal particles with principal lengths $w_i^{\rm I}$ surrounded by a distributional ellipsoid with principal lengths $w_i^{\rm D}$. The distributional ellipsoid characterizes—through the two-point probability function of the microstructure—the average distance between the particles in different directions. The principal axes of both ellipsoids are assumed to be aligned, so that we can use the same set of unit vectors, $\hat{\mathbf{e}}_i$, to define the orientation of both ellipsoids. We can then write the shape tensors $\boldsymbol{Z}_0^{\rm I}$ and $\boldsymbol{Z}_0^{\rm D}$, defining the shape and initial distribution of the inclusions, in the forms

$$\boldsymbol{Z}_0^{\rm I} = \sum_{i=1}^{3} w_i^{\rm I} \hat{\mathbf{e}}_i \otimes \hat{\mathbf{e}}_i, \text{ and } \boldsymbol{Z}_0^{\rm D} = \sum_{i=1}^{3} w_i^{\rm D} \hat{\mathbf{e}}_i \otimes \hat{\mathbf{e}}_i. \tag{7.1}$$

Under the above microstructural hypotheses, the MRE exhibits orthotropic symmetry and is such that no rotations will be induced in the microstructure if the magnetic and mechanical fields are aligned with the symmetry axes defined by the vectors $\hat{\mathbf{e}}_i$. Thus, the composite is assumed to be loaded magnetically along the k-th direction, so that

$$\bar{\mathbf{b}} = \bar{b}\hat{\mathbf{e}}_k, \tag{7.2}$$

where $\bar{b}$ is the magnitude of the magnetic flux. The deformation is also aligned (coaxial) with the symmetry axes, so the deformation gradient is described by

$$\bar{\boldsymbol{F}} = \bar{\boldsymbol{U}} = \sum_{i=1}^{3} \bar{\lambda}_i \hat{\mathbf{e}}_i \otimes \hat{\mathbf{e}}_i, \tag{7.3}$$

where $\bar{\lambda}_i$ is the principal stretch in the $\hat{\mathbf{e}}_i$ direction.

Under these conditions, the average magnetization in the MRE is given by

$$\bar{\mathbf{m}}(\bar{\mathbf{b}}) = \frac{1}{\mu_0} \tilde{\boldsymbol{X}}_L(\bar{\boldsymbol{U}}, \chi_L)\bar{\mathbf{b}}, \tag{7.4}$$

where $\tilde{\boldsymbol{X}}_L(\bar{\boldsymbol{U}}, \bar{\mathbf{b}})$ is the effective magnetic susceptibility of a linear comparison composite (see Ponte Castañeda (1992, 1998)) with linear magnetic susceptibility χ_L in the matrix phase. Using the linear homogenization procedure of Ponte Castañeda and Willis (1995) for the above-defined microstructure, the following expression is

obtained

$$\tilde{\boldsymbol{X}}_L(\bar{\boldsymbol{U}},\chi_L) = \frac{c^{\mathrm{I}}}{\bar{J}}\left[\frac{\boldsymbol{I}}{\chi_L} - \boldsymbol{I} + \boldsymbol{P}^{\mathrm{I}} + \frac{c^{\mathrm{I}}}{\bar{J}}\boldsymbol{I} - c^{\mathrm{I}}\boldsymbol{P}^{\mathrm{D}}(\bar{\boldsymbol{U}})\right]^{-1}, \tag{7.5}$$

where c^{I} is the concentration of inclusions, and $\boldsymbol{P}^{\mathrm{I}}$ and $\boldsymbol{P}^{\mathrm{D}}$ are microstructural tensors, characterizing the effects of the inclusions and distribution. They are given by

$$\boldsymbol{P}^{\mathrm{I}} = \frac{\det\, \boldsymbol{Z}_0^{\mathrm{I}}}{4\pi}\int_{|\xi|=1} \xi\otimes\xi|\boldsymbol{Z}_0^{\mathrm{I}}\xi|^{-3}dS(\xi), \tag{7.6}$$

and

$$\boldsymbol{P}^{\mathrm{D}}(\bar{\boldsymbol{U}}) = \frac{\det\, \boldsymbol{Z}_0^{\mathrm{D}}}{4\pi}\int_{|\xi|=1} \xi\otimes\xi|\boldsymbol{Z}_0^{\mathrm{D}}\bar{\boldsymbol{U}}\xi|^{-3}dS(\xi). \tag{7.7}$$

In addition, the comparison susceptibility χ_L is determined from the solution of the "secant" linearization equation (Ponte Castañeda, 1998)

$$\frac{1}{\mu_0 c^{\mathrm{I}}}\tilde{\boldsymbol{X}}_L(\bar{\boldsymbol{U}},\chi_L)\bar{\mathbf{b}} = \mathbf{m}\left(\mathbf{b} = \frac{\tilde{\boldsymbol{X}}_L(\bar{\boldsymbol{U}},\chi_L)\bar{\mathbf{b}}}{c^{\mathrm{I}}\chi_L}\right), \tag{7.8}$$

where

$$\mathbf{m}(\mathbf{b}) = \frac{m_{\mathrm{s}}}{b}\left[\coth\left(\frac{3\chi b}{\mu_0 m_{\mathrm{s}}}\right) - \frac{\mu_0 m_{\mathrm{s}}}{3\chi b}\right]\mathbf{b}. \tag{7.9}$$

Even though this equation is a vector equation, $\mathbf{m}(\mathbf{b})$ is such that both sides of the equation are parallel, producing only one independent equation to determine χ_L. Also it may appear in equation (7.4) that the magnetization $\bar{\mathbf{m}}$ is linear in the applied magnetic field; however χ_L depends on $\bar{\mathbf{b}}$ so the magnetization is nonlinear in the magnetic flux and also depends on the deformation through $\bar{J}$ and $\boldsymbol{P}^{\mathrm{D}}(\bar{\boldsymbol{U}})$.

Correspondingly, the total Cauchy stress is given from expression (3.73) as

$$\begin{aligned}\bar{\boldsymbol{T}} = \bar{\boldsymbol{T}}^{\mathrm{me}}(\bar{\boldsymbol{U}}) - \frac{1}{2\mu_0}(\bar{\mathbf{b}}\cdot\bar{\mathbf{b}})\boldsymbol{I} + \frac{1}{\mu_0}\bar{\mathbf{b}}\otimes\bar{\mathbf{b}} + (\bar{\mathbf{m}}\cdot\bar{\mathbf{b}})\boldsymbol{I} - \bar{\mathbf{m}}\otimes\bar{\mathbf{b}} \\ - \frac{\mu_0}{2}(\bar{\mathbf{m}}\cdot\bar{\mathbf{m}})\boldsymbol{I} - \frac{\mu_0}{2}\bar{J}\frac{\partial}{\partial\bar{\boldsymbol{U}}}\left[\bar{\mathbf{m}}\cdot\boldsymbol{P}^{\mathrm{D}}(\bar{\boldsymbol{U}})\bar{\mathbf{m}}\right]\bar{\boldsymbol{U}},\end{aligned} \tag{7.10}$$

where

$$\bar{\boldsymbol{T}}^{\mathrm{me}}(\bar{\boldsymbol{F}}) = \frac{\rho}{\rho_0}\frac{\partial\widetilde{W}^{\mathrm{me}}(\bar{\boldsymbol{F}})}{\partial\bar{\boldsymbol{F}}}\bar{\boldsymbol{F}}^{\mathrm{T}} \tag{7.11}$$

is the purely mechanical stress, and $\bar{\mathbf{m}}$ is given in terms of $\bar{\boldsymbol{U}}$ and $\bar{\mathbf{b}}$ via expression (7.4). Note, however, that the derivatives with respect to $\bar{\boldsymbol{U}}$ in equation (7.10) are

taken with $\bar{\mathbf{m}}$ held fixed.

By comparing expression (7.10) for the homogenized stress with expression (2.13) for the stress in a general magnetoelastic material, it can be seen that, in addition to the usual magnetic terms, and to the purely mechanical stress, there are two additional terms arising from the derivatives of the effective free-energy with respect to the deformation that are quadratic in the magnetization. The first is a hydrostatic pressure which can be directly related to changes in the concentration of the particles with the deformation, while the second involves changes in the shape of the two-point distribution of the particles with the deformation. They both come from the additional terms in the effective energy function, which describe the nonlinear magnetic susceptibility of the composite. In this context, it is interesting to remark that while the particle-particle forces have *not* been computed directly, the estimate (7.10) for the macroscopic stress does include these two-point interactions between the particles, as has just been remarked. In fact, this new method for determining the macroscopic stress of the MRE requires only the computation of derivatives of the nonlinear magnetic susceptibility of the composite. As a consequence, it is simpler to implement and generalize than other methods requiring the direct computation of the particle-particle forces (Borcea and Bruno, 2001; Yin and Sun, 2006), which is much more involved in practice.

Since the loading is aligned with the principal axes, which are symmetry axes for the composite, the second-order tensors $\bar{\boldsymbol{T}}$, $\tilde{\boldsymbol{X}}_L$, $\boldsymbol{P}^{\mathrm{I}}$ and $\boldsymbol{P}^{\mathrm{D}}$ can be written in terms of their principal values as

$$\begin{aligned} \bar{\boldsymbol{T}} = \sum_{i=1}^{3} \bar{T}_i \hat{\mathbf{e}}_i \otimes \hat{\mathbf{e}}_i, \quad \tilde{\boldsymbol{X}}_L = \sum_{i=1}^{3} \tilde{X}_{L_i} \hat{\mathbf{e}}_i \otimes \hat{\mathbf{e}}_i, \\ \boldsymbol{P}^{\mathrm{I}} = \sum_{i=1}^{3} P_i^{\mathrm{I}} \hat{\mathbf{e}}_i \otimes \hat{\mathbf{e}}_i, \quad \text{and} \quad \boldsymbol{P}^{\mathrm{D}} = \sum_{i=1}^{3} P_i^{\mathrm{D}} \hat{\mathbf{e}}_i \otimes \hat{\mathbf{e}}_i. \end{aligned} \tag{7.12}$$

Therefore, the magnetization is aligned with the $\mathbf{b}$ field, as given by expression (7.2), so that $\bar{\mathbf{m}} = \bar{m}\hat{\mathbf{e}}_k$ with

$$\bar{m} = \tilde{X}_{L_k} \bar{b} = \frac{c^{\mathrm{I}} \chi_L \bar{b}}{1 - \chi_L \left[1 - P_k^{\mathrm{I}} + c^{\mathrm{I}} (P_k^{\mathrm{D}} - 1)\right]}, \tag{7.13}$$

where it is recalled that the P_k^{D} are functions of the principal stretches $\bar{\lambda}_i$. Thus,

expression (7.13) provides the average magnetization in the MRE resulting from the application of a $\mathbf{b}$ field in the k-direction, as a function of $\bar{b}$ and the $\bar{\lambda}_i$, for a given volume fraction of the particles and particle and distribution shapes.

A corresponding expression can be also obtained from expression (7.10) for the principal components $\bar{T}_i$ of the average stress, as functions of $\bar{b}$ and the $\bar{\lambda}_i$. However, as we have already seen in the context of expression (2.38), the actual tractions $\bar{t}_i$ that would need to be applied on the boundaries of a representative volume element of the MRE would be different from the principal stresses $\bar{T}_i$, and would depend on the boundary normals. Assuming that the boundaries of the specimen are perpendicular to the symmetry directions, such that $\mathbf{n}_i = \hat{\mathbf{e}}_i$, expression (2.38) gives the following results in each of the 3 symmetry directions

$$\bar{t}_i = \bar{T}_i - \frac{\bar{b}^2}{2\mu_0} \text{ for } i = k, \quad \text{and} \quad \bar{t}_i = \bar{T}_i + \frac{\mu_0 \bar{h}^2}{2} \text{ for } i \neq k, \tag{7.14}$$

where it is recalled that k is a fixed number denoting the magnetic field direction, and that $\bar{h}$ is defined by $\bar{\mathbf{h}} = \bar{h}\hat{\mathbf{e}}_k$. Then, making use of equation (7.10) for the total stress components, the following magnetoelastic traction-stretch relations are obtained

$$\bar{t}_i = \bar{T}_i^{\text{me}}(\bar{\lambda}_i) - \frac{\mu_0}{2}\bar{m}^2\delta_{ik} - \frac{\mu_0}{2}\bar{J}\bar{m}^2\frac{\partial P_k^{\text{D}}}{\partial \bar{\lambda}_i}\bar{\lambda}_i \qquad \text{no sum, i=1...3,} \tag{7.15}$$

where $\bar{T}_i^{\text{me}}$ is the principal component of the purely mechanical stress tensor (7.11), and δ_{ij} is the Kronecker delta (meaning that the second term only contributes when i is in the direction of the applied field k).

It is evident from expression (7.15) that the traction depends on the magnetic field only through the magnetization (i.e., $\bar{m}^2$), even though the total stress, as given by (7.10), includes terms that are proportional to $\bar{b}^2$ and $\bar{b}\,\bar{m}$. This means that while the total stress continues to rise in the MRE as the magnetic field is increased, the traction will necessarily saturate with magnetization, which is consistent with experimental observation for actual MREs (Bednarek, 1999; Ginder et al., 2002; Guan et al., 2008). In addition, noting that the average magnetization is linear in the particle concentration to leading order, it is easily deduced that the magnetic part of the traction, again to leading order, is of second order in the concentration, even though the total Cauchy stress includes terms that are of first order in the concentration. This result means that the first-order contributions to the total stress must cancel exactly with

the magnetic stresses that are set up by the MRE just outside the specimen. This result is physically consistent, since at low concentrations, each particle behaves like an isolated particle in a uniform magnetic field and experiences no net magnetic force and therefore does not contribute to the traction. This result is also consistent with experimental results, as we shall see below.

7.1.1 Specialization to small-strain results

The traction-stretch relations (7.15) are valid for large strains, and arbitrary magnetic fields. In this work, however, we are interested in the limit of small strains (but still arbitrary magnetic fields), when the general expressions (7.13) and (7.15) for the average magnetization and traction, as functions of the stretch and magnetic field, simplify. The infinitesimal strain tensor $\bar{\boldsymbol{\epsilon}}$ is aligned with the stretch tensor $\bar{\boldsymbol{U}}$, as given by (7.3), so that

$$\bar{\boldsymbol{\epsilon}} = \sum_{i=1}^{3} \bar{\epsilon}_i \hat{\mathbf{e}}_i \otimes \hat{\mathbf{e}}_i, \tag{7.16}$$

where $\bar{\epsilon}_i = \bar{\lambda}_i - 1$ and $|\bar{\epsilon}_i| \ll 1$. It then follows that the magnetization can be expanded for small strains, and equation (7.13) can be written as

$$\bar{m} = \bar{m}^{(0)}(\bar{b}) + \sum_{i=1}^{3} \bar{m}_i^{(1)}(\bar{b})\bar{\epsilon}_i + o(\bar{\epsilon}^2), \tag{7.17}$$

where

$$\bar{m}^{(0)}(\bar{b}) = \bar{m}\Big|_{\bar{\lambda}_1=\bar{\lambda}_2=\bar{\lambda}_3=1} \quad \text{and} \quad \bar{m}_i^{(1)}(\bar{b}) = \frac{\partial \bar{m}}{\partial \bar{\lambda}_i}\Big|_{\bar{\lambda}_1=\bar{\lambda}_2=\bar{\lambda}_3=1}. \tag{7.18}$$

In these expressions, and in the expressions to follow, the vertical bars mean with their arguments (in this case, $\bar{\lambda}_1, \bar{\lambda}_2, \bar{\lambda}_3$) held fixed (equal to 1).

The tractions can also be expanded for small strains, and under the aligned loading assumption, they reduce to expressions of the form

$$\bar{t}_i = \bar{t}_i^{(0)}(\bar{b}) + \sum_{j=1}^{3} \tilde{C}_{ij}^{\text{tot}}(\bar{b})\bar{\epsilon}_j + o(\bar{\epsilon}^2), \tag{7.19}$$

where $\bar{t}_i^{(0)}$ denote the tractions at zero strain, also called the actuation stresses, and

are functions of $\bar{b}$. They are given by

$$\bar{t}_i^{(0)} = -\frac{\mu_0}{2}\left(\bar{m}^{(0)}(\bar{b})\right)^2\left[\delta_{ik} + \left.\frac{\partial P_k^{\mathrm{D}}}{\partial \bar{\lambda}_i}\right|_{\bar{\lambda}_1=\bar{\lambda}_2=\bar{\lambda}_3=1}\right]. \tag{7.20}$$

On the other hand, $\tilde{C}_{ij}^{\mathrm{tot}}(\bar{b})$ is a matrix representing the effective total modulus of the composite. It should be noted that the elements of $\tilde{C}_{ij}^{\mathrm{tot}}$ are not the components of any general fourth-order elasticity tensor, but simply relate the axial tractions to the axial strains in this test. It should also be noted that $\tilde{C}_{ij}^{\mathrm{tot}}(\bar{b})$ can be broken into a purely mechanical and a magnetic contribution, according to

$$\tilde{C}_{ij}^{\mathrm{tot}}(\bar{b}) = \tilde{C}_{ij}^{\mathrm{me}} + \tilde{C}_{ij}^{\mathrm{mag}}(\bar{b}). \tag{7.21}$$

The magnetic contribution of the modulus is given by

$$\begin{aligned}\tilde{C}_{ij}^{\mathrm{mag}} = \frac{\mu_0\left(\bar{m}^{(0)}(\bar{b})\right)^2}{2}&\left[-\left.\frac{\partial P_k^{\mathrm{D}}}{\partial \bar{\lambda}_i \partial \bar{\lambda}_j}\right|_{\bar{\lambda}_1=\bar{\lambda}_2=\bar{\lambda}_3=1} - (1+\delta_{ij})\left.\frac{\partial P_k^{\mathrm{D}}}{\partial \bar{\lambda}_i}\right|_{\bar{\lambda}_1=\bar{\lambda}_2=\bar{\lambda}_3=1}\right] \\ &+ \mu_0\left(\bar{m}^{(0)}(\bar{b})\right)\left(\bar{m}_j^{(1)}(\bar{b})\right)\left[-\delta_{ik} - \left.\frac{\partial P_k^{\mathrm{D}}}{\partial \bar{\lambda}_i}\right|_{\bar{\lambda}_1=\bar{\lambda}_2=\bar{\lambda}_3=1}\right] \qquad \text{(no sum)},\end{aligned} \tag{7.22}$$

while the purely mechanical component is extracted from the elasticity modulus $\tilde{\mathbb{C}}^{\mathrm{me}}$ of the MRE relating the mechanical stress $\bar{\boldsymbol{T}}^{\mathrm{me}}$ to the strain $\bar{\boldsymbol{\epsilon}}$ via

$$\bar{\boldsymbol{T}}^{\mathrm{me}} = \tilde{\mathbb{C}}^{\mathrm{me}}\bar{\boldsymbol{\epsilon}}. \tag{7.23}$$

For rigid inclusions, the effective modulus of the composite can be given in terms of the matrix modulus $\mathbb{C}^{\mathrm{mat}}$, as

$$\tilde{\mathbb{C}}^{\mathrm{me}} = \mathbb{C}^{\mathrm{mat}} + c^{\mathrm{I}}\left(\mathbb{P}^{\mathrm{I}} - c^{\mathrm{I}}\mathbb{P}^{\mathrm{D}}\right)^{-1} \tag{7.24}$$

where $\mathbb{P}^{\mathrm{I}}$ and $\mathbb{P}^{\mathrm{D}}$, are microstructural tensors, respectively describing the particle and distribution shapes (Ponte Castañeda and Willis, 1995). Note that $\tilde{C}_{ij}^{\mathrm{me}} = \tilde{\mathbb{C}}_{iijj}^{\mathrm{me}}$ (no sum) for aligned loadings.

7.1.2 Spheroidal microstructure with incompressible matrix

The previous results apply for general ellipsoidal shapes for the particles and the distribution. However, in this section, we specialize these general results for the case where both the particles and the distribution exhibit a spheroidal shape with the same symmetry axes. Then, the MRE becomes transversely isotropic with the symmetry axis given by the axis of revolution of the particles, which we identify with $\hat{\mathbf{e}}_1$. In addition, we have that $w_2^{\mathrm{I}} = w_3^{\mathrm{I}} = w_2^{\mathrm{D}} = w_3^{\mathrm{D}} = 1$ with $w^{\mathrm{D}} = w_1^{\mathrm{D}}$ and $w^{\mathrm{I}} = w_1^{\mathrm{I}}$, and we can obtain explicit analytical expressions for the relevant microstructural tensors, and the corresponding expressions for the effective properties simplify considerably. Thus, the zero-strain average magnetization associated with the magnetic load (7.2) is obtained from expression (7.13), and given by

$$\bar{m}^{(0)}(\bar{b}) = \frac{c^{\mathrm{I}}\chi_L \bar{b}}{1 - \chi_L \left(1 - P_k(w^{\mathrm{I}}) + c^{\mathrm{I}} \left[P_k(w^{\mathrm{D}}) - 1\right]\right)} \tag{7.25}$$

where

$$P_1(w) = \begin{cases} \frac{1}{1-w^2} - \frac{w \arccos(w)}{(1-w^2)^{3/2}} & w < 1 \\ 1/3 & w = 1\,, \\ \frac{1}{1-w^2} + \frac{w \operatorname{arccosh}(w)}{(-1+w^2)} & w > 1 \end{cases} \tag{7.26}$$

and

$$P_2(w) = P_3(w) = \begin{cases} \frac{w^2}{2(-1+w^2)} + \frac{w \arccos(w)}{2(1-w^2)^{3/2}} & w < 1 \\ 1/3 & w = 1\,. \\ \frac{w^2}{2(-1+w^2)} - \frac{w \operatorname{arccosh}(w)}{2(-1+w^2)^{3/2}} & w > 1 \end{cases} \tag{7.27}$$

Note that $w^{\mathrm{D}} \neq w^{\mathrm{I}}$, in general.

The corresponding expression for the linear comparison susceptibility χ_L, obtained from (7.8) specialized to the Langevin model, is given by

$$\begin{aligned} \frac{\bar{b}}{\mu_0 m_{\mathrm{s}}} \frac{\chi_L}{1 - \chi_L \left[1 - P_k^{\mathrm{I}} + c^{\mathrm{I}}(P_k^{\mathrm{D}} - 1)\right]} = & \\ \coth\left(\frac{\bar{b}}{\mu_0 m_{\mathrm{s}}} \frac{3\chi}{\left(1 - \chi_L \left[1 - P_k^{\mathrm{I}} + c^{\mathrm{I}}(P_k^{\mathrm{D}} - 1)\right]\right)}\right) & \\ - \frac{\mu_0 m_{\mathrm{s}}}{\bar{b}} \frac{\left(1 - \chi_L \left[1 - P_k^{\mathrm{I}} + c^{\mathrm{I}}(P_k^{\mathrm{D}} - 1)\right]\right)}{3\chi}. & \end{aligned} \tag{7.28}$$

Explicit expressions for $\bar{t}_i^{(0)}$ can also be obtained for spheroidal microstructures from equation (7.20), together with the expressions in Appendix C for the derivatives of the $\boldsymbol{P}^{\mathrm{D}}$ with respect to $\boldsymbol{U}$. On the other hand, the expressions for $\bar{m}_i^{(1)}(\bar{b})$ and $\tilde{C}_{ij}^{\mathrm{mag}}$ are more complicated and will not be given explicitly here. However, we will provide special forms for these quantities further below in the important limits of small and large magnetic fields.

In applications, it is important to consider incompressible matrix materials, leading to an indeterminate hydrostatic pressure p in the traction-strain relation (7.19) for the composite, such that

$$\bar{t}_i = -p + \bar{t}_i^{(0)} + \sum_{j=1}^{3} \tilde{C}_{ij}^{\mathrm{tot}} \bar{\epsilon}_j \tag{7.29}$$

where the constraint that $\bar{\epsilon}_1 + \bar{\epsilon}_2 + \bar{\epsilon}_3 = 0$ must be enforced. In this case, the expressions for the elasticity moduli of the transversely isotropic composite simplify (Ponte Castañeda and Willis, 1995), and the components of $\tilde{\mathbb{C}}^{\mathrm{me}}$ can be expressed in terms of three different shear moduli, $\tilde{G}_{\mathrm{p}}$, $\tilde{G}_{\mathrm{n}}$ and $\tilde{G}_{\mathrm{a}}$, corresponding to shear transverse to the fiber axis, longitudinal shear in the direction of the fiber axis and axisymmetric shear, respectively. They are given in terms of the shear modulus of the matrix G as

$$\frac{\tilde{G}_{\mathrm{p}}(w^{\mathrm{I}}, w^{\mathrm{D}})}{G} = 1 + c^{\mathrm{I}} 4 \left[\frac{3h(w^{\mathrm{I}}) - 2(w^{\mathrm{I}})^2}{(1-(w^{\mathrm{I}})^2)} - c^{\mathrm{I}} \frac{3h(w^{\mathrm{D}}) - 2(w^{\mathrm{D}})^2}{(1-(w^{\mathrm{D}})^2)} \right]^{-1}, \tag{7.30}$$

$$\frac{\tilde{G}_{\mathrm{n}}(w^{\mathrm{I}}, w^{\mathrm{D}})}{G} = 1 + c^{\mathrm{I}} 2 \left[\frac{\left[(1+(w^{\mathrm{I}})^2)(2-3h(w^{\mathrm{I}}))\right]}{(1-(w^{\mathrm{I}})^2)} - c^{\mathrm{I}} \frac{\left[(1+(w^{\mathrm{D}})^2)(2-3h(w^{\mathrm{D}}))\right]}{(1-(w^{\mathrm{D}})^2)} \right]^{-1}, \tag{7.31}$$

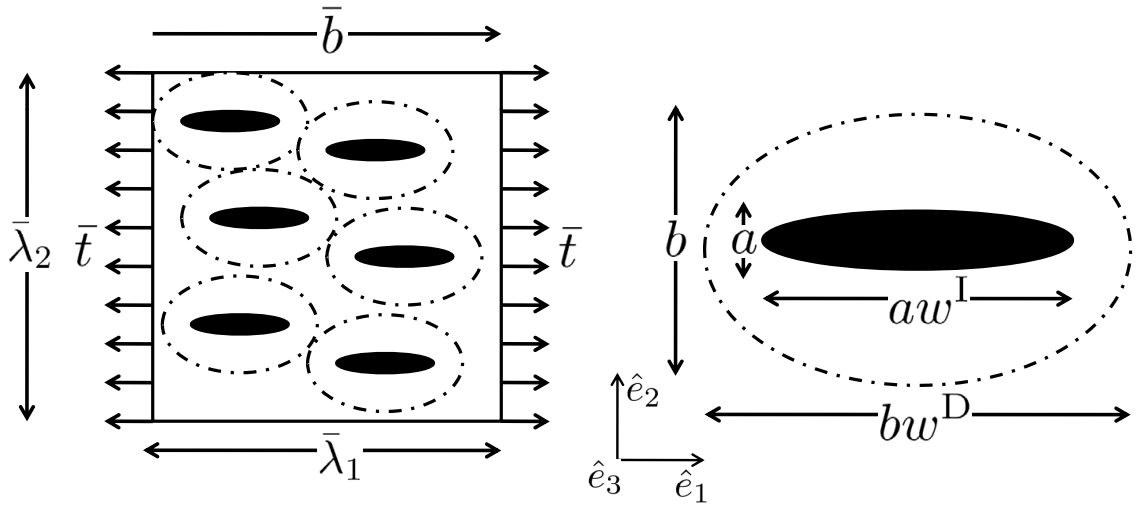

Figure 7.2: Relevant loading conditions and material variables for composites with axial symmetry. The composite consists of spheroidal particles with aspect ratio w^{I} and distributional spheroid with aspect ratio w^{D}. The magnetic field and stretch are aligned with the particle aspect ratio and the normal traction on the surface.

$$\frac{\tilde{G}_{\mathrm{a}}(w^{\mathrm{I}},w^{\mathrm{D}})}{G} = 1 + c^{\mathrm{I}}\frac{2}{3}\left[\frac{\left[h(w^{\mathrm{I}}) - 2(w^{\mathrm{I}})^2 + 2(w^{\mathrm{I}})^2 h(w^{\mathrm{I}})\right]}{(1-(w^{\mathrm{I}})^2)} - c^{\mathrm{I}}\frac{\left[h(w^{\mathrm{D}}) - 2(w^{\mathrm{D}})^2 + 2(w^{\mathrm{D}})^2 h(w^{\mathrm{D}})\right]}{(1-(w^{\mathrm{D}})^2)}\right]^{-1}, \quad (7.32)$$

with

$$h(w) = \begin{cases} \frac{w\left[\arccos(w) - w\sqrt{1-w^2}\right]}{(1-w^2)^{3/2}} & w < 1 \\ 2/3 & w = 1 \\ \frac{w\left[w\sqrt{w^2-1} - \operatorname{arccosh}(w)\right]}{(w^2-1)^{3/2}} & w > 1 \end{cases}. \quad (7.33)$$

In any case, under the aligned loading conditions assumed here, only the transverse and axisymmetric shear moduli are relevant, and they can be related to the components of $\tilde{C}^{\mathrm{me}}_{ij}$ via

$$\begin{bmatrix} \tilde{C}^{\mathrm{me}}_{11} & \tilde{C}^{\mathrm{me}}_{12} & \tilde{C}^{\mathrm{me}}_{13} \\ \tilde{C}^{\mathrm{me}}_{21} & \tilde{C}^{\mathrm{me}}_{22} & \tilde{C}^{\mathrm{me}}_{23} \\ \tilde{C}^{\mathrm{me}}_{31} & \tilde{C}^{\mathrm{me}}_{32} & \tilde{C}^{\mathrm{me}}_{33} \end{bmatrix} = \begin{bmatrix} \frac{4}{3}\tilde{G}_{\mathrm{a}} & -\frac{2}{3}\tilde{G}_{\mathrm{a}} & -\frac{2}{3}\tilde{G}_{\mathrm{a}} \\ -\frac{2}{3}\tilde{G}_{\mathrm{a}} & \frac{1}{3}\tilde{G}_{\mathrm{a}} + \tilde{G}_{\mathrm{p}} & \frac{1}{3}\tilde{G}_{\mathrm{a}} - \tilde{G}_{\mathrm{p}} \\ -\frac{2}{3}\tilde{G}_{\mathrm{a}} & \frac{1}{3}\tilde{G}_{\mathrm{a}} - \tilde{G}_{\mathrm{p}} & \frac{1}{3}\tilde{G}_{\mathrm{a}} + \tilde{G}_{\mathrm{p}} \end{bmatrix}. \quad (7.34)$$

The theory developed in the previous section for spheroidal inclusions and dis-

tributions is valid for $w^{\mathrm{D}} \neq w^{\mathrm{I}}$; however, in this section, for simplicity, it will be assumed that $w = w^{\mathrm{D}} = w^{\mathrm{I}}$. In addition, we let $\hat{\mathbf{e}}_1$ be the axis of symmetry for the inclusion and distributional spheroids, and assume that the magnetic field is aligned with this symmetry direction such that $\bar{\mathbf{b}} = \bar{b}\hat{\mathbf{e}}_1$. Similarly, we consider axial traction such that $\bar{t}_1 = \bar{t}$ with $\bar{t}_2 = \bar{t}_3 = 0$ consistent with Figure 7.2. Under these conditions, the isotropic symmetry in the transverse plane defined by $\hat{\mathbf{e}}_2$ and $\hat{\mathbf{e}}_3$, together with the incompressibility constraint imply that the system can be described by a single strain parameter $\bar{\epsilon} = \bar{\epsilon}_1 = -2\bar{\epsilon}_2 = -2\bar{\epsilon}_3$.

7.1.3 Magnetization response

In terms of $\bar{\epsilon}$, the magnetization can then be written as

$$\bar{m} = \bar{m}^{(0)}(\bar{b}) + \left[\bar{m}_1^{(1)}(\bar{b}) - \frac{\bar{m}_2^{(1)}}{2}(\bar{b}) - \frac{\bar{m}_3^{(1)}}{2}(\bar{b})\right]\bar{\epsilon} = \bar{m}^{(0)}(\bar{b}) + \bar{m}^{(1)}(\bar{b})\bar{\epsilon}. \tag{7.35}$$

Because of the nonlinear magnetic behavior, the expressions for $\bar{m}^{(0)}$ and $\bar{m}^{(1)}$, as functions of $\bar{b}$, are complicated. However, simple expressions can be obtained by considering the limits of small and large $\bar{b}$, respectively, corresponding to linear and saturation magnetization responses.

Small $\bar{b}$ limit

For the case of small $\bar{b}$, the magnetization is proportional to the magnetic flux so that

$$\mu_0\bar{m} = \tilde{\chi}_{\mathrm{i}}\bar{b} \tag{7.36}$$

where $\tilde{\chi}_{\mathrm{i}}$ represents the initial susceptibility of the composite, which depends on the strain, but not on $\bar{b}$. It can thus be written as

$$\tilde{\chi}_{\mathrm{i}} = \left.\frac{\partial\bar{m}}{\partial\bar{b}}\right|_{\bar{b}=0} = \tilde{\chi}_{\mathrm{i}}^{(0)} + \tilde{\chi}_{\mathrm{i}}^{(1)}\bar{\epsilon}, \tag{7.37}$$

where $\tilde{\chi}_{\mathrm{i}}^{(0)}$ is the initial susceptibility of the composite at zero strain given by

$$\tilde{\chi}_{\mathrm{i}}^{(0)} = \mu_0 \frac{\partial \bar{m}^{(0)}}{\partial \bar{b}}\bigg|_{\bar{b}=0} = \begin{cases} -\frac{c^{\mathrm{I}}\chi(1-w^2)^{3/2}}{\sqrt{1-w^2}(w^2[\chi(c^{\mathrm{I}}-1)+1]-1)-w\chi(c^{\mathrm{I}}-1)\arccos(w)} & w<1 \\ \frac{3c^{\mathrm{I}}\chi}{3+2(c^{\mathrm{I}}-1)\chi} & w=1 \\ \frac{c^{\mathrm{I}}\chi(-1+w^2)^{3/2}}{\sqrt{-1+w^2}(w^2[\chi(c^{\mathrm{I}}-1)+1]-1)-w\chi(c^{\mathrm{I}}-1)\operatorname{arccosh}(w)} & w>1 \end{cases} \tag{7.38}$$

and $\tilde{\chi}_{\mathrm{i}}^{(1)}$ is a correction accounting for the strain given by

$$\tilde{\chi}_{\mathrm{i}}^{(1)} = \mu_0 \frac{\partial \bar{m}^{(1)}}{\partial \bar{b}}\bigg|_{\bar{b}=0} = \begin{cases} \frac{3w\left(c^{\mathrm{I}}\right)^2\chi^2\sqrt{1-w^2}\left[3w\sqrt{1-w^2}-\left(1+2w^2\right)\arccos(w)\right]}{2\left[\sqrt{1-w^2}(w^2[\chi(1-c^{\mathrm{I}})-1]+1)+w\chi(c^{\mathrm{I}}-1)\arccos(w)\right]^2} & w<1 \\ \frac{18\left(c^{\mathrm{I}}\right)^2\chi^2}{5[3+2(c^{\mathrm{I}}-1)\chi]^2} & w=1 \\ \frac{3w\left(c^{\mathrm{I}}\right)^2\chi^2\sqrt{-1+w^2}\left[3w\sqrt{-1+w^2}-\left(1+2w^2\right)\operatorname{arccosh}(w)\right]}{2\left[\sqrt{-1+w^2}(w^2[\chi(1-c^{\mathrm{I}})-1]+1)+w\chi(c^{\mathrm{I}}-1)\operatorname{arccosh}(w)\right]^2} & w>1 \end{cases}. \tag{7.39}$$

Large $\bar{b}$ limit

In the limit as $\bar{b} \to \infty$, the composite will reach magnetic saturation with magnetization given by

$$\bar{m}_{\mathrm{s}} = \lim_{\bar{b}\to\infty} \bar{m} = \bar{m}_{\mathrm{s}}^{(0)} + \bar{m}_{\mathrm{s}}^{(1)}\bar{\epsilon}, \tag{7.40}$$

where

$$\bar{m}_{\mathrm{s}}^{(0)} = \lim_{\bar{b}\to\infty} \bar{m}^{(0)} = c^{\mathrm{I}} m_{\mathrm{s}}, \tag{7.41}$$

and

$$\bar{m}_{\mathrm{s}}^{(1)} = \lim_{\bar{b}\to\infty} \bar{m}^{(1)} = 0. \tag{7.42}$$

These expressions can be easily derived by considering the composite saturation at finite strain. In the limit as $\bar{b} \to \infty$, all the particles saturate so the composite magnetization will be the product of the particle saturation magnetization and the current volume fraction. For an incompressible composite the particle concentration is fixed; therefore, $\bar{m}_{\mathrm{s}} = c^{\mathrm{I}} m_{\mathrm{s}}$, independently of the strain. This result is consistent with the recent experimental and theoretical predictions given by Diguet et al. (2010).

7.1.4 Mechanical response

Under uniaxial loading, the composite symmetry and incompressibility allow the reduction of equations (7.29) to the following expression for the uniaxial traction

$$\bar{t} = \bar{t}^{(0)}(\bar{b}) + \tilde{E}^{\mathrm{tot}}(\bar{b})\bar{\epsilon}. \tag{7.43}$$

In this expression, $\bar{t}^{(0)}$ corresponds to the traction at $\bar{\epsilon} = 0$. It is the effective uniaxial actuation stress of the composite, and is given by

$$\bar{t}^{(0)}(\bar{b}) = \mu_0 \left(\bar{m}^{(0)}(\bar{b})\right)^2 D^{(0)}(w), \tag{7.44}$$

where $D^{(0)}(w)$ is a geometric factor defined by

$$\begin{aligned} D^{(0)}(w) &= \left(-1/2 - \frac{1}{2}\frac{\partial P_1^{\mathrm{D}}}{\partial \bar{\lambda}_1} + \frac{1}{2}\frac{\partial P_1^{\mathrm{D}}}{\partial \bar{\lambda}_2}\right)\Bigg|_{\bar{\lambda}_1=\bar{\lambda}_2=\bar{\lambda}_3=1} \\ &= \begin{cases} -\frac{2+5w^2+2w^2}{4(-1+w^2)^2} + \frac{3w(1+2w^2)\arccos\,(w)}{4(1-w^2)^{5/2}} & w < 1 \\ -3/10 & w = 1 \\ -\frac{2+5w^2+2w^2}{4(-1+w^2)^2} + \frac{3w(1+2w^2)\mathrm{arccosh}\,(w)}{4(-1+w^2)^{5/2}} & w > 1 \end{cases}. \end{aligned} \tag{7.45}$$

On the other hand, $\tilde{E}^{\mathrm{tot}}$ is the effective total Young's modulus for the composite, which can be broken up into a purely mechanical part and a part depending on $\bar{b}$, such that

$$\tilde{E}^{\mathrm{tot}}(\bar{b}) = \tilde{E}^{\mathrm{me}} + \tilde{E}^{\mathrm{mag}}(\bar{b}). \tag{7.46}$$

Thus, $\tilde{E}^{\mathrm{me}}$ is the mechanical Young's modulus for the composite in the axial direction, such that $\tilde{E}^{\mathrm{me}} = 3\tilde{G}_{\mathrm{a}}$, where $\tilde{G}_{\mathrm{a}}$ is given by equation (7.33). The magnetic modulus $\tilde{E}^{\mathrm{mag}}$ depends on the applied magnetic field $\bar{b}$ in a complicated fashion; however, as was the case for the magnetization, simpler expressions may be generated by considering the small and large $\bar{b}$ limits.

Small $\bar{b}$ limit

In the limit of small $\bar{b}$, it is found that

$$\bar{t}^{(0)} = \beta_{\mathrm{i}}\bar{b}^2 + O(\bar{b}^4), \tag{7.47}$$

where β_{i} is a material parameter characterizing the initial growth of $\bar{t}^{(0)}$ with $\bar{b}$, such that

$$\beta_{\mathrm{i}} = \frac{1}{2}\frac{\partial^2 \bar{t}^{(0)}}{\partial \bar{b}^2}\bigg|_{\bar{b}=0} = \frac{\left(\tilde{\chi}_{\mathrm{i}}^{(0)}\right)^2 D^{(0)}(w)}{\mu_0}. \tag{7.48}$$

In addition, in the limit of small $\bar{b}$, it is also found that

$$\tilde{E}^{\mathrm{tot}} = \tilde{E}^{\mathrm{me}} + o(\bar{b}^2), \tag{7.49}$$

so that the effective modulus reduces to the purely mechanical modulus in this limit.

Large $\bar{b}$ limit

As previously noted, the applied traction in equation (7.43) depends only on the magnetic fields through the magnetization; therefore in the limit of large $\bar{b}$, the magneto-mechanical effects must also saturate. The saturation value of the traction, $\bar{t}_{\mathrm{s}}$, depends on the strain, and can be written as

$$\bar{t}_{\mathrm{s}} = \lim_{\bar{b}\to\infty} \bar{t} = \bar{t}_{\mathrm{s}}^{(0)} + \tilde{E}_{\mathrm{s}}^{\mathrm{tot}}\bar{\epsilon} \tag{7.50}$$

where $\bar{t}_{\mathrm{s}}^{(0)}$ and $\tilde{E}_{\mathrm{s}}^{\mathrm{tot}}$ are the saturation values of $\bar{t}^{(0)}$ and $\tilde{E}^{\mathrm{tot}}$, respectively. In this limit, it can be shown that

$$\bar{t}_{\mathrm{s}}^{(0)} = \mu_0 m_{\mathrm{s}}^2 \left(c^{\mathrm{I}}\right)^2 D^{(0)}(w), \tag{7.51}$$

while

$$\tilde{E}_{\mathrm{s}}^{\mathrm{tot}} = \tilde{E}^{\mathrm{me}} + \tilde{E}_{\mathrm{s}}^{\mathrm{mag}}, \tag{7.52}$$

with

$$\tilde{E}_{\mathrm{s}}^{\mathrm{mag}} = \mu_0 m_{\mathrm{s}}^2 \left(c^{\mathrm{I}}\right)^2 D^{(1)}(w), \tag{7.53}$$

where

$$D^{(1)}(w) = \left(-\frac{\partial P_1^{\mathrm{D}}}{\partial \bar{\lambda}_1 \partial \bar{\lambda}_1} + 2\frac{\partial P_1^{\mathrm{D}}}{\partial \bar{\lambda}_1 \partial \bar{\lambda}_2} - \frac{1}{2}\frac{\partial P_1^{\mathrm{D}}}{\partial \bar{\lambda}_2 \partial \bar{\lambda}_2} \right.$$
$$\left. -\frac{1}{2}\frac{\partial P_1^{\mathrm{D}}}{\partial \bar{\lambda}_3 \partial \bar{\lambda}_2} - \frac{\partial P_1^{\mathrm{D}}}{\partial \bar{\lambda}_1} - \frac{1}{2}\frac{\partial P_1^{\mathrm{D}}}{\partial \bar{\lambda}_2} \right) \Bigg|_{\bar{\lambda}_1=\bar{\lambda}_2=\bar{\lambda}_3=1}$$
$$= \begin{cases} \frac{-8+251w^2+299w^4-2w^6}{32(-1+w^2)^3} + \frac{3w(7+125w^2+48w^4)\arccos(w)}{32(1-w^2)^{7/2}} & w < 1 \\ -3/35 & w = 1 \\ \frac{-8+251w^2+299w^4-2w^6}{32(-1+w^2)^3} - \frac{3w(7+125w^2+48w^4)\operatorname{arccosh}(w)}{32(-1+w^2)^{7/2}} & w > 1 \end{cases} . \quad (7.54)$$

7.1.5 Magnetostriction

For magnetically susceptible materials, the magnetostrictive strain, $\bar{\epsilon}^{\mathrm{m}}$ is a very important property. It corresponds to the magnetically induced deformation when no mechanical traction is applied. An expression for the magnetostrictive strain is obtained by setting $\bar{t} = 0$ in equation (7.43), and solving for $\bar{\epsilon}$, with the result that

$$\bar{\epsilon}^{\mathrm{m}}(\bar{b}) = \frac{-\bar{t}^{(0)}(\bar{b})}{\tilde{E}^{\mathrm{me}} + \tilde{E}^{\mathrm{mag}}(\bar{b})}. \quad (7.55)$$

However, equation (7.55) must be consistent with the small-strain approximation. The terms $\bar{t}^{(0)}$ and $\tilde{E}^{\mathrm{mag}}$ can be shown to be of the same order of magnitude, and the small-strain requirement implies that $\bar{t}^{(0)}$ and $\tilde{E}^{\mathrm{mag}}$ must be assumed to be small compared to $\tilde{E}^{\mathrm{me}}$. Since $\bar{t}^{(0)}$ saturates to $\bar{t}_{\mathrm{s}}^{(0)}$, the strain will be small for all magnetic fields provided that

$$\left| \frac{-\bar{t}_{\mathrm{s}}^{(0)}}{\tilde{E}^{\mathrm{me}}} \right| = \frac{\mu_0 m_{\mathrm{s}}^2 \left(c^{\mathrm{I}}\right)^2 \left|D^{(0)}(w)\right|}{3\tilde{G}_{\mathrm{a}}} \ll 1. \quad (7.56)$$

This condition is satisfied when the dimensionless parameter

$$\kappa = \frac{\mu_0}{G} m_{\mathrm{s}}^2 \quad (7.57)$$

is small enough. The parameter κ relates the magnetic forces among the particles at saturation to the stiffness of the matrix. Higher values for κ indicate strong magnetic effects relative to the stiffness of the matrix. For known magnetic materials, $\mu_0 m_{\mathrm{s}} \leq 2.44\mathrm{T}$, but κ can still be large if the matrix is soft enough (i.e., G is small), see Table 7.1.

Table 7.1: Typical values of κ for different constituent materials (Kaye and Laby, 2008)

Matrix	G	Inclusions	$\mu_0 m_\mathrm{s}$	κ
Elastomer	0.01 - 10 MPa	High Purity Iron	2.16 Tesla	371 - .370
Elastomer	0.01 - 10 MPa	Cast Iron	1.70 Tesla	230 - .230
Elastomer	0.01 - 10 MPa	Nickel Alloys	0.77 Tesla	47.2 - .0472
Elastomer	0.01 - 10 MPa	Cobalt-Iron Alloy	2.35 Tesla	439 - .439
Silicon Rubber	0.1 Mpa	Steels	2.00 - 2.15 Tesla	31.8 - 36.8

When κ is such that condition (7.56) is satisfied, equation (7.55) reduces to

$$\bar{\epsilon}^\mathrm{m}(\bar{b}) = \frac{-\bar{t}^{(0)}(\bar{b})}{\tilde{E}^\mathrm{me}}. \tag{7.58}$$

More explicit expressions can then be obtained in the limits of small and large $\bar{b}$, as given next.

Small $\bar{b}$ limit

In this limit, $\bar{t}^{(0)}$ is given by expression (7.47), and it follows that

$$\bar{\epsilon}^\mathrm{m}(\bar{b}) = \alpha_\mathrm{i}\bar{b}^2 + o(\bar{b}^4) \tag{7.59}$$

where

$$\alpha_\mathrm{i} = \frac{1}{2}\frac{\partial^2 \bar{\epsilon}^\mathrm{m}}{\partial \bar{b}^2}\bigg|_{\bar{b}=0} = \frac{-\left(\tilde{\chi}_\mathrm{i}^{(0)}\right)^2 D^{(0)}(w)}{3\mu_0 \tilde{G}_\mathrm{a}} \tag{7.60}$$

is a parameter describing $\bar{\epsilon}^\mathrm{m}$ in the linear magnetization regime, where, according to (7.59), $\bar{\epsilon}^\mathrm{m}$ grows quadratically with $\bar{b}$.

Large $\bar{b}$ limit

For large $\bar{b}$, the magnetization saturates and $\bar{\epsilon}^\mathrm{m}$ is given by

$$\bar{\epsilon}_\mathrm{s}^\mathrm{m} = \lim_{\bar{b}\to\infty} \bar{\epsilon}^\mathrm{m} = \frac{-\bar{t}_\mathrm{s}^{(0)}}{3\tilde{G}_\mathrm{a}} = \frac{-\mu_0 m_\mathrm{s}^2 \left(c^\mathrm{I}\right)^2 D^{(0)}(w)}{3\tilde{G}_\mathrm{a}}, \tag{7.61}$$

which is proportional to κ and to the square of the volume fraction c^I (for small c^I).

7.1.6 Actuator energy density

The actuation stress $\bar{t}_{\mathrm{s}}^{(0)}$ and the magnetostriction $\bar{\epsilon}_{\mathrm{s}}^{\mathrm{m}}$ are both important measures of actuator performance. However, in applications, the actuation energy density, describing the potential for energy transfer, is often more important (Pelrine et al., 2000).

At saturation, the actuation energy density for the uniaxial loading conditions of this section can be estimated as

$$\bar{e}_{\mathrm{a}} = \left|\bar{\epsilon}_{\mathrm{s}}^{\mathrm{m}} \bar{t}_{\mathrm{s}}^{(0)}\right| = \frac{\mu_0^2 m_{\mathrm{s}}^4 \left(c^{\mathrm{I}}\right)^4 \left(D^{(0)}(w)\right)^2}{3\tilde{G}_{\mathrm{a}}}, \tag{7.62}$$

which can also be written in terms of the parameter κ as

$$\bar{e}_{\mathrm{a}} = \kappa \mu_0 m_{\mathrm{s}}^2 \frac{G}{3\tilde{G}_{\mathrm{a}}} \left(c^{\mathrm{I}}\right)^4 \left(D^{(0)}(w)\right)^2. \tag{7.63}$$

This means that, for combinations of G and m_{s} resulting in the same κ, the energy density is maximized for the largest value of m_{s}. Also, note that, at saturation, the energy transfer is proportional to the volume fraction c^{I} to the fourth power (for small c^{I}).

7.2 Discussion of the results for uniaxial loading

Figure 7.3 shows the magnetization curves for the composite when $\bar{\epsilon} = 0$, as determined by the nonlinear variational estimate (equations (7.25) - (7.28)). The plots are normalized by the magnetic saturation m_{s}. The initial slope of these curves is $\tilde{\chi}_{\mathrm{i}}^{(0)}$ and the value as $\bar{b} \to \infty$ is the magnetic saturation $\bar{m}_s$. Figure 7.3a shows how the saturation magnetization and the initial susceptibility increase with the inclusion concentration. In agreement with expression (7.41), the results show that the saturation magnetization scales linearly with the concentration, while the initial susceptibility has a more complicated dependence on concentration. On the other hand, Figure 7.3b shows that the initial susceptibility of the composite has a marked dependence on particle shape, while the saturation magnetization is independent of particle shape. Figures 7.3c and 7.3d depict the effect of particle initial susceptibility χ on the properties of the composite. Examining both plots we can see that changing the

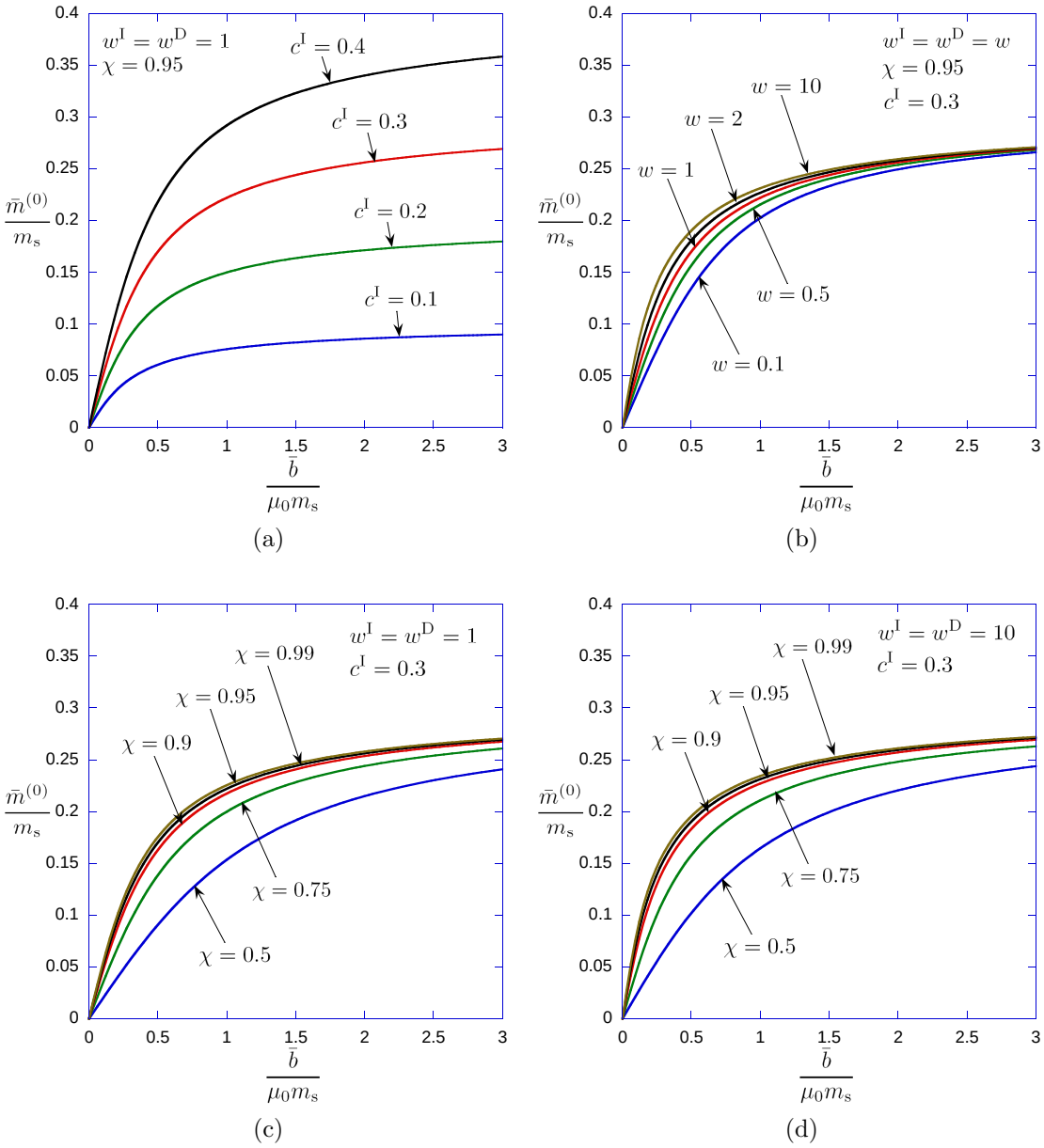

Figure 7.3: The magnetization in the unstrained composite $\bar{m}^{(0)}(\bar{b})$ as a function of magnetic flux $\bar{b}$ for various microstructures. (a) The magnetization curves for various concentrations c^{I} with spherical aspect ratio $w = 1$. (b) The curves for a fixed concentration c^{I} and a variety of aspect ratios w. (c) The magnetization curves for spherical aspect ratios $w = 1$ for different particle susceptibilities χ. (d) The magnetization curves for elongated aspect ratios $w = 10$ for different particle susceptibilities χ.

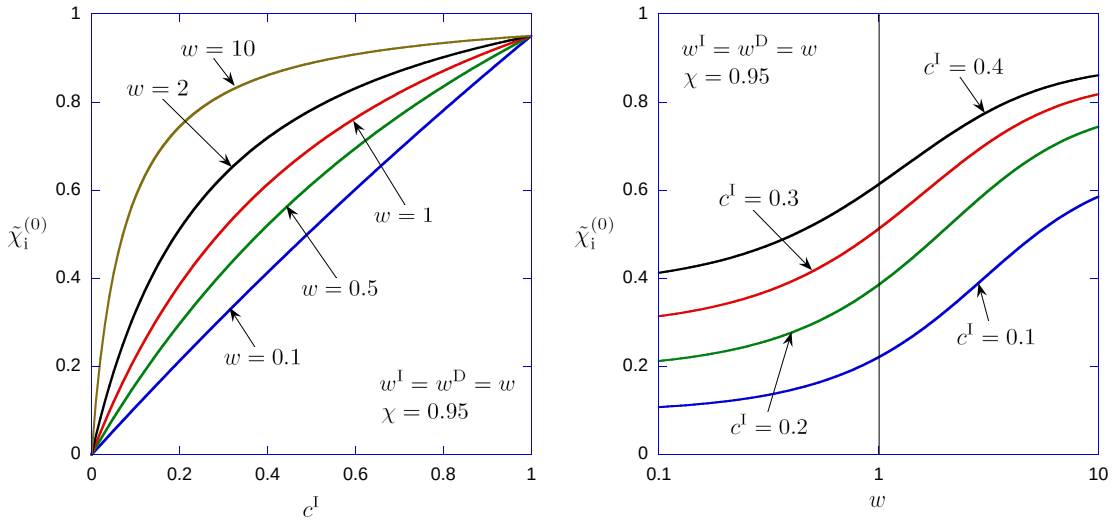

(a) (b)

Figure 7.4: The initial susceptibility of the unstrained composite $\tilde{\chi}_{\mathrm{i}}^{(0)}$ for different microstructures. The particle initial susceptibility is $\chi = 0.95$. (a) $\tilde{\chi}_{\mathrm{i}}^{(0)}$ as a function of concentration c^{I}. (b) $\tilde{\chi}_{\mathrm{i}}^{(0)}$ as a function of aspect ratio w.

initial susceptibility of the particles affects the initial susceptibility of the composite, but not the corresponding saturation values.

Figure 7.4 shows more detailed plots of the effect of microstructure on the zero-strain initial susceptibility of the composite $\tilde{\chi}_{\mathrm{i}}^{(0)}$. Elongated initial shapes ($w > 1$) lead to larger initial susceptibilities for the composite. This makes sense because elongated, isolated particles (with $w > 1$) magnetize more easily than disk shaped particles (with $w < 1$). The composite susceptibility also depends on the particle susceptibility, but the focus here is on values of χ close to 1, where the change in χ has a relatively small effect on the behavior of the composite. The effect of the strain $\bar{\epsilon}$ on the initial susceptibility $\tilde{\chi}_{\mathrm{i}}$ may be obtained via expression (7.37), but is relatively small and will not be shown here. Also, as already mentioned, the strain $\bar{\epsilon}$ has no effect on the saturation magnetization of the composite.

Figure 7.5 shows the initial susceptibility $\tilde{\chi}_{\mathrm{i}}$ as a function of strain $\bar{\epsilon}$ via expression (7.37). The resulting effect is quite small and only becomes noticeable for higher values of the concentration, where the effects of particle interactions are more significant. The deformation affects the susceptibility of the composite through the particle

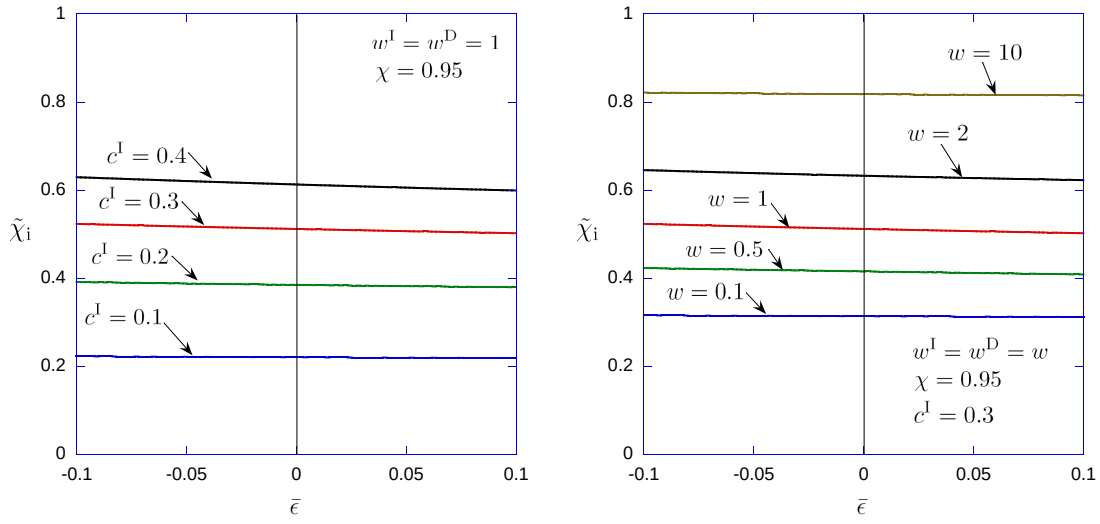

(a) (b)

Figure 7.5: The initial susceptibility of the composite $\tilde{\chi}_{\mathrm{i}}$ as a function of the strain $\bar{\epsilon}$ for various microstructures. The particle susceptibility is $\chi = 0.95$. (a) Spherical microstructure $w = 1$ at different concentrations c^{I}. (b) Different aspect ratios w at fixed concentration $c^{\mathrm{I}} = 0.3$.

distribution, and the effect is largest for the spherical distributions even though the total change is negligible as shown in Figure 7.5a. Considering also that the saturation magnetization does not depend on strain, we can conclude that the deformation has a minimal effect on the magnetization behavior of the composite. Overall the effects are of order strain so the effects are necessarily small, even for compressible composites.

Figure 7.6 depicts the effects of the magnetic field on the traction-strain curve. The traction is non-dimensionalized by the shear modulus of the matrix phase. Figure 7.6a shows the magnetic field has the effect of shifting the curve downwards; essentially, this means that a compressive traction would be necessary to prevent the sample from elongating. The value of this traction is specified by the vertical intercept of the curves and is the actuation stress $\bar{t}^{(0)}$. The corresponding horizontal displacement defines the magnetostrictive strain, $\bar{\epsilon}^{\mathrm{m}}$. As the magnetic field increases, the plots approach the saturation traction-strain curve whose vertical and horizontal intercepts are $\bar{t}_{\mathrm{s}}^{(0)}$ and $\bar{\epsilon}_{\mathrm{s}}^{\mathrm{m}}$ respectively. These plots were obtained neglecting the contribution of $\tilde{E}^{\mathrm{mag}}(\bar{b})$ because the effect of $\tilde{E}^{\mathrm{mag}}(\bar{b})$ is small, as we will show. Figure 7.6b shows the effect of

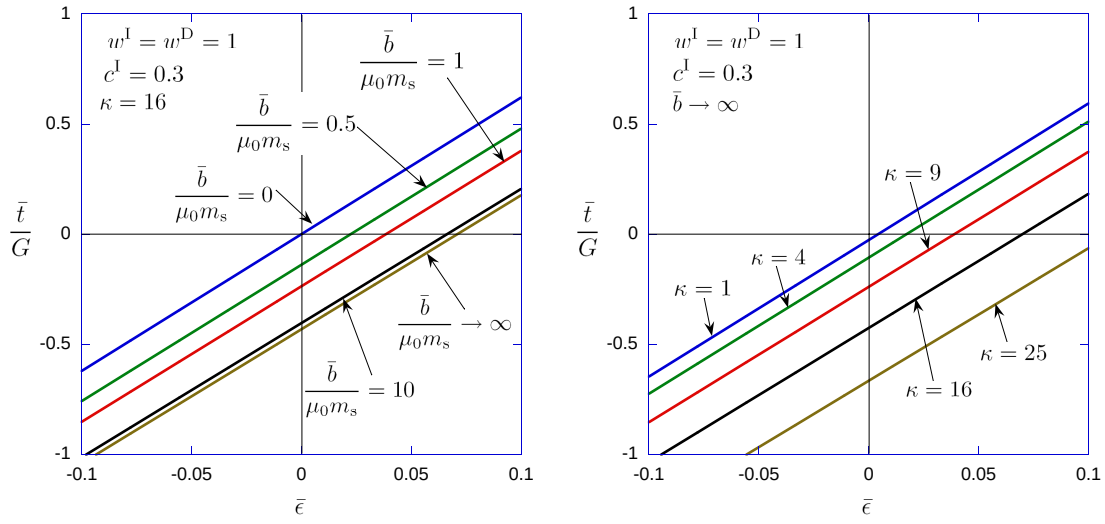

Figure 7.6: The traction $\bar{t}$ as a function of the strain $\bar{\epsilon}$ for different magnetic loadings and material parameters. (a) The traction-strain curves for different magnetic flux $\bar{b}$. (b) The saturation traction-strain curves for different values of κ.

increasing κ on the saturation traction-strain curves. As expected for larger κ, there is a more pronounced effect of the magnetic field indicating that the magnetic effects are stronger compared to the mechanical effects.

Figure 7.7 shows the traction as a function of the strain for $\kappa = 16$. The plots are for $\bar{b} = 0$ and $\bar{b} \to \infty$. The different slopes in Figures 7.7a and 7.7c illustrate the mechanical reinforcement effect of the particles on the composite. They depend on the particle shape and concentration. Figures 7.7b and 7.7d show the corresponding plots when a magnetic field is applied. The slope of the curve remains the same but there is a shift downwards. The vertical shift increases monotonically with concentration, but shows a more complex dependence on the particle aspect ratio. There is a very small change in the slope of the curves due to the magnetic field, which is not visible here, but will be discussed next when we look at the modulus curves.

Figure 7.8 depicts the magnetoelastic moduli of the composite at high magnetic field normalized by the shear modulus of the matrix. The total modulus $\tilde{E}_{\mathrm{s}}^{\mathrm{tot}}$ depends on the magnetic field, but $\tilde{E}_{\mathrm{s}}^{\mathrm{mag}}$ is small relative to the mechanical contribution even though the magnetic field is large enough to bring all the particles to saturation. Thus, the primary effects seen in Figures 7.8a and 7.8c are the role of aspect ratio

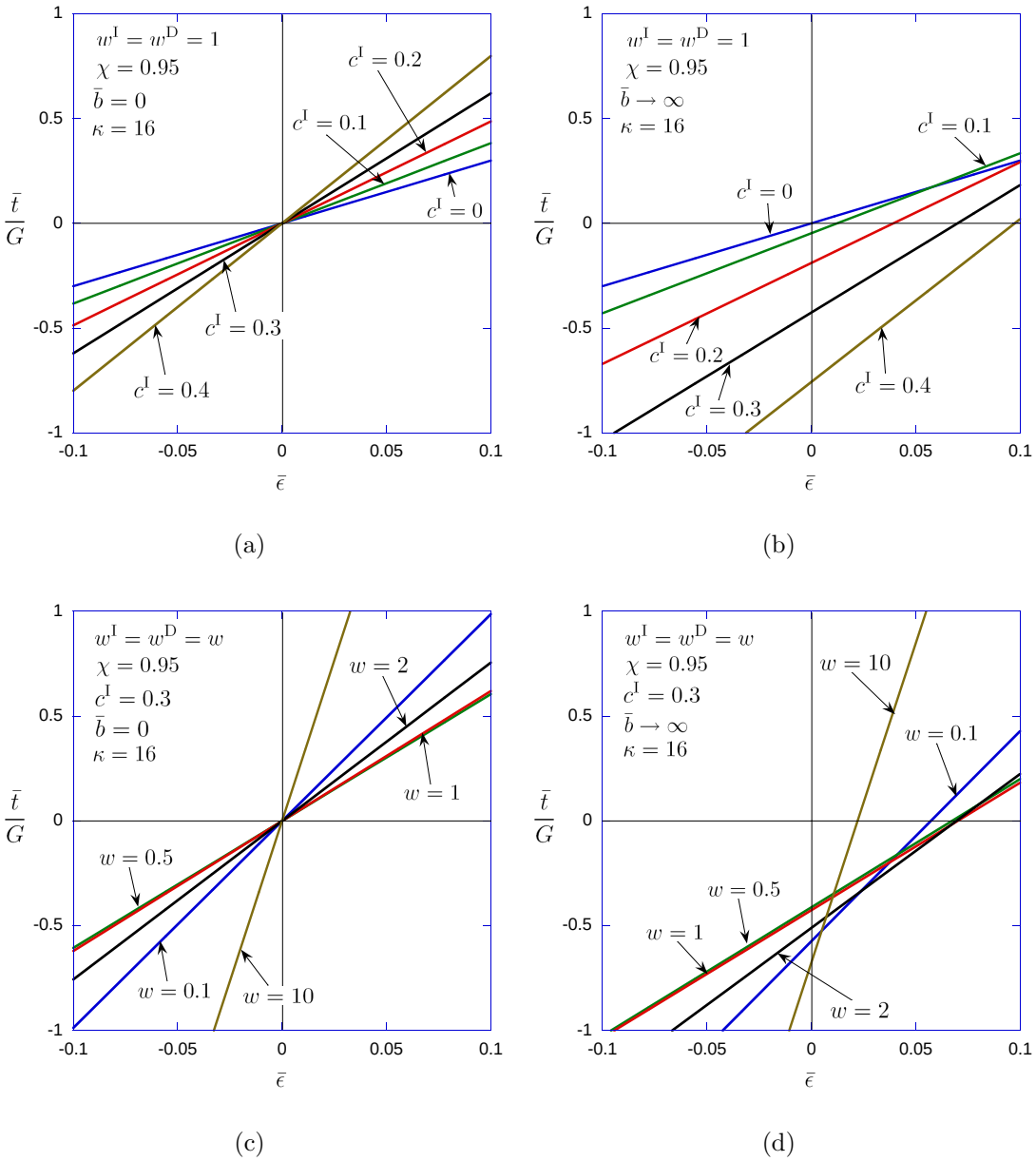

Figure 7.7: The traction $\bar{t}$ vs strain $\bar{\epsilon}$ with no magnetic field and with high magnetic field $\bar{b} \to \infty$. (a) The traction-strain curves for spherical aspect ratio $w = 1$ at different concentrations c^{I} when the magnetic field is off. (b) Corresponding plots when the magnetic field is large enough to saturate the composite. (c) The traction-strain curves for $c^{\mathrm{I}} = 0.3$ and different aspect ratios w when the magnetic field is off. (d) Corresponding plots when the magnetic field is large enough to saturate the composite.

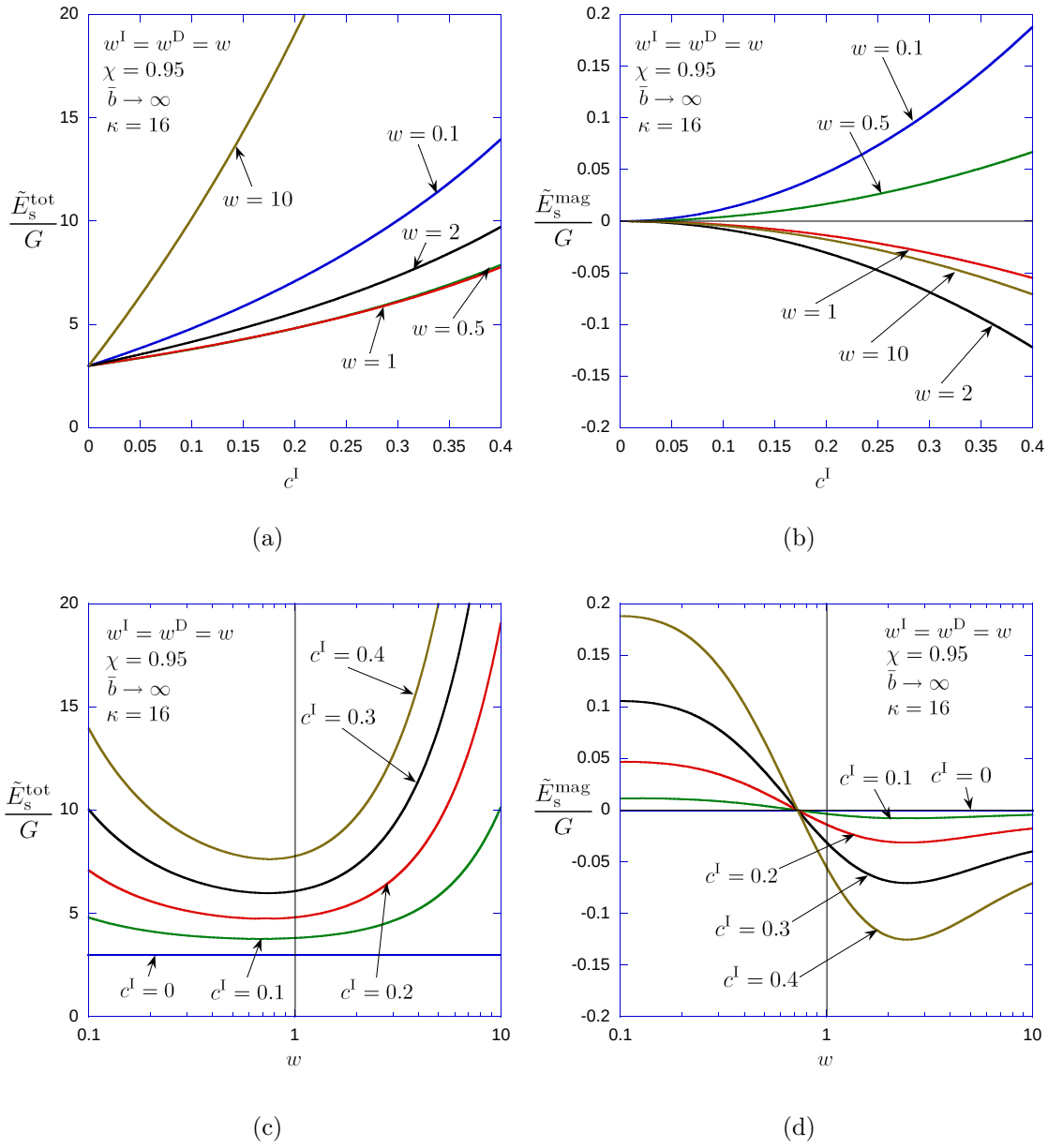

Figure 7.8: The total magnetoelastic Young's modulus $\tilde{E}_{\mathrm{s}}^{\mathrm{tot}}$ and the magnetic contribution to the modulus $\tilde{E}^{\mathrm{mag}}$ when the field is large enough to bring all the particles to saturation. (a) The total Young's modulus of the composite as a function of concentration c^{I}. (b) The corresponding magnetic part of the Young's modulus. (c) The total Young's modulus of the composite as a function of aspect ratio w. (d) The corresponding magnetic part of the Young's modulus.

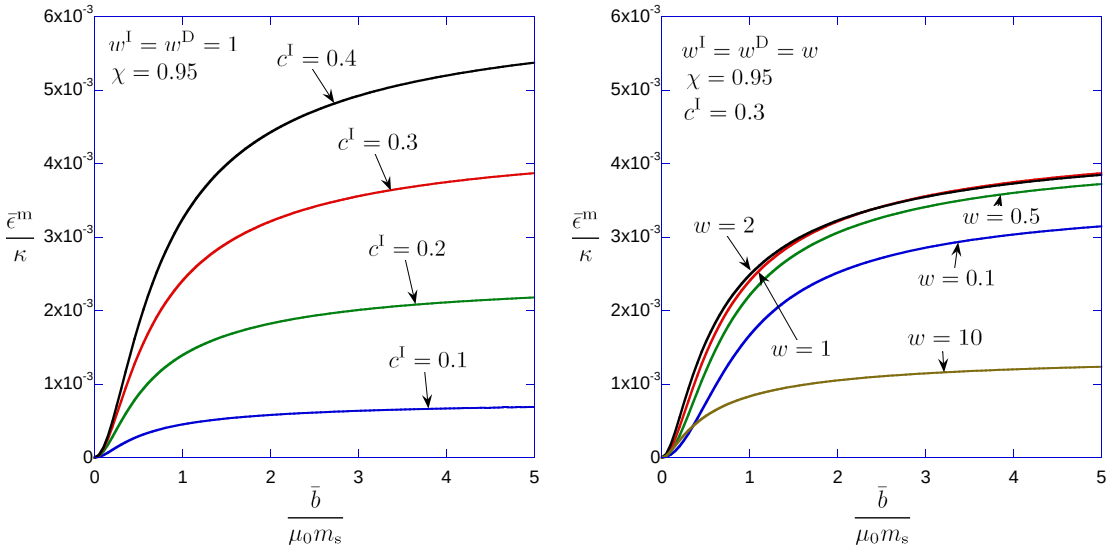

Figure 7.9: The magnetostriction $\bar{\epsilon}^{\mathrm{m}}$ as a function of the applied magnetic field $\bar{b}$ for different microstructures. (a) The magnetostriction for different concentrations c^{I} with spherical aspect ratio $w = 1$. (b) The magnetostriction for different aspect ratios w and concentration $c^{\mathrm{I}} = 0.3$.

w and concentration c^{I} on the purely mechanical reinforcement of the composite. It is interesting that even though the magnetic modulus is small, it can be negative or positive depending on particle aspect ratio, as shown in Figures 7.8b and 7.8d. This magnetic modulus is due to the magnetic forces on particles changing relative positions with the deformation. These particle forces depend in a complicated way on the microstructure; subsequently, the modulus depends on how the microstructure changes with the deformation. In principle we could also consider fixed $\mathbf{m}$, fixed $\mathbf{h}$, and fixed $\mathbf{b}$ moduli which would be different for magnetic fields below saturation; however since the magnetic field would be smaller the overall effect would also be minimal.

Figure 7.9 shows the magnetostriction $\bar{\epsilon}^{\mathrm{m}}$ as a function of $\bar{b}$ for different aspect ratios w and concentrations c^{I}. The magnetostriction is normalized by κ indicating that, for fixed microstructure, magnetostriction is a balance between the magnetic saturation of the particle and the stiffness of the matrix, and can be increased by softening the matrix. The effect is initially quadratic in $\bar{b}$ but then saturates. The range of $\bar{b}$ where the magnetostriction is quadratic is the range where the magneti-

zation is linear. The initial curvature of the lines is determined by the parameter α_{i}, defined by (7.60), and the limiting value of magnetostriction by $\bar{\epsilon}_{\mathrm{s}}^{\mathrm{m}}$, defined by (7.61). The predicted effect is always extension in the direction of the applied magnetic field regardless of aspect ratio and concentration. This is confirmed by experiments on spherical particles (Ginder et al., 2002; Guan et al., 2008).

Figure 7.10 shows the effect of concentration c^{I} and the aspect ratio w on the initial and saturation behavior of magnetostriction. Figures 7.10a and 7.10c characterize the magnetostriction when the composite is magnetically linear, while Figures 7.10b and 7.10d show the magnetostriction at saturation. The two effects are clearly different. The saturation magnetostriction depends on the distribution of the particles, the saturation magnetization, and the mechanical reinforcement. For fixed concentration, the mechanical reinforcement is minimized for aspect ratios below 1 so the maximum $\bar{\epsilon}_{\mathrm{s}}^{\mathrm{m}}$ is obtained when $c^{\mathrm{I}} \approx 0.61$ and $w \approx 0.67$. The initial behavior depends on the same parameters and on the composite susceptibility. The composite susceptibility is larger for elongated particles, $w > 1$, which initially leads to large magnetostriction despite the additional stiffening effect. Both effects tend to vanish as $c^{\mathrm{I}} \to 1$ or w is far from 1 because the composite is becoming mechanically rigid. Overall, for fixed κ, magnetostriction is maximized by increasing the magnetic forces produced by the inclusions and minimizing their reinforcement of the composite.

Figure 7.11 shows the actuation stress $\bar{t}^{(0)}$ normalized by $\mu_0 m_{\mathrm{s}}^2$ as a function of $\bar{b}$ for different aspect ratios w and concentrations c^{I}. The effect is initially quadratic in $\bar{b}$ but then saturates as $\bar{b}$ becomes large. The range of $\bar{b}$ where the actuation stress is quadratic is the range where the magnetization is linear. The initial curvature of the lines is the parameter β_{i} and the limiting value of actuation stress is $\bar{t}_{\mathrm{s}}^{(0)}$, as given by expressions (7.48) and (7.51), respectively. These curves are independent of the matrix and the mechanical stiffening. They correspond to a property of the initial configuration of magnetic particles and represent the net magnetic force generated by the current distribution of magnetic particles.

Figure 7.12 shows the effect of the concentration c^{I} and aspect ratio w on the initial and saturation behaviors of the actuation stress. Figures 7.12a and 7.12c characterize the actuation stress when the composite is magnetically linear, while Figures 7.12b and 7.12d show the actuation stress at saturation. $\bar{t}_{\mathrm{s}}^{(0)}$ is quadratic in the concentration because it depends only on the saturation magnetization and the distribution of the particles. It is not compensated for by the mechanical reinforcement

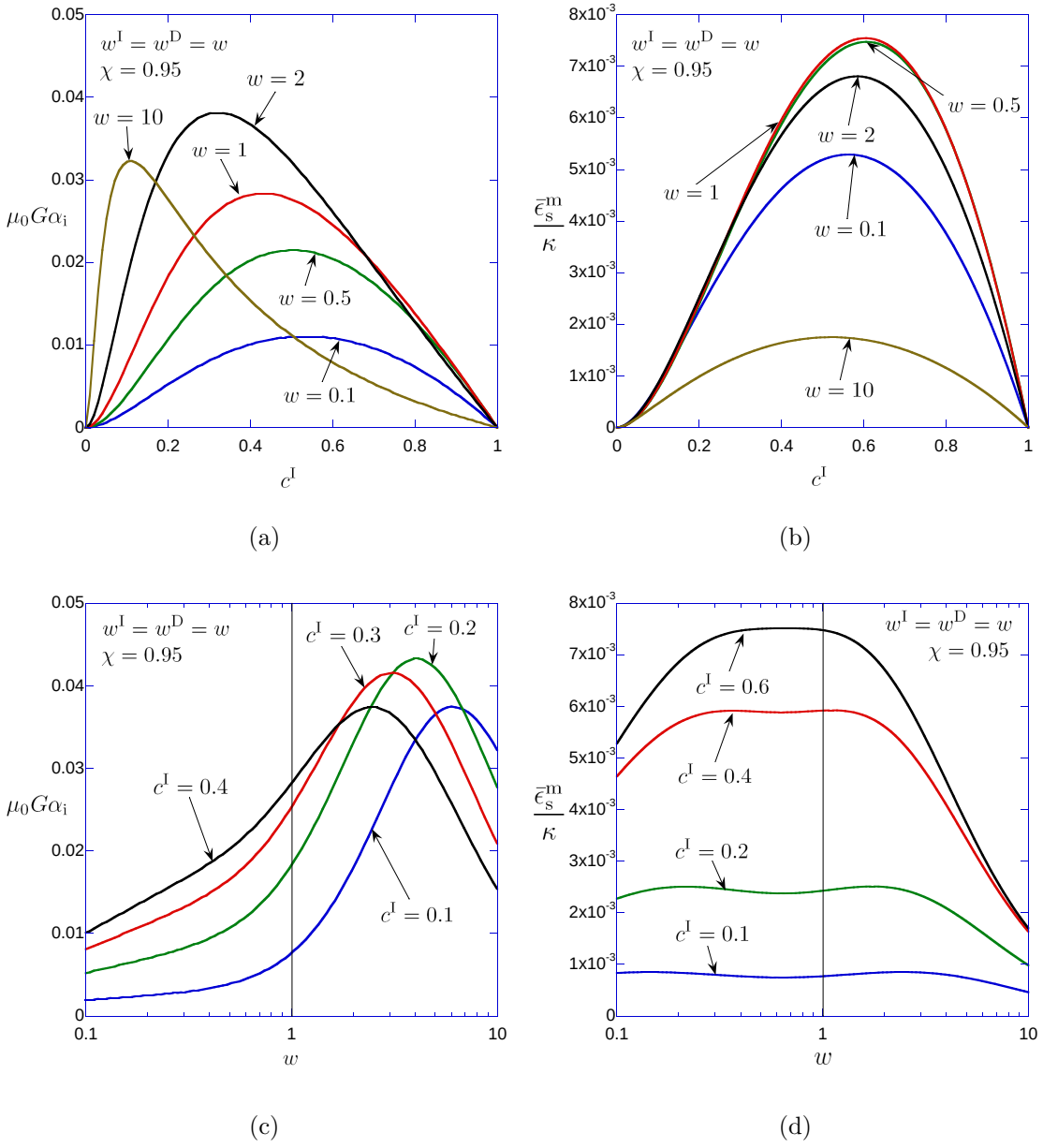

Figure 7.10: The coefficient of magnetostriction α_{i} and the saturation magnetostriction $\bar{\epsilon}_{\mathrm{s}}^{\mathrm{m}}$ for different microstructures. The results correspond to the magnetostriction in the range of linear magnetization and the saturation magnetization. (a) The coefficient of magnetostriction α_{i} and (b) the saturation magnetostriction $\bar{\epsilon}_{\mathrm{s}}^{\mathrm{m}}$ as a function of the concentration c^{I}. (c) The coefficient of magnetostriction α_{i} and (d) the saturation magnetostriction $\bar{\epsilon}_{\mathrm{s}}^{\mathrm{m}}$ as a function of the aspect ratio w.

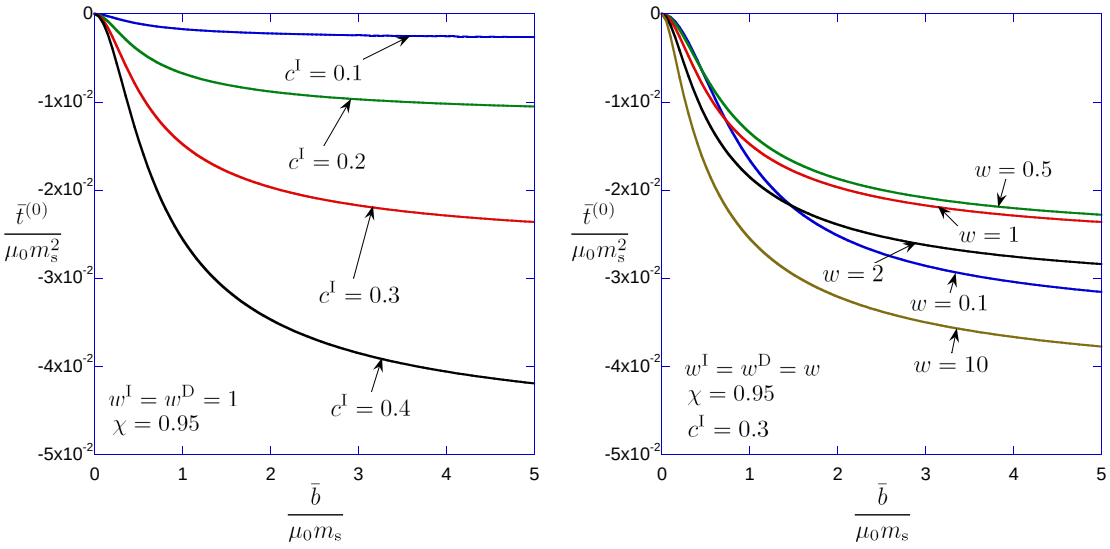

Figure 7.11: The actuation stress $\bar{t}^{(0)}$ as a function of the applied magnetic field $\bar{b}$ for different microstructures. (a) The actuation stress $\bar{t}^{(0)}$ for different concentrations c^{I} with spherical aspect ratio $w = 1$. (b) The actuation stress $\bar{t}^{(0)}$ for different aspect ratios w and concentration $c^{\mathrm{I}} = 0.3$.

like the magnetostriction. In the range of linear magnetic behavior, the composite susceptibility also affects the actuation stress which leads to the more complicated behavior for β_{i}. Prolate shapes (with $w > 1$) tend to have a bigger effect on β_{i} than oblate shapes (with $w < 1$), but both prolate and oblate shapes tend to increase the saturation traction $|\bar{t}_{\mathrm{s}}^{(0)}|$. This indicates that both prolate and oblate shapes can lead to a greater actuation stress, but in the linear regime oblate shapes are slower to magnetize, limiting the actuation stress of the composite.

Figure 7.13 shows the actuation energy density $\bar{e}_{\mathrm{a}}$ as a function of the concentration c^{I} and aspect ratio w. The actuation energy density is quartic to leading order in the concentration, so that even for concentrations up to 40 percent, it is relatively small. The dependence on the aspect ratio is more subtle, showing that for a set concentration there are two local maxima for the energy density. This effect is the result of a complex dependence on the magnetic and mechanical properties of the composite. The actuation energy also goes to zero when $c^{\mathrm{I}} \to 1$ or w is far from 1 because the composite is becoming mechanically rigid. On the other hand, when $c^{\mathrm{I}} = 0$, the magnetic energy is unavailable to the composite because the magnetization vanishes.

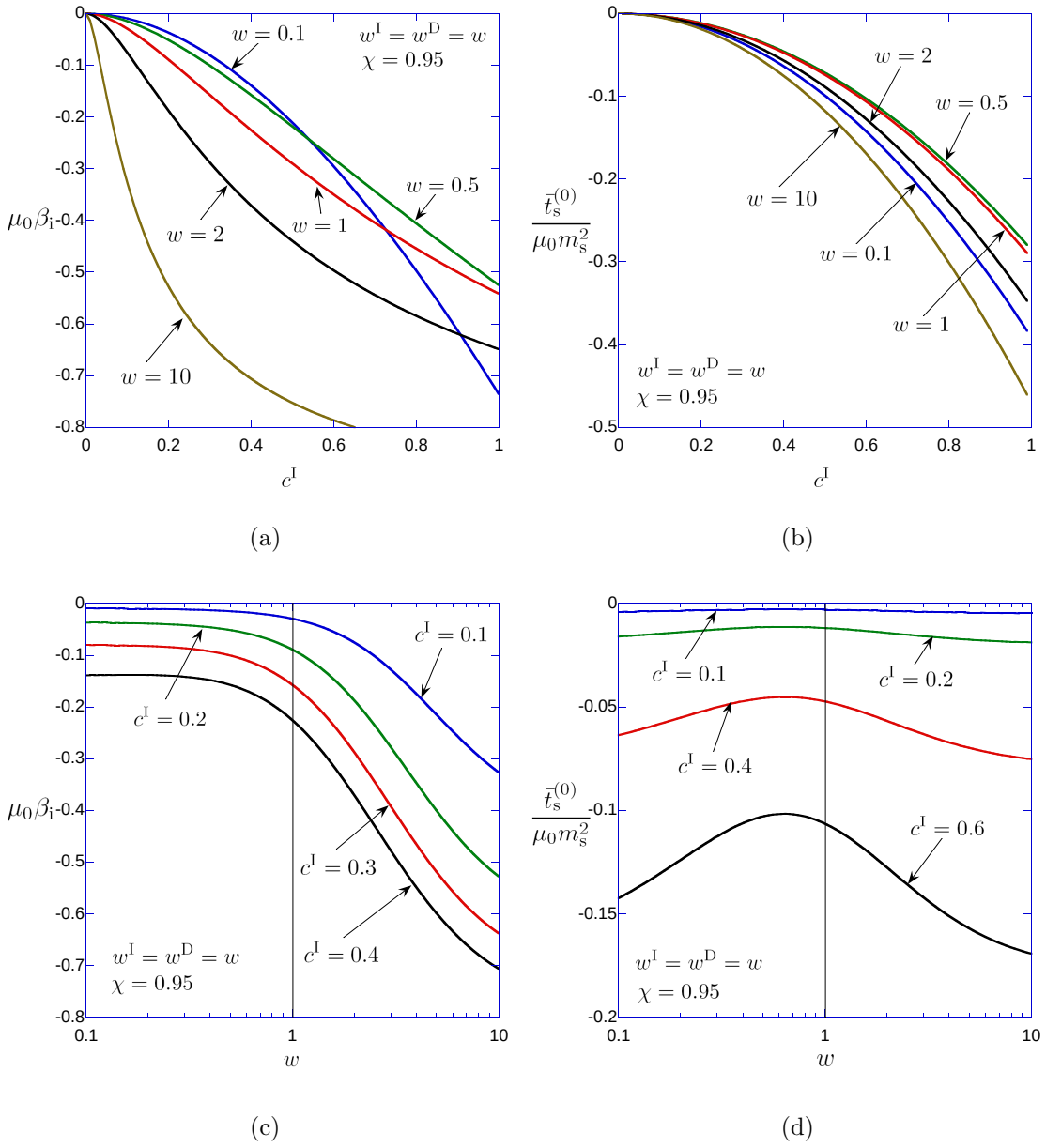

Figure 7.12: The coefficient of actuation stress β_{i} and the saturation actuation stress $\bar{t}_{\mathrm{s}}^{(0)}$ for different microstructures. The results correspond to the actuation stress in the range of linear magnetization and the saturation actuation stress. (a) The coefficient of actuation stress β_{i} and (b) the saturation actuation stress $\bar{t}_{\mathrm{s}}^{(0)}$ as a function of the concentration c^{I}. (c) The coefficient of actuation stress β_{i} and (d) the saturation actuation stress $\bar{t}_{\mathrm{s}}^{(0)}$ as a function of the aspect ratio w.

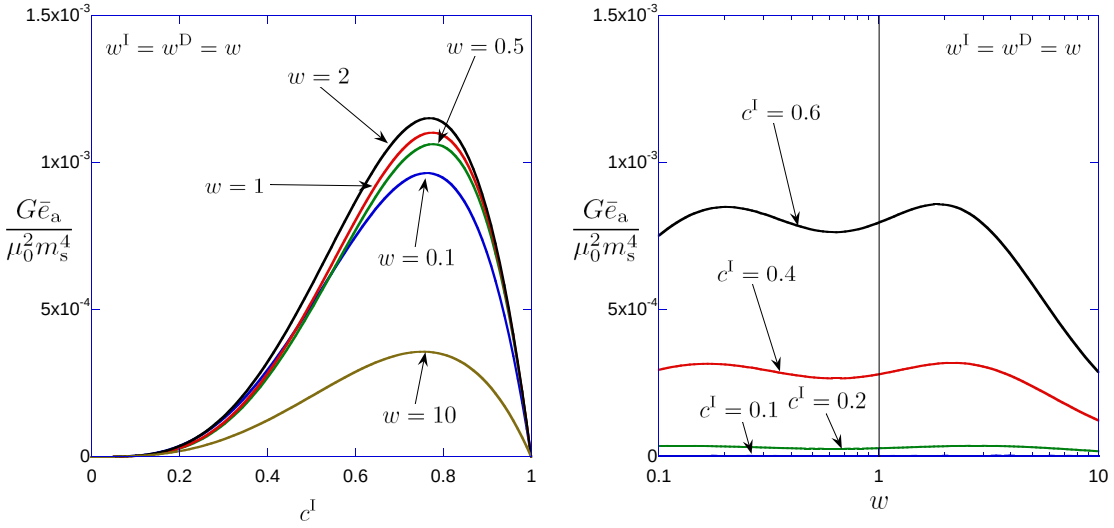

(a) (b)

Figure 7.13: The actuation energy density $\bar{e}_{\mathrm{a}}$ for different microstructures. (a) Actuator energy density $\bar{e}_{\mathrm{a}}$ as a function of concentration c^{I}. (b) Actuator energy density $\bar{e}_{\mathrm{a}}$ as a function of aspect ratio w.

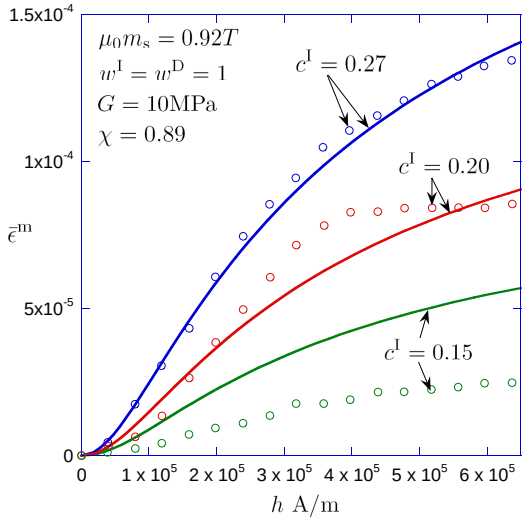

Figure 7.14: The predicted magnetostriction $\bar{\epsilon}^{\mathrm{m}}$ as a function of $\bar{h}$ compared against the experimental results of Guan et al. (2008). The solid lines are theoretical results and the discrete values are the experimental results. The experimental materials exhibit hysteresis so the plot compares the initial loading vs. the theoretical results.

Figure 7.14 provides a comparison of the predictions of the theory against the experiments of Guan et al. (2008), for the magnetostriction $\bar{\epsilon}^{\mathrm{m}}$ as a function of the magnetic intensity $\bar{h}$. Even though the precise material properties for the matrix and particles were not provided by the authors, it was still possible to infer values of the properties in our model to achieve a reasonable match to the experimental data. The model does predict a somewhat weaker effect of particle concentration than the experiments. This is consistent with the use of estimates of the Hashin-Shtrikman type for the magnetic and elastic effects, which are known to underestimate the effect of particle interactions, especially at large volume fractions. However, given the uncertainties involved in the experimental data, the model does capture very well the qualitative features of the experiments, and can even provide reasonably good predictive capabilities. In addition, it should be noted that Guan et al.'s experiments exhibited hysteresis, which is not accounted for in our theory. The hysteresis of the particles themselves is very difficult to describe and including these effects in the homogenization is beyond the scope of the present work.

It is also relevant to mention that Diguet et al. (2010) have measured experimentally the magnetostriction of a cylinder made of an MRE. However, their results depend on the aspect ratio of the cylinder (which is not the same as the aspect ratio of the inclusions) and do not correspond to the magnetostriction defined in this paper, which is a shape-independent (i.e., a material) property. However the results are qualitatively consistent and of the same order of magnitude.

7.3 Magnetostriction with magnetic loading transverse to the microstructure

We can also consider magnetostriction when the magnetic field is perpendicular to the symmetry axis of the microstructure such that $\mathbf{b} = \bar{b}\hat{e}_2$. $\hat{e}_1$ is still the symmetry axis of the microstructure but now there is no symmetry between the $\hat{e}_2$ and $\hat{e}_3$ directions. This means that magnetic effects can produce different strain in all three directions. The incompressibility constraint still allows us to solve for p and remove one of the equations. Since the magnetic contribution to the modulus is negligible, the magnetostriction can be given in terms of the mechanical moduli for the composite. If all surfaces are traction-free, the result is two equilibrium equations which determine

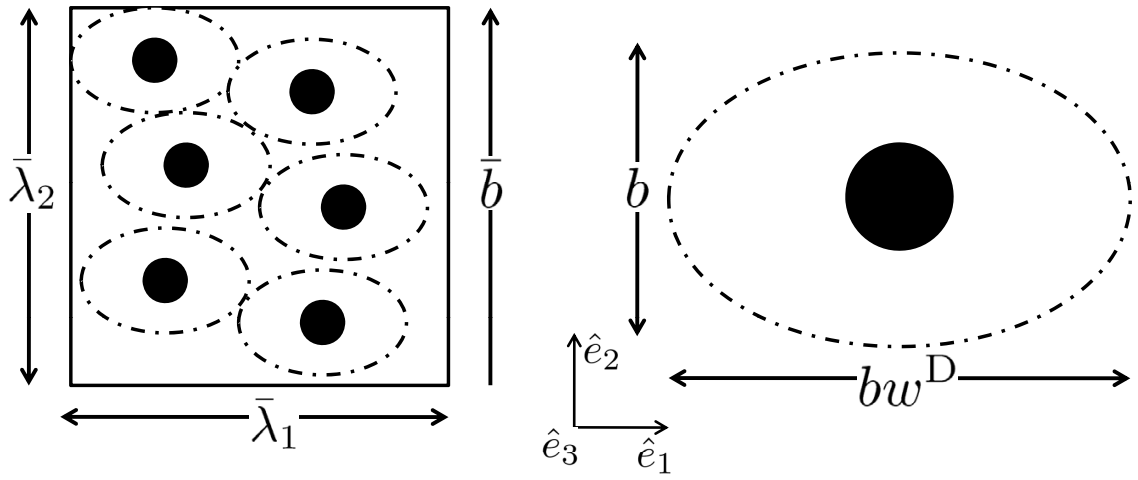

Figure 7.15: The relevant loading conditions and material variables for magnetic loading transverse to the composite. This model consists of spherical particles with distributional spheroid w^{D}. There is no traction applied on any surface and the material responds by straining in all three directions.

the magnetostriction as a function of the magnetization

$$\begin{bmatrix} \bar{\epsilon}_1^{\mathrm{m}} \\ \bar{\epsilon}_2^{\mathrm{m}} \end{bmatrix} = -\frac{1}{14\tilde{G}_{\mathrm{a}}\tilde{G}_{\mathrm{p}} - 2\tilde{G}_{\mathrm{p}}^2} \begin{bmatrix} \tilde{G}_{\mathrm{a}} & \tilde{G}_{\mathrm{a}} - 3\tilde{G}_{\mathrm{p}} \\ -2\tilde{G}_{\mathrm{p}} & 3\tilde{G}_{\mathrm{a}} + \tilde{G}_{\mathrm{p}} \end{bmatrix} \begin{bmatrix} \bar{t}_1^{(0)} - \bar{t}_3^{(0)} \\ \bar{t}_2^{(0)} - \bar{t}_3^{(0)} \end{bmatrix} + o(\bar{\epsilon}^2). \tag{7.64}$$

with

$$\bar{\epsilon}_3^{\mathrm{m}} = -\bar{\epsilon}_1^{\mathrm{m}} - \bar{\epsilon}_2^{\mathrm{m}} \tag{7.65}$$

$\bar{t}_i^{(0)}$, and $\bar{\epsilon}_i^{\mathrm{m}}$ reach a saturation value similar to the axial loading case. Rather than introduce a subscript to denote the saturation values, we will point out that the saturation magnetostriction is given by using the saturation value for

$$\bar{t}_i^{(0)} = -\frac{\mu_0}{2}\bar{m}_{\mathrm{s}}^2 \left[\delta_{ik} + \left. \frac{\partial P_k^{\mathrm{D}}}{\partial \bar{\lambda}_i} \right|_{\bar{\lambda}=1} \right] \tag{7.66}$$

in equation (7.64).

It is of particular interest to consider the case where spherical particles are distributed spheroidally perpendicular to the applied field so that $w^{\mathrm{I}} = 1$ and w^{D} is allowed to vary. These microstructures in some sense characterize chain distributions when $w^{\mathrm{D}} < 1$. It is important to note that there is a restriction on the w^{I}, w^{D} and c^{I} which ensures the validity of the results specifically (Ponte Castañeda and Willis,

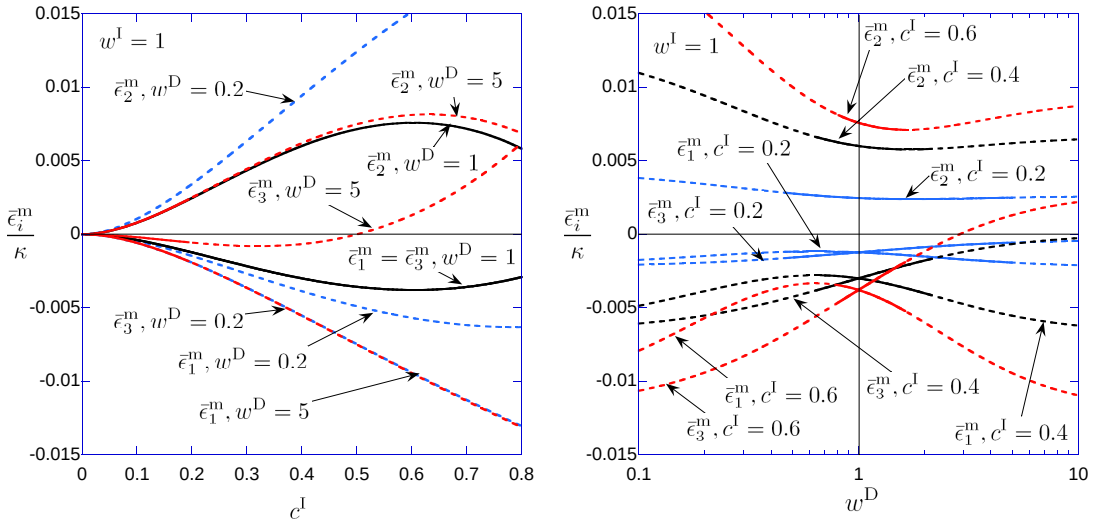

(a) (b)

Figure 7.16: The saturation magnetostriction for $\bar{\epsilon}_1^{\mathrm{m}}$, $\bar{\epsilon}_2^{\mathrm{m}}$ and $\bar{\epsilon}_3^{\mathrm{m}}$. The magnetic field is applied in the $\hat{e}_2$ direction perpendicular to the $\hat{e}_1$, the symmetry axis of the distributional spheroid. The lines become dashed when the condition (7.67) on w^{I}, w^{D} and c^{I} fails.

1995).

$$c^{\mathrm{I}} \left(\frac{w^{\mathrm{I}}}{w^{\mathrm{D}}} \right)^2 \leq 1 \text{ when } w^{\mathrm{D}} \leq w^{\mathrm{I}}, \text{ and } c^{\mathrm{I}} \frac{w^{\mathrm{D}}}{w^{\mathrm{I}}} \leq 1 \text{ when } w^{\mathrm{D}} > w^{\mathrm{I}}. \tag{7.67}$$

Figure 7.16 shows the saturation magnetostriction when the particles are spherical for different concentrations and distributions. The magnetic effects cause different strain in all three directions. The strain is always positive in the direction of the magnetic field and negative in the other two directions. When $w^{\mathrm{D}} < 1$ the general effect is to be more like a chain-structured MRE Guan et al. (2008). The results predict that the effects will increase for both extremes when w^{D} is far from 1. The magnetostriction is, as in the aligned case, a balance between the magnetic forces that are generated and the mechanical stiffness of the composite.

7.4 Concluding remarks

In this work, estimates have been developed for the magnetoelastic properties of spheroidal-particle MREs under aligned loading conditions. The properties include the magnetostrictive strain, the field-dependent Young's modulus, the actuation stress, and the actuation energy density. The results are based on the finite-strain homogenization framework and partial decoupling approximation introduced in Ponte Castañeda and Galipeau (2011), which provides estimates for the total stress and magnetization in MREs with rigid magnetic inclusions. In particular, expressions for the applied traction on the composite are derived from the total stress by accounting for the magnetic stress outside the sample. The results are formulated in the finite strain context, but then specialized for small strains, where we define appropriate parameters characterizing the magnetoelastic behavior of the composites.

The magnetoelastic effects in these systems are found to be of second order in the particle concentration and limited by the magnetic saturation of the particles. In this context, it should be emphasized that while the macroscopic stress inside a given MRE specimen includes contributions that are of first order in the concentration, such contributions drop out from the corresponding expressions for the external traction (on the specimen), because of the Maxwell stresses that surround the specimen. This result is consistent with the fact that for small (dilute) concentrations, the particles do not interact and the net forces on the particles vanish, producing no magnetoelastic coupling effects. In addition, the magnetoelastic coupling is seen to arise from the dependence of the (nonlinear) magnetic susceptibility of the MRE on the deformation, and has been linked to certain microstructural tensors characterizing the two-point correlation function for the random distribution of the particles in the elastomer matrix. However, the thermodynamically consistent approach followed in this work is different from earlier approaches (Borcea and Bruno, 2001; Yin and Sun, 2006), which estimated the average stress in the composite by means of a direct computation of the inter-particle forces. Although the specific results developed in this work made use of variational estimates (Ponte Castañeda and Willis, 1995) incorporating up to two-point statistics for the distribution of the particle in the composite, the method is more general and could, in principle, be generalized to include the effects of higher-order statistics, to obtain more accurate estimates at higher particle concentrations.

Concerning the specific results of this work, it is important to distinguish between

two different regimes: the linear magnetization regime and the saturation magnetization regime. In the linear regime, the magnetoelastic coupling is largely controlled by the composite susceptibility, with microstructures that magnetize easily favoring strong magnetoelastic effects. In the saturation regime, the effects are controlled by the saturation magnetization of the particles and their distribution in space. For small applied magnetic fields $\bar{b}$, the magnetostrictive strain grows quadratically with $\bar{b}$. The corresponding coefficient increases and then decreases with the particle concentration and aspect ratio (from oblate to prolate shapes), reaching a maximum effect for a particle concentration of about 0.2 and a prolate particle shape with aspect ratio of about 4. On the other hand, for large values of $\bar{b}$, the effect saturates and scales with the dimensionless parameter $\kappa = \mu_0 m_s^2/G$, characterizing the relative strengths of the magnetic to the elastic forces in the MRE systems. The maximum magnetostrictive strain is reached at saturation for a particle concentration of about 0.61 and an oblate particle shape with aspect ratio of about 0.67. These different results for different regimes demonstrate clearly the need to account for the magnetic nonlinearity of the material when seeking to optimize the microstructure in these MRE systems. Predictions for the optimal microstructure based on the (linear) magnetic susceptibility of the material do not continue to hold when the magnetic saturation of the particles—corresponding to the largest possible magnetostrictive strain that the composite material can sustain—is accounted for. Corresponding predictions for the actuation stress (at saturation) show that the effect is enhanced by larger concentrations of particles and by both strongly oblate and prolate shapes. Now, while the optimal microstructures for the magnetostrictive strain and the actuation stress are somewhat contradictory, in applications, a more useful figure of merit is the actuation energy density of the material, which is found to be optimized by relatively large volume fractions in the order of 75% and either slightly prolate shapes, or somewhat oblate shapes (with aspect ratios of 2 and 0.2, respectively). Finally, the effect of the magnetic field on the Young's modulus of the material was found to be relatively small compared to the purely mechanical modulus of the composite, although it is worth emphasizing that prolate shapes can be used to reduce the total modulus of the MRE under application of a magnetic field.

The results presented in this paper have focused on magnetic and mechanical loadings that are aligned with the uniaxial symmetry axes of the particles. We have also considered magnetic loadings that are perpendicular to this symmetry axis, and

investigated the effects of particle distributions in an attempt to model chain distributions of spherical particles. However, the characterization of such systems requires consideration of more general orthotropic symmetries for the material behavior, leading to significantly more complex expressions and results. More generally, if the magnetic and/or mechanical loading axis are not aligned with the particle axes, additional effects are expected due to the particle rotations that would be generated by the magnetic and elastic torques on the particles. The particle rotations generated by a non-aligned magnetic field have been addressed recently by Siboni and Ponte Castañeda (2012a) in the context of small strains and rotations. Such particle rotations, whether induced mechanically or magnetically, have been shown to produce effects that are of the same order as the particle concentration, and a dilute theory has been developed accordingly by (Siboni and Ponte Castañeda, 2012b), again in the small-strain/small-rotation context.

Finally, it should be noted that the results of this work concerning the effects of particle shape for MREs are also expected to be relevant for certain types of dielectric elastomer composites. Indeed, it has been shown recently Siboni and Ponte Castañeda (2012a) that the framework of Ponte Castañeda and Galipeau (2011) for magnetoelastic composites can be extended to certain classes of electroactive polymer composites consisting of stiff dielectric (ferroelectric) particles that are randomly distributed in a soft dielectric elastomer matrix that can be idealized as having a deformation-independent dielectric coefficient.

Chapter 8

Conclusion

In this thesis energy functions were obtained which characterize the effective macroscopic behavior of MREs. The estimates are valid for finite deformation and large magnetic field and include the effect of saturation. The estimates account for the properties of the constituent materials including the stiffness and nonlinear behavior of the elastomer matrix as well as the initial susceptibility and magnetic saturation of the particles. The estimates also account for the microstructure of the composite including the shape, distribution, and concentration of the inclusion phases.

The proposed energy functions are based on an extension of the formulation of Hill (1972) for the effective behavior of the mechanical composite at finite strain using a Lagrangian description of magnetoelasticity initially proposed by Dorfmann and Ogden (2004). This homogenization framework is the basis for describing magnetoelastic composites as well as electro-active composites at finite strain and large magnetic fields. This homogenization framework, advantageously, has a form where "linear comparison" methods (Ponte Castañeda and Tiberio, 2000) can be applied directly.

Motivated by interest in MREs where the inclusions are effectively rigid, a "partial decoupling approximation" was proposed which simplifies the homogenization problem into a purely mechanical and purely magnetic homogenization problem, both of which are non-linear and can be evaluated using the previously mentioned "linear comparison" methods. This separation allows us to use previously obtained results for the purely mechanical problem to derive relatively explicit estimates for the coupled magnetoelastic constitutive behavior of MREs. This "partial decoupling approximation" also clarifies the essential connection between microstructure evolution and magnetoelastic coupling in MREs. The energy function obtained using the "partial decoupling approximation" provides reasonable predictions for the full mechanical and magnetic behavior of the composite material. These energy functions may be the first to provide physically consistent results through this large range of validity.

We examined the effective behavior of magnetorheological elastomers with random and periodic distribution of the particles. We analyzed the role of the concentration, distribution and shape of the particles on the magnetomechanical response of the composites. In particular, the random and periodic rectangular and quasi-hexagonal microstructures with varying concentrations and shape of the particles were considered. Motivated by the potential applications for "linear actuators," we specifically examined the materials subjected to uniaxial loading in the presence of a magnetic

field. The primary parameters governing the performance of the MREs is the susceptibility with respect to strain.

The energy functions obtained using the partial decoupling approximation were then evaluated by considering the traction on the surface of the materials. This provided a means to account for the underlying Maxwell stress within the magnetoelastic material in a way that is consistent with experiments. These materials were evaluated by considering the actuation traction, magnetostriction, magnetization, and magnetoelastic modulus of these materials. These properties were considered over a broad range of microstructures in both the 2D and 3D cases. Through this effort it was shown that when the materials' symmetry axis and the applied magnetic field are not aligned, torques develop on the composite which appear in the applied traction. This makes certain effects such as magnetostriction and modulus effects difficult to define despite the fact that the coupling is in general stronger in these cases.

To exploit the stronger coupling effects of particle rotation, we proposed using the particulate MRE material energy function in a laminated microstructure, thereby making a multiscale composite. This laminated composite was able to produce large magnetoelastic effects including magnetostriction, actuation traction, and modulus effects because it uses the effects of the particle rotation. Instabilities which depend on the magnetic field were observed in this context. In this case the magnetic field has the potential to aggravate or stabilize an existing mechanical instability affecting all the relevant magnetoelastic properties.

There are a myriad of future directions which arise from this work. At the fundamental level the "linear comparison methods" could be brought directly to bear on the magnetoelastic homogenization problem without using the "partial decoupling approximation." More specific estimates for magnetoelastic coupling could be obtained at a cost of more computational effort. Homogenization efforts of this type could capture the evolution of the microstructure due solely to the magnetic field which the partial decoupling approximation does not account for. It is also of interest to further develop the loss of ellipticity and examine instabilities in magnetoelastic composites. This work has shown that such instabilities are affected by the magnetic field and it is anticipated that these effects could produce composites with favorable properties.

The methods employed here to homogenize MREs with rigid particles circumvent the need to compute torques on particles and inter-particle force interactions, which has many advantages. However the interaction between the rigid particles and the

matrix is in theory entirely controlled by the net force and torques on the particles. It would be very interesting to reconcile these two points of view.

In conclusion it is clear that the theoretical results presented here could help guide the development of magnetorheological elastomers with improved properties. This work lacks comparisons to experimental data because suitable experimental data could not be found in the literature. Therefore it would be useful to apply some of the microstructures considered here to experimental results. This comparison would hopefully validate these results and produce composites with favorable magnetoelastic properties. It would also be of interest to generate the laminated microstructure studied here.

Appendix

A Relationships between volume averaged quantities

In this appendix a detailed derivation of the relationships

$$\bar{\boldsymbol{T}} = \bar{J}^{-1}\bar{\boldsymbol{S}}\,\bar{\boldsymbol{F}}^{T}, \quad \bar{\mathbf{h}} = \bar{\boldsymbol{F}}^{-T}\overline{\mathbf{H}}, \quad \text{and} \quad \bar{\mathbf{b}} = \bar{J}^{-1}\bar{\boldsymbol{F}}\,\overline{\mathbf{B}}, \tag{A1}$$

as given by equation (3.13) is provided. The proof of the first relation in the magnetoelastic case is identical to the proof in the mechanical context so we will not repeat it here. For the latter two, recall that we consider magneto-mechanical excitation of a region Ω_0 subject to affine excitation conditions. This region deforms to some region Ω. The mechanical excitation condition can be specified by either defining the deformation or the normal component of the stress. However as is typical in elasticity, we will only consider the case of specifying

$$\mathbf{x} = \bar{\boldsymbol{F}}\mathbf{X} \quad \text{on} \quad \partial\Omega_0. \tag{A2}$$

The volume average of Lagrangian variables will be defined in terms of the reference configuration specifically,

$$\bar{\mathbf{H}} = \frac{1}{|\Omega_0|}\int_{\Omega_0} \mathbf{H}\; dV \quad \text{and} \quad \bar{\mathbf{B}} = \frac{1}{|\Omega_0|}\int_{\Omega_0} \mathbf{B}\; dV. \tag{A3}$$

Correspondingly, the volume average of Eulerian variables will be defined in terms of a deformed configuration volume average as

$$\bar{\mathbf{h}} = \frac{1}{|\Omega|}\int_{\Omega} \mathbf{h}\; dv \quad \text{and} \quad \bar{\mathbf{b}} = \frac{1}{|\Omega|}\int_{\Omega} \mathbf{b}\; dv. \tag{A4}$$

A0.1 Proof that $\bar{\mathbf{b}} = \bar{J}^{-1}\bar{\boldsymbol{F}}\,\overline{\mathbf{B}}$

First address the volume average of $\mathbf{b}$. Transferring to the Lagrangian variables and transferring the integral to the reference configuration yields

$$\bar{\mathbf{b}} = \frac{1}{|\Omega|}\int_{\Omega_0} \boldsymbol{F}\mathbf{B}\; dV. \tag{A5}$$

Decomposing the deformation gradient into its definition and using the fact that Div $\mathbf{B} = 0$, we can write

$$\bar{b}_i = \frac{1}{|\Omega|} \int_{\Omega_0} \left(\frac{\partial x_i}{\partial X_j} B_j + x_i \frac{\partial B_j}{\partial X_j} \right) dV. \tag{A6}$$

This allows us to compress the derivative to yield

$$\bar{b}_i = \frac{1}{|\Omega|} \int_{\Omega_0} \frac{\partial}{\partial X_j} \left(x_i B_j \right) dV \tag{A7}$$

Now application of the divergence theorem yields

$$\bar{b}_i = \frac{1}{|\Omega|} \int_{\partial\Omega_0} x_i B_j N_j \; dS \tag{A8}$$

where $\mathbf{N}$ is the normal to the region in question. We use the prescribed mechanical boundary condition to find that

$$\bar{b}_i = \frac{1}{|\Omega|} \int_{\partial\Omega_0} \bar{F}_{ik} X_k B_j N_j \; dS. \tag{A9}$$

Next removing the constant terms and applying the divergence theorem again yields

$$\bar{b}_i = \frac{\bar{F}_{ik}}{|\Omega|} \int_{\Omega_0} \left(B_k + X_k \frac{\partial B_j}{\partial X_j} \right) dV. \tag{A10}$$

The divergence of $\mathbf{B}$ is zero; we also substitute from the definition of $\bar{\mathbf{B}}$ to arrive at

$$\bar{\mathbf{b}} = \frac{\bar{\boldsymbol{F}} \bar{\mathbf{B}} \, |\Omega_0|}{|\Omega|} = \frac{\bar{\boldsymbol{F}} \bar{\mathbf{B}}}{\bar{J}}. \tag{A11}$$

A0.2 Proof that $\bar{\mathbf{h}} = \bar{\boldsymbol{F}}^{-T} \overline{\mathbf{H}}$

Our goal now is to perform a similar analysis for $\bar{\mathbf{h}}$. Starting with the definition

$$\bar{\mathbf{h}} = \frac{1}{|\Omega|} \int_{\Omega} \mathbf{h} \; dv. \tag{A12}$$

We know that $\mathbf{h}$ is the gradient of a potential Π. This can be substituted into the previous expression to yield

$$\bar{h}_i = \frac{1}{|\Omega|} \int_\Omega \frac{\partial \Pi}{\partial x_i} \, dv. \tag{A13}$$

Using the divergence theorem to bring the integral to the boundary yields

$$\bar{h}_i = \frac{1}{|\Omega|} \int_{\partial\Omega} \Pi n_i \, ds \tag{A14}$$

where $\mathbf{n}$ is the normal to the boundary in the deformed configuration. We now transfer this integral to the reference boundary using Nanson's relation to arrive at

$$\bar{h}_i = \frac{1}{|\Omega|} \int_{\partial\Omega_0} \Pi \bar{J} \bar{F}^{-1}_{ji} N_j \, dS. \tag{A15}$$

The constants can be removed and we can apply the divergence theorem to the terms inside the integral to yield

$$\bar{h}_i = \frac{\bar{J}\bar{F}^{-1}_{ji}}{|\Omega_0|} \int_{\partial\Omega} \frac{\partial \Pi}{\partial X_j} \, dV. \tag{A16}$$

Since $\mathbf{H} = \text{Grad } \Pi$ we can write

$$\bar{h}_i = \frac{\bar{J}\bar{F}^{-1}_{ji}}{|\Omega|} \int_{\Omega_0} H_j \, dV. \tag{A17}$$

Using the definition for $\bar{\mathbf{H}}$ we obtain the expected relation

$$\bar{\mathbf{h}} = \bar{\boldsymbol{F}}^{-T} \bar{\mathbf{H}}. \tag{A18}$$

Notice that these results do not assume a particular magnetic boundary condition. This result is therefore valid for either magnetic boundary condition, provided that the mechanical boundary condition is applied.

B Decoupling approximation for the magneto-elastic energy function

Consider a two phase composite. Phase (1), the matrix phase, is an isotropic, non-magnetically susceptible material. The inclusion phase, phase (2), is a material which is magnetically susceptible and mechanically rigid. Phase (1), the matrix phase, will have an energy function of the form

$$W^{(1)}(\boldsymbol{F}, \mathbf{B}) = \rho_0^{(1)} W_{me}^{(1)}(\boldsymbol{F}) + \frac{1}{2\mu_0 J}(\boldsymbol{F}\mathbf{B}) \cdot (\boldsymbol{F}\mathbf{B}). \tag{B1}$$

The second term ensures that the material is not magnetically susceptible, which means it has the same magnetic constitutive relation as a vacuum.

The constitutive relation of the inclusion phase can initially be assumed to have an energy function of the following form

$$W^{(2)}(\boldsymbol{F}, \mathbf{B}) = \rho_0^{(2)} W_{me}^{(2)}(\boldsymbol{F}) + \frac{1}{2\mu_0 J}(\boldsymbol{F}\mathbf{B}) \cdot (\boldsymbol{F}\mathbf{B}) + \rho_0^{(2)} \Phi^{(2)}(\boldsymbol{F}, \mathbf{B}). \tag{B2}$$

If we have a large region subject to the appropriate affine boundary conditions, we can define the homogenized energy function. We can determine an exact homogenized energy function if we know the exact solutions for the $\boldsymbol{F}$ and $\mathbf{B}$ fields on the micro-scale. Assuming that $\boldsymbol{F}$ and $\mathbf{B}$ are the exact solution to the complete homogenization problem, the exact homogenized energy is given by

$$\tilde{W}(\bar{\boldsymbol{F}}, \bar{\mathbf{B}}) = \frac{1}{|\Omega_0|} \int_{\Omega_0} W(\mathbf{X}, \boldsymbol{F}, \mathbf{B}) dV. \tag{B3}$$

The integral can be divided into two regions, $\Omega_0^{(1)}$ the region occupied by the matrix, and $\Omega_0^{(2)}$, the region occupied by the inclusions to yield

$$\tilde{W}(\bar{\boldsymbol{F}}, \bar{\mathbf{B}}) = \frac{1}{|\Omega_0|} \int_{\Omega_0^{(1)}} W^{(1)}(\boldsymbol{F}, \mathbf{B}) dV + \frac{1}{|\Omega_0|} \int_{\Omega_0^{(2)}} W^{(2)}(\boldsymbol{F}, \mathbf{B}) dV. \tag{B4}$$

Collecting all the terms containing $\mathbf{B}$ and grouping them together

$$\tilde{W}(\bar{\boldsymbol{F}},\bar{\mathbf{B}}) = \frac{1}{|\Omega_0|}\left[\int_{\Omega_0}\frac{1}{2\mu_0 J}(\boldsymbol{F}\mathbf{B})\cdot(\boldsymbol{F}\mathbf{B})dV + \int_{\Omega_0^{(2)}}\rho_0^{(2)}\Phi_{mag}^{(2)}(\boldsymbol{F},\mathbf{B})dV\right] + \frac{1}{|\Omega_0|}\int_{\Omega_0}\rho_0 W_{me}(\mathbf{X},\boldsymbol{F})dV. \quad \text{(B5)}$$

It is now useful to transfer the first two integrals to the deformed configuration. Therefore we can rewrite this in terms of $\mathbf{b}$

$$\bar{J}\tilde{w}_{mag}(\bar{\mathbf{b}};\boldsymbol{F}) = \frac{1}{|\Omega|}\left[\int_{\Omega}\frac{1}{2\mu_0}\mathbf{b}\cdot\mathbf{b}dv + \int_{\Omega^{(2)}}\rho^{(2)}\varphi_{mag}^{(2)}(\boldsymbol{F},\mathbf{b})dv\right] \quad \text{(B6)}$$

The integral given above is a magnetic homogenization problem in the deformed configuration with $\mathbf{b}\cdot\mathbf{n} = \bar{\mathbf{b}}\cdot\mathbf{n}$ on $\partial\Omega$ (as shown in Appendix A $\bar{\mathbf{b}} = \bar{\boldsymbol{F}}\bar{\mathbf{B}}/J$). The rearrangement at this stage is exact because we have simply written the original integral in terms of the deformed configuration. This provides a simplification because the expression does not depend on the details of the deformation inside the matrix. The problem in general is still very difficult because in principle this is a homogenization with infinitely many different inclusion phases since $\varphi_{mag}^{(2)}(\boldsymbol{F},\mathbf{b})$ depends on $\boldsymbol{F}$. This implies that at each point the magnetic constitutive relations can be a different function of $\mathbf{b}$ even within the same particle.

If we assume that the particles are in fact rigid, this implies that ρ is a constant and $\boldsymbol{F}$ is a rotation $\boldsymbol{R}$, the homogenization problem can be reduced to:

$$\bar{J}\tilde{w}_{mag}(\bar{\mathbf{b}};\boldsymbol{F}) = \frac{1}{|\Omega|}\left[\int_{\Omega}\frac{1}{2\mu_0}\mathbf{b}\cdot\mathbf{b}dv + \int_{\Omega^{(2)}}\rho_0^{(2)}\varphi_{mag}^{(2)}(\boldsymbol{R},\mathbf{b})dv\right] \quad \text{(B7)}$$

In the previous homogenization problem, equation (B6), each point can have a different magnetic constitutive relation. Here the rigid particle assumption forces each individual inclusion to have the same constitutive relation providing a significant simplification. This problem is more simple but still requires knowledge of the microstructure and rotations of the particles. In principle we would need to know both the positions of the particles and their rotations in the deformed configuration to use a homogenization estimate.

If we knew the required information about the deformed configuration microstructure, we could write the above integral as an effective energy as a function of $\bar{\mathbf{b}}$ which

depends on the deformation via two distinct ways: through the microstructure and through the boundary conditions.

Substituting this back into equation (B5) we get

$$\tilde{W}(\bar{\boldsymbol{F}}, \bar{\mathbf{B}}) = \bar{J}\tilde{w}_{mag}(\bar{\mathbf{b}}; \boldsymbol{F}) + \frac{1}{|\Omega_0|}\int_{\Omega_0} W_{me}(\mathbf{X}, \boldsymbol{F})dV \tag{B8}$$

This equation suggests using the homogenized energy for the purely mechanical case in the place of the integral. In general there is energy coupled in the magnetic homogenization which does not allow us to make a clear distinction between magnetic and deformation energy. However in the rigid particle case, all of the mechanical strain energy is contained in the matrix phase and a clear distinction between the mechanical and magnetic energy can be drawn.

Even in the case of rigid particles, the exact $\boldsymbol{F}$ will depend on the magnetic field. This means that the total sum of the strain energy in the matrix will be different from the total sum of the strain energy when there is no magnetic excitation. Despite this, an estimate for the effective mechanical energy could be determined by just using the homogenization result in the purely mechanical case. In the process this will also provide predictions for the microstructure evolution needed to compute the magnetic energy.

B0.3 The effect of the partial decoupling approximation

We have an estimate for the effective energy function of the composite based on the effective energy function in the purely mechanical case and the associated predictions for the microstructure evolution, but more insight can be gained about the approximation we are making.

Consider the intergrals which provide the homogenized energy function as the minimization of the energy over trial fields $\boldsymbol{F}$ and $\mathbf{B}$. Call $\boldsymbol{F}_{PD}$ the exact solution when there is no magnetic field (or the particles are not magnetically susceptible). Call $\mathbf{B}_{PD}$ the minimizing magnetic field if the deformation is held at $\boldsymbol{F}_{PD}$. Similarly name $\boldsymbol{F}_{mel}$ and $\mathbf{B}_{mel}$ the exact solution for the magnetoelastic case. $\boldsymbol{F}_{mel}$ is a kinematically admissible $\boldsymbol{F}$. Using the minimum energy principle for the purely mechanical case we know that

$$\int_{\Omega_0} W_{me}(\mathbf{X}, \boldsymbol{F}_{mel})dV \geq \int_{\Omega_0} W_{me}(\mathbf{X}, \boldsymbol{F}_{PD})dV. \tag{B9}$$

This equation shows that using the homogenized energy function obtained from the purely mechanical homogenization is an underestimation for the strain energy in the elastic matrix for the full magnetoelastic problem.

The fields $\mathbf{B}_{PD}$ and $\boldsymbol{F}_{PD}$ are also trial fields for the magneto-elastic problem. From the minimum energy principle, we again can show the inequality

$$\bar{J}\tilde{w}_{mag}(\bar{\mathbf{b}};\boldsymbol{F}_{PD}) + \int_{\Omega_0} W_{me}(\mathbf{X},\boldsymbol{F}_{PD})dV \geq \bar{J}\tilde{w}_{mag}(\bar{\mathbf{b}};\boldsymbol{F}_{mel}) + \int_{\Omega_0} W_{me}(\mathbf{X},\boldsymbol{F}_{mel})dV. \quad \text{(B10)}$$

Adding the negative of equation (B9) to equation (B10) we can derive the inequality

$$\tilde{w}_{mag}(\bar{\mathbf{b}};\boldsymbol{F}_{PD}) \geq \tilde{w}_{mag}(\bar{\mathbf{b}};\boldsymbol{F}_{mel}). \quad \text{(B11)}$$

This expression shows that by using the deformed configuration microstructure obtained in the purely mechanical case to determine the magnetic energy, we are overestimating the magnetic energy. This is logical because when applying a magnetic field to a rigid particle mechanical system the magnetic energy will be reduced at the expense of increasing the mechanical energy in the matrix.

Since the partial decoupling approximation overestimates the magnetic energy and underestimates the mechanical energy, the errors may cancel each other out provided that the overall corrections are small. It is also important to consider that we are primarily interested in the stresses that are predicted by derivatives of the energy with respect to deformation. In this regard as long as the trend in microstructural evolution is consistent with the purely mechanical problem the stresses predicted should be consistent.

This formulation also makes a precise connection between microstructure evolution and the magnetoelastic energy. In this sense when designing magnetoelastic composites the most important consideration is to connect the microstructure evolution to the applied deformation. This is the source of magnetoelastic stresses which lead to the coupled behavior. No additional stresses will be generated unless the microstructure changes with respect to the macroscopic deformation even if the microstructure evolves because of the applied magnetic field.

It should be noted that in practice $\boldsymbol{F}_{PD}$ is not known exactly and the deformation predicted by the purely mechanical homogenization $\boldsymbol{F}_m$ is an estimate of the defor-

mation. Additionally only certain statistic charaterising $\boldsymbol{F}_m$ are known. Because of these two approximations the partial decoupling approximation is not a bound in a precise sense. However the partial decoupling approximation is in spirit a trial field for the exactly magnetoelastic homogenization problem.

C The derivatives of $\boldsymbol{P}^{\mathrm{D}}$.

In this appendix, we provide the derivatives of the distribution tensor $\boldsymbol{P}^{\mathrm{D}}(\boldsymbol{U})$, evaluated when $\bar{\lambda}_1 = \bar{\lambda}_2 = \bar{\lambda}_3 = 1$, for spheroidal distributions aligned with the $\hat{\mathbf{e}}_1$ axis. Note that in these expressions $w = w^{\mathrm{D}}$.

$$\left.\frac{\partial P_1^{\mathrm{D}}}{\partial \bar{\lambda}_1}\right|_{\bar{\lambda}_1=\bar{\lambda}_2=\bar{\lambda}_3=1} = \begin{cases} \frac{4w^2-1}{(-1+w^2)^2} - \frac{3w^3 \mathrm{arccos}\,(w)}{(1-w^2)^{5/2}} & w < 1 \\ -3/5 & w = 1 \\ \frac{4w^2-1}{(-1+w^2)^2} - \frac{3w^3 \mathrm{arccosh}\,(w)}{(-1+w^2)^{5/2}} & w > 1 \end{cases}$$

$$\left.\frac{\partial P_1^{\mathrm{D}}}{\partial \bar{\lambda}_2}\right|_{\bar{\lambda}_1=\bar{\lambda}_2=\bar{\lambda}_3=1} = \left.\frac{\partial P_1^{\mathrm{D}}}{\partial \bar{\lambda}_3}\right|_{\bar{\lambda}_1=\bar{\lambda}_2=\bar{\lambda}_3=1} = \begin{cases} \frac{-2-w^2}{2(1-w^2)^2} + \frac{3w \mathrm{arccos}\,(w)}{2(1-w^2)^{5/2}} & w < 1 \\ -1/5 & w = 1 \\ \frac{-2-w^2}{2(1-w^2)^2} + \frac{3w \mathrm{arccosh}\,(w)}{2(-1+w^2)^{5/2}} & w > 1 \end{cases}$$

$$\left.\frac{\partial P_2^{\mathrm{D}}}{\partial \bar{\lambda}_1}\right|_{\bar{\lambda}_1=\bar{\lambda}_2=\bar{\lambda}_3=1} = \left.\frac{\partial P_3^{\mathrm{D}}}{\partial \bar{\lambda}_1}\right|_{\bar{\lambda}_1=\bar{\lambda}_2=\bar{\lambda}_3=1} = \begin{cases} \frac{-2w^2-w^4}{2(-1+w^2)^2} + \frac{3w^3 \mathrm{arccos}\,(w)}{2(1-w^2)^{5/2}} & w < 1 \\ -1/5 & w = 1 \\ \frac{-2w^2-w^4}{2(-1+w^2)^2} + \frac{3w^3 \mathrm{arccosh}\,(w)}{2(-1+w^2)^{5/2}} & w > 1 \end{cases}$$

$$\left.\frac{\partial P_2^{\mathrm{D}}}{\partial \bar{\lambda}_2}\right|_{\bar{\lambda}_1=\bar{\lambda}_2=\bar{\lambda}_3=1} = \left.\frac{\partial P_3^{\mathrm{D}}}{\partial \bar{\lambda}_3}\right|_{\bar{\lambda}_1=\bar{\lambda}_2=\bar{\lambda}_3=1} = \begin{cases} \frac{15w^2-6w^4}{8(-1+w^2)^2} - \frac{9w \mathrm{arccos}\,(w)}{8(1-w^2)^{5/2}} & w < 1 \\ -3/5 & w = 1 \\ \frac{15w^2-6w^4}{8(-1+w^2)^2} - \frac{9w \mathrm{arccosh}\,(w)}{8(-1+w^2)^{5/2}} & w > 1 \end{cases}$$

$$\left.\frac{\partial P_2^{\mathrm{D}}}{\partial \bar{\lambda}_3}\right|_{\bar{\lambda}_1=\bar{\lambda}_2=\bar{\lambda}_3=1} = \left.\frac{\partial P_3^{\mathrm{D}}}{\partial \bar{\lambda}_2}\right|_{\bar{\lambda}_1=\bar{\lambda}_2=\bar{\lambda}_3=1} = \begin{cases} \frac{5w^2-2w^4}{8(-1+w^2)^2} - \frac{3w \mathrm{arccos}\,(w)}{8(1-w^2)^{5/2}} & w < 1 \\ -1/5 & w = 1 \\ \frac{5w^2-2w^4}{8(-1+w^2)^2} - \frac{3w \mathrm{arccosh}\,(w)}{8(-1+w^2)^{5/2}} & w > 1 \end{cases}$$

$$\left.\frac{\partial P_1^{\mathrm{D}}}{\partial\bar{\lambda}_1\partial\bar{\lambda}_1}\right|_{\bar{\lambda}_1=\bar{\lambda}_2=\bar{\lambda}_3=1}=\begin{cases}\frac{-2+6w^2-19w^4}{(-1+w^2)^3}-\frac{3w^3(1+4w^2)\arccos\,(w)}{(1-w^2)^{7/2}} & w<1\\ 54/35 & w=1\\ \frac{-2+6w^2-19w^4}{(-1+w^2)^3}+\frac{3w^3(1+4w^2)\operatorname{arccosh}\,(w)}{(-1+w^2)^{7/2}} & w>1\end{cases}$$

$$\left.\frac{\partial P_1^{\mathrm{D}}}{\partial\bar{\lambda}_2\partial\bar{\lambda}_2}\right|_{\bar{\lambda}_1=\bar{\lambda}_2=\bar{\lambda}_3=1}=\left.\frac{\partial P_1^{\mathrm{D}}}{\partial\bar{\lambda}_3\partial\bar{\lambda}_3}\right|_{\bar{\lambda}_1=\bar{\lambda}_2=\bar{\lambda}_3=1}=\begin{cases}\frac{-16-31w^2+2w^4}{8(-1+w^2)^3}-\frac{3w(11+4w^2)\operatorname{arccosh}\,(w)}{8(1-w^2)^{7/2}} & w<1\\ 8/35 & w=1\\ \frac{-16-31w^2+2w^4}{8(-1+w^2)^3}+\frac{3w(11+4w^2)\operatorname{arccosh}\,(w)}{8(-1+w^2)^{7/2}} & w>1\end{cases}$$

$$\left.\frac{\partial P_1^{\mathrm{D}}}{\partial\bar{\lambda}_2\partial\bar{\lambda}_1}\right|_{\bar{\lambda}_1=\bar{\lambda}_2=\bar{\lambda}_3=1}=\left.\frac{\partial P_1^{\mathrm{D}}}{\partial\bar{\lambda}_3\partial\bar{\lambda}_1}\right|_{\bar{\lambda}_1=\bar{\lambda}_2=\bar{\lambda}_3=1}=\begin{cases}\frac{-2+14w^2+3w^4}{2(-1+w^2)^3}+\frac{15w^3\operatorname{arccosh}\,(w)}{2(1-w^2)^{7/2}} & w<1\\ 3/7 & w=1\\ \frac{-2+14w^2+3w^4}{2(-1+w^2)^3}-\frac{15w^3\operatorname{arccosh}\,(w)}{2(-1+w^2)^{7/2}} & w>1\end{cases}$$

$$\left.\frac{\partial P_1^{\mathrm{D}}}{\partial\bar{\lambda}_3\partial\bar{\lambda}_2}\right|_{\bar{\lambda}_1=\bar{\lambda}_2=\bar{\lambda}_3=1}=\begin{cases}\frac{-8w^2-9w^4+2w^6}{8(-1+w^2)^3}-\frac{15w^3\operatorname{arccosh}\,(w)}{8(1-w^2)^{7/2}} & w<1\\ 1/7 & w=1\\ \frac{-8w^2-9w^4+2w^6}{8(-1+w^2)^3}+\frac{15w^3\operatorname{arccosh}\,(w)}{8(-1+w^2)^{7/2}} & w>1\end{cases}$$

Bibliography

J. M. Ball. Convexity conditions and existence theorems in nonlinear elasticity. *Arch. Ration. Mech. Anal.*, 63:337–403, 1977.

S Bednarek. The giant magnetostriction in ferromagnetic composites within an elastomer matrix. *Applied Physics A: Materials Science & Processing*, 68:63–67, 1999.

K. Bertoldi and M. Gei. Instabilities in multilayered soft dielectrics. *J. Mech. Phys. Solids*, 59:18–42, 2011.

L. Borcea and O. Bruno. On the magneto-elastic properties of elastomer-ferromagnet composites. *J. Mech. Phys. Solids*, 49:2877–2919, 2001.

A. Braides. Homogenization of some almost periodic coercive functionals. *Rendiconti della Accademia Nazionale delle Scienze detta dei XL*, 9:313–322, 1985.

A. Braides and A. Defrancheschi. *Homogenization of Multiple Integrals*. Oxford University Press, 1998.

I. A. Brigadnov and A. Dorfmann. Mathematical modeling of magneto-sensitive elastomers. *Int. J. Solids Struct.*, 40:4659–4674, 2003.

W. F. Brown. *Micromagnetics*. Wiley, New York, 1963.

W. F. Brown. *Magnetoelastic Interactions*. Springer-Verlag, New York, 1966.

R. Bustamante, A. Dorfmann, and R.W. Ogden. On variational formulations in nonlinear magnetoelastostatics. *Math. Mech. Solids*, 13:725–745, 2008.

J. D. Carson and M. R. Jolly. MR fluid, foam and elastomer devices. *Mechatronics*, 10:555–569, 2000.

K. Danas, S. V. Kankanala, and N. Triantafyllidis. Experiments and modeling of iron-particle-filled magnetorheological elastomers. *J. Mech. Phys. Solids*, 60:120–138, 2012.

G. deBotton. Transversely isotropic sequentially laminated composites in finite elasticity. *J. Mech. Phys. Solids*, 53:1334–1361, 2006.

G. deBotton, L. Tevel-Deree, and D. A. Socolsky. Electroactive heterogeneous polymers: Analysis and applications to laminated composites. *Mechanics of Advanced Materials and Structures*, 14:13–22, 2007.

A. DeSimone. Energy minimizers for large ferromagnetic bodies. *Arch. Ration. Mech. Anal.*, 125:99–143, 1993.

A. DeSimone and R.D. James. A constrained theory of magnetoelasticity. *J. Mech. Phys. Solids*, 20:283–320, 2002.

M. Destrade and R. Ogden. On magneto-acoustic waves in finitely deformed elastic solids. *Math. Mech. Solids*, 16:594–604, 2011.

G. Diguet, E. Beaugnon, and J. Y. Cavaille. Shape effect in the magnetostriction of ferromagnetic composites. *J. Magn. Magn. Mater.*, 322:3337–3341, 2010.

A. Dorfmann and R. W. Ogden. Nonlinear magnetoelastic deformations. *Q. J. Mech. Appl. Math*, 57:599–622, 2004.

A. Dorfmann and R. W. Ogden. Nonlinear electroelastostatics: Incremental equations and stability. *Int. J. Eng. Sci.*, 48:1–14, 2010.

T. A. Duenas and G. P. Carman. Large magnetostrictive response of terfenol-d resin composites (invited). *J. Appl. Phys.*, 87:4696–4701, 2000.

A. C. Eringen and G. A. Maugin. *Electrodynamics of Continua*. Springer-Verlag, New York, 1990.

J. D. Eshelby. The determination of the elastic field of an ellipsoidal inclusion and related problems. *Proc. R. Soc. Lond. A*, 241:376–396, 1957.

E. Galipeau and P. Ponte Castañeda. The effect of particle shape and distribution on the macroscopic behavior of magnetoelastic composites. *Int. J. Solids Struct.*, 49:1–17, 2012.

E. Galipeau and P. Ponte Castañeda. A finite-strain constitutive model for magnetorheological elastomers: magnetic torques and particle rotations. *Submitted*, 2013.

E. Galipeau, S. Rudykh, G. deBotton, and P Ponte Castañeda. On the effective behavior of magnetorheological elastomers with periodic and randomn distribution of particles. *In preparation*, 2013.

A. N. Gent. A new constitutive relation for rubber. *Rubber Chem. Technol.*, 69:59–61, 1996.

G. Geymonat, S. Müller, and N. Triantafyllidis. Homogenization of nonlinearly elastic materials, microscopic bifurcation and macroscopic loss of rank-one convexity. *Arch. Ration. Mech. Anal.*, 122:231–290, 1993.

J. M. Ginder, M. E. Nichols, L. D. Elie, and J. L. Tardiff. Magnetorheological elastomers: Properties and applications. *Smart Material Technologies. Proc. of SPIE.*, 3675:Wuttig, M., 1999.

J. M. Ginder, S. M. Clark, W. F. Schlotter, and M. E. Nichols. Magnetostrictive phenomena in magnetorheological elastomers. *Int. J. Mod. Phys. B*, 16:2412–2418, 2002.

X. Guan, X. Dong, and J. Ou. Magnetostrictive effect of magnetorheological elastomer. *J. Magn. Magn. Mater.*, 320:158–163, 2008.

R. Hill. On constitutive macrovariables for heterogenous solids at finite strain. *Proc. R. Soc. Lond. A*, 326:131–147, 1972.

A. Hoger. The elasticity tensor of a residually stressed material. *J. of Elasticity*, 31: 219–237, 1993.

M. I. Idiart and P. Ponte Castañeda. Variational linear comparison bounds for nonlinear composites with anisotropic phases. I. General results. *Proc. R. Soc. Lond. A*, 463:907–924, 2007.

J. D. Jackson. *Classical Electrodynamics*. Wiley, New York, 2 edition, 1975.

R. D. James and D. Kinderlehrer. Theory of magnetostriction with applications to $Tb_xDy_{1-x}Fe_2$. *Philos. Mag.*, 68:237–274, 1993.

M. R. Jolly, J. D. Carlson, and B. C. Munoz. A model of the behaviour of magnetorheological materials. *Smart Mater. Struct.*, 5:607–614, 1996.

M. Kailasam and P. Ponte Castañeda. A general constitutive theory for linear and nonlinear particulate media with microstructure evolution. *J. Mech. Phys. Solids*, 46:427–465, 1998.

M. Kailasam, P. Ponte Castañeda, and J.R. Willis. The effect of particle size, shape, distribution and their evolution on the constitutive response of nonlinearly viscous composites. I. Theory. *Philos. Trans. R. Soc. Lon. A*, 335:1835–1852, 1997.

S. V. Kankanala and N. Triantafyllidis. On finitely strained magnetorheological elastomers. *J. Mech. Phys. Solids*, 52:2869–2908, 2004.

S. V. Kankanala and N. Triantafyllidis. Magnetoelastic buckling of a rectangular block in plane strain. *J. Mech. Phys. Solids*, 56:1147–1169, 2008.

Kaye and Laby. Magnetic properties of materials. *Tables of Physical and Chemical Constants. 2.1.2 Barometry*, Online Version 1.1, 2008. URL `http://www.kayelaby.npl.co.uk/general_physics/2_6/2_6_6.html`.

A. Kovetz. *Electromagnetic Theory*. Oxford University Press, New York, 2000.

L. Lanotte, G. Ausanio, C. Hison, V. Iannotti, and C. Luponio. The potentiality of composite elastic magnets as novel materials for sensors and actuators. *Sens. Actuators, A*, 106:56–60, 2003a.

L. Lanotte, G. Ausanio, V. Iannotti, and C. Luponio. Influence of particle preorientation on elastomagnetic effect in a composite material of ellipsoidal Ni microparticles in a silicone matrix. *Applied Physics A: Materials Science & Processing*, 77:953–958, 2003b.

L. P. Liu, R. D. James, and P. H. Leo. Magnetostrictive composites in the dilute limit. *J. Mech. Phys. Solids*, 54:951–974, 2006.

O. Lopez-Pamies and P. Ponte Castañeda. On the overall behavior, microstructure evolution, and macroscopic stability in reinforced rubbers at large deformations: II - Application to cylindrical fibers. *J. Mech. Phys. Solids*, 54:831–863, 2006a.

O. Lopez-Pamies and P. Ponte Castañeda. On the overall behavior, microstructure evolution, and macroscopic stability in reinforced rubbers at large deformations: I—Theory. *J. Mech. Phys. Solids*, 54:807–830, 2006b.

O. Lopez-Pamies and P. Ponte Castañeda. Microstructure evolution in hyperelastic laminates and implications for overall behavior and macroscopic stability. *Mechanics of Materials*, 41:364–374, 2009.

P. Marcellini. Periodic solutions and homogenization of nonlinear variational problems. *Annali di Matematica Pura ed Applicata*, 4:139–152, 1978.

G. A. Maugin and A. C. Eringen. Deformable magnetically saturated media. 1. Field equations. *J. Math Phys.*, 13:143–155, 1972.

J.-C. Michel, O. Lopez-Pamies, P. Ponte Castañeda, and N. Triantafyllidis. Microscopic and macroscopic instabilities in finitely strained porous elastomers. *J. Mech. Phys. Solids*, 55:900–938, 2007.

J.-C. Michel, O. Lopez-Pamies, P. Ponte Castañeda, and N. Triantafyllidis. Microscopic and macroscopic instabilities in finitely strained fiber-reinforced elastomers. *J. Mech. Phys. Solids*, 58:1776–1803, 2010.

G. W. Milton. *The Theory of Composites*. Cambridge University Press, New York, 2001.

S. Müller. Homogenization of nonconvex integral functionals and cellular elastic materials. *Arch. Ration. Mech. Anal.*, 99:189–212, 1987.

H. Ohanian. *Classical Electrodynamics*. Infinity Science Press LLC, 2 edition, 2006.

M. Ottenio, M. Destrade, and R. Ogden. Incremental magnetoelastic deformations, with application to surface instability. *J. of Elasticity*, 90:19–42, 2008.

R. Pelrine, R. Kornbluh, J. Joseph, R. Heydt, Q. B. Pei, and S. Chiba. High-field deformation of elastomeric dielectrics for actuators. *Materials Science & Engineering, C: Biomimetic and Supramolecular Systems*, 11:89–100, 2000.

P. Ponte Castañeda. The effective mechanical properties of nonlinear isotropic composites. *J. Mech. Phys. Solids*, 39:45–71, 1991.

P. Ponte Castañeda. Bounds and estimates for the properties of nonlinear heterogeneous systems. *Philos. Trans. R. Soc. Lon. A*, 340:531–567, 1992.

P. Ponte Castañeda. Exact second-order estimates for the effective mechanical properties of nonlinear composite materials. *J. Mech. Phys. Solids*, 44:827–862, 1996.

P. Ponte Castañeda. Three-point bounds and other estimates for strongly nonlinear composites. *Phys. Rev. B*, 57:12077–12083, 1998.

P. Ponte Castañeda. Second-order theory for nonlinear composite dielectrics incorporating field fluctuations. *Phys. Rev. B*, 64:214205, 2001.

P. Ponte Castañeda. Second-order homogenization estimates for nonlinear composites incorporating field fluctuations: I — theory. *J. Mech. Phys. Solids*, 50:737–757, 2002.

P. Ponte Castañeda and E. Galipeau. Homogenization-based constitutive models for magnetorheological elastomers at finite strain. *J. Mech. Phys. Solids*, 59:194–215, 2011.

P. Ponte Castañeda and M. H. Siboni. A finite-strain constitutive theory for electroactive polymer composites via homogenization. *Int. J. Nonlinear Mech.*, 47:293–306, 2011.

P. Ponte Castañeda and P. Suquet. Nonlinear composites. *Advances in Applied Mechanics*, 34:171–302, 1998.

P. Ponte Castañeda and E. Tiberio. A second-order homogenization procedure in finite elasticity and applications to black-filled elastomers. *J. Mech. Phys. Solids*, 48:1389–1411, 2000.

P. Ponte Castañeda and J. R. Willis. The effect of spatial distribution on the effective behavior of composite materials and cracked media. *J. Mech. Phys. Solids*, 43: 1919–1951, 1995.

P. Ponte Castañeda and J. R. Willis. Variational second-order estimates for nonlinear composites. *Proc. R. Soc. Lond. Ser. A Math. Phys. Eng. Sci.*, 455:1799–1811, 1999.

P. Ponte Castañeda and M. Zaidman. Constitutive models for porous materials with evolving microstructure. *J. Mech. Phys. Solids*, 42:1459–1497, 1994.

P Ponte Castañeda, G Debotton, and G LI. Effective properties of nonlinear inhomogeneous dielectrics. *Phys. Rev. B*, 46:4387–4394, 1992.

Z. Rigbi and L. Jilken. The response of an elastomer filled with soft ferrite to mechanical and magnetic influences. *J. Magn. Magn. Mater.*, 37:267–276, 1983.

S. Rudykh and G. deBotton. Stability of anisotropic electroactive polymers with application to layered media. *Z. Angew. Math. Phys.*, 62:1131–1142, 2011.

S. Rudykh and G. deBotton. Instabilities of hyperelastic fiber composites: micromechanical versus numerical analyses. *J. of Elasticity*, 106:123–147, 2012.

M. H. Siboni and P. Ponte Castañeda. Dielectric elastomer composites: Small-deformation theory and applications. *Submitted*, 2012a.

M. H. Siboni and P. Ponte Castañeda. A magnetically anisotropic, ellipsoidal inclusion subjected to a non-aligned magnetic field in an elastic medium. *Comptes Rendus Mécanique*, 340:205–218, 2012b.

G. B. Sohoni and J. E. Mark. Anisotropic reinforcement in elastomers containing magnetic filler particles. *J. Appl. Polym. Sci.*, 34:2553–2859, 1987.

Z. Suo, X. Zhao, and W. H. Greene. A nonlinear field theory of deformable dielectrics. *J. Mech. Phys. Solids*, 56:467–486, 2008.

P. Suquet. Overall potentials and extremal surfaces of power law or ideally plastic materials. *J. Mech. Phys. Solids*, 41:981–1002, 1993.

D. R. S. Talbot and J. R. Willis. Variational principles for inhomogeneous nonlinear media. *IMA Journal of Applied Mathematics*, 35:39–54, 1985.

H. F. Tiersten. Coupled magnetomechnical equations for magnetically saturated insulators. *J. Math Phys.*, 5:1298–1318, 1964.

H. F. Tiersten. Variational principle for saturated magnetoelastic insulators. *J. Math Phys.*, 6:779–787, 1965.

R. Toupin. The elastic dielectric. *J. Ration. Mech. Analysis*, 5:849–915, 1956.

N. Triantafyllidis and B. N. Maker. On the comparison between microscopic and macroscopic instability mechanisms in a class of fiber-reinforced composites. *J. App. Mech.*, 52:794–800, 1985.

C. Truesdell and R. Toupin. The classical field theories. *Handbuch der Physik*, III, 1960.

P. von Lockette, S. Lofland, J. Biggs, J. Roche, J. Mineroff, and M. Babcock. Investigating new symmetry classes in magnetorheological elastomers: cantilever bending behavior. *Smart Mater. Struct.*, 20:105022, 2011.

D. K. Vu and P. Steinmann. Nonlinear electro- and magneto-elastostatics: Material and spatial settings. *Int. J. Solids Struct.*, 44:7891–7905, 2007.

J. R. Willis. Bounds and self-consistent estimates for overall properties of anisotropic composites. *J. Mech. Phys. Solids*, 25:185–202, 1977.

H. M. Yin and L. Z. Sun. Magnetoelastic modelling of composites containing randomly dispersed ferromagnetic particles. *Philos. Mag.*, 86:4367–4395, 2006.

H. M. Yin, L. Z. Sun, and J. S. Chen. Magneto-elastic modeling of composites containing chain-structured magnetostrictive particles. *J. Mech. Phys. Solids*, 54: 975–1003, 2006.